



University of HUDDERSFIELD

University of Huddersfield Repository

Fennessy, Rebecca Valerie

Synthesis of polydentate ligands and their self-assembly into helicates, meso-helicates and cyclic helicates

Original Citation

Fennessy, Rebecca Valerie (2013) Synthesis of polydentate ligands and their self-assembly into helicates, meso-helicates and cyclic helicates. Doctoral thesis, University of Huddersfield.

This version is available at <http://eprints.hud.ac.uk/id/eprint/23326/>

The University Repository is a digital collection of the research output of the University, available on Open Access. Copyright and Moral Rights for the items on this site are retained by the individual author and/or other copyright owners. Users may access full items free of charge; copies of full text items generally can be reproduced, displayed or performed and given to third parties in any format or medium for personal research or study, educational or not-for-profit purposes without prior permission or charge, provided:

- The authors, title and full bibliographic details is credited in any copy;
- A hyperlink and/or URL is included for the original metadata page; and
- The content is not changed in any way.

For more information, including our policy and submission procedure, please contact the Repository Team at: E.mailbox@hud.ac.uk.

<http://eprints.hud.ac.uk/>

**SYNTHESIS OF POLYDENTATE LIGANDS AND THEIR SELF-
ASSEMBLY INTO HELICATES, *MESO*-HELICATES AND CYCLIC
HELICATES**



University of
HUDDERSFIELD

Rebecca Fennessy

A thesis submitted to the University of Huddersfield in partial fulfilment of the requirements for the degree of Doctor of Philosophy

Department of Chemical and Biological Sciences
The University of Huddersfield

August 2013

Copyright statement

- i. The author of this thesis (including any appendices and/or schedules to this thesis) owns any copyright in it (the "Copyright") and she has given The University of Huddersfield the right to use such copyright for any administrative, promotional, educational and/or teaching purposes.
- ii. Copies of this thesis, either in full or in extracts, may be made only in accordance with the regulations of the University Library. Details of these regulations may be obtained from the Librarian. This page must form part of any such copies made.
- iii. The ownership of any patents, designs, trademarks and any and all other intellectual property rights except for the Copyright (the "Intellectual Property Rights") and any reproductions of copyright works, for example graphs and tables ("Reproductions"), which may be described in this thesis, may not be owned by the author and may be owned by third parties. Such Intellectual Property Rights and Reproductions cannot and must not be made available for use without the prior written permission of the owner(s) of the relevant Intellectual Property Rights and/or Reproductions

Acknowledgements

Firstly I would like to thank my supervisor Prof. Craig Rice, in addition to solving the numerous crystal structures, for his constructive guidance, advice and support. My thanks also goes to past and present members of the Rice research group, in particular Samantha Bullock, all of whom have been a pleasure to work with over the years.

The following people have given their assistance and support with various aspects of the research I would therefore like to thank them; Dr. Thomas Riis-Johannessen and Dr. Michaele Hardie for crystal structure refinement, Dr. Neil McLay for NMR and Mass Spectroscopy, Dr. Lindsay Harding for assistance with Mass Spectrometry, Dr. Simon Pope for photophysical experiments, Dr. Nicholas Fletcher for CD spectroscopy experiments and Dr. David Cooke for molecular modelling calculations.

I would like to thank the University of Huddersfield for providing this great opportunity and the necessary funding to perform this research. I would also like to thank other members within the Department of Chemical and Biological Sciences.

I would like to express my deepest appreciation to all my family and friends who have supported me throughout my studies. Last but not least I would like to thank Simon for his support.

Abstract

Described here is the synthesis and coordination chemistry of various ligands, $L^1 - L^{17}$. Some of the ligands presented form interesting supramolecular assemblies upon reaction with selected metal ions.

Chapter 1 provides a general introduction to supramolecular chemistry and self-assembly.

Chapter 2 introduces a new class of potentially hexadentate symmetrical ligands, $L^1 - L^5$. These ligands consist of two tridentate binding sites separated by a 1,3-phenylene spacer unit. Reaction of L^1 with Zn(II) ions results in the formation of a pentanuclear circular helicate $[Zn_5(L^1)_5]^{10+}$, within the structure all five zinc ions are six-coordinate arising from coordination of two tridentate domains from two different ligand strands. This structure was shown to exist in both the solid state and in solution. Incorporation of various enantiopure units allowed variation of the terminal functional group of the ligand, $L^2 - L^5$. These ligands, upon coordination with Zn(II) ions, were shown to form supramolecular assemblies analogous to the pentanuclear species observed for L^1 . Additionally these ligands were shown to be diastereoselective, controlling the resulting supramolecular architecture giving up to 80% diastereomeric excess.

Described in Chapter 3 are a number of potentially hexadentate N-donor ligands, $L^6 - L^{14}$. Each ligand possesses the same thiazole-pyridyl-pyridyl tridentate domains, with variation of the spacer unit. Upon coordination with selected transition metal ions these ligands resulted in the formation of dinuclear species. Reaction of L^9 with Cd(II) results in the formation of a dinuclear double helicate, in which the two tridentate domains coordinate each metal ion and the ligands twist in the centre generating an 'over and under' arrangement. However, reaction of L^9 with Co(II) results in the formation of a dinuclear *meso*-helicate, in which the ligands adopt a side-by-side configuration. This difference in structure is attributed to unfavourable steric interactions which prevent the formation of the Co(II) double helicate. Reaction

of two of these ligands L^{10} , which possesses an ethylene glycol chain, and L^{11} , containing an amine group, with Cd(II) and camphorsulfonic acid results in the formation of a heteroleptic one-dimensional chain. Hydrogen bonding interactions between the protonated amine of L^{11} and the glycol chains of L^{10} results in a structure which contains both of these *meso*-helicite structures in an extended one-dimensional arrangement $(([Cd_2(L^{10})_2][Cd_2(L^{11}-H)_2])(ClO_4)_{10})_n$.

Chapter 4 reports the synthesis of three ligands, $L^{15} - L^{17}$, each containing the same central phenol unit, and either a hydroxyl, pyridine or pyridine-*N*-oxide terminal unit. Reaction of each ligand with various trivalent lanthanide ions results in the formation of a dinuclear double helicite. In each structure the central phenol unit is deprotonated and bridges the two lanthanide ions giving $[L_2M_2]^{4+}$. L^{17} , which possesses the pyridine-*N*-oxide as the terminal group, effectively encompasses the cations minimising access for the coordination of any anions or solvent molecules. Photophysical measurements show that this ligand forms emissive complexes with a number of lanthanide ions, whilst the magnitude of the lifetime for $[(L^{17})_2Yb_2]^{4+}$ ($\tau = 21.0 \mu s$) suggests that both Yb(III) ions are well-shielded from excited state quenching phenomena.

Contents	
Acknowledgements	i
Abstract	ii
Contents	i
List of figures	viii
List of schemes	xiv
List of tables	xv
List of abbreviations	xvi
1. Introduction	1
1.1 Supramolecular chemistry	1
1.1.1 Foundations of supramolecular chemistry	1
1.2 Supramolecular interactions	2
1.2.1 Ion-ion interactions	3
1.2.2 Ion-dipole interactions.....	3
1.2.5 π - π stacking interactions	4
1.3 Host-guest chemistry	5
1.3.1 Crown ethers	7
1.4 Self-assembly	12
1.4.1 Rotaxanes.....	13
1.5 Metallosupramolecular chemistry	15
1.5.1 Grids	17
1.5.2 Ladders.....	19
1.5.3 Racks.....	20
1.5.4 Cages	21
1.6 Helicates.....	25
1.6.1 Nomenclature	26
1.6.2 Homotopic helicates	27
1.6.3 Heterotopic helicates	28
1.6.4 Unsaturated helicates	30
1.6.5 Heteroleptic helicates	32

1.6.6 Heteronuclear helicates	33
1.6.7 Chirality in helicates.....	35
1.6.8 <i>Meso</i> -helicates.....	41
1.7 Circular helicates	42
1.7.1 Anion templation	43
1.7.2 Alternatives to anion templation.....	46
1.7.3 Directional and heteroleptic circular helicates.....	47
1.7.4 Diastereoselective circular helicates.....	50
1.7.5 Circular <i>meso</i> -helicates	51
1.8 Allosteric interactions.....	53
1.8.1 Ditopic ligands	56
1.9 Ligand design	58
1.9.1 Ligand programming.....	59
1.9.2 Ligand recognition	63
2. Diastereoselective assembly of pentanuclear circular helicates	67
2.1 Ligand synthesis.....	68
2.1.1 Synthesis of L^1	68
2.1.2 Synthesis of $L^2 - L^4$	70
2.2 Coordination chemistry	71
2.2.1 Complexes of L^1 with zinc(II)	71
2.3 Solution studies	76
2.3.1 Solution state characterisation of $[Zn_5(L^1)_5]^{10+}$	76
2.3.2 Solution state characterisation of $L^2 - L^4$	78
2.4 Conclusion.....	83
3 Steric control over the formation of dinuclear double helicate and dinuclear <i>meso</i>-helicate assemblies.....	84
3.1 Ligand synthesis.....	91
3.1.1 Synthesis of L^6	91
3.1.2 Synthesis of $L^7 - L^{14}$	93
3.2 <i>Coordination chemistry</i>	98

3.2.1 Complexes of L^6 with copper(II)	98
3.2.2 Complexes of L^7 with iron(II)	100
3.2.4 Complexes of L^9	105
3.2.5 Complexes of L^{10} with iron(II).....	111
3.2.6 Complexes of L^{11} with cadmium(II)	115
3.2.7 Complexes of L^{12} with zinc(II)	119
3.2.8 Complexes of L^{13} with zinc(II)	120
3.2.9 Complexes of L^{14} with cadmium(II)	123
3.3 <i>Solution studies</i>	126
3.3.1 Solution state characterisation of complexes of L^9	126
3.3.2 Solution state characterisation of complexes of L^{14}	127
3.4 <i>Discussion</i>	129
3.5 <i>Conclusion</i>	135
4. Emissive lanthanide-containing dinuclear double stranded helicates	136
4.1 Ligand synthesis	141
4.1.1 Synthesis of L^{15}	141
4.1.2 Synthesis of L^{16} and L^{17}	143
4.2 Coordination chemistry	145
4.2.1 Complex of L^{15} with europium(III)	145
4.2.2 Complex of L^{16} with lanthanum(III)	148
4.2.3 Complex of L^{17} with terbium(III)	152
4.3 Photophysical measurements.....	154
4.4 Discussion	158
4.5 Conclusion.....	159
5. Conclusion	160
6. Experimental	163
6.1 Preparation of diastereoselective ligands (L^1 - L^4).....	164
6.1.1 Synthesis of picolinamide derivative 1a ¹⁷⁰	164
6.1.2 Synthesis of picolinamide derivative 1b	165
6.1.3 Synthesis of picolinamide derivative 1c	165

6.1.4 Synthesis of picolinamide derivative 1d	166
6.1.5 Synthesis of picolinamide-N-oxide derivative 2a	167
6.1.6 Synthesis of picolinamide-N-oxide derivative 2b	168
6.1.7 Synthesis of picolinamide-N-oxide derivative 2c	168
6.1.8 Synthesis of picolinamide-N-oxide derivative 2d	169
6.1.9 Synthesis of 6-cyanopicolinamide derivative 3a	170
6.1.10 Synthesis of 6-cyanopicolinamide derivative 3b	171
6.1.11 Synthesis of 6-cyanopicolinamide derivative 3c	171
6.1.12 Synthesis of 6-cyanopicolinamide derivative 3d	172
6.1.13 Synthesis of picolinamide-6-thioamide derivative 4a	173
6.1.14 Synthesis of picolinamide-6-thioamide derivative 4b	174
6.1.15 Synthesis of picolinamide-6-thioamide derivative 4c	174
6.1.16 Synthesis of picolinamide-6-thioamide derivative 4d	175
6.1.17 Synthesis of L¹	176
6.1.18 Synthesis of L²	177
6.1.19 Synthesis of L³	178
6.1.20 Synthesis of L⁴	179
6.2 Preparation of phenyl-spacer ligands (L⁶ - L¹⁴).....	180
6.2.1 Synthesis of 3, 3'-Bis (2-bromoacetyl) biphenyl (8).....	180
6.2.2 Synthesis of L⁶	181
6.2.3 Synthesis of 12	182
6.2.4 Synthesis of 13	183
6.2.5 Synthesis of L⁷	184
6.2.6 Synthesis of 15	185
6.2.7 Synthesis of 16	185
6.2.8 Synthesis of L⁸	186
6.2.9 Synthesis of 1,3-dibromo-2-methoxy-5-methylbenzene (18) ¹⁷¹	187

6.2.10 Synthesis of 19	188
6.2.11 Synthesis of 20	189
6.2.12 Synthesis of L⁹	190
6.2.13 Synthesis of 23 ¹⁷²	191
6.2.14 Synthesis of 24	192
6.2.15 Synthesis of 25	193
6.2.16 Synthesis of 26	194
6.2.17 Synthesis of ligand L¹⁰	195
6.2.18 Synthesis of 28	196
6.2.19 Synthesis of 29	197
6.2.20 Synthesis of L¹¹	198
7.2.21 Synthesis of 30 ¹⁷³	199
6.2.22 Synthesis of 31	200
6.2.23 Synthesis of 32	201
6.2.24 Synthesis of L¹²	202
6.2.25 Synthesis of N-(2,6-dibromo-4-methyl-phenyl)benzamide (33)....	203
6.2.26 Synthesis of 34	204
6.2.27 Synthesis of 35	205
6.2.28 Synthesis of L¹³	206
6.2.29 Synthesis of 36	207
6.2.30 Synthesis of 37	208
6.2.31 Synthesis of 38	209
6.2.32 Synthesis of L¹⁴	210
6.3 Preparation of (L¹⁵- L¹⁷).....	211
6.3.1 Synthesis of 8-hydroxyquinoline-2-carbothioamide 40	211
6.3.2 Synthesis of 42	212
6.3.3 Synthesis of L¹⁵	213

6.3.4 Synthesis of L^{16}	214
6.3.5 Synthesis of 6'-cyano-2,2'-bipyridine-N-oxide (44) ¹⁶⁹	215
6.3.6 Synthesis of Synthesis of N-oxide-2,2'-bipyridine-6'-thioamide (45) ¹⁶⁹	216
6.3.7 Synthesis of L^{17} ¹⁶⁹	217
6.4 Synthesis of complexes	218
6.4.1 Synthesis of $[Zn_5(L^1)_5](CF_3SO_3)_{10}$	218
6.4.2 Synthesis of the complex $[Cu_2(L^6)_2](ClO_4)_4$	218
6.4.3 Synthesis of the complex $[Fe_2(L^7)_2](ClO_4)_4$	219
6.4.4 Synthesis of the complex $[Hg_2(L^8)_2](ClO_4)_4$	219
6.4.5 Synthesis of L^9 complexes	219
6.4.6 Synthesis of the complex $[Fe_2(L^{10})_2](ClO_4)_4$	220
6.4.7 Synthesis of the complex $[Cd_2(L^{11})_2](ClO_4)_4$	220
6.4.8 Synthesis of the complex $[Zn_2(L^{12})_2](ClO_4)_4$	220
6.4.9 Synthesis of the complex $[Zn_2(L^{13})_2](ClO_4)_4$	221
6.4.10 Synthesis of the complex $[Cd_2(L^{14})_2](ClO_4)_4$	221
6.4.11 Synthesis of the complex $[Cd_2(L^{10})_2][Cd_2(L^{12}-H)_2](ClO_4)_{10}$	221
6.4.12 Synthesis of the complex $[(L^{15})_2Eu_2(H_2O)_2](CF_3SO_3)_4$	222
6.4.13 Synthesis of the complex $[(L^{16})_2La_2(H_2O)_2(CF_3SO_3)_2](CF_3SO_3)_4$	222
6.4.14 Synthesis of the complex $[(L^{17})_2Tb_2](CF_3SO_3)_4$	222
References	223
Appendix 1: Crystal data tables	234
Table A1. Crystallographic data of L^1 complex $[Zn_5(L^1)_5]^{10+}$	236
Table A2. Crystallographic data of L^6 complex $[Cu_2(L^6)_2]^{4+}$	237
Table A3. Crystallographic data of L^7 complex $[Fe_2(L^7)_2]^{4+}$	238
Table A4. Crystallographic data of L^8 complex $[Hg_2(L^8)_2]^{4+}$	239
Table A5. Crystallographic data of L^9 complex $[Zn_2(L^9)_2]^{4+}$	240
Table A6. Crystallographic data of L^9 complex $[Co_2(L^9)_2]^{4+}$	241
Table A7. Crystallographic data of L^9 complex $[Cd_2(L^9)_2]^{4+}$	242

Table A8. Crystallographic data of L^{10} complex $[Fe_2(L^{10})_2]^{4+}$	243
Table A9. Crystallographic data of L^{11} complex $[Cd_2(L^{11})(L^{11}-H)]^{5+}$	244
Table A10. Crystallographic data of L^{12} complex $[Zn_2(L^{12})_2]^{4+}$	245
Table A11. Crystallographic data of L^{13} complex $[Zn_2(L^{13})_2]^{4+}$	246
Table A12. Crystallographic data of L^{14} complex $[Cd_2(L^{14})_2]^{4+}$	247
Table A13. Crystallographic data of L^{10} and L^{11} complex $[Cd_2(L^{10})_2][Cd_2(L^{11}-H)_2]^{10+}$	248
Table A14. Crystallographic data of L^{15} complex $[(L^{15})_2Eu_2]^{4+}$	249
Table A15. Crystallographic data of L^{16} complex $[(L^{16})_2La_2]^{4+}$	250
Table A16. Crystallographic data of L^{17} complex $[(L^{17})_2Tb_2]^{4+}$	251
Appendix 2: Crystal packing	252
A2.1. Packing of L^1 complex $[Zn_5(L^1)_5]^{10+}$	252
A2.2 Packing of L^6 complex $[Cu_2(L^6)_2]^{4+}$	252
A2.3. Packing of L^7 complex $[Fe_2(L^7)_2]^{4+}$	253
A2.4. Packing of L^8 complex $[Hg_2(L^8)_2]^{4+}$	253
A2.5. Packing of L^9 complex $[Co_2(L^9)_2]^{4+}$	254
A2.6. Packing of L^9 complex $[Cd_2(L^9)_2]^{4+}$	254
A2.7. Packing of L^{10} complex $[Fe_2(L^{10})_2]^{4+}$	255
A2.8. Packing of L^{11} complex $[Cd_2(L^{11})(L^{11}-H)]^{5+}$	255
A2.9. Packing of L^{13} complex $[Zn_2(L^{13})_2]^{4+}$	256
A2.10. Packing of L^{14} complex $[Cd_2(L^{14})_2]^{4+}$	256
A2.11. Packing of L^{15} complex $[(L^{15})_2Eu_2]^{4+}$	257
A2.13. Packing of L^{17} complex $[(L^{17})_2Tb_2]^{4+}$	258
Appendix 3: Publications	259

List of figures

Figure 1.1 Early macrocyclic ligands in supramolecular chemistry	2
Figure 1.2 Ion-ion interactions ¹³	3
Figure 1.3 Example of ion-dipole interaction.....	3
Figure 1.4 Dipole-dipole interactions in carbonyls	4
Figure 1.5 Example of hydrogen bonding	4
Figure 1.6 Possible orientations for π - π stacking interactions.....	5
Figure 1.7 Illustration of the co-ordination difference between cavitands and clathrands	6
Figure 1.8 Spatial arrangements between host and guest ⁵	6
Figure 1.9 Intended synthesis for bis[2(o-hydroxy-phenoxy)ethyl]ether ⁴	8
Figure 1.10 Dibenzo [18]crown-6 (or 2,3,11,12-dibenzo-1,4,7,10,13,16-hexaoxacyclooctadeca-2,11-diene)	9
Figure 1.11 Examples of crown ethers	9
Figure 1.12 Representation of a) [2]-rotaxane b) [2]-pseudorotaxane ³⁴	13
Figure 1.13 Method of synthesis for the first [2]-rotaxane ³²	14
Figure 1.14 Illustration showing methods for rotaxane synthesis ⁴⁰	15
Figure 1.15 Examples of metal directed assemblies a) molecular square ⁴⁷ , b) Helicate and c) a supramolecular cube ⁴⁸	16
Figure 1.16 Schematic representations of A) racks, B) ladders and c) a grid ⁵⁰	17
Figure 1.17 Self-assembly of [2x2] grid architecture.....	18
Figure 1.18 Self-assembly of two- and three-“rung” ladders.....	20
Figure 1.19 Self-assembly of a rack with rotaxane character ⁵⁷	21
Figure 1.20 Three-dimensional supramolecular cage	23
Figure 1.21 Ligand Tp ^{py}	24
Figure 1.22 Examples of aromatic hydrocarbon spacer ligands	25
Figure 1.23 Trinuclear saturated homotopic double stranded helicate	28
Figure 1.24 Directional helicates from asymmetrically substituted quaterpyridine	30
Figure 1.25 Dinuclear unsaturated heterotopic double stranded homoleptic helicate	31
Figure 1.26 Trinuclear saturated homotopic double stranded heteroleptic helicate	33

Figure 1.27 Representation of the first structurally characterized heterodinuclear double helicate	35
Figure 1.28 Illustration representing a right-handed (P-plus) and a left-handed (M-minus) helix (where l is the pitch and z gives the helical axis).....	36
Figure 1.29 a) Ligands L^L and L^M b) schematic representation of the possible HH and HT diastereomeric dinuclear double helicates from the reaction of chiral ligands L^L and L^M with Cu(I) (S^* = homochiral compounds, (S,S) or (R,R)) ⁹¹ ...	38
Figure 1.30 Chiral ligand produced to control the chirality of helicates	39
Figure 1.31 4,5-Chiragen-type ligand produced for diastereoselective formation of helicates.....	40
Figure 1.32 Stereoselective self-assembly of a single-stranded helicate.....	40
Figure 1.33 Illustration of the assembly of a dinuclear heteroleptic mesocate .	42
Figure 1.34 Self-assembly of a pentanuclear circular helicate.....	44
Figure 1.35 Self-assembly of a tetranuclear circular helicate from four L^t ligands and four Fe(II) ions	45
Figure 1.36 Ligand, L^u , employed for the self-assembly of a circular helicate .	47
Figure 1.37 L^v used in the self-assembly of a head-to-tail circular helicate.	48
Figure 1.38 L^u and L^w used in the self-assembly of a heteroleptic circular helicate $[Cu_5(L^u)_3(L^w)_2]^{10+}$	50
Figure 1.39 L^x ligand utilised in the diastereoselective self-assembly of a circular helicate.....	51
Figure 1.40 a) Ligands utilized for the self-assembly of circular mesocates b) Schematic representation of a hexanuclear mesocate with Cu(II)	52
Figure 1.41 Representation of binding-induced conformational changes within a synthetic system ¹¹⁴	55
Figure 1.42 Ligand L^c and the two complex cations $[Hg_2(L^c)_2Na_2]^{6+}$ and $[Hg(L^c)Ba]^{4+115}$	57
Figure 1.43 Ligands, L^D and L^E , from previous research. Combination of these ligands produced a more complex ligand, L^F	60
Figure 1.44 Self-assembly modes of ligand, L^F , and metal ions of different coordination geometries ¹²⁰	61
Figure 1.45 Thiazole-containing ligands which self-assemble into different helicates, L^G triple helicate and L^H double helicate, upon coordination to Cu(II)	62

Figure 1.46 Self-recognition in the self-assembly of double helicates from a mixture of oligobipyridine ligand strands	64
Figure 1.47 Self-recognition in the self-assembly of a double helicate and triple helicate from a mixture of oligobipyridine ligand strands (L^S , L^J) with Cu(I) and Ni(II)	65
Figure 2.1 New class of helicands $L^1 - L^4$	67
Figure 2.2 Aromatic regions in the 1H NMR (400 MHz, $CDCl_3$) spectra of (1a) picolinamide derivative, (2a) picolinamide- <i>N</i> -oxide, (3a) 6-cyanopicolinamide, (4a) picolinamide-6-thioamide and Ligand 1 (L^1)	70
Figure 2.3 Solid state structure of the complex cation $[Zn_5(L^1)_5]^{10+}$	71
Figure 2.4 Structure of L^1 (i) diagram showing the two tridentate domains separated by the a 1,3-phenylene space unit and (ii) the partitioning seen within the crystal structure for L^1	74
Figure 2.5 Space-filling picture of L^1 showing atoms with their van der Waal's radii	75
Figure 2.6 Aromatic region in the 1H NMR (400 MHz, CD_3NO_2) spectrum of L^1 with Zn(II)	76
Figure 2.7 ESI-MS spectrum of $[Zn_5(L^1)_5](CF_3SO_3)_{10}$	77
Figure 2.8 Aromatic region of the 1H NMR spectra of (a) $[Zn_5(L^1)_5]^{10+}(CD_3NO_2)$, (b) $[Zn_5(L^2)_5]^{10+}(CD_3NO_2)$, (c) $[Zn_5(L^3)_5]^{10+}(CD_3NO_2)$ and (d) $[Zn_5(L^4)_5]^{10+}(CD_3NO_2)$:	79
Figure 2.9 L^5 , (R,R)- enantiomer of ligand L^3	80
Figure 2.10 The CD spectra of (a) ligand L^3 (red) and L^5 (blue) and (b) the resulting complexes upon the addition of one equivalent of Zn (II) in acetonitrile (298 K, concentration of 2.5×10^{-5} mol dm^{-3})	82
Figure 3.1 A schematic representation of the enantiomeric forms of a dinuclear triple helicate (left: $\Delta\Delta$, centre: $\Lambda\Lambda$) and the <i>meso</i> -helicate (right: $\Lambda\Delta$) ⁽⁹⁹⁾	84
Figure 3.2 Dicatechol ligand, L^M , employed to investigate the diastereoselectivity of helicates versus mesocate ⁽¹⁰⁰⁾	85
Figure 3.3 Bis(2,2'-bypyridine) ligand, L^N ⁽¹³⁵⁾	86
Figure 3.4 Chemical structure of ligand, L^O ⁽¹³⁷⁾	87
Figure 3.5 Chemical structure of pre-ligands, L^P ⁽¹³⁹⁾	88
Figure 3.6 Chemical structure of ligand, L^Q ⁽¹³⁹⁾	88
Figure 3.7 New class of ligands $L^6 - L^{14}$	90

Figure 3.8 Two views for the solid state structure of the complex cation $[\text{Cu}_2(\text{L}^6)_2]^{4+}$	98
Figure 3.9 Two views for the solid state structure of the complex cation $[\text{Fe}_2(\text{L}^7)_2]^{4+}$	100
Figure 3. 10 ESI-MS of $[\text{Fe}_2(\text{L}^7)_2](\text{ClO}_4)_4$ with the found (top) and predicted (bottom) isotopic distribution pattern of $\{[\text{Fe}_2(\text{L}^7)_2](\text{ClO}_4)_3\}^+$ (inset).....	101
Figure 3.11 Solid state structure of the complex cation $[\text{Hg}_2(\text{L}^8)_2]^{4+}$	103
Figure 3.12 Two views for the solid state structure of the complex cation $[\text{Co}_2(\text{L}^9)_2]^{4+}$	105
Figure 3.13 Two views for the solid state structure of the complex cation $[\text{Cd}_2(\text{L}^9)_2]^{4+}$	108
Figure 3.14 (i) Structure of L^9 , (ii) ligand coordination within the complex cation $[\text{Cd}_2(\text{L}^9)_2]^{4+}$	109
Figure 3.15 Two views for the solid state structure of the complex cation $[\text{Fe}_2(\text{L}^{10})_2]^{4+}$	111
Figure 3.16 solid state structure of the complex cation $[\text{Fe}_2(\text{L}^{10})_2]^{4+}$. One ligand shown in yellow to better illustrate the “side-by-side” conformation of the ligand strands	112
Figure 3. 17 ESI-MS of $[\text{Fe}_2(\text{L}^{10})_2](\text{ClO}_4)_4$ with the found (top) and predicted (bottom) isotopic distribution pattern of $\{[\text{Fe}_2(\text{L}^{10})_2](\text{ClO}_4)_3\}^+$ (inset)	113
Figure 3.18 Solid state structure of the complex cation $[\text{Cd}_2(\text{L}^{11})(\text{L}^{11}\text{-H})]^{5+}$	115
Figure 3.19 Two views of the complex cation $[\text{Cd}_2(\text{L}^{11})(\text{L}^{11}\text{-H})]^{5+}$ (i) Solid state structure including the water molecule within the cavity; (ii) Solid state structure showing hydrogen bonding.	117
Figure 3.20 Solid state structure of the complex cation $[\text{Zn}_2(\text{L}^{12})_2]^{4+}$	119
Figure 3.21 Two views for the solid state structure of the complex cation $[\text{Zn}_2(\text{L}^{13})_2]^{4+}$, solvent molecule omitted for clarity.	120
Figure 3.22 Two views of the complex cation $[\text{Zn}_2(\text{L}^{13})_2]^{4+}$ (i) Solid state structure; (ii) a space-filling picture showing all atoms and their van der Waal’s radii.....	121
Figure 3.23 Two views for the solid state structure of the complex cation $[\text{Cd}_2(\text{L}^{14})_2]^{4+}$	123
Figure 3.24 Space-filling picture of the complex cation $[\text{Cd}_2(\text{L}^{14})_2]^{4+}$ showing all atoms and their van der Waal’s radii.....	124

Figure 3.25 Aromatic region of the ^1H NMR spectra (CD_3NO_2) of a) $[\text{Zn}_2(\text{L}^9)_2]^{4+}$ (\bullet = mesocate), b) $[\text{Cd}_2(\text{L}^9)_2]^{4+}$, c) $[\text{Zn}_2(\text{L}^{14})_2]^{4+}$ and d) $[\text{Cd}_2(\text{L}^{14})_2]^{4+}$	127
Figure 3.26 Aromatic region of the ^1H - ^1H COSY spectrum of $[\text{Zn}_2(\text{L}^{14})_2]^{4+}$ in CD_3NO_2	128
Figure 3.27 Space-filling view of the crystal structures of a) $[\text{Fe}_2(\text{L}^7)_2]^{4+}$, b) $[\text{Co}_2(\text{L}^9)_2]^{4+}$	130
Figure 3.28 The $[\text{Cd}_2(\text{L}^{10})_2]^{4+}$ section of the one-dimensional $([\text{Cd}_2(\text{L}^{10})_2][\text{Cd}_2(\text{L}^{11}\text{-H})_2])^{10+}_n$ heteroleptic chain assembly.	132
Figure 3.29 The $[\text{Cd}_2(\text{L}^{11}\text{-H})_2]^{6+}$ section of the one-dimensional chain $([\text{Cd}_2(\text{L}^{10})_2][\text{Cd}_2(\text{L}^{11}\text{-H})_2])^{10+}_n$ assembly containing the two hydrogen-bond acceptor water molecules	133
Figure 3.30 The X-ray crystal structure of the mesocate-containing one-dimensional chain $([\text{Cd}_2(\text{L}^{10})_2][\text{Cd}_2(\text{L}^{11}\text{-H})_2])^{10+}_n$ showing the hydrogen-bonding interaction	134
Figure 4.1 Basic ligand, $\text{L}^{\text{R}'}$, employed to investigate lanthanide-containing helicates ¹⁵⁴⁻¹⁵⁸	137
Figure 4.2 Ligands, $\text{L}^{\text{S}'}$ and $\text{L}^{\text{T}'}$, employed for the self-assembly of heterodinuclear d-f helicates ⁽¹⁶⁰⁾	138
Figure 4.3 A new group of multidentate ligands $\text{L}^{15} - \text{L}^{17}$	140
Figure 4.4 Two views for the solid state structure of the complex cation $[(\text{L}^{15})_2\text{Eu}_2(\text{H}_2\text{O})_2]^{4+}$	145
Figure 4.5 ESI-MS of $[(\text{L}^{15})_2\text{Eu}_2](\text{CF}_3\text{SO}_3)_4$ with the found (top) and predicted (bottom) isotopic distribution pattern of $\{[(\text{L}^{15})_2\text{Eu}_2](\text{CF}_3\text{SO}_3)_3\}^+$ (inset)	146
Figure 4.6 Two views for the solid state structure of the complex cation $[(\text{L}^{16})_2\text{La}_2(\text{H}_2\text{O})_2(\text{CF}_3\text{SO}_3)_2]^{2+}$	148
Figure 4.7 ESI-MS of $[(\text{L}^{16})_2\text{La}_2](\text{CF}_3\text{SO}_3)_4$ with the found (top) and predicted (bottom) isotopic distribution pattern of $\{[(\text{L}^{16})_2\text{La}_2](\text{CF}_3\text{SO}_3)_3\}^+$ (inset)	149
Figure 4.8 Two views for the solid state structure of the complex cation $[(\text{L}^{17})_2\text{Tb}_2]^{4+}$	152
Figure 4.9 ESI-MS of $[(\text{L}^{17})_2\text{Gd}_2](\text{CF}_3\text{SO}_3)_4$ with the found (top) and predicted (bottom) isotopic distribution pattern of $\{[(\text{L}^{17})_2\text{Gd}_2](\text{CF}_3\text{SO}_3)_3\}^+$ (inset)	155
Figure 4.10 Total emission spectrum of $[(\text{L}^{17})_2\text{Eu}_2]^{2+}$ recorded in acetonitrile ($\lambda_{\text{ex}} = 290 \text{ nm}$).	156

Figure 4.11 a) Steady state emission spectrum of $[(L^{17})_2Yb_2]^{2+}$ and $[(L^{17})_2Nd_2]^{2+}$ recorded in acetonitrile ($\lambda_{ex} = 370$ nm); b) fitted decay profile for $[(L^{17})_2Yb_2]^{2+}$ ($\lambda_{ex} = 355$ nm).....	157
Figure 4.12 Structure of the complex cation $[(L^{15})_2Eu_2(H_2O)_2]^{4+}$ showing the $\{Eu(\mu-O_2)Eu\}$ core.....	158
Figure 4.13 End-on view of the space-filled X-ray structures of complexes a) $[(L^{15})_2Eu_2]^{4+}$, b) $[(L^{16})_2La_2]^{4+}$ and c) $[(L^{17})_2Tb_2]^{4+}$ (c). Coordinated anions/water molecules omitted for clarity	159

List of schemes

Scheme 2.1 Synthesis of $L^1 - L^4$	69
Scheme 3.1 Synthesis of L^6	92
Scheme 3.2 Synthesis of $L^7 - L^{13}$	96
Scheme 3.3 Synthesis of L^{14}	97
Scheme 4.1 Synthesis of L^{15}	142
Scheme 4. 2 Syntheses of L^{16} and L^{17}	144

List of tables

Table 1.1 Cation ionic diameters with a selection of crown ether cavity sizes .	10
Table 2.1 Selected bond lengths (Å) for the complex cation $[\text{Zn}_5(\text{L}^1)_5]^{10+}$	72
Table 2.2 Selected bond angles (°) for the complex cation $[\text{Zn}_5(\text{L}^1)_5]^{10+}$	74
Table 3.1 Selected bond lengths (Å) for the complex cation $[\text{Cu}_2(\text{L}^6)_2]^{4+}$	99
Table 3.2 Selected bond angles (°) for the complex cation $[\text{Cu}_2(\text{L}^6)_2]^{4+}$	99
Table 3.3 Selected bond lengths (Å) for the complex cation $[\text{Fe}_2(\text{L}^7)_2]^{4+}$	102
Table 3.4 Selected bond angles (°) for the complex cation $[\text{Fe}_2(\text{L}^7)_2]^{4+}$	102
Table 3.5 Selected bond lengths (Å) for the complex cation $[\text{Hg}_2(\text{L}^8)_2]^{4+}$	104
Table 3.6 Selected bond angles (°) for the complex cation $[\text{Hg}_2(\text{L}^8)_2]^{4+}$	104
Table 3.7 Selected bond lengths (Å) for the complex cation $[\text{Co}_2(\text{L}^9)_2]^{4+}$	106
Table 3.8 Selected bond angles (°) for the complex cation $[\text{Co}_2(\text{L}^9)_2]^{4+}$	107
Table 3.9 Selected bond lengths (Å) for the complex cation $[\text{Cd}_2(\text{L}^9)_2]^{4+}$	110
Table 3.10 Selected bond angles (°) for the complex cation $[\text{Cd}_2(\text{L}^9)_2]^{4+}$	110
Table 3.11 Selected bond lengths (Å) for the complex cation $[\text{Fe}_2(\text{L}^{10})_2]^{4+}$	113
Table 3.12 Selected bond angles (°) for the complex cation $[\text{Fe}_2(\text{L}^{10})_2]^{4+}$	114
Table 3.13 Selected bond lengths (Å) for the complex cation $[\text{Cd}_2(\text{L}^{11})(\text{L}^{11}\text{-H})]^{5+}$	118
Table 3.14 Selected bond angles (°) for the complex cation $[\text{Cd}_2(\text{L}^{11})(\text{L}^{11}\text{-H})]^{5+}$	118
Table 3.15 Selected bond lengths (Å) for the complex cation $[\text{Zn}_2(\text{L}^{13})_2]^{4+}$	122
Table 3.16 Selected bond angles (°) for the complex cation $[\text{Zn}_2(\text{L}^{13})_2]^{4+}$	122
Table 3.17 Selected bond lengths (Å) for the complex cation $[\text{Cd}_2(\text{L}^{14})_2]^{4+}$	124
Table 3.18 Selected bond angles (°) for the complex cation $[\text{Cd}_2(\text{L}^{14})_2]^{4+}$	125
Table 4.1 Selected bond lengths (Å) for the complex cation $[(\text{L}^{15})_2\text{Eu}_2(\text{H}_2\text{O})_2]^{4+}$	147
Table 4.2 Selected bond angles (°) for the complex cation $[(\text{L}^{15})_2\text{Eu}_2(\text{H}_2\text{O})_2]^{4+}$	147
Table 4.3 Selected bond lengths (Å) for the complex cation $[(\text{L}^{16})_2\text{La}_2(\text{H}_2\text{O})_2(\text{CF}_3\text{SO}_3)_2]^{2+}$	150
Table 4.4 Selected bond angles (°) for the complex cation $[(\text{L}^{16})_2\text{La}_2(\text{H}_2\text{O})_2(\text{CF}_3\text{SO}_3)_2]^{2+}$	151
Table 4.5 Selected bond lengths (Å) for the complex cation $[(\text{L}^{17})_2\text{Tb}_2]^{4+}$	153
Table 4.6 Selected bond angles (°) for the complex cation $[(\text{L}^{17})_2\text{Tb}_2]^{4+}$	154

List of abbreviations

α	Alpha
Al_2O_3	Aluminium oxide
Å	Angstroms
(aq)	Aqueous
Ar	Aromatic
Bz	Benzoyl
Bn	Benzyl
Br_2	Bromine
$\text{CHCl}_3/\text{CDCl}_3$	Chloroform/Deuterated
CD	Circular Dichroism
COSY	Correlation spectroscopy
J	Coupling constant
$^\circ\text{C}$	Degree Celsius
d.H ₂ O	Deionised water
δ	Delta (chemical shift)
d.e	Diastereomeric excess
DCM	Dichloromethane
DMSO/DMSO-d ₆	Dimethyl sulfoxide/ Deuterated
DMF	Dimethylformamide
d	Doublet
ESI-MS	Electrospray ionisation mass spectrometry
EtOH	Ethanol
Et ₂ O	Ether
(g)	Gas
g	Gram
Hz	Hertz
h	Hours
HCl	Hydrogen chloride
H ₂ O	Hydrogen sulfide
MgSO ₄	Magnesium sulfate
m/z	mass/charge
Mhz	Megahertz
<i>m</i> -CPBA	Meta-Chloroperoxybenzoic acid
MeOH	Methanol
<i>ml</i>	Mililitre
mmol	Milimoles
mol	Moles
M	Moles per litre
m	Multiplet
NMR	Nuclear magnetic resonance
ppm	Parts per million, δ (delta), chemical shift
Ph	Phenyl
Py	Pyridine
RT	Room temperature

SiO ₂	Silica
s	singlet
Na	Sodium
NaCl	Sodium chloride
Na ₂ HCO ₃	Sodium hydrogen carbonate
s.g	Specific gravity
THF	Tetrahydrofuran
Tz	Thiazole
TLC	Thin layer chromatography
TOF-LC	Time of flight liquid chromatography
t	Triplet

1. Introduction

1.1 *Supramolecular chemistry*

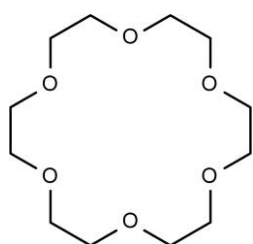
Supramolecular chemistry is a vast area of research; as such it is difficult to give a precise definition. However, Jean-Marie Lehn, seen as one of the founding fathers of supramolecular chemistry, referred to it as 'chemistry of molecular assemblies and of the intermolecular bond, more commonly quoted as 'chemistry beyond the molecule'.¹ This may seem simplistic but allows interpretation and adaptation to incorporate all possible architectures from the many disciplines (physical chemistry, inorganic chemistry, organic synthesis, computational chemistry and even biochemistry) which have contributed to this maturing research field.²

The key feature of supramolecular chemistry is the use of reversible intermolecular interactions for the generation of the final architecture. In comparison to classical molecular chemistry, which is focused on the making and breaking of strong molecular bonds (covalent bond) providing new molecules,³ supramolecular chemistry takes these preformed molecules and through intermolecular interactions provides a structure which is greater than the sum of its parts.⁴

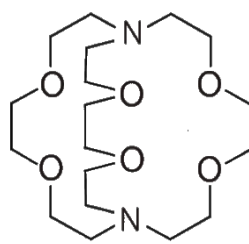
1.1.1 Foundations of supramolecular chemistry

The very beginning of supramolecular chemistry is hard to define exactly. It is generally accepted that the main developments were achieved in the 1960's,⁵ from this time research in this field has expanded exponentially. Early work focused on macrocyclic ligands for coordination of metal cations. The principles of these systems were researched by groups Curtis,⁶ Jäger,⁷ Busch⁸ and Pederson,⁹ providing the foundations for future development. Also worth a note here for their contributions to this emerging field are Cram and Lehn.

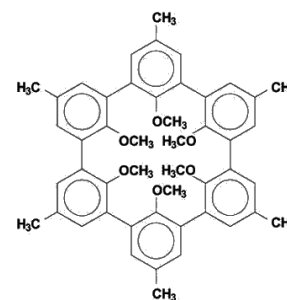
Pederson is known for creating crown ethers as well as Lehn who introduced the structurally similar cryptands.¹⁰ Cram further modified these systems to give ligands that were more pre-organised for cation binding becoming known as spherands¹¹ (figure 1.1). This initial research introduced principles of selective recognition of cations based on ion and shape as well as pre-organisation of ligands. Pederson, Lehn and Cram were recognised for their contributions to this field being awarded the Nobel Prize in 1987.



Pederson: 18-crown-6



Lehn; [2.2.2] cryptand¹⁰



Cram: Spherand¹¹

Figure 1.1 Early macrocyclic ligands in supramolecular chemistry

1.2 Supramolecular interactions

Reversible intermolecular interactions are implemented, as opposed to covalent bonds, in the assembly of components in supramolecular systems. Intermolecular interactions may be attractive as well as repulsive, which means for the most stable complex to form the components must possess a complementary arrangement of binding sites. There is an enormous range of forces which can potentially be employed by the supramolecular chemist. The main ones of note are electrostatic interactions (ion-ion, ion dipole and dipole-dipole), hydrogen bonding and π - π stacking interactions. However the interactions between the components do not occur in isolation so other factors may also influence the system, for example solvation.¹²

1.2.1 Ion-ion interactions

Ionic bonding is comparable in energy to covalent bonding. In basic terms the formation of an ionic bond results from the loss of an electron from a metal to a non-metal forming ions of opposite charge, leading to electrostatic attraction. A well-known example is NaCl, which is composed of an ionic lattice of Na^+ ions surrounded by Cl^- ions in the solid state (figure 1.2). This type of interaction is rarely seen in supramolecular chemistry.

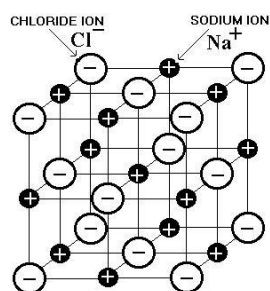


Figure 1.2 Ion-ion interactions¹³

1.2.2 Ion-dipole interactions

There are numerous examples in supramolecular chemistry of ion-dipole interactions. An ion-dipole force occurs when an ion interacts with a polar molecule. The complexes of crown ethers and alkali metal cations are a perfect example to illustrate this type of interaction (figure 1.3); here the oxygen lone pairs are attracted to the positive charge of the potassium ion.

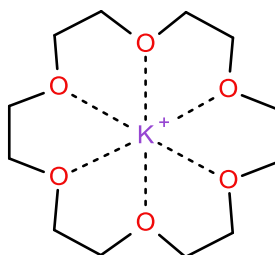


Figure 1.3 Example of ion-dipole interaction

1.2.3 Dipole-dipole interactions

Association of one dipole with another can be useful for bringing molecules into alignment. Organic carbonyl compounds are good examples that exhibit this type of interaction (figure 1.4).

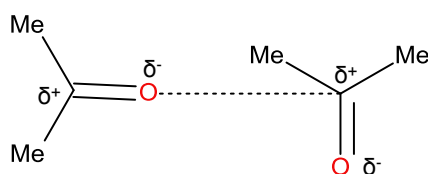


Figure 1.4 Dipole-dipole interactions in carbonyls

1.2.4 Hydrogen bonding

Hydrogen bonding is considered as a special example of dipole forces. This occurs when a hydrogen atom which is attached to an electronegative atom (for example nitrogen) is attracted to a dipole in an adjacent molecule or functional group (figure 1.5). This bonding is highly directional and relatively strong which is why it is of some significance in supramolecular chemistry. There are a wide variety of bond lengths, strengths and geometries for hydrogen bonds; they are significant for the formation of proteins, the double helix of DNA and much more besides.

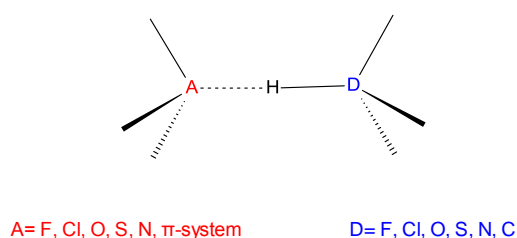


Figure 1.5 Example of hydrogen bonding

1.2.5 π - π stacking interactions

These interactions occur within systems containing aromatic rings; it is believed that the interaction is a weak electrostatic interaction. This results when the negative charged π -electron cloud of one system is attracted to the positive σ -framework of an adjacent molecule. More than one orientation of the rings

involved is possible giving rise to face-to-face or edge-to-face interactions (figure 1.6).¹⁴

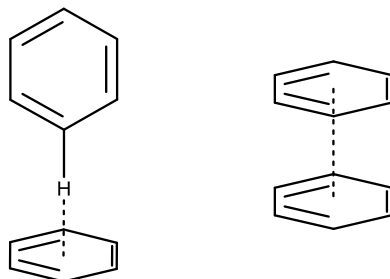


Figure 1.6 Possible orientations for π - π stacking interactions

1.3 Host-guest chemistry

As mentioned supramolecular chemistry is the binding of components using intermolecular forces, the next step is to identify what is partaking in the binding. Obviously for binding to occur at least two components are required, for host-guest chemistry one molecule binds another forming a complex or supramolecule. Generally the host is identified as the larger (higher molecular weight) component of the system.⁴ Cram identified the components of a complex as “The host component is the molecular entity whose binding sites converge in the complex... the guest component is any molecule whose binding sites diverge in the complex”.¹⁵

A number of categories of host compounds have been identified based on the association between host and guest within the supramolecule. Two main categories that have been acknowledged are cavitands and clathrands (figure 1.7). Cavitands are hosts which already possess intermolecular cavities, with the capability of encapsulating the guest. As the cavity is already present within the host these complexes exist both in solution and in the solid state. Clathrands produce extra-molecular cavities which form between two or more of the host molecules. As these cavities are not an intrinsic molecular property of the host component these cavities only exist in the solid or crystalline state.⁵

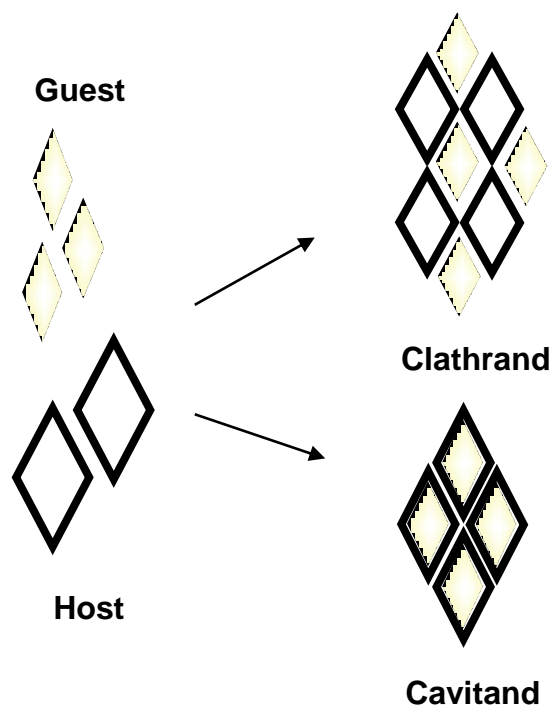


Figure 1.7 Illustration of the co-ordination difference between cavitands and clathrands

The previous examples of host guest complexes illustrate the two extremes of the possible supramolecule. There exist a number of intermediate types for host guest coordination, based on the spatial arrangements of the guest and host when forming the complex, resulting in further subdivision of the two broad categories.

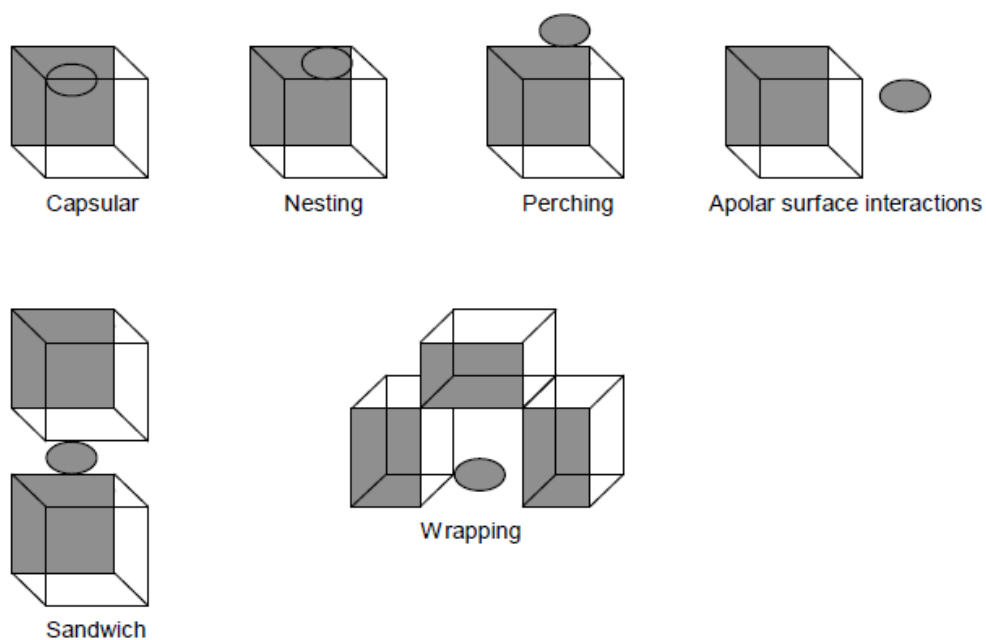


Figure 1.8 Spatial arrangements between host and guest⁵

At first glance this area of supramolecular chemistry may seem simplistic; host-guest chemistry is, however, extremely significant. The idea of the host-guest complex is reminiscent of the enzyme-substrate complex seen in biology. The principal ideas are effectively the same in each instance, the host (enzyme) must possess certain binding domains which are complimentary to those of the desired guest (substrate). This is more commonly known as the “lock and key principle” introduced by Emil Fischer in 1894.¹⁶ In this analogy, the lock (enzyme) and key (substrate) must be correctly sized to fit together to allow the lock to be opened. Incorrect geometric shape or size of a key (substrate) does not fit into the lock (enzyme); this forms the basis of molecular recognition. Therefore the shape and size of the host cavity must be complementary for a particular guest if the coordination is to be selective and specific. This plays a critical part in the formation of supramolecules leading to increased likelihood of coordination to the guest and increased stability of the complex.

1.3.1 Crown ethers

The serendipitous discovery of the first crown ether was due to an impure starting material being used in the synthesis of bis[2(o-hydroxyphenoxy)ethyl]ether (figure 1.9) by Pederson working for DuPont in New Jersey, USA. He was initially interested in making multidentate ligands for coordination of copper and vanadium. Pederson isolated a small quantity of white crystalline by-product (0.4 % yield) while attempting to purify the desired pentadentate ligand.¹⁷

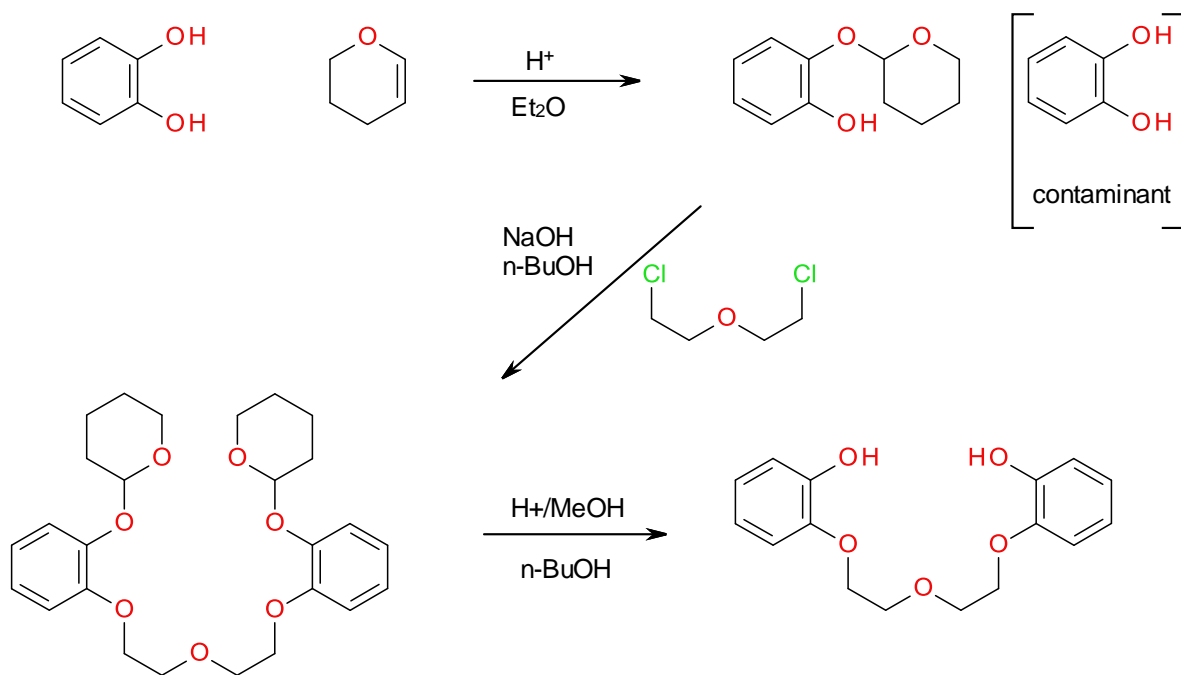


Figure 1.9 Intended synthesis for bis[2(o-hydroxy-phenoxy)ethyl]ether⁴

This unexpected by-product, a crystalline substance, was of some interest to Pederson due to the properties observed for the compound. It was sparingly soluble in methanol but was solubilised upon addition of sodium hydroxide. On further investigation it was actually identified that alkali metals solubilised the compound, thus the solubilisation was due to the sodium cation not the addition of base. The UV analysis was of a phenolic compound, with the spectrum being altered upon the addition of sodium.¹⁸

The elemental analysis was consistent with the structure being benzo-9-crown-3, a possible product of the reaction. However, the structure was finally identified after molecular weight determination; with the molecular weight being double that of benzo-9-crown-3 indicating the compound was actually dibenzo-18-crown-6 (figure 1.10). As the chemical names of these compounds are enormous, a more trivial nomenclature was implemented.¹⁷ Eventually these compounds became known as crown ethers, supposedly due to the crown-like conformation of the complexes. It was observed by a space-filling model that the sodium cations sit in the cavity of the macrocyclic polyether by way of electrostatic ion-dipole interactions with the oxygen atoms.

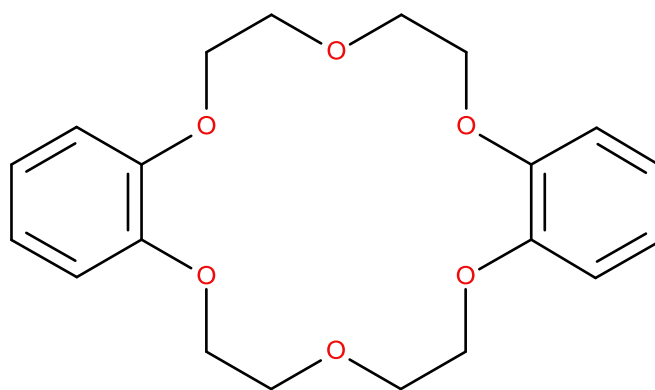


Figure 1.10 Dibenzo [18]crown-6 (or 2,3,11,12-dibenzo-1,4,7,10,13,16-hexaoxacyclooctadeca-2,11-diene)

Before this there were no known examples of synthetic compounds capable of forming complexes with alkali metal cations. With this realisation of the significance of such a compound no time was wasted in producing a whole family of macrocyclic polyethers (figure 1.11), followed by in-depth determination of their interactions with inorganic cations.^{17, 19}

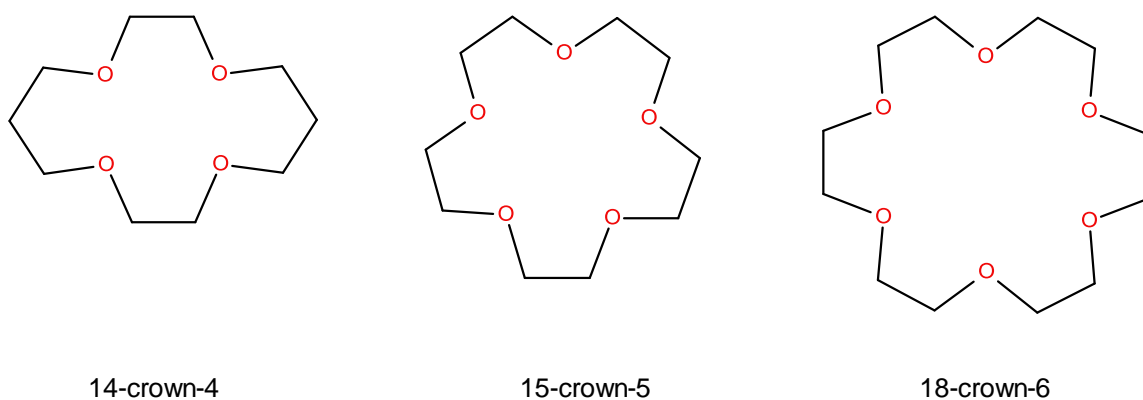


Figure 1.11 Examples of crown ethers

Early research undertaken by Frensdorff²⁰ provided information relating to the strength of complexation in solution dependent on the polyether structure, cation size and solvent. The stability constants of several cyclic polyethers with different cations in methanol and aqueous solution were determined using potentiometry. Frensdorff determined that the stability constants of 1:1 complexes were significantly higher using methanol as solvent, due to the

cation being more highly solvated in water. The main finding was that selectivity towards different cations depended on the polyether ring size, with the optimum ring size being the one that the cation just fits into the cavity. This relationship between cation size and ring size is clear from the results, for example, potassium ions (K^+) form a more stable complex with 18-crown-6 than sodium (table 1.1). However, sodium (Na^+), being a smaller ion, binds more strongly with the smaller 15-crown-5.

This is further supported by structural data as the cavity size and cation diameter are most complementary between potassium and 18-crown-6 (table 1.1). The 1:1 complexation is strongest when the host and guest are complementary; the cation (guest) when matched with the complementary crown ether (host) is able to fully sit in the cavity within the plane of the oxygen atoms where the charge density is highest. If the crown is too large there are insufficient interactions with all the available oxygen atoms. This relationship between cationic radius, cavity size and stability of the complex is a concept known as *optimal spatial fit*.

Cation	Ionic Diameter (Å)	Polyether Ring	Cavity Size (Å)
Li^+	1.36	14-crown-4	1.20-1.50
Na^+	1.94	15-crown-5	1.70-2.20
K^+	2.66	18-crown-6	2.60-3.20
Rb^+	2.94	21-crown-7	3.40-4.30
Cs^+	3.38		
Ag^+	2.52		

Table 1.1 Cation ionic diameters with a selection of crown ether cavity sizes

It should be noted that stoichiometries of cation to crown ether, other than 1:1, are also possible. A complex may still form even if the sizes are not complementary between the two components, this results in a “sandwich complex” where two “smaller” crowns coordinate a “larger” cation.²¹

Crown ethers, which have been shown to coordinate s-block cations, consist of a cyclic array of ether oxygen atoms linked by an organic spacer (commonly –CH₂-CH₂-), mono-dentate ether molecules, for example diethyl ether, are very poor with regards to metal ion coordination. This leads to the question as to why this isn't the case for crown ethers and even podands such as pentaethyleneglycol (acyclic ether). This ability to form a stable coordination complex is due to what is known as the macrocyclic effect and chelate effect, which are well established principles in coordination chemistry.²²

Following on from the work of Pederson, Lehn moved crown ethers into 3-dimensions by introducing macro-bicyclic structures: the cryptands.²³ This resulted in the guest interacting to a greater degree with the host, giving more stable complexes with group one and two metal cations than analogous crown ethers.²⁴ The most common cryptand is the [222] cryptand (figure 1.1). Upon inspection of the crystal structures of the complexes produced by crown ethers and cryptands with s-block metal ions, Cram noticed that the binding sites within these macrocycles were not completely convergent. Thus for complexation to occur the ligands require some degree of rearrangement. This realisation prompted the idea to produce a rigid host which contains fixed binding sites in an octahedral arrangement around an enforced cavity, leading to the synthesis of the more pre-organised macrocycles the spherands.²⁵ These macrocycles showed enhanced binding constants in comparison to the aforementioned macrocycles due to the structure being more pre-organised towards the desired guest.²⁶

Since this pioneering research these macrocyclic ligands are now ubiquitous in supramolecular chemistry, with research groups introducing new functionalities and properties into the simple crown ether motif.²⁷ The simplest variations are those which have substituted the heteroatom, using such atoms as nitrogen,²⁸ sulfur, or arsenic²⁹ in place of the oxygen atoms, making up the family collectively known as *corands*. More drastic alterations have given other classes such as Lariat ethers,³⁰ which are essentially crown ethers which possess a side arm with additional donor atoms for coordination to the guest giving desirable properties of both podands and crown ethers. These structures

have found a number of potential uses, such as building blocks in other supramolecular systems, for example, within rotaxanes and catenanes.

1.4 Self-assembly

The previous section focused on macrocycles, pre-organisation and molecular recognition: the origins of supramolecular chemistry. Another concept that has emerged within supramolecular chemistry is self-assembly. The definition of self-assembly is the spontaneous and reversible generation of well-defined supramolecular architectures from their component parts under a given set of conditions to provide the most thermodynamically stable assembly. The components, or tectons, contain intrinsic information which is used to direct the assembly.³

A wide variety of biological systems and structures rely on self-assembly processes for their construction. Self-assembly is ubiquitous in nature; formation of the DNA double helix being the most common example. Natural systems exhibit efficient control over complex molecular assemblies using a number of relatively weak intermolecular interactions. It is from here that the supramolecular chemist gains inspiration to replicate such principles within synthetic systems, with the desire to produce assemblies with the same degree of selectivity, specificity and precision as those found in nature.³¹

This area of supramolecular chemistry may allow access to molecular architectures which may be inaccessible using classical synthesis methods or if they are accessible the synthesis would be greatly time-consuming and non-trivial. The molecular architectures result when simple, appropriately designed sub-units combine under certain conditions, these complex assemblies may have a number of potential uses.² A simple example is the production of catenanes; the first method of synthesis, “the statistical approach”, gave very small yields (< 1 %). The use of self-assembly techniques was subsequently implemented in their construction, providing improved yields and more reliable synthesis methods.³² Within nanotechnology it is desired that one day similar

principles will be applied to electronic devices, the bottom-up or engineering up approach, to provide access to the ever reducing size of electronic devices.³³

1.4.1 Rotaxanes

These supramolecules acquire their name from Latin: *rota* (wheel) and *axis* (axle), as Rotaxanes consist of a long relatively linear component which is threaded through a macrocyclic ring, giving a similar result to threading a piece of cotton through the eye of a needle. A true rotaxane cannot be separated into its constituent parts without the breaking of a chemical bond, thus the reason why the linear chain is frequently terminated by bulky functional groups which are unable to fit through the macrocyclic component. The group of supramolecules which does not possess these barriers to stop the separation of the components, allowing unthreading of the structure, are known as pseudorotaxanes (figure 1.12).⁵

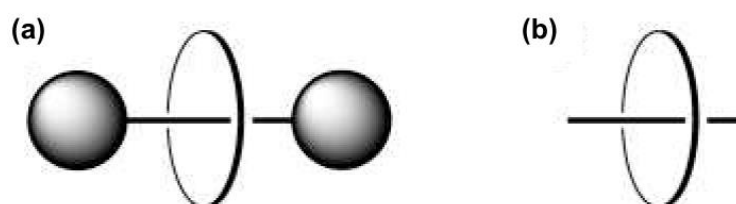


Figure 1.12 Representation of a) [2]-rotaxane b) [2]-pseudorotaxane³⁴

There are a number of methods that have been employed for the assembly of these structures. The first method utilised in their initial synthesis was “the statistical approach”, this relies on there being a small chance that macrocyclisation may occur while a linear precursor is threaded through a macrocyclic component.³⁵ The first example of a rotaxane using the “statistical approach” was reported by Harrison *et al.*³⁶ In this it was suggested that the structure be called a hooplane, the method was to attach a cyclic ketone with a carboxylic acid functionality to Merrifield’s peptide resin.³⁷ A column of this resin, bound to the macrocycle, was washed with decane-1, 10-diol and triphenylmethyl chloride a number of times (70 in total), after which the reagents and other materials were washed from the column leaving only the

reaction product to be hydrolysed from the resin support. This method was unreliable and initial reactions gave yields between 1-6 % (figure 1.13). Due to low yields of this approach other methods of synthesis were investigated.³⁸

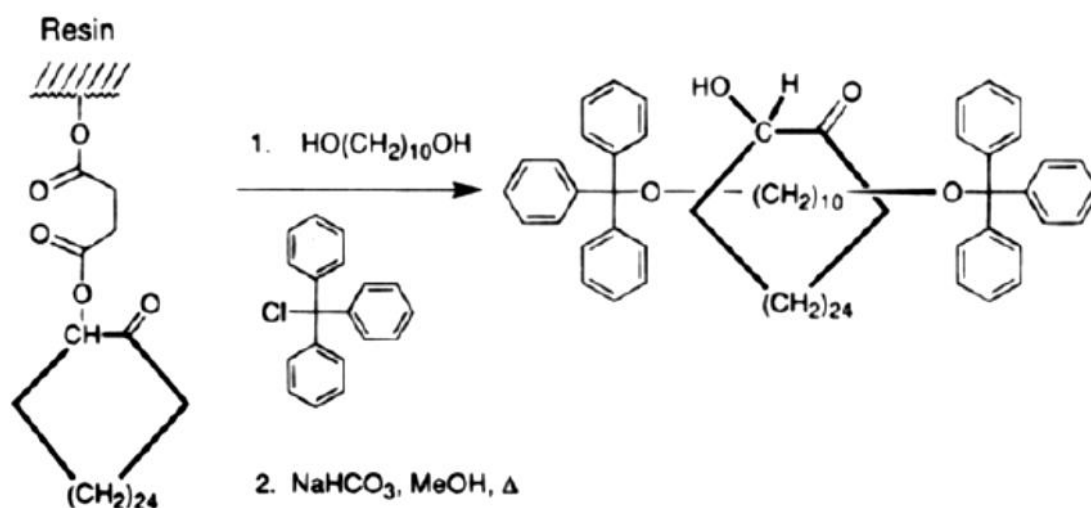


Figure 1.13 Method of synthesis for the first [2]-rotaxane³²

The directed synthesis, self-assembly, of rotaxanes allowed more control over the process. A number of methods were produced for the successful synthesis of these interlocked structures. Three main methods were identified, threading, clipping³⁹ and slipping. For threading, a molecule is threaded through a preformed ring, this is achieved by the two tectons containing complementary binding sites to assemble the sub-units, which is followed by stoppering of one or both ends of the linear section. Pseudorotaxanes produced by self-assembly followed by termination at one or both ends of the linear component by bulky groups gives the rotaxane, if however the linear component reacts intramolecularly (ring closure) then a catenane is produced, another family of supramolecules. Clipping is achieved by attaching a macrocycle onto a preformed dumbbell, and slipping is achieved by slipping the ring over the ends of a preformed dumbbell (figure 1.14).²

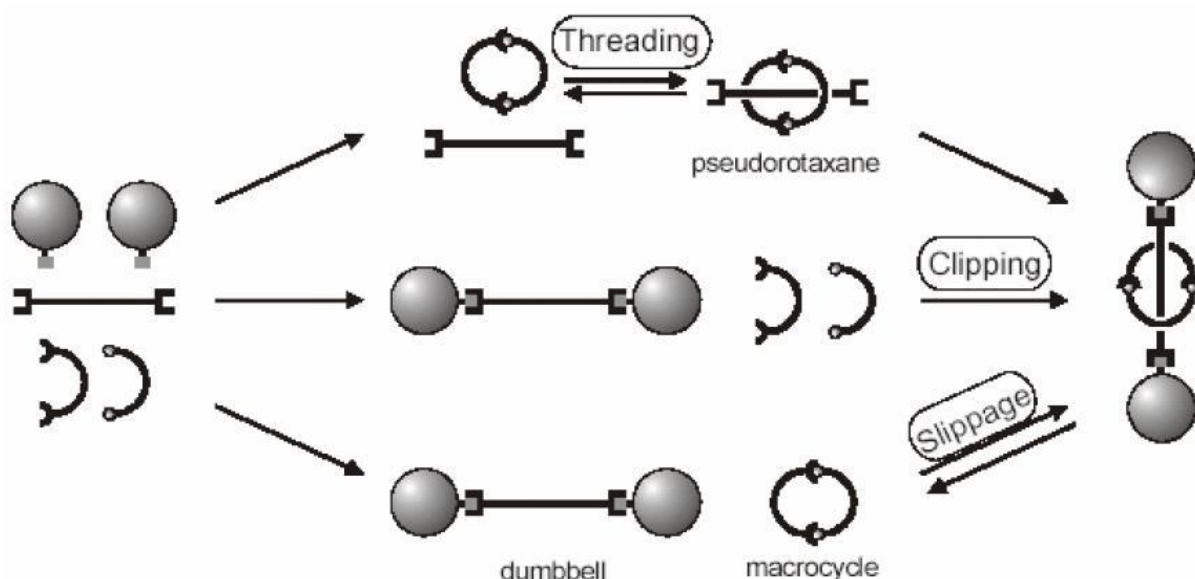


Figure 1.14 Illustration showing methods for rotaxane synthesis⁴⁰

Slipping is achieved as the bulky end groups may be able to slip through the axle as a result of elevated temperature. Harrison⁴¹ first demonstrated this by heating a mixture of macrocycles with 1,10-bis(triphenylmethoxy) decane to 120°C which resulted in the formation of a small concentration of an interlocked [2]-rotaxane; this [2]-rotaxane structure was shown to decompose on heating. It was demonstrated here that the size of the macrocycle is important for slipping as if it is too small slipping will not occur and if it is too large only transient compounds are formed. This method has been used by other research groups to produce rotaxanes.⁴²

It is possible to produce [3]-rotaxanes which contain one axle and two macrocycles within the final structure.⁴³ Further to this rotaxanes with interesting functions are known such as molecular shuttles, where the axle contains two 'stations' for the macrocycle and with manipulation of the system the macrocycle favours one of the 'stations'.⁴⁴ Rotaxane assembly may also be directed by means of coordination with metal centres.⁴⁵

1.5 Metallosupramolecular chemistry

The use of transition metal centres for organising molecular building blocks into complex architectures is an area of study frequently seen in supramolecular

chemistry. There are a number of reasons why metal centres are employed. It is well known that metal ions are able to be coordinated by donor atoms or groups of atoms, through a form of ion-dipole interaction. Additionally these dative bonds are directional, thermodynamically strong, are available in a range of kinetic stabilities and have a variety of geometries depending on the metal centre, which add significantly to directing the self-assembly process. The formation of these coordination complexes can lead to architectures which may be one-, two- or three- dimensional.⁴ As this strategy has been vastly employed in self-assembly it has become known as metallosupramolecular chemistry. This term was first introduced in 1994 by Constable, describing the metal centres as a type of 'glue' holding the structure together.⁴⁶

There are numerous examples of supramolecular architectures which have taken advantage of metal ion centres for their self-assembly. For example grids, racks ladders, various polygons, rotaxanes and helicates to name a few (figure 1.15). Through careful selection of metal ion and ligand the supramolecular chemist is able to impart some control over the outcome of the assembly. The self-assembly processes are directed by the information encoded within the covalent framework, resulting in organisation of the components via interactions and recognition events. This concept of components containing molecular information which directs the assembly is analogous to an algorithm which controls a computer programme. The idea that information can be stored at the molecular level is a concept introduced by Lehn.³

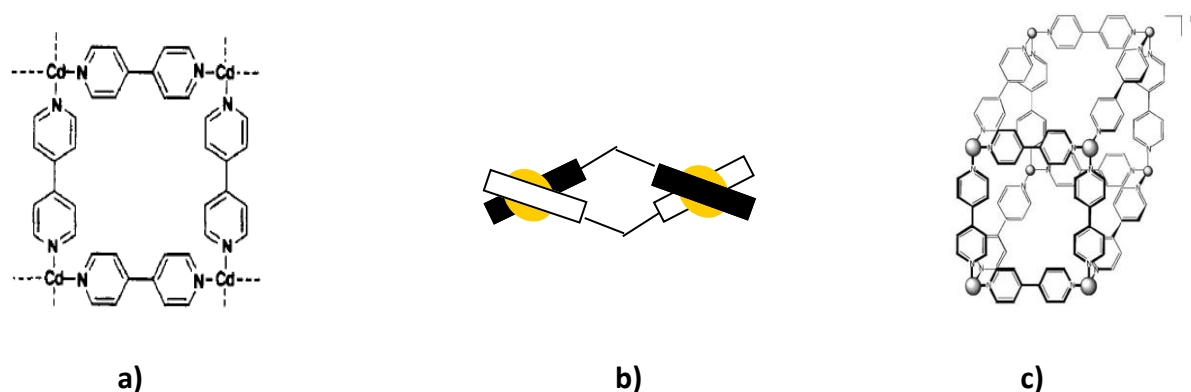


Figure 1.15 Examples of metal directed assemblies a) molecular square⁴⁷, b) Helicate and c) a supramolecular cube⁴⁸

1.5.1 Grids

Self-assembly of metal directed arrays are of particular interest such as racks, ladders and grids (figure 1.16), which have extensively been researched, particularly the latter due to potential use as molecular electronic devices.⁴⁹ The grid architecture, denoted as $[n \times m]\text{grid}$ or $[n \times m]\text{G}$, consists of square or rectangular tiles with metal ions as the corners. The ligands used within the assembly may be the same or different depending on the desired architecture. For construction of a square grid the n and m ligands must be equivalent, for the rectangular arrangement n and m must be different. The metal ions may be tetrahedral or octahedral; however the ligands must possess complementary binding domains for the assembly to be directed to the grid array.

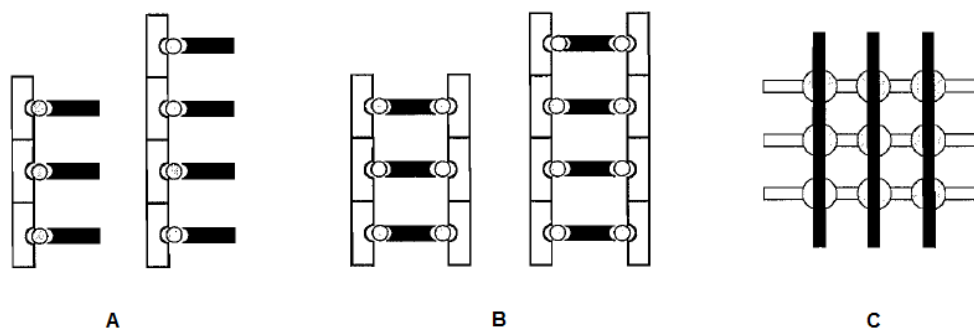


Figure 1.16 Schematic representations of A) racks, B) ladders and c) a grid⁵⁰

For the construction of a square grid architecture utilising tetrahedral metal ions (e.g. Ag^+ , Cu^+) the n -topic linear rigid ligands would require bidentate binding sites for coordination to the tetrahedral ions. Within these structures the two ligand sets may be on opposite sides of the metal ions, one above and one below the plane of the metal. This can however become more complex by the ligands twisting and binding over and under the metal ions at opposite ends introducing the possibility of having chiral grids.⁴

Grids have been extensively researched by Lehn *et al.* This is primarily due to the interesting reversible switching processes, optical, magnetic and redox, in response to changes from external parameters.^{51, 52}

One of the early reported [2x2] grids reported by Lehn *et al.*,⁵³ was assembled using ligands containing pyridine and pyrimidine units to provide the donor atoms for coordination. Three ligands were used in this research with variation of substituents present on the central pyrimidine ring and the 5-position of the terminal pyridine rings ($R = H$ or Me). The variation within the ligands was incorporated to allow possible further functionalisation to provide more complex architectures. Upon mixing equimolar quantities of cobalt acetate tetrahydrate with one of the ligands in methanol and heating at reflux temperature the [2x2]G tetracobalt(II) complex is formed in high yields. Elemental analysis and mass spectroscopy confirmed the formation of the desired structures. Single crystals were obtained after slow diffusion of methanol into a saturated solution of the complex in acetonitrile, allowing structural determination by X-ray crystallography (figure 1.17). The complex was shown to consist of four ligands and four cobalt metal cations in a [2x2]G array, with the metal centres displaying a distorted octahedral coordination to the perpendicularly orientated ligand fragments.

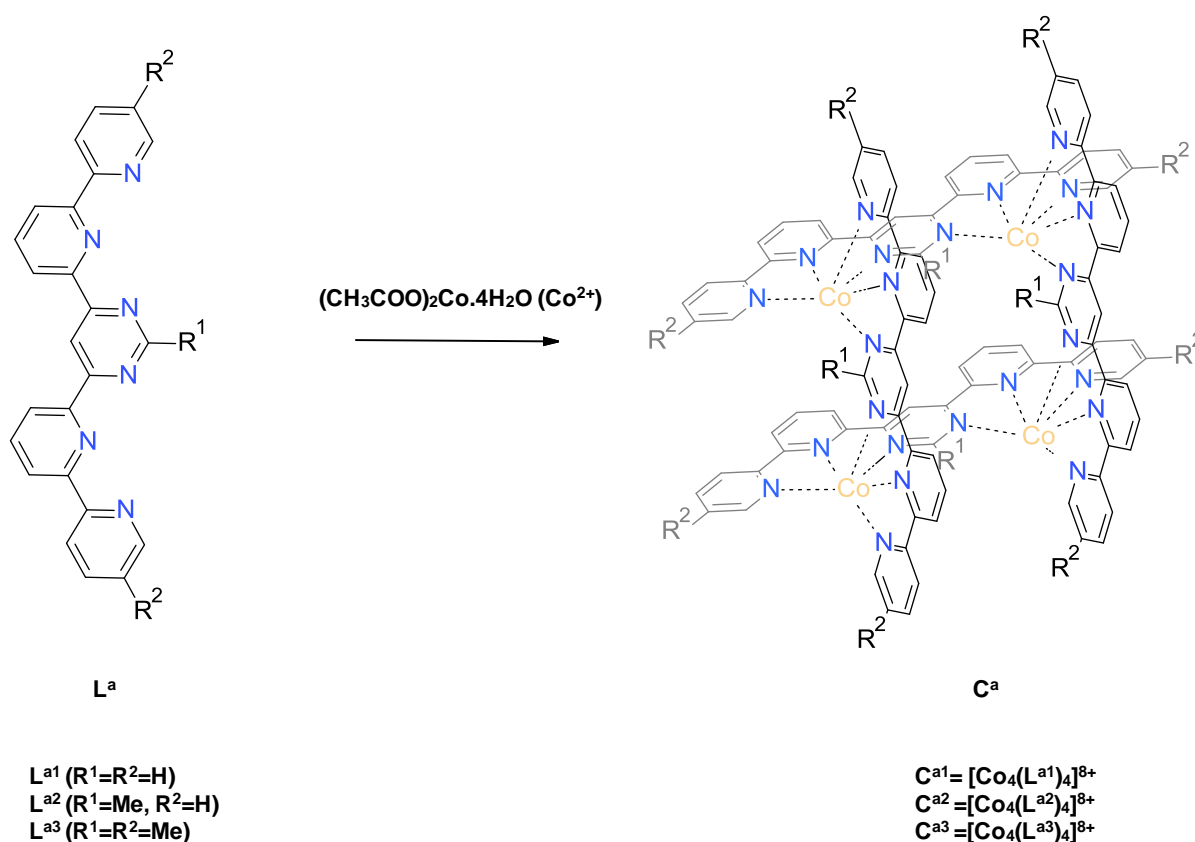


Figure 1.17 Self-assembly of [2x2] grid architecture

1.5.2 Ladders

Ladders are similar to grids, in that the self-assembly occurs due to the interplay between the polydentate ligand and coordination to metal ions. Ladders are described by using [2.n]L nomenclature, where 2 signifies the two sides of the ladder to which the “rungs” are attached and n refers to the number of “rung” ligands present.⁵⁴ In these structures, unlike grids, a second ligand is always required, so in addition to a rigid rod like ligand to form the backbone of the structure an additional ligand for the “rungs” of the ladder is necessary. Such metal arrays have not been as extensively investigated as the related grid architectures.

Common ligands which are instrumental in these self-assembled metal arrays are those containing pyridine and pyrimidine aromatic rings.⁵⁵ An example of a [2.2] and [2.3] ladder has been reported by Lehn *et al.*⁵⁶ which is produced upon mixing the preorganised ligands, L^b and L^c , with Cu(I) metal ions in the correct stoichiometries (figure 1.18). This is an example of a mixed-ligand self-assembly, which requires some form of recognition between the components for the formation of the discrete complex to occur. The structure of complexes of L^b and L^c were unambiguously assigned based on 1H and ^{13}C NMR, with the 1H NMR spectrum being extremely simple indicating a single highly symmetrical species. Other analysis of the complexes was conducted (COSY, ROESY and ESMS) with these results also corresponding to the formation of the ladder type complexes (C^{b1c} and C^{b2c}

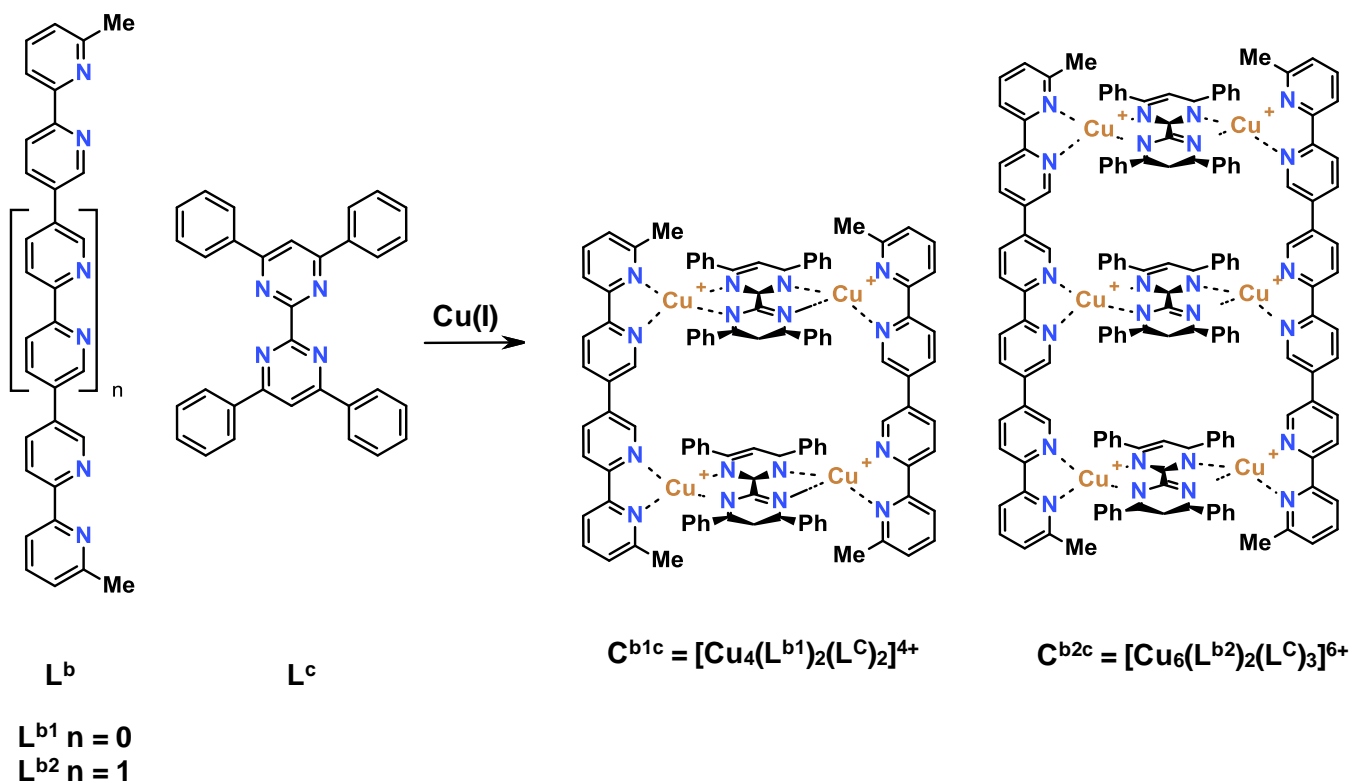


Figure 1.18 Self-assembly of two- and three-“rung” ladders

1.5.3 Racks

Racks are closely related to grids and ladders. Racks are designated by $[n]$ Rack, where n represents the nuclearity of the species. These arrays consist of a single linear rigid poly-topic ligand and several monotopic ligands which upon coordination to metal ion linkers results in the monotopic ligand pointing perpendicularly away from the poly-topic ligand backbone. For this to be achieved the components must be complementary, therefore the ligands and metal centre must be appropriately selected. Thus if the metal ion selected is tetrahedral then binding domains of the ligand must satisfy this geometry, to achieve this each ligand requires bidentate donor moieties. These architectures can be assembled using octahedral or tetrahedral metal centres.⁵⁴

Lehn *et al.* have produced a number of different racks by using these simple principles for their self-assembly. One such example produced upon reaction of $Cu(I)$ with oligobipyridine ligand L^d and ligand L^e (figure 1.19) results in the formation of a rigid rack, with a slight rotaxane character due to the use of a

macrocycle as one of the ligands. The structure of this rack has been determined through analysis of the crystal structure.⁵⁷

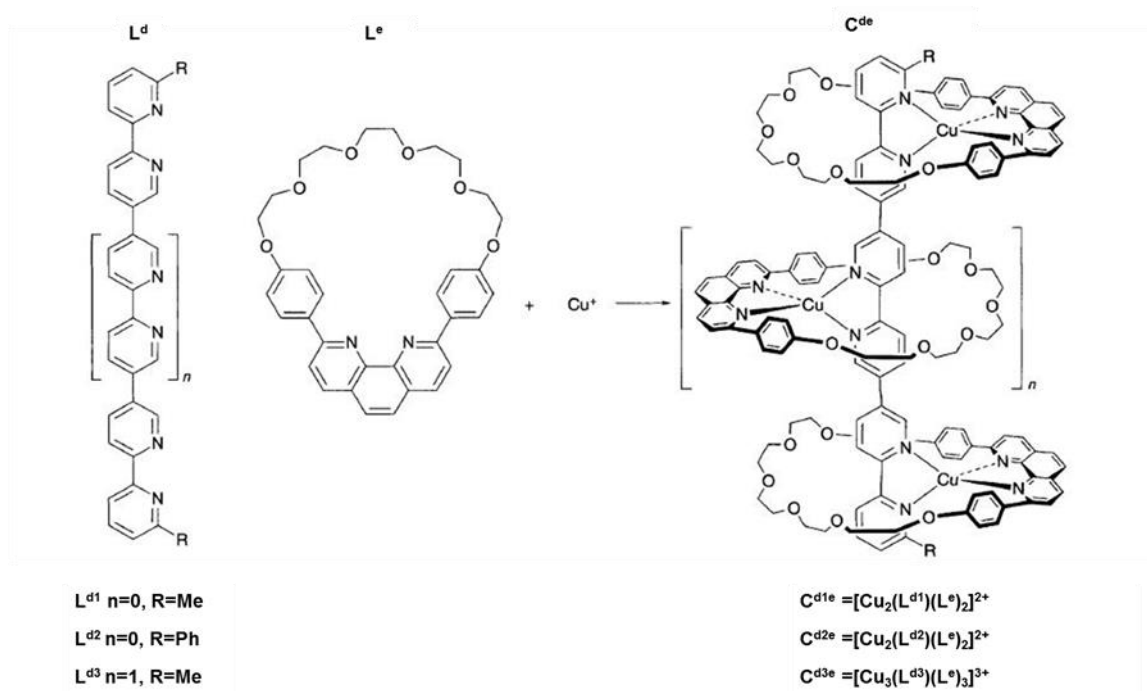


Figure 1.19 Self-assembly of a rack with rotaxane character⁵⁷

1.5.4 Cages

The metal-directed self-assembled cage architectures fall into the category of molecular containers or capsules. Hydrogen bonded self-assembled capsules are known, which are also able to encapsulate guest species.⁴ A remarkable amount of progress in the construction of three dimensional structures has, however, been made since the incorporation of metal centres. There are two methods available for the construction of metallocapsules; these methods depend on the type of ligand(s) employed. The ligand selected may be one-dimensional or two-dimensional. Ligands which are one-dimensional are only able to bridge two metal centres. These ligands are equivalent to the straight edges of the structure. This method of forming self-assembled molecular capsules is known as molecular scaffolding (also known as edge-directed self-assembly).⁵⁸ One such example was reported by Thomas *et al.*, in which a supramolecular cube was produced from 8 octahedral metal ions, the corners, and 12 ligands, the edges, via self-assembly (diagram c, figure 1.15).⁴⁸

Additionally two-dimensional ligands may be employed in the production of molecular cages. In this case the ligand is able to bridge more than two metal ions and the ligands make up the faces of the structure. This approach is known as molecular panelling or face-directed assembly.⁵⁹ An excellent example by Fujita and co-workers demonstrates the assembly of an octahedral 3D structure.⁶⁰ The idea to use 90° coordination angles of transition metals led to the production of a *cis*-protected square-planar metal (\mathbf{C}^* , figure 1.20). The prepared ethylenediamine-protected Pd(II) complex was shown to form simple 2D square assemblies with 4,4'-bipyridine, a one-dimensional ligand. This structure was produced upon mixing equimolar amounts of *cis*-protected Pd(II) and 4,4'-bipyridine in aqueous solution, addition of ethanol to the reaction solution led to precipitation of the pure product. The tetranuclear square compound results due to the 180° divergence of the ligand and the nature of the *cis*-protected metal giving a 90° coordination angle. These architectures are now known as molecular squares (diagram a, figure 1.15).⁶¹

The use of two-dimensional ligands with the square-planar protected metal ions afforded 3D assemblies. Fujita and co-workers⁴⁷ have produced some fascinating self-assembled three-dimensional molecular cages, which show potential as synthetic receptors. When ligand \mathbf{L}^f is exposed to \mathbf{C}^* , a symmetrical cage complex containing four ligands and six metal ions forms (figure 1.20). The cage has a large spherical central cavity with a diameter of ca. 11 Å, which is able to accommodate four molecules of adamantane carboxylate. This clathrate complex has been fully characterized by X-ray crystallography.⁶² Further investigations of these cage complexes have dealt with such aspects as selective recognition of the guest species, as well as variation of the *cis*-protected metal employed within the assembly. A Pt(II) containing complex was shown to be more stable upon exposure to harsh conditions, changes in pH and nucleophile addition, in comparison to a Pd(II) complex.⁶³ The numerous examples which employ 2-dimensional organic components as molecular panelling illustrate that this is an efficient method in constructing large 3D architectures.

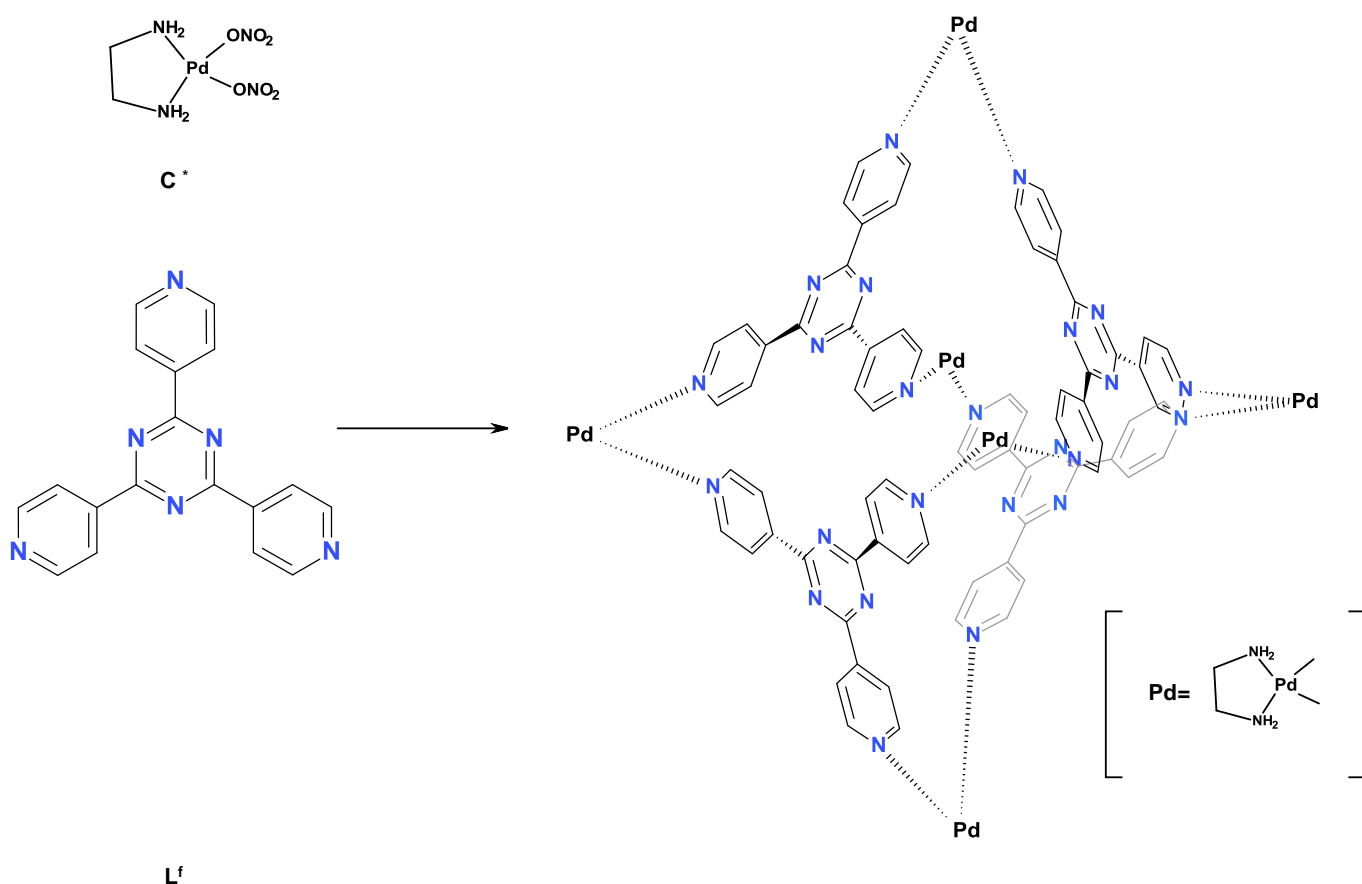


Figure 1.20 Three-dimensional supramolecular cage

Ward *et al.*⁶⁴⁻⁶⁷ have also contributed a considerable quantity to the research of supramolecular cage complexes. This research focuses on multinucleating ligands all of which are based on pyrazolyl-pyridine chelating units linked to a central head-group. Initially the desire to extend the chemistry of the tris(pyrazolyl)borate ligand led to the incorporation of various substituents at the C3 position of the pyrazolyl rings.⁶⁸ One such example was a hexadentate podand ligand hydrotris[3-(2-pyridyl)pyrazol-1-yl]borate. This derivative of tris(pyrazolyl)borate incorporates 2-pyridyl substituents at the C3 positions of the pyrazolyl rings giving a ligand which possesses three bidentate arms (Tp^{py}) (figure 1.21). This was designed to encapsulate large metal ions, in many cases this is how the ligand behaves. Upon exposure to lanthanide metal ions mononuclear complexes result and the stoichiometries may be 1:1 or 1:2 (metal: ligand).⁶⁹

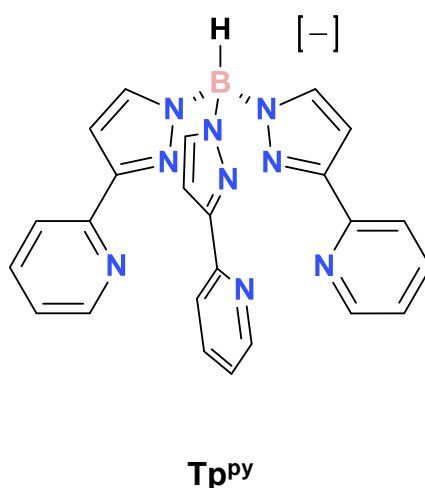


Figure 1.21 Ligand Tp^{py}

On reaction of the hexadentate ligand with Co(II) a mononuclear complex is formed, in contrast reaction with Mn(II) or Zn(II) forms tetrahedral clusters.⁷⁰ Reaction with Co(II) salts results in the formation of a 1:1 metal:ligand complex [Co(Tp^{py})] [PF₆], in which the Co(II) ion is coordinated in a trigonal prismatic geometry which is imposed by the steric constraints of the ligand strand, to give a relatively undistorted ligand. Reaction of Tp^{py} with Mn(II) or Zn(II) salts and subsequent elemental analyses suggested a 1 : 1 metal: ligand ratio, however, the electrospray mass spectrum of each complex contained a weak peak corresponding to the presence of a tetranuclear species. The crystal structure for each complex confirmed the formation of a tetranuclear complex cation [M₄(Tp^{py})₄] [PF₆]₄ (M= Mn or Zn). The two complex cations display very similar structures, each ligand is spread out so each of the bidentate arms coordinates a different metal ion. In order for this to happen the tris(pyrazolyl)borate core adopts an inverted geometry such that the apical hydrogen is directed inwards. Each metal ion displays a pseudo-octahedral coordination geometry from three bidentate pyrazolyl-pyridine groups from three different ligands. It was realised that this was the only way in which an octahedral geometry could be produced, since it would not be possible for the three arms of one ligand to provide an octahedral donor set to encapsulate one metal ion.

Following on from this initial research into the coordination behaviour of poly(pyrazolyl)borate ligands it was identified that extension of this class of

bridging ligands through substitution of the spacer group would be valuable. Consequently aromatic hydrocarbon spacers provided a suitable alternative as a bridging unit to separate the two binding sites (figure 1.22).^{65-67, 71}

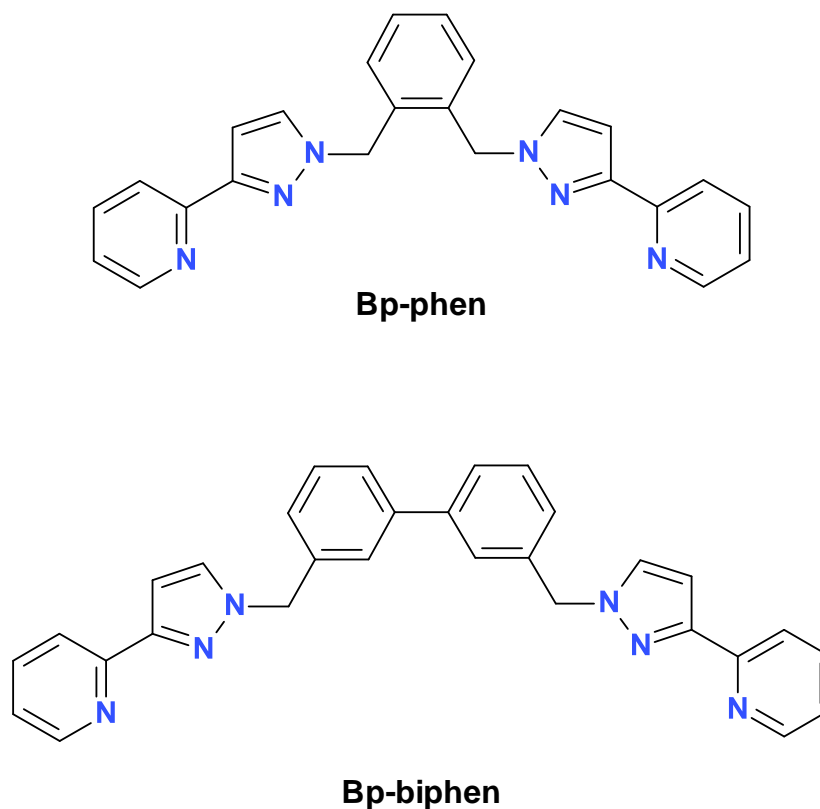


Figure 1.22 Examples of aromatic hydrocarbon spacer ligands

1.6 Helicates

Metallosupramolecular chemistry has provided access to architectures of higher complexity through self-assembly. There has been substantial contribution from numerous research groups to this area of chemistry, presenting a wide variety of eye catching and innovative architectures. Inspiration for such systems can be ascribed to nature. With the precision and accuracy of self-assembly and self-organisation observed in biological systems, it is no surprise chemists wish to mimic these processes to better understand them as well as to master non-covalent interactions within synthetic systems. The spontaneous association of complementary base pairs leading to the formation of the DNA double helix has been an area of intense interest. It has been shown that the entwining of the two strands for the formation of the

double helix occurs in two stages. Initially there is nucleation; the two strands come together. This association is thermodynamically unfavourable due to the loss in entropy. However, subsequent hydrogen bonding between every additional base pair leading to the complete double helix more than compensates for this initial loss.⁵ This is just one of the many remarkable examples of self-assembly observed in a biological system.

An example of an inorganic helix was reported by Lehn in 1987, with the introduction of the term 'helicate' to describe the polymetallic helical double-stranded complex.⁷² The ligand strands used in the formation of a helicate are known as helicands, reaction of a helicand with an appropriate metal centre resulting in the formation of a complex gives a "helicate".⁴ The formation of a helicate requires one or more organic strands, containing multiple binding sites, which are able to wrap around two or more metal centres defining a helical axis. A coiled spring is a good example of a helix, as helices can run in either right or left direction a special property of a helix is chirality.

The successful assembly of a helicate from its components is dependent on the design of the ligands and metal ions selected, similar to the self-assembly of the metal-directed arrays seen previously. Helicates have similarities to the self-assembly of ladders in that they are assembled from linear molecular threads which coordinate a number of metal centres, however, helicates require more flexible ligands to allow twisting around the metal ions to form a helical structure. These structures are interesting as achiral ligands may be used for the assembly and a chiral architecture may result.

1.6.1 Nomenclature

To communicate clearly the components of a metallosupramolecular helicate some form of unambiguous naming of the structure is required. As new structures being produced display better control over the self-assembly and ever more interesting features this nomenclature can become complicated. Initially a few aspects can easily be determined for the naming process: i) the number of ligands ii) the number of metal centres. Following this a simple helicate can be identified from the number of ligands and the number of metal

ions. For example a helicate containing two ligands is a double helicate, three ligands a triple helicate, with each additional ligand adding to this naming. The number of metal ions is expressed by dinuclear, trinuclear, tetranuclear, pentanuclear... for two, three, four (and so on) metal ions. From this point other nomenclature can be introduced into the name depending on other features of the metal ions or ligand strands.

Within a complex the ligand strands may be of one type (homoleptic or homostranded), use of different ligand strands provides heteroleptic or heterostranded helicates. The other possible difference between molecular strands for helicate formation is variation of binding domains. A ligand containing identical binding domains is a homotopic ligand, different coordination sites along a strand are known as heterotopic ligands. Two isomeric forms exist if a heterotopic ligand strand is employed. Depending on the orientations of the ligands upon coordination this may give a head-to-head (HH) or a head-to-tail (HT) configuration. Additionally these sections of helicates can be further divided to take into account the nature of coordination to the metal centre, giving saturated helicates when the coordination sites of the metal ion are fulfilled by the donor atoms of the ligand strands. Unsaturated helicates occur when other atoms (possibly from solvent molecules) are required to satisfy the coordination requirements of the metal centre.⁷³

1.6.2 Homotopic helicates

There are many examples of homotopic helicates. These are produced from the self-assembly of molecular strands containing identical binding domains along the ligand strand and a suitable metal centre. Ideally homotopic helicates give complexes with a constant pitch (palindromic helices). One such example can be found in the early work published by Lehn *et al.*⁷² in which ligand strands containing two or three 2,2'-bipyridine units separated by oxapropylene bridges and their coordination properties with metal ions was investigated. Of particular interest was the result produced upon complexation with copper(I). Determination of the crystal structure of the complex between ligand (L^9) and Cu^+ was found to be a trinuclear double helicate (figure 1.23). This structure

results due to the intrinsic information provided by the metal ions and the structure of the ligand. The ligand is flexible enough to allow twisting of the strand around the metal ions but sufficiently rigid to prevent coordination to one metal ion. As the stereochemical requirements of the metal ion are fulfilled this is also an example of a saturated helicate. Bipyridine and oligobipyridine derivatives are now frequently employed in the formation of helicates.

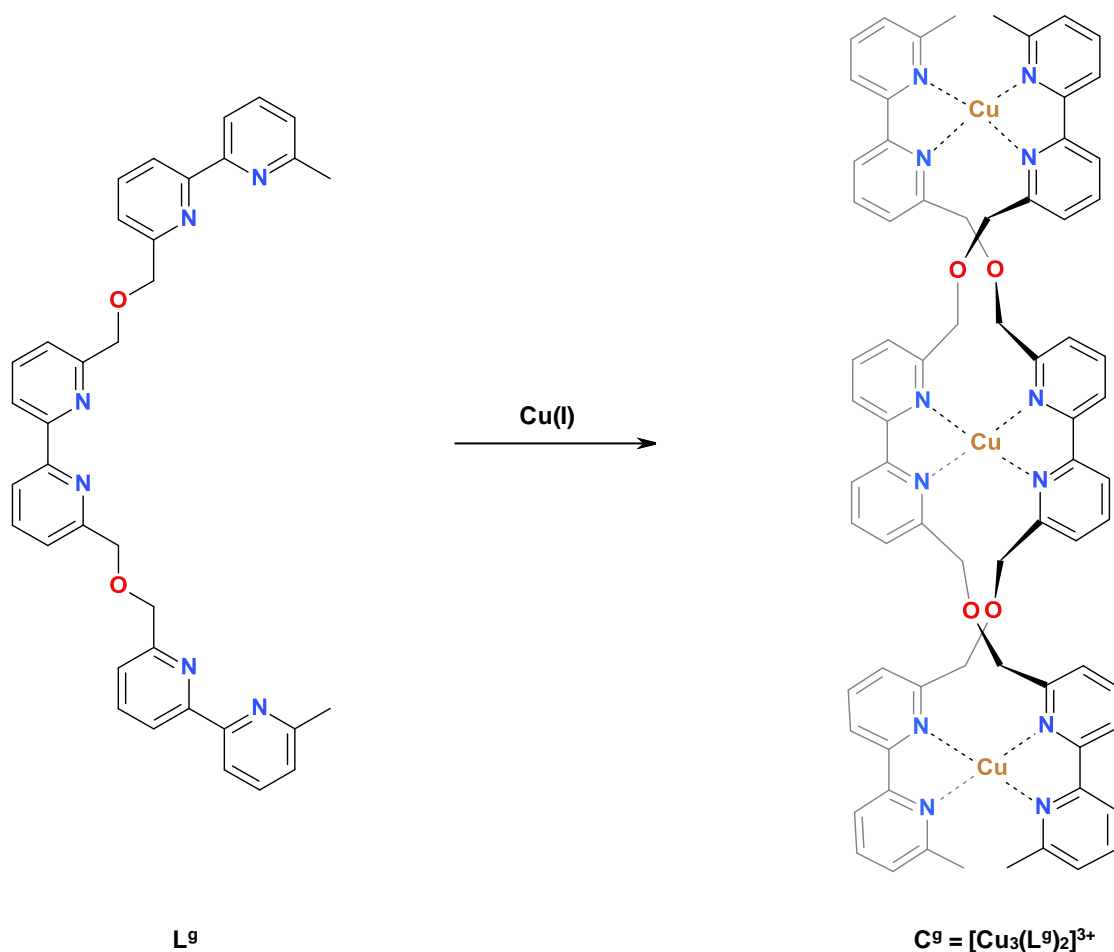


Figure 1.23 Trinuclear saturated homotopic double stranded helicate

1.6.3 Heterotopic helicates

As with homotopic helicates ligands focused on pyridine and bipyridine functionalities have been popular in the research of heterotopic assemblies. Heterotopic ligands contain different binding sites; this difference could be introduced by variation of the number or type of donor atoms present. This

leads to the possibility of two isomeric forms depending on the various arrangement of the molecular strand, giving directionality to ligand strands. Constable *et al.* demonstrate this well with the coordination of asymmetrically substituted 2,2':6',2'':6'',2'''-quaterpyridine to copper(I). Initial attempts to demonstrate selectivity for the formation of a single conformational isomer produced only a small excess of the less hindered isomer.⁷⁴ Synthesis of other asymmetrically substituted 2,2':6',2'':6'',2'''-quaterpyridines however provided better results.⁷⁵ As can be seen, two additional ligands were produced with variation in the substituent located at the 4 (R) and 4' (R') position of the pyridine rings (figure 1.24).

Complexes of the ligands were obtained upon treatment of methanolic solutions of the ligand (L^{h2} or L^{h3}) with excess metal ($[Cu(MeCN)_4][PF_6]$) under an atmosphere of argon, resulting in the formation of dark brown solutions from which the brown complexes $[Cu_2(L)_2][PF_6]_2$ ($L = L^{h2}$ or L^{h3}) could be obtained. Diffusion of diethyl ether into acetonitrile solutions of the complexes gave sufficiently pure crystals for structural analysis. It was determined from the data that a dinuclear species was present. From the NMR and subsequent COSY and NOESY assignment the data suggest a 1:1 mixture of the two conformational (HH and HT) isomers for L^{h2} , while only one isomer is present in the data for the other ligand L^{h3} . Problems with crystal formation, stability and disorder only allowed comment on the gross structural features; this did however confirm the presence of only one isomer (HH) for the L^{h3} ligand. Through molecular modelling the reasoning for the preferential formation of this conformer was attributed to short contacts between the tert-butyl substituent in the other isomer.⁷⁶

quinquepyridine ligand (L^i) was used. This ligand may be seen as a bipyridyl, bidentate unit, and terpyridyl, tridentate unit, joined together giving heterotopic binding domains. Reaction of the ligand with copper(II), cobalt(II), zinc(II) or nickel(II) acetate in boiling methanol followed by addition of $[NH_4][PF_6]$ allowed isolation of the complex salt $[M_2L_2]^{4+}$. From the copper(II) acetate reaction a number of species were isolated. These species contained a varying number of ancillary ligands. Analysis of a complex from the copper reaction shows the formation of a dinuclear unsaturated heterotopic double homoleptic helicate, with each ligand within the assembly acting as a bidentate donor to one metal and a tridentate donor to the other metal centre forming the head-to-head conformer. One copper ion has a distorted octahedral coordination geometry and the other copper centre has a highly distorted trigonal bipyramidal geometry. This second copper centre is coordinated by the two bidentate bipyridyl sections of the ligand and an oxygen atom from an acetate group (figure 1.25).⁷⁹

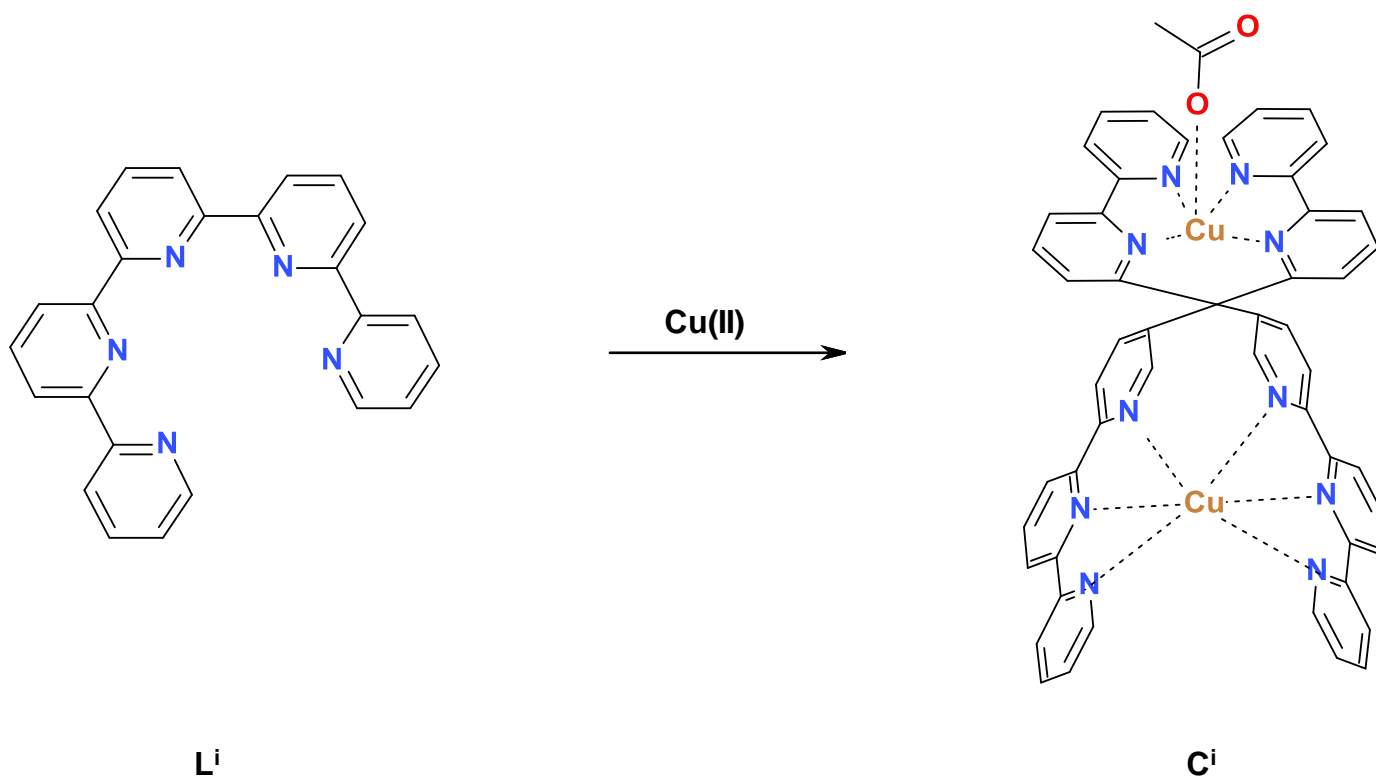


Figure 1.25 Dinuclear unsaturated heterotopic double stranded homoleptic helicate

1.6.5 Heteroleptic helicates

The helicates, discussed previously, have all contained identical ligand strands within the helicate i.e. are homostranded helicates. It is possible, however, to incorporate different strands within a helicate resulting in heterostranded or heteroleptic helicates. Hasenknopf *et al.* provided one example for the synthesis of a heteroleptic helicate.⁸¹ The assembly of a heteroleptic helicate through programming of the components was seen as the next step in the self-assembly of helicates. The two ligands selected had previously been produced and shown to form homoleptic helicates, copper(I)⁷² with L^k and iron(II)⁸² or nickel(II)⁸³ with L^j . Reaction of three equivalents of $Cu(CF_3SO_3)_2$ (in acetonitrile solution) and one equivalent of each ligand strand in chloroform gave a blue green solution upon reaction completion. The crystal structure was obtained which confirmed the formation of the desired trinuclear heteroleptic helicate, in which each metal ion is pentacoordinated by one terpyridyl unit of L^j and a bipyridyl group from L^k (figure 1.26). This example demonstrates well how the self-assembly may be directed by the binding information within the ligand strands and metal ion selected.

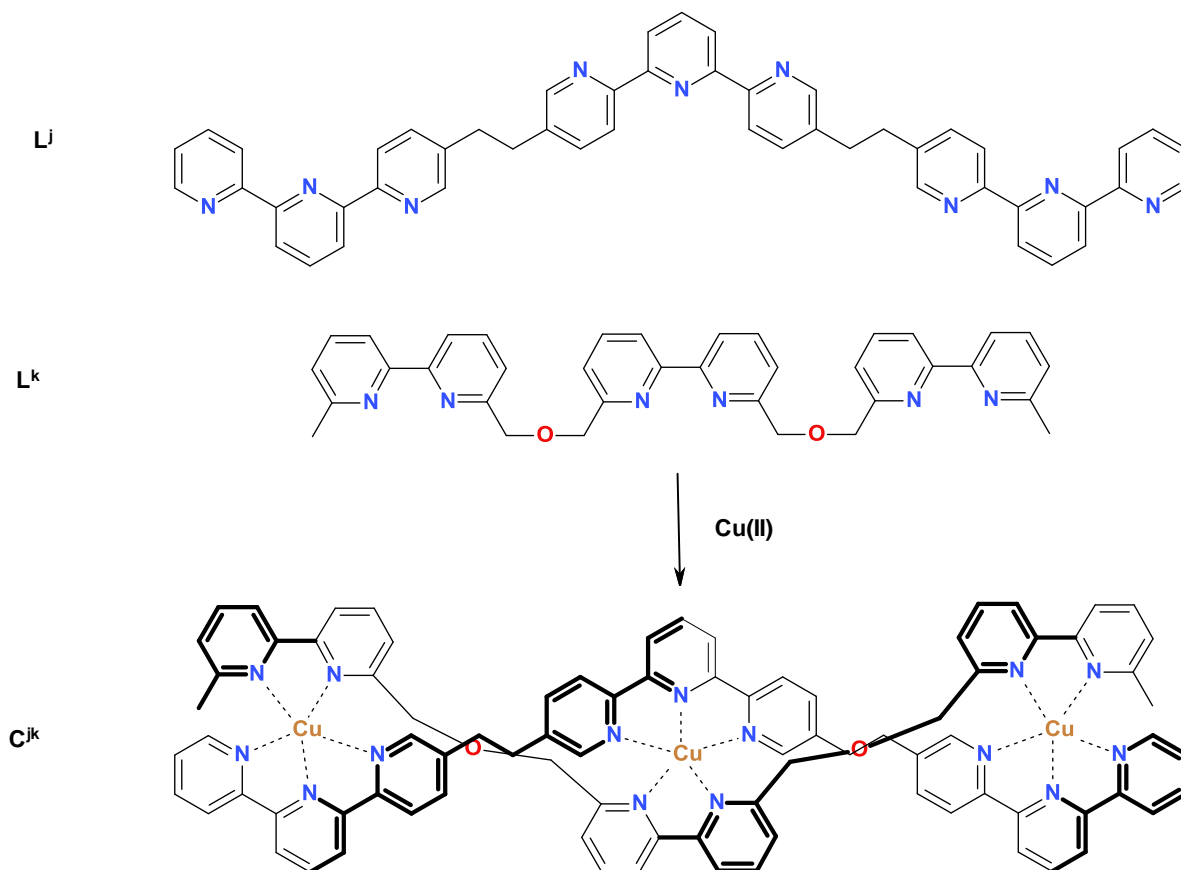


Figure 1.26 Trinuclear saturated homotopic double stranded heteroleptic helicate

1.6.6 Heteronuclear helicates

It is clear from the previous examples that different metal ions can be used in the self-assembly of helicates. For the self-assembly to be successful the metal ions must be complementary to the ligand. Tetrahedral metal centres form double stranded helicates with molecular strands possessing multiple bidentate domains; octahedral metal ions forming double stranded helicates require molecular strands with tridentate sites. An octahedral metal ion can also form triple stranded helicates with ligands consisting of bidentate domains. These general rules for matching the intrinsic information to direct the self-assembly of a helicate may not be applicable to every system. For example copper(II) is known to display a number of distorted coordination geometries, with five-coordinate complexes being a common occurrence.⁸⁴ As seen within the section relating to unsaturated helicates the 2,2':6',2'':6'',2''':6''',2''''-quinquepyridine ligand was shown to coordinate two copper ions, with each copper ion within the assembly displaying a different coordination geometry.

The different geometries within the complex were due to the binding sites available within the ligand strand. As this ligand is heterotopic, it possesses different binding domains, the ligand can be seen as being split into a bidentate and a tridentate domain.

The examples so far have incorporated one type of metal ion within each complex i.e. a homonuclear helicate. Constable *et al.* have contributed a substantial amount of research into the self-assembly of metal ions with oligopyridines.^{75, 85, 86} By using helicates already known it was rationalised that it would be possible to convert a mono-helical cobalt(II) complex to a heterobimetallic double helicate upon exposure to a compatible metal ion such as copper(I) or silver(I).⁷⁸ This research was conducted using a variety of 2,2':6',2'':6'',2''':6''',2''''-quinquepyridine derived ligands (L^I). Reaction of solutions containing $[Co(L^I)(MeCN)_2]^{2+}$ with half an equivalent of silver(I) or copper(I) resulted in the precipitation of solids after treatment with $[NH_4][PF_6]$ or $Na[BF_4]$. This initial research did not successfully produce good quality crystals. Subsequent investigation along the same lines resulted in the successful formation of heterodinuclear double helicates in the solid state upon reaction of one equivalent of 2,2':6',2'':6'',2''':6''',2''''-quinquepyridine with half an equivalent of each metal ion, cobalt(II) and silver(I) (figure 1.27).⁸⁷

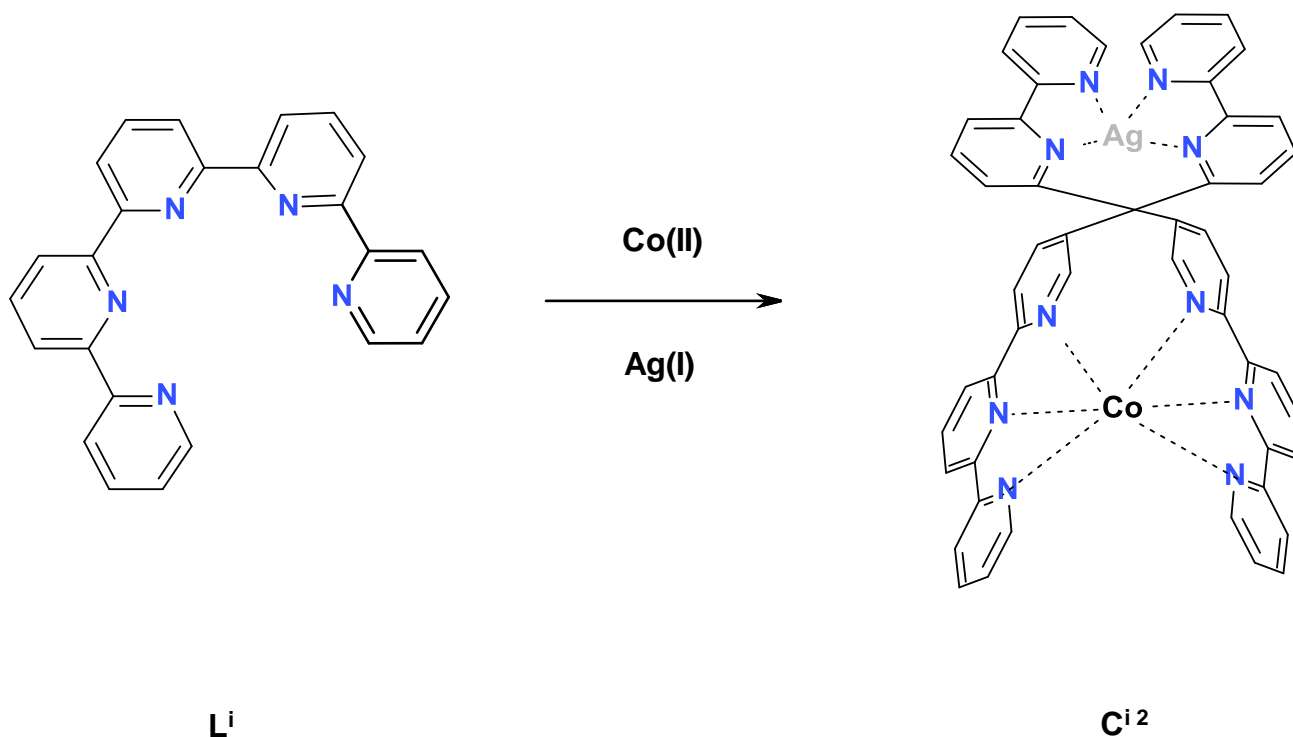


Figure 1.27 Representation of the first structurally characterized heterodinuclear double helicate

So far only octahedral and tetrahedral metal ions have been considered for the formation of helicates. It is, however, possible to use other metal centres with higher coordination numbers, such as lanthanide metal ions.⁸⁸ These metals can display a range of coordination geometries (generally 6-12). If a tricapped trigonal prismatic geometry (9 coordination geometry) is displayed then the metal centre has the potential to form triple stranded helicates with molecular strands possessing tridentate domains.⁸⁹

1.6.7 Chirality in helicates

A helix is generated from the motion of a point around and along a line, the helical axis. The helix is characterised by its helical axis, a screw sense (i.e. chirality) and a pitch (rate of axially linear to angular properties). In an ideal example the axis is a straight line and the two kinds of motion, linear and circular, give a helix with a constant radius (constant distance from axis, r) and constant pitch (palindromic). The direction of the circular motion may be right

handed (P, plus) or left handed (M, minus). So if the direction of the rotation of a helix is clockwise from the end closest to the viewer to the end which is distant this gives the P helix while a rotation anticlockwise gives the M helix (figure 1.28).⁹⁰

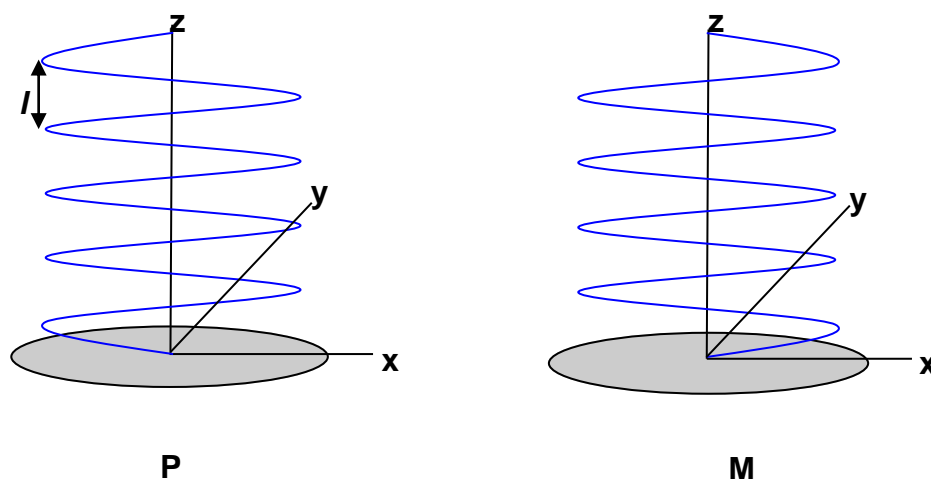


Figure 1.28 Illustration representing a right-handed (P-plus) and a left-handed (M-minus) helix (where l is the pitch and z gives the helical axis)

Chirality operates at the molecular and supramolecular levels. As such supramolecules, as with molecules, can express chirality with enantiomeric and diastereomeric forms. Within the metal-directed assembly of helicates the helices are a racemic mixture of the plus (P) and minus (M) enantiomers. The ability to selectively form one of the helicates, P or M, shows a higher level of control over the assembly. This is of importance as chirality is seen in biological systems and has been an issue within medical research.

Chiral ligands have been employed for the self-assembly of helicates. When chiral ligands are used the P and M forms are diastereomers. Enantiomers possess identical chemical and physical properties except for the direction they rotate plane-polarised light, whereas diastereomers express different chemical and physical properties. Thus one diastereomer could be more thermodynamically stable than others resulting in one isomer being produced in excess. The use of chiral ligands to direct self-assembly has been an area of

some interest. With contributions from numerous research groups some remarkable results have been produced.⁷³

Constable *et al.* have a background in the self-assembly of helicates using oligopyridine and oligobipyridine which is known as a robust method for helicate formation with carefully selected metal ions. With the use of chiral oligopyridine ligand strands Constable *et al.* have demonstrated the diastereoselective formation of helicates.⁹¹ A pair of enantiomeric 2,2':6'2''-terpyridine ligands (L^L and L^m) was prepared by reaction of 6-bromo-6''-methyl-2,2' : 6',2''-terpyridine with the sodium salts of (1*S*)-(-) or (1*R*)-(+)-borneol (figure 1.29). It is known that the coordination of terpyridines to copper(I) produces dinuclear double species. In this example using the chiral terpyridine and copper(I) a number of possible double helicates may result. This ligand is directional so head-to-head and head-to-tail isomers are possible for the P or M conformers as the helicate itself is chiral. Reaction of the ligand, L^L or L^m , with $[Cu(MeCN)_4][PF_6]$ in acetonitrile gave an orange-red solution from which a precipitate was isolated upon addition of $[NH_4][PF_6]$. X-ray structural determination was achieved from crystals produced from the recrystallisation of the crude $[Cu_2(L^L)_2][PF_6]_2$ or $[Cu_2(L^m)_2][PF_6]_2$ complexes from acetonitrile by slow diffusion of diethyl ether. This confirmed the formation of the head-to-tail isomer and the diastereoselective formation of (S)(S)-(M)-HT isomer for L^L and (R)(R)(P)-HT isomer of L^m . The preferential formation of the HT helicate is due to reduced steric interactions between the chiral groups in relation to the head-to-tail isomer. The reasoning for the preferential formation of a given diastereoisomer is not as clear cut.

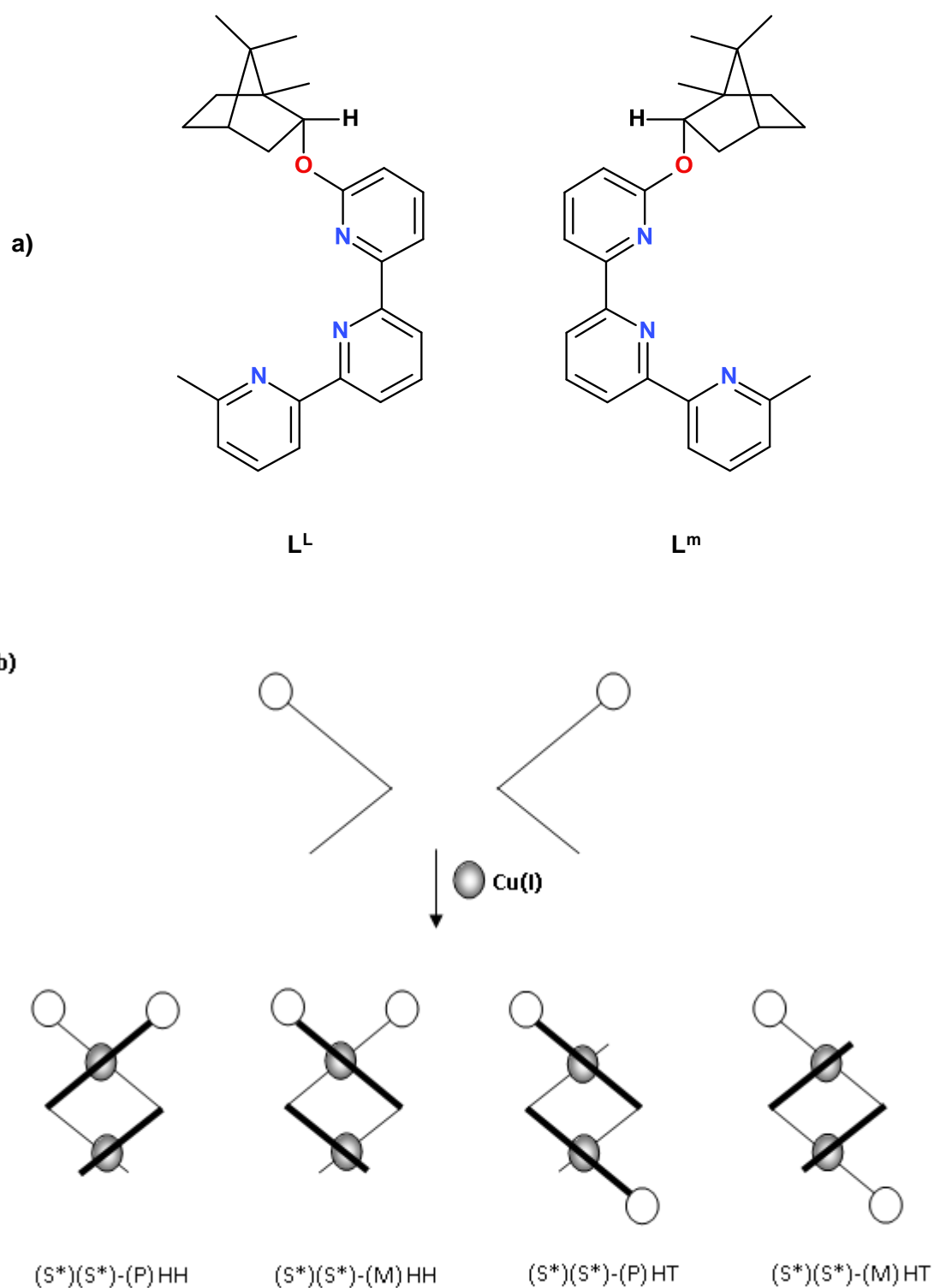


Figure 1.29 a) Ligands L^L and L^M b) schematic representation of the possible HH and HT diastereomeric dinuclear double helicates from the reaction of chiral ligands L^L and L^M with $Cu(I)$ (S^* = homochiral compounds, (S,S) or (R,R))⁹¹

Following this research relating to the formation of diastereoselective helicates other ligands were produced which upon complexation to different metal ions displayed a greater level of diastereoselectivity. In the previous example the ^1H NMR spectrum of each complex showed two species in solution with a d.e (diastereomeric excess) of 75%. Subsequent ligands (for example figure 1.30) produced by Constable *et al.* showed 95% d.e with silver(I)⁹² and 98.7% with copper(I).⁹³

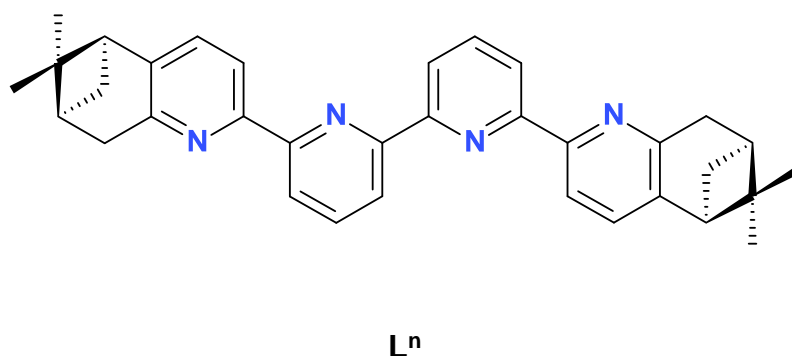
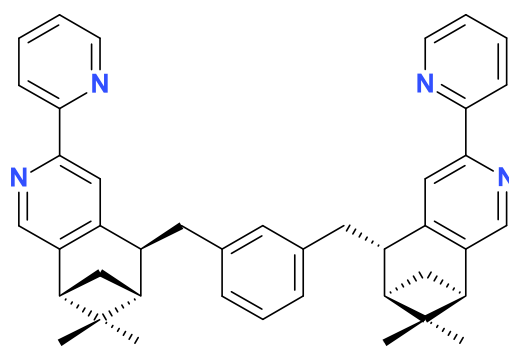


Figure 1.30 Chiral ligand produced to control the chirality of helicates

Another researcher within this area of chiral control of helicates is Von Zelewsky. Early research focused on ruthenium(II) complexes produced by coordination to a number of bridging chiral bisbipyridine ligands, becoming known as “chiragen” ligands.⁹⁴ Von Zelewsky reports the application of chiragen-type ligands in the self-assembly of helicates.⁹⁵ One of these chiragen-type ligands, 4,5-chiragen (L^0 , figure 1.31), has been shown to form complexes with a number of octahedral metal ions (Cd(II), Zn(II) and Fe(II)). Through analysis it was determined that the major species produced is a dinuclear triple helicate which shows preferential formation of one of the stereoisomers.⁹⁶



L°

Figure 1.31 4,5-Chiragen-type ligand produced for diastereoselective formation of helicates

The research so far has involved double- or triple-stranded helicates; however, as chirality is an intrinsic property of a helix, single stranded helicates also exhibit chirality. Kwong *et al.* have reported the synthesis of a new chiral quaterpyridine ligand (L^P) which forms a stereoselective single-stranded dinuclear helical complex with palladium.⁹⁷ Each Pd atom adopts a distorted square-planar geometry. X-ray crystal structure and CD analyses confirm the complex structure to be stereoselective in the assembly giving the *M*-[Pd₂(η³-C₃H₅)₂(L^P)] complex (figure 1.32).

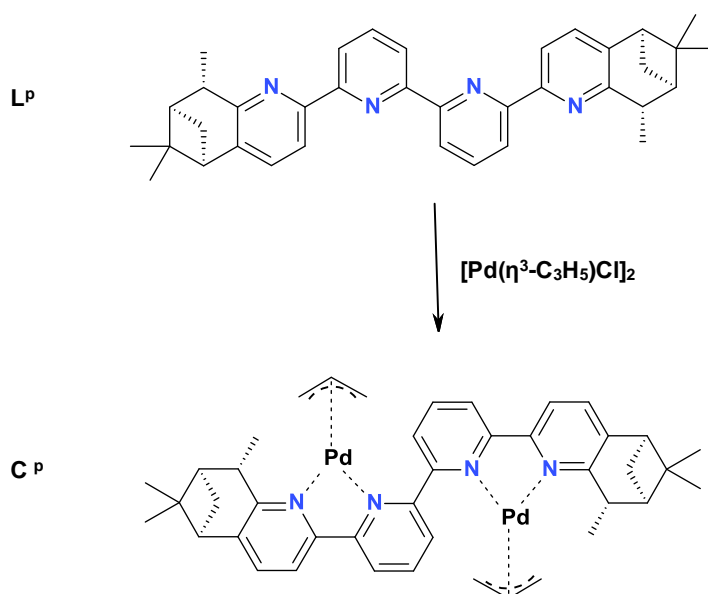


Figure 1.32 Stereoselective self-assembly of a single-stranded helicate

1.6.8 Meso-helicates

The term *meso-helicate* was introduced around 1995; also at the same time additional terms, 'side-by-side complex'⁹⁸ and 'mesocate', were introduced to describe the same kind of coordination array. In the formation of helicates the ligands within the assembly twist around the metal ions forming a helix, in *meso-helicates* the ligands adopt a 'side by side' arrangement. The ligands in a *meso-helicate* do not twist around the metal ion in a helical rotation and thus the *meso-helicate* gives an achiral product from the self-assembly.⁹⁹ There has been some interest in the factors which drive the assembly toward the formation of the achiral *meso-helicate* in preference to the chiral helicate. Albrecht's research led to the suggestion that the length of alkyl spacers between bidentate binding domains of alkyl bridged dicatechol ligands could be used to predict the selective formation of *meso-helicates*.¹⁰⁰

An interesting example of a mixed-ligand mesocate has been reported by Ward *et al.*¹⁰¹ Two bisbidentate ligands which possess two N,O-donor pyrazolyl-phenol units (L^q and L^r) have been shown previously¹⁰² to form conventional double helicates with Co(II), Cu(II) and Zn(II) in which the metals adopt a distorted tetrahedral geometry. A 1:1 mixture of each ligand (L^q , L^r), with triethylamine to deprotonate the phenol donors, was treated with metal salts in methanol. The product formed was isolated by filtration and analysed to determine the distribution of the three possible structures. From the reaction between L^q , L^r and Zn(II) crystals were obtained; X-ray structural determination revealed the structure to be the 'face to face' arrangement of the two ligands giving an achiral heteroleptic mesocate (figure 1.33).

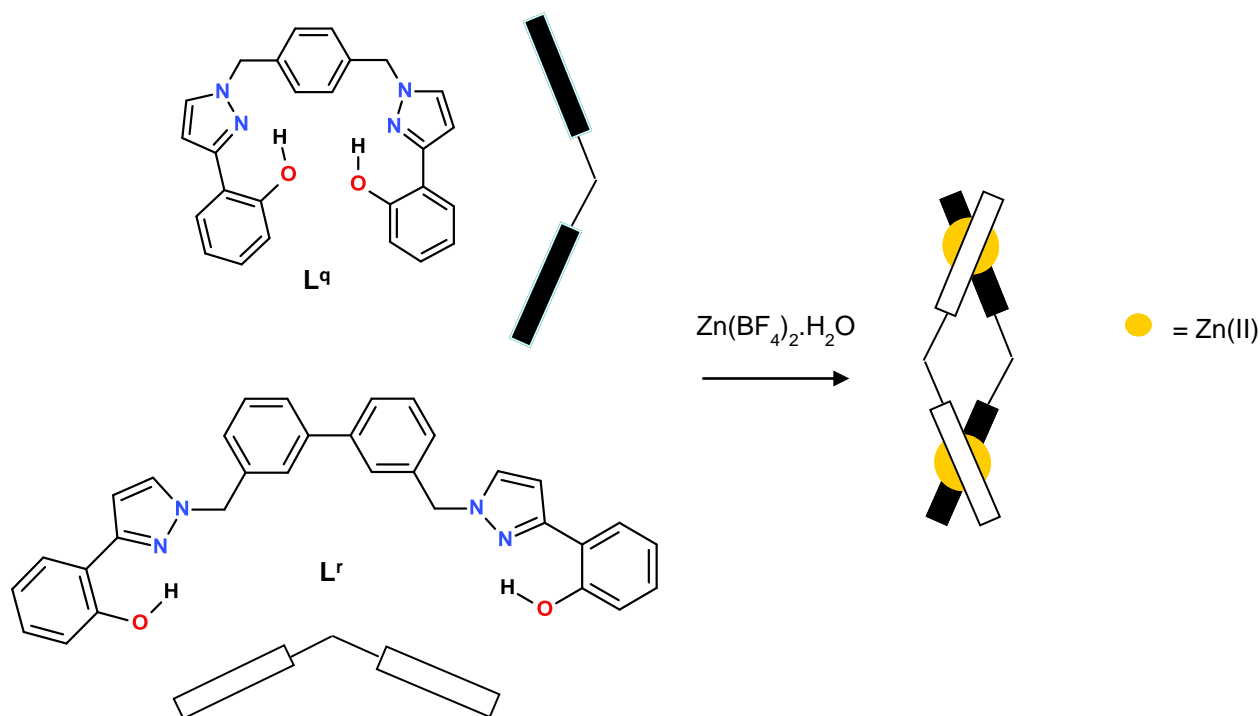


Figure 1.33 Illustration of the assembly of a dinuclear heteroleptic mesocate

1.7 Circular helicates

The principles for the successful formation of helicates are now generally well known. The self-assembly of these linear polynuclear structures results from the careful selection of complementary ligands and metal centres. Contributions from many research groups have produced a vast array of ligands which are able to coordinate a whole host of metal ions and through self-assembly lead to helicates. Numerous architectures from the simple dinuclear double helicates to other polynuclear double-, triple- and even quadruple-stranded helicates are now known.^{80-82, 84} As seen in previous sections these structures can be further controlled or varied through incorporation of different features within the ligand strand or variation of stereochemistry of the metal centres.

In comparison to helicates the self-assembly of circular helicates, a higher nuclearity assembly, is less well understood. This is partially due to the design principles of these architectures which are essentially the same as their linear counterparts. For the self-assembly of helicates and circular helicates a ligand containing at least two suitable binding sites that coordinate different metal ions

is required. However, for the self-assembly of a circular helicate the entropically favoured linear assembly must be prevented. The assembly of linear helicates could be hindered through intermolecular interactions such as templation by anions or intramolecular interactions which stabilise the formation of a circular structure. The nomenclature employed in the identification of circular helicates is essentially the same as that used for linear helicates.

1.7.1 Anion templation

As with linear helicates the vast majority of circular helicates are produced using homotopic ligands, ligands which contain the same binding domains. The first example of a circular helicate was reported by Lehn and co-workers.¹⁰³ Reaction of tris-bipyridyl ligand (L^5) and an equimolar quantity of Fe(II)chloride in ethylene glycol gave a red-orange solution; addition of ammonium hexafluorophosphate afforded a red precipitate. This was separated and the structure confirmed using 1H NMR, mass spectroscopy and X-ray crystal structure determination. The structure was found to contain five Fe(II) ions, five ligands and a chloride ion $[(Fe_5L^5_5)Cl]^{9+}$. Three bipyridine groups, belonging to three different ligands, are coordinated to each metal ion giving each Fe(II) a distorted octahedral coordination geometry. The short linkers between the bipyridyl groups prevent the terminal and central bipyridyl units coordinating the same metal ion; in addition to this the two terminal bipyridyl groups are unable to coordinate the same metal centre as this would distort the central unit. The metals almost lie in one plane and form the corners of a pentagon, with the ligands wrapped helically around the metals forming the sides of the pentagon. The structure has been identified as a pentanuclear circular helicate $[5]cH$ (figure 1.34). The cavity of the structure is occupied by a chloride ion, with no exchange of anion occurring even with excess of other anions (PF_6^- , $CF_3SO_3^-$) demonstrating ion selectivity of the receptor for Cl^- .

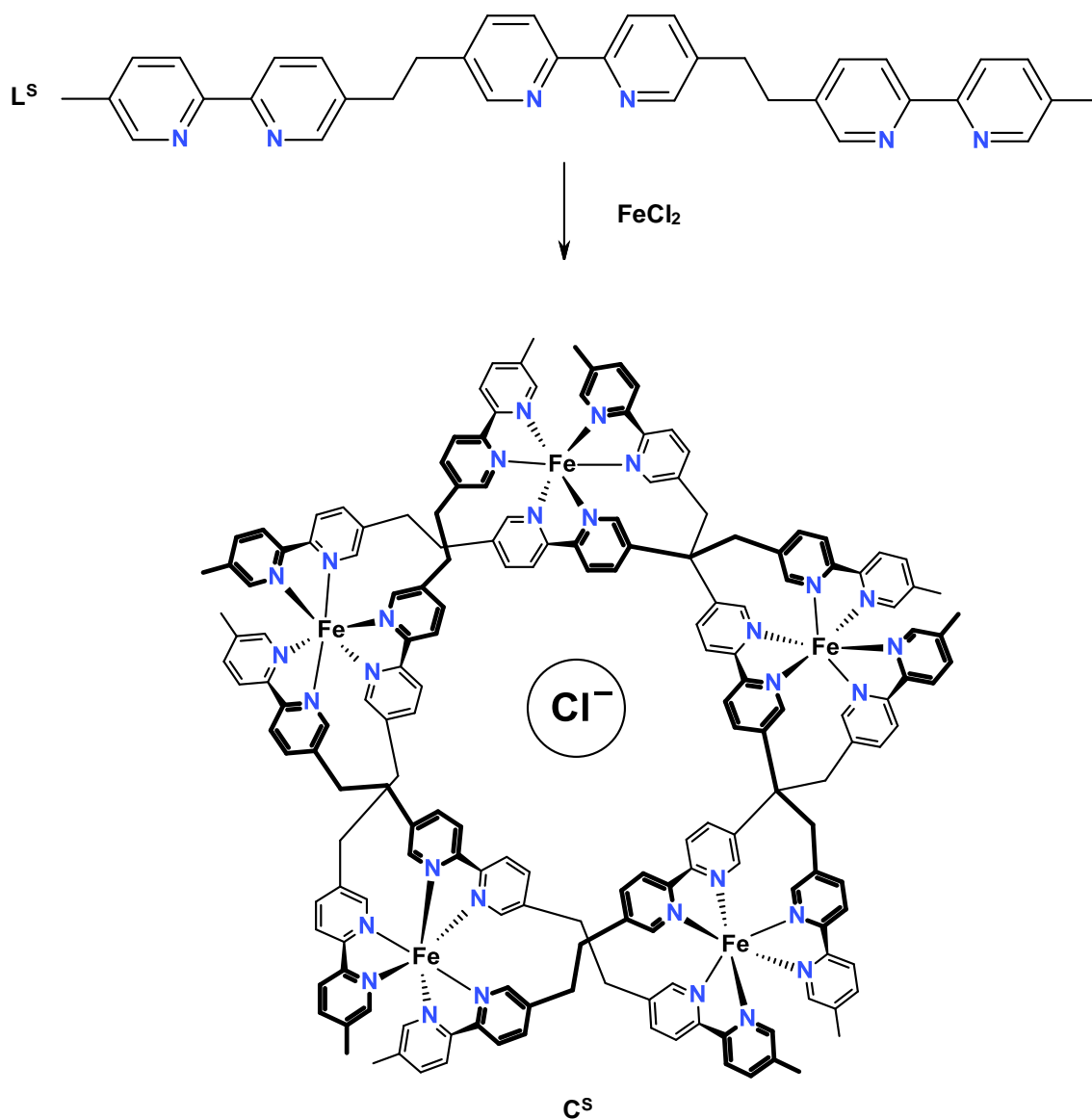


Figure 1.34 Self-assembly of a pentanuclear circular helicate

Further understanding of the factors controlling this self-assembly was required. Lehn and co-workers¹⁰⁴ subsequently investigated how variation in the system components, such as metal salt and structure of the ligand, would affect the outcome of the self-assembly. With variation in the metal salt (FeSO_4) a hexagonal circular double-helicate, $[6]\text{cH}$, was produced. The idea that the size of the circular double helicate could somehow be dependent on the anion prompted further inspection. Other metal salts employed produced circular helicates and it was determined that the charge of an anion had little influence on the structure (i.e. mono- or divalent). The important feature was shown to be

size of the anion; the size of the circular helicate was dependent on the size of the anion used, suggesting the role of the anion is to act as a template for the self-assembly of these circular helicates. As well as variation in anions a different ligand was also synthesised to identify the role of the ligand structure in the self-assembly. Exchange of the ethylene bridges for oxypropylene bridges gave a longer ligand (L^t) displaying a higher level of flexibility in comparison to the ethylene bridges. Reaction of this ligand with Fe(II) ions results in the assembly of a tetrameric circular assembly $[4]cH$. This structure is produced due to the increased length of the ligand, giving a larger cavity, and higher flexibility allowing more bending of the ligand to form a square (figure 1.35).

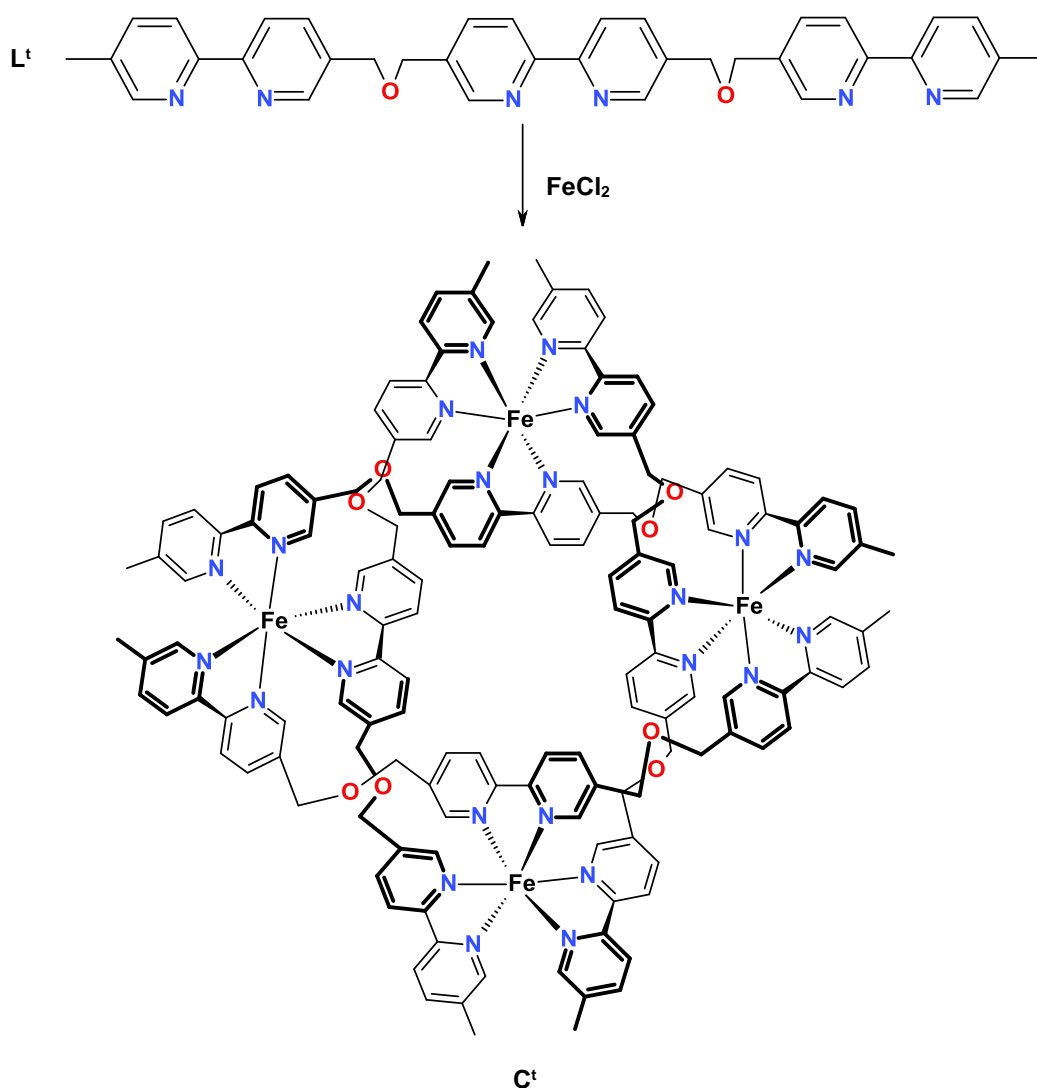


Figure 1.35 Self-assembly of a tetranuclear circular helicate from four L^t ligands and four Fe(II) ions

1.7.2 Alternatives to anion templation

Following on from the initial research conducted by Lehn *et al.* other groups have reported circular helicates which are not dependent on anion templation. Thummel and co-workers produced ligands for coordination with metal ions which contained a pyrene unit which due to its ability to form well organised π -stacked arrays dictates the nuclearity of the complex in this case forming a trimeric species.¹⁰⁵ Hannon¹⁰⁶ demonstrated that the coordination geometry of the metal ion employed can influence the self-assembly, showing that reaction of bis-pyridylimine ligands containing a 1,3-bis(aminomethyl) benzene spacer unit with tetrahedral metal centres gives linear dimers while coordination to octahedral metal ions produces a triangular circular helicate.

An elegant example by Rice *et al.*¹⁰⁷ demonstrates the self-assembly of circular helicates controlled by inter-ligand interactions, which is dependent on the size of the metal ion used. The ligand (L^u) consists of two tridentate domains, containing thiazole–pyridyl–pyridyl units, separated by a phenylene spacer (figure 1.36). Reaction with $Cd(ClO_4)_2 \cdot 6H_2O$ in nitromethane produced crystals upon diffusion of dichloromethane. The structural determination showed a dinuclear double stranded helicate in which the cadmium(II) metal centres adopt a distorted octahedral coordination geometry due to coordination with one tridentate, thiazole–pyridyl–pyridyl, domain from each ligand strand. Reaction with $Zn(CF_3SO_3)_2$ in acetonitrile gave a colourless solution which upon layering with ether resulted in the formation of crystals; structural analysis revealed the formation of a pentanuclear cyclic helicate. The Zn^{2+} metal ions within the assembly are six-coordinate again due to the coordination with two tridentate domains, thiazole–pyridyl–pyridyl, from two different ligands. The ligands wrap around the metal ions in an ‘over and under’ conformation, giving the helical cyclic oligomer. To rule out the possibility that the difference in architecture could be due to use of different metal salts 1H NMR solution studies were conducted to monitor any effect upon addition of another anion. This showed, even with addition of an excess of the second anion, no observable influence. The vast difference seen between the structures has been assigned to the difference in size between the metal ions, which causes unfavourable inter-ligand steric interactions.

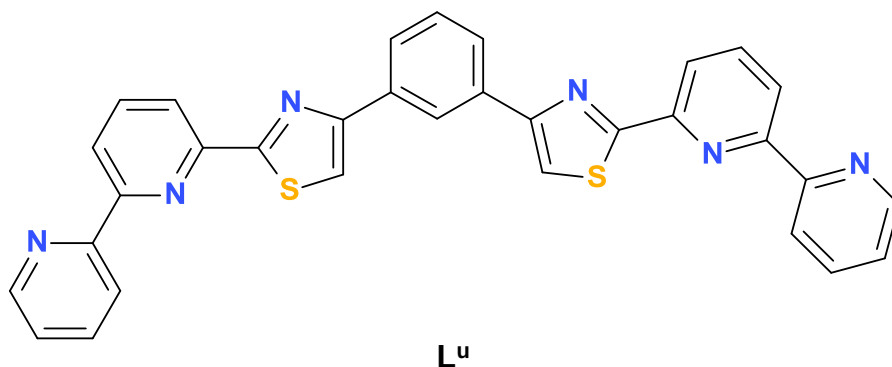


Figure 1.36 Ligand, L^u , employed for the self-assembly of a circular helicate

1.7.3 Directional and heteroleptic circular helicites

As discussed above linear helicites may be programmed to express a variety of structural features, from the standard dinuclear double helicate to polynuclear double-, triple- and quadruple-stranded assemblies. They can also be programmed to give architectures which display a higher level of complexity, such as directionality and heteroleptic structures. The programming of such helicites is through the ligands selected and metal centres. To control the directionality of a helicate the ligand strand must contain at least two different binding domains, such as a tridentate and bidentate unit, which upon coordination gives a head-to-head or head-to-tail arrangement. The conformer which results may be controlled with the selection of metal ion, thus if a metal ion which possesses a geometry which forms five-coordinate species is employed the preferential coordination of one bidentate and one tridentate domain will give the head-to-tail isomer. The formation of the head-to-head isomer may likewise be programmed for self-assembly by using two metal ions one of which is tetrahedral, for binding the bidentate domains, and one which is octahedral, for the tridentate domains, assembling the ligand in a head-to-head conformation.

Until recently these principles for directing structures of higher complexity had not been applied to the assembly of circular helicites. Rice *et al.*¹⁰⁸ elegantly demonstrated the application of these simple principles for the formation of a

higher complexity circular helicate. The principles which govern the assembly of circular helicates are essentially the same as those which are applicable to linear helicates, with the additional proviso that the formation of the linear dimer must be hindered. A few methods for the stabilisation of the circular architecture have been reported,^{103, 104, 107, 108} in this instance the formation of the circular helicate was driven by repulsion between protons located on the central phenyl group within the ligand.

The use of a phenyl spacer within the ligands has provided a reliable and robust method for the self-assembly of circular helicates. Variations in the structure of the ligand, L^u , led to the synthesis of L^v and L^w providing new structures for the investigation of higher complexity circular assemblies (figures 1.37 and 1.38). L^v was used to probe the possibility of directionality within these higher nuclearity species. Using similar design principles as those for the assembly of linear analogues a ligand containing a bidentate and tridentate domain separated by a 1,3-phenylene spacer was produced, reasoning that one bidentate and one tridentate domain is required to satisfy the stereochemical requirements for a metal ion displaying a pentacoordinate geometry, resulting in the assembly of a head-to-tail motif. Reaction of L^v with one equivalent of $Cu(ClO_4)_2 \cdot 6H_2O$ in acetonitrile gave a crystalline solid after diffusion of chloroform. Structural analysis confirmed the head-to-tail pentanuclear circular helicate $[Cu_5(L^v)_5](ClO_4)_{10}$ (figure 1.37).

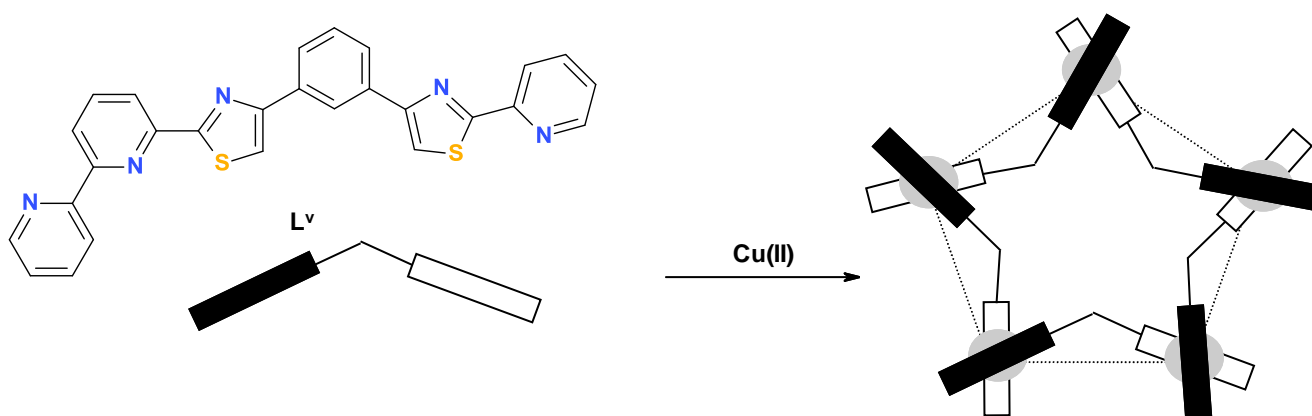


Figure 1.37 L^v used in the self-assembly of a head-to-tail circular helicate.

As expected the bidentate and tridentate domains of the ligand coordinate two different metal centres, with each centre adopting a distorted square-based pyramidal geometry. This is an excellent example of a head-to-tail circular helicate.

In addition to demonstrating the possibility of producing a circular helicate displaying head-to-tail conformation, the assembly of a heteroleptic circular helicate was investigated. For this experiment L^u , a bis(tridentate)ligand, and L^w , bis(bidentate) ligand, were utilised. The arrangement of these ligands in a circular array has the potential to produce any number of different structures. Initial attempts using mixed metals to form a heteroleptic species were unsuccessful, which resulted in the use of copper(II) as it may display more than one coordination geometry. Reaction of Cu(II) with L^u and L^w in a 5:3:2 ratio gave the desired pentanuclear heteroleptic complex $[Cu_5(L^u)_3(L^w)_2]^{10+}$, however, this reaction gave a mixture of other species as well as the desired heteroleptic circular helicate. In order to force the equilibrium towards a heteroleptic helicate the component ratios were altered giving a 2:1:1 ratio of Cu^{2+} : L^u : L^w . ESI-MS of the complex in acetonitrile showed a number of peaks which potentially corresponded to a heteroleptic species. Crystallisation of the complex from nitromethane was achieved after slow diffusion of ethyl acetate. X-ray analysis confirmed the presence of a heteroleptic circular helicate in which five copper(II) ions are coordinated by three strands of L^u and two L^w strands. One of the metal ions is octahedrally coordinated by two tridentate domains and the remaining metal ions are bound by one tridentate and one bidentate domain making them five-coordinate (figure 1.38).

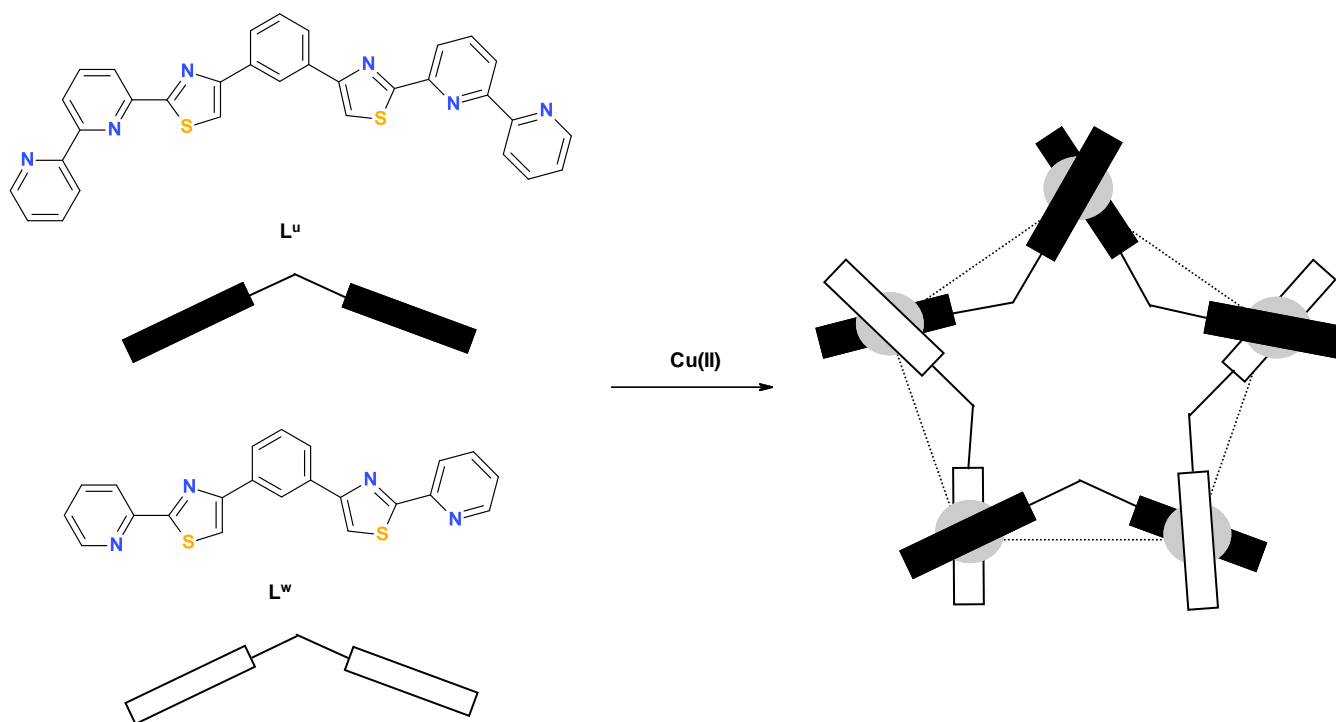


Figure 1.38 L^u and L^w used in the self-assembly of a heteroleptic circular helicate $[Cu_5(L^u)_3(L^w)_2]^{10+}$

1.7.4 Diastereoselective circular helicites

Circular helicites are also intrinsically chiral so the architectures which result within an assembly are a racemic mixture of the two enantiomers. In a similar way to the linear analogous the chirality may be influenced by incorporation of chiral centres within the ligand strands. An elegant example by Von Zelewsky and co-workers demonstrates the application of the principles used in the formation of linear helicites is applicable in the formation of circular assemblies to selectively provide one diastereomer.

From previous research a family of ligands which incorporate a number of pinene-2,2'-bipyridine moieties into one ligand strand have been synthesised.^{95, 96} Due to steric constraints L^x (figure 1.39) is unable to coordinate in a tetradentate manner to one coordination centre. The interaction of L^x with labile coordination centres was tested for the possibility of producing polynuclear self-assembled structures. A mixture of a 1:1 molar ratio of L^x and $AgPF_6$ in

acetonitrile solution followed by slow diffusion of diethyl ether provided crystals. X-ray diffraction analysis of the silver complex shows a hexameric single-stranded circular helicate which displays a P handedness of the resulting helix. The silver centres are tetrahedrally coordinated by four nitrogen atoms from two different ligands. This is the first example of a self-assembled hexanuclear structure which is a circular helicate with a predetermined configuration.¹⁰⁹

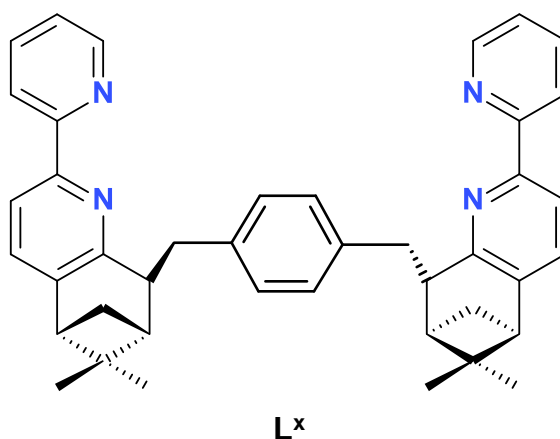


Figure 1.39 L^x ligand utilised in the diastereoselective self-assembly of a circular helicate

1.7.5 Circular *meso*-helicates

In comparison to helicates the occurrence of circular and *meso*-helicates is rare, while examples of circular *meso*-helicates are even more uncommon. Gloe *et al.*¹¹⁰ have created some beautiful architectures, which present the first examples of circular *meso*-helicates. Using ligands L^y , L^z and L^a (figure 1.40) the bis-pyridylimine ligands differ in the central linking component between the two binding domains. Previous studies have shown these ligands form a variety of supramolecular structures depending on the metal ion employed.^{111,112}

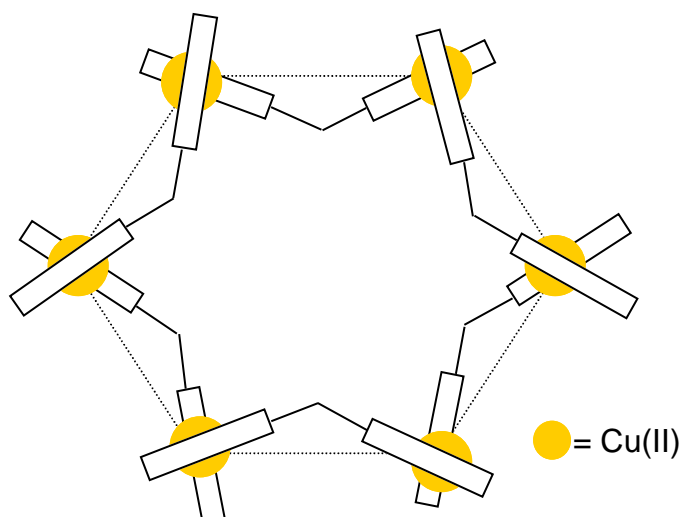
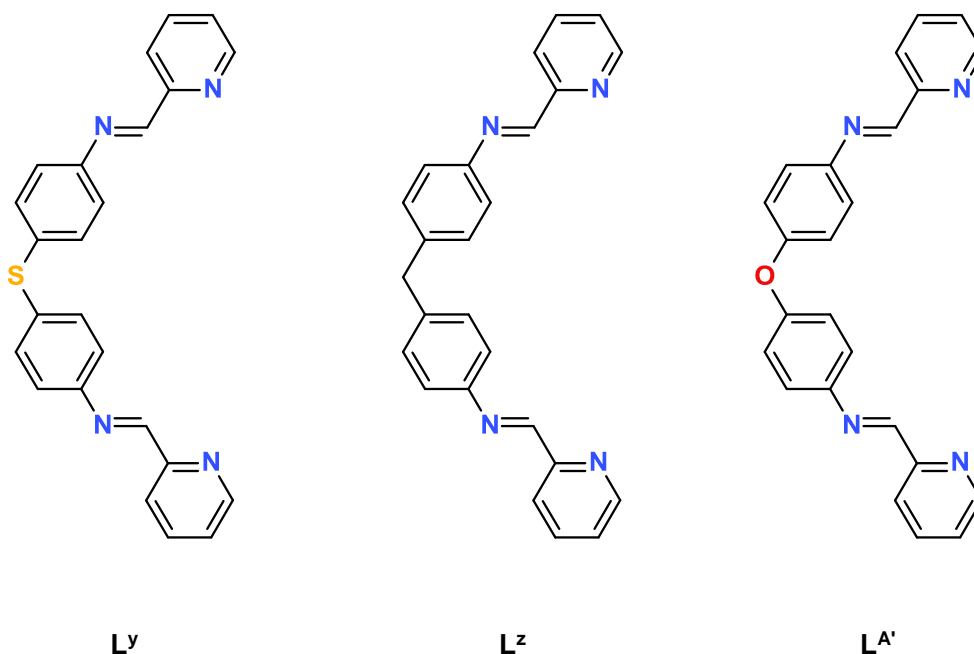


Figure 1.40 a) Ligands utilized for the self-assembly of circular mesocates b) Schematic representation of a hexanuclear mesocate with Cu(II)

Reaction of L^y , L^z or $L^{A'}$ with $\text{CuSO}_4 \cdot 5\text{H}_2\text{O}$ in a mixed solvent system (methanol /water/acetonitrile) followed by slow diffusion of diethyl ether gave crystals suitable for X-ray structural determination. Each of the complexes formed from the three ligands is essentially the same; the Cu(II) ions have alternating L- and D- configurations leading to the *meso*-helicite. Each metal centre has a distorted octahedral coordination geometry with binding to two bidentate pyridylimine strands of different ligands and one sulfate ion, resulting in a neutral hexanuclear complex with six anions associated with the molecule. The

anions have been shown to play a major role within the formation of these assemblies as substitution of the anion for alternatives (e.g. ClO_4^- or NO_3^-) yields a non-cyclic structure under otherwise identical reaction conditions. The hexanuclear *meso*-helicates produced are the first examples of neutral circular *meso*-helicates. As well as hydrogen bonding and π - π stacking interactions, the assembly is controlled by association with the sulfate anions which provide a double stranded rather than a triple-stranded structure around the metal ions. The variation of linkers within the ligands surprisingly showed little influence over the resulting complexes.

The examples given demonstrate a whole host of inspiring architectures. This research has expanded upon the principles determined for the successful assembly of linear helicates and applied them to the higher nuclearity species known as circular helicates, showing that complex architectures may result due to complementarity of the chemical information stored within the covalent framework of the ligands and the intrinsic properties of the metal centres. Other components, such as anions and solvents, may also play important roles within these assemblies.

1.8 Allosteric interactions

For self-assembly and self-organisation to occur components containing two or more interaction sites are required; this introduces the possibility of allosteric interactions which can play a significant role within self-processes. Allostery results when occupation at one site influences the binding features of another. This may mean the binding at the second site is favoured or disfavoured, giving positive co-operativity and negative co-operativity respectively.¹ Allosteric interactions are important within biological systems, for example hemoglobin is an extremely important protein present in red blood cells. This respiratory protein is responsible for the transport of oxygen into tissues and the removal of carbon dioxide. The binding of oxygen atoms by this protein is cooperative; the binding of one oxygen atom leads to favourable binding of additional oxygen atoms. Enzymes are another example of biological systems capable of

displaying allosteric effects. Enzymes are seen as biological catalysts, they are responsible for a number of biologically important processes and functions within nature. A simple enzyme may contain an active site which is specific for a particular substrate; in addition to the active site another, allosteric, site may be present. The allosteric site could potentially bind to a species which activates the enzyme to bind the substrate or an inhibitor may be present at the allosteric site which can turn off the enzyme's activity. This simplified explanation of allosteric effects within enzymes provides the basic ideas of what takes place in order to regulate enzyme activity. These features of enzyme activity are a target for application within synthetic systems.¹¹³

The initial application of allosteric effects to synthetic systems was proposed by Rebek *et al.*¹¹³ Identification of the minimum requirements for an allosteric effect, i.e. an active site, a remote site (also known as an allosteric site) and a conformational mechanism which connects the two, provided a starting point for developing supramolecular systems capable of mimicking this type of behaviour. A macrocyclic polyether incorporating a 2,2'-bipyridyl and crown ether site within the same structure ($L^{B'}$) gave a system containing two binding sites required for allosteric behaviour (figure 1.41).¹¹⁴ The polyethers are known to bind alkali metal ions and the 2,2'-bipyridyl unit to chelate transition metals. Although the two sites are separated from one another they are not expected to behave independently. The binding at one site forces conformational restrictions on the other site thereby altering its receptivity to binding.

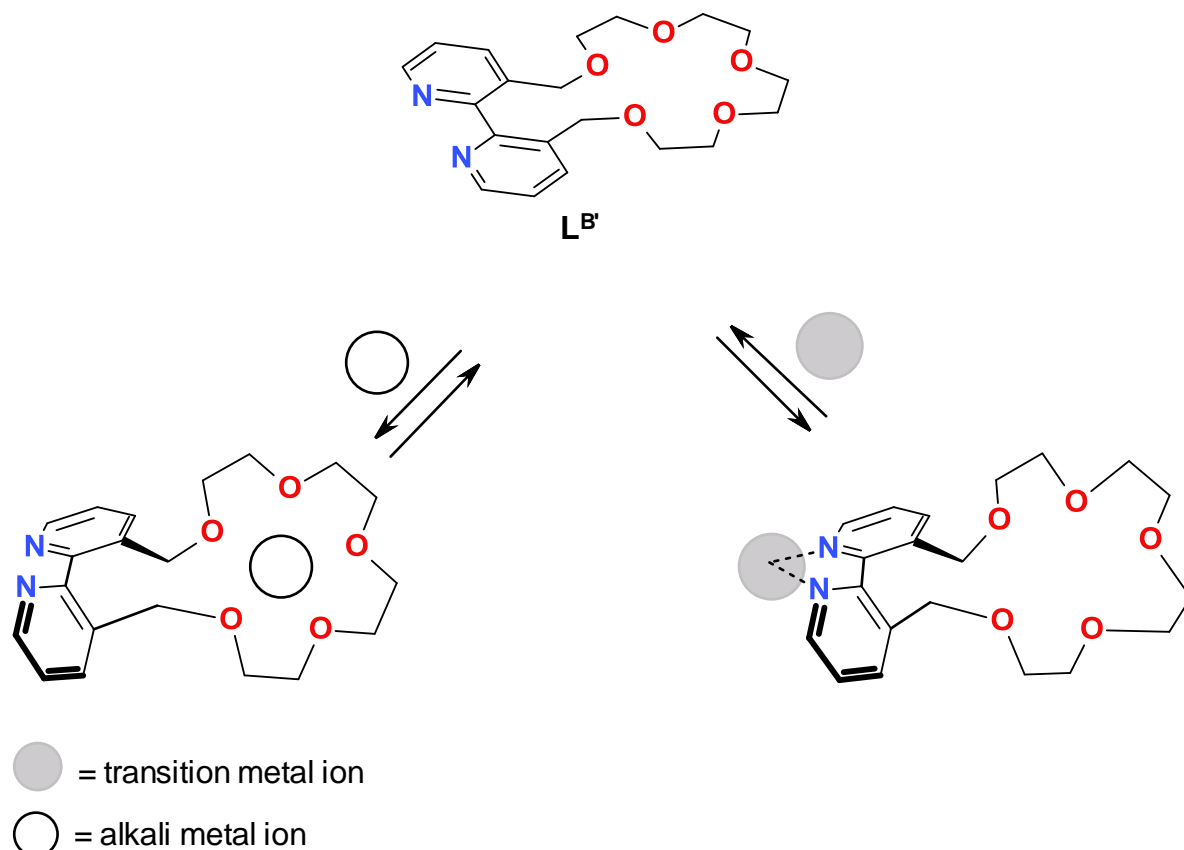


Figure 1.41 Representation of binding-induced conformational changes within a synthetic system¹¹⁴

In this example the allosteric effect was determined by ion transport experiments. Transport of ions, Li^+ , Na^+ , and K^+ , across a chloroform liquid membrane with $\text{L}^{\text{B}'}$ containing tungsten (W) was examined within a U-tube. The free macrocyclic crown was shown to preferentially transport K^+ , while the complex of $\text{L}^{\text{B}'}$ showed preferential transport of the smaller ions. This difference was attributed to the availability of the oxygen atom within the crown. The chelation of metal ions at the 2,2'-bipyridyl unit forces the aromatic groups towards co-planarity and consequently the oxygen atoms of the ether are directed away from one another. This means the oxygen atoms are no longer able to function as part of the ether cavity. Rebek and co-workers have provided numerous examples which beautifully demonstrate allosteric effects with increased selectivity with a goal to produce synthetic systems that better resemble those seen in nature. From this initial research supramolecular systems displaying allosteric effects have been investigated to advance these synthetic systems.

1.8.1 Ditopic ligands

The investigation of allosteric effects within supramolecular systems has allowed further diversification of the known architectures. Ligands are able to partition into distinct binding domains which influence the formation of the metallosupramolecular assembly. The ligands are thus designed and synthesised to contain different binding domains which give, upon reaction with metal ions, a desired supramolecular entity. The covalent information within the ligands can thus be selected to direct the system to a given architecture. The information is permanently contained within the covalent framework of the ligand once it has been synthesised, which can be thought of as a 'pre-programmed' component. A number of ditopic ligands have been reported, however, which allow the binding modes of the ligands to be altered or 'reprogrammed'. This is related to the allosteric effect demonstrated by Rebek *et al.* seen in the previous section.

A ditopic ligand reported by Rice *et al.*¹¹⁵ elegantly demonstrates the reprogramming of a dinuclear double helicate. The ligand, L^C , contains a potentially tetradentate pyridyl-thiazole chain and an additional crown ether binding site connecting the two halves of the ligand chain. Reaction of an equimolar amount of L^C and $Hg(ClO_4)_2 \cdot 3H_2O$ in acetonitrile resulted in the self-assembly of a dinuclear double helicate $[Hg_2(L^C)_2]^{4+}$. Addition of excess $NaClO_4$ to the complex give $[Hg_2(L^C)_2Na_2]^{6+}$. The Hg(II) centres have a distorted tetrahedral geometry from coordination of the two thiazole-pyridyl units, one from each ligand. The ligands are twisted around the bond between the central pyridyl rings. Both crown ethers partially coordinate sodium ions; the sodium ions are unable to coordinate all the oxygen atoms of the crown ether which is to be expected as the crown used is known to be too large to optimally coordinate sodium cations. In comparison, on reaction of the dimercury complex with excess $Ba(ClO_4)_2$ a mononuclear complex $[Hg(L^C)Ba]^+$ is produced. The ligand is near planar with a slight twist due to steric interactions between the methylene substituents on the central bipyridyl core. In this structure the Hg(II) centres display a distorted octahedral geometry from the nitrogen atoms of the two thiazole-pyridyl units of the ligand and two

perchlorate anions. The Ba(II) cation is ten-coordinate and bonded by all six oxygen atoms of the crown ether, with additional coordination to perchlorate anions. The Ba(II) ion is coordinated by all the oxygen atoms of the crown ether moiety demonstrating the better size match between this cation and crown (figure 1.42). This control over the self-assembly may be attributed to one of two factors; an electrostatic effect as coordination of barium to the helicate would produce a higher charged 8+ ion, consequently the disassembly of the double helicate to the mononuclear species lowers electrostatic repulsion and increases the entropy; alternatively, this change in structure may be due to an allosteric effect. Either way this demonstrates how ligand-binding domains may be altered or 'reprogrammed'.

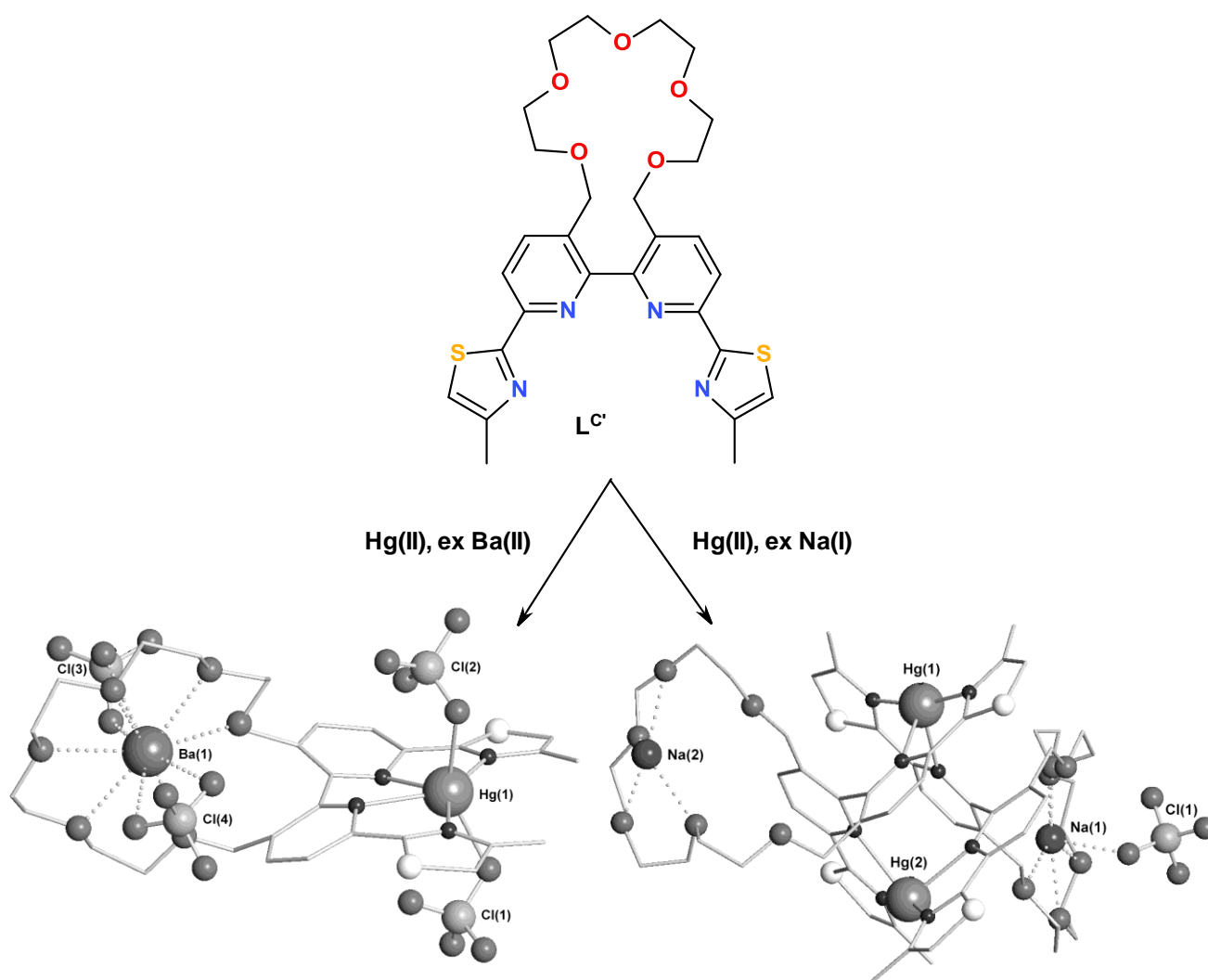


Figure 1.42 Ligand $L^{C'}$ and the two complex cations $[Hg_2(L^{C'})_2Na_2]^{6+}$ and $[Hg(L^{C'})Ba]^{4+115}$

These types of interactions are useful in the development of sensors, as the coordination of a guest is signalled at the secondary connected site. Sensors often consist of a selective coordination site, connected by a communication bridge to a secondary site which is capable of a physical response. A number of artificial allosteric receptors and catalysts are now known.^{116, 117}

1.9 Ligand design

Self-organisation and self-assembly, i.e. self-processes, are now a major theme of supramolecular chemistry. The incorporation of metal ions provides access to new and varied architectures, this subdivision becoming known as metallosupramolecular chemistry. Well-researched examples are the helicates; as seen previously an enormous quantity of research has been directed towards their synthesis and understanding of their formation. Self-organisation of a system occurs when the components converge to produce a larger, and generally more complicated, assembly.

Taking helicates as an example, the components within these assemblies are the metal ions and helicands (ligands which form helicates). The metal ions are selected as they possess, to some degree, known coordination geometries. Certain metals are known to form octahedral coordination compounds for example Zn(II) and Co(II), others form tetrahedral geometries such as Ag(I) and Cu(I). These two examples are the most commonly utilised geometries, however, the incorporation of lanthanides, which possess higher coordination numbers, is increasingly being employed^{118, 119}. The important aspect with regards to helicate formation is that the metal ion selected must be complementary to the binding domains within the ligand. Ligands are the organic component of the system; they must contain sufficient donor atoms to interact with the metal centres. Specifically, for a helicate the ligand must contain at least two binding sites which are positioned such that both sites within the ligand are unable to coordinate the same metal ion. The ligand employed can have a significant influence on the resulting architecture and potentially gives the supramolecular chemist some control over the assembly.

1.9.1 Ligand programming

Chemical systems with molecular building blocks which contain all the necessary information (size, shape, electronic properties) to selectively produce the desired architecture represent pre-programmed systems. Through self-processes; self-organisation and self-assembly, the molecular instructions contained within the components lead to the generation of a well-defined supramolecular entity. This concept of molecular information is seen as one of the basic principles within supramolecular chemistry.

Self-assembly may be directed towards a particular architecture based on the design of the ligand and coordination geometries of the metal ions. The processing of the same ligand information by different interaction algorithms, metal ions, allows the self-organization of different architectures, resulting in multiple expressions of the molecular information. An elegant example by Lehn *et al.* demonstrates how the molecular instructions within a ligand may generate different structures upon exposure to different metal ions. From previous research it was established that L^D , when treated with octahedral metal ions, provides a square [2x2] grid assembly,⁵³ and L^E gives dinuclear double helicate complexes with tetrahedral metal ions.⁷² By combining the binding domains of L^D and L^E a new ligand, L^F ,¹²⁰ was produced (figure 1.43). By designing this ligand it was hoped that, as the ligand contains both bidentate and tridentate binding sites, the assembly may be directed towards a different architecture by careful selection of metal centre, in contrast to previous investigations in which only one metal ion could be complexed by the ligand strand.¹²¹ A suspension of L^F in acetonitrile was treated with one equivalent of $[Cu(CH_3CN)_4]ClO_4$ and two equivalents of $Cu(ClO_4)_2 \cdot 6H_2O$. Addition to an aqueous solution of ammonium hexafluorophosphate produced a precipitate. Upon diffusion of benzene into a solution of the complex single crystals were obtained. X-ray structural determination revealed a large complex ion $[Cu_{12}(L^F)_4]^{20+}$ for the compound. The Cu(I) centres display a distorted tetrahedral coordination geometry while the Cu(II) centres have a severely distorted trigonal bipyramidal geometry. The ligands are wrapped around each other linking four double helical sections with 12 crossing points (figure 1.44).

The structure contains two types of duplexes of opposite helicity which are connected in an alternating fashion resulting in the formation of an achiral, or *meso*, form.

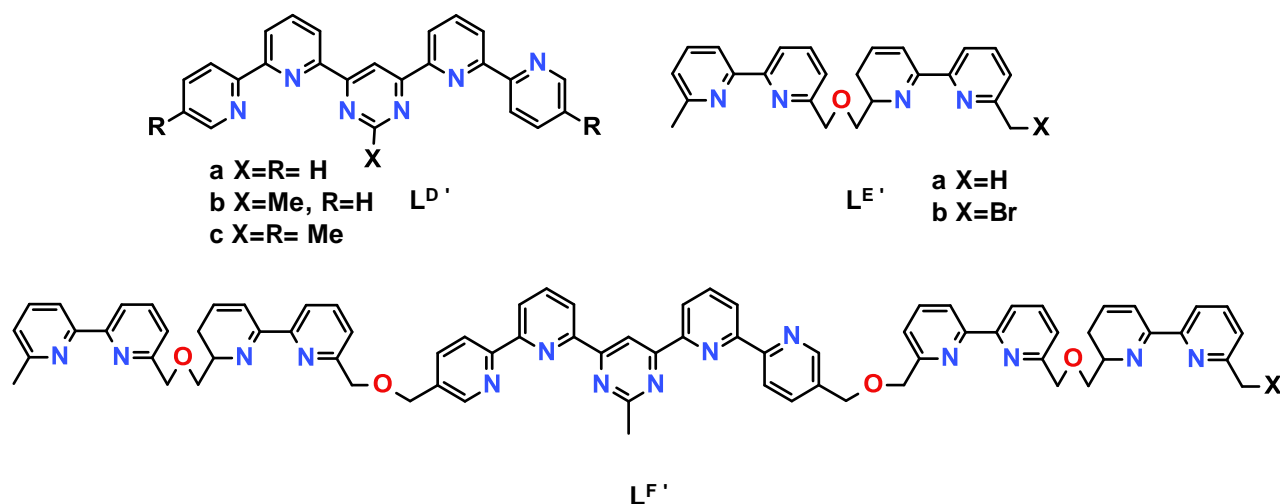


Figure 1.43 Ligands, $L^{D'}$ and $L^{E'}$, from previous research. Combination of these ligands produced a more complex ligand, $L^{F'}$

Reactions of $L^{F'}$ with Cu(I) and M(II) (M= Fe, Co, Ni, Cu) ClO_4^- salts in acetonitrile in a 1:2:1 ratio ($L^{F'}:\text{Cu(I)}:\text{M(II)}$) gave $[\text{M}_4\text{Cu}_8(L^{F'})_4](\text{ClO}_4)_{16}$ complexes. All the spectrometric results obtained for these structures point towards the formation of a complex with the structure shown in figure 1.44 which may be seen to combine the [2x2] grid (of $L^{D'}$) in the centre and four helicate units (of $L^{E'}$) at the corner of the central grid. This demonstrates the controlled generation of two different supramolecular architectures from the same ligand, $L^{F'}$, by processing of molecular information by different coordination algorithms, in this case different sets of metal ions.

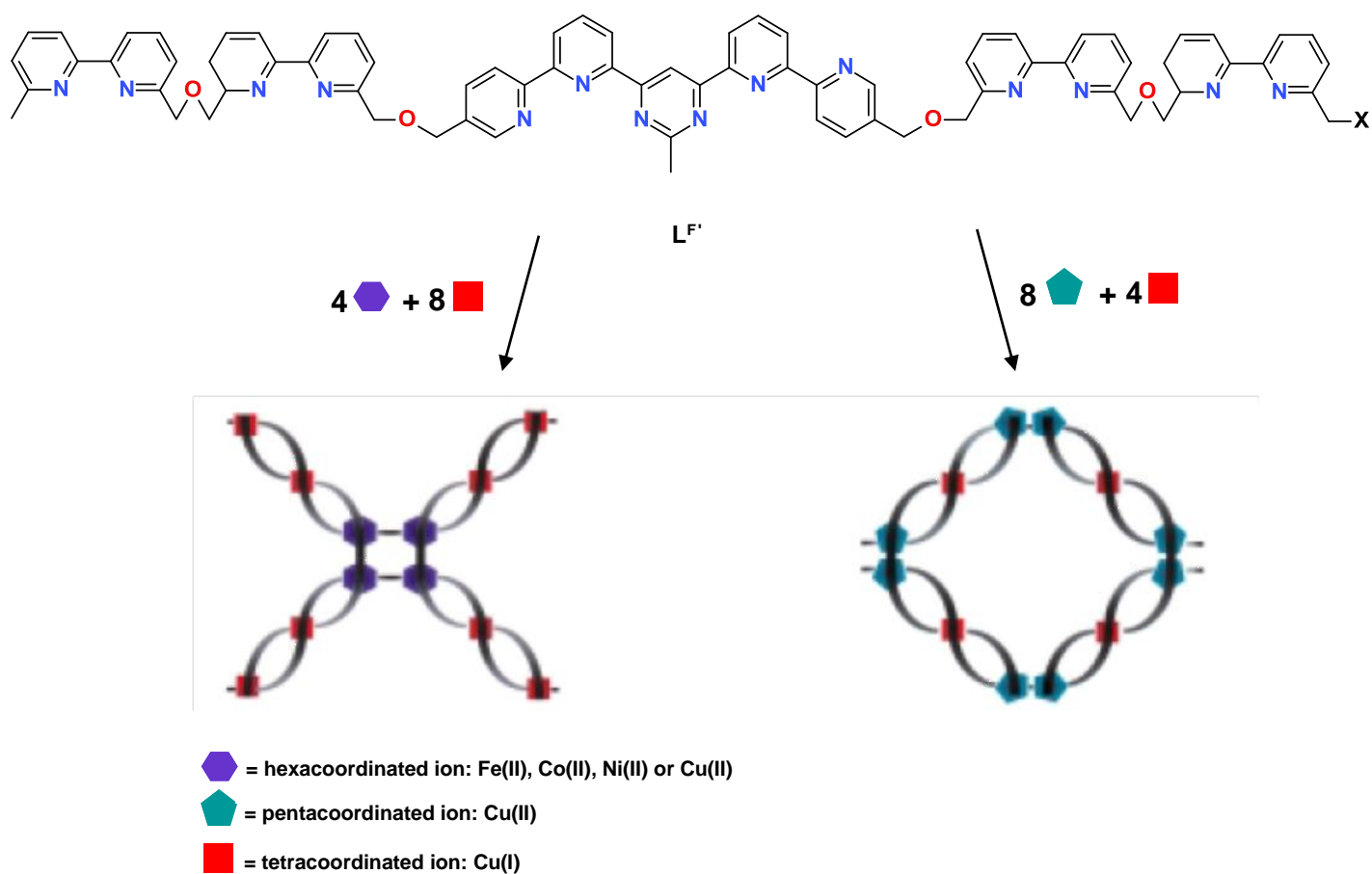


Figure 1.44 Self-assembly modes of ligand, $L^{F'}$, and metal ions of different coordination geometries¹²⁰

Constable and co-workers also produced a number of metallosupramolecular assemblies with sexipyridine showing that different metal ions can produce remarkably different structures depending on the stereochemical requirements of the metal centres.¹²² Rice *et al.* reported the synthesis of a new group of thiazole-containing polydentate ligands for the self-assembly of helicates with Cu(II) (figure 1.45).¹²³ In this instance the same metal ion is used and different ligands employed to produce different architectures. These ligands are of interest as the ligands naturally partition into distinct binding domains as adjacent thiazolyl units are unable to coordinate the same metal ion. Reaction of L^G and two equivalents of $\text{Cu}(\text{PF}_6)_2$ in acetone under an atmosphere of ethyl acetate produced crystals. X-ray structural determination showed two Cu(II) ions coordinated to three L^G ligands in a triple helical assembly with each metal ion in a pseudo-octahedral coordination geometry formed from three thiazole-

pyridyl unit from each of the ligand strands. In contrast reaction of L^H with $Cu(ClO_4)_2$ in acetonitrile gives double helicates, with the metal centres in a pseudo-octahedral arrangement by coordination of two thiazolyl-phenanthroline tridentate domains from each ligand. The thiazole ligand examples shown here are only a few of the ligands which have been produced which contain this natural partition for the self-assembly of helicates.^{124, 125}

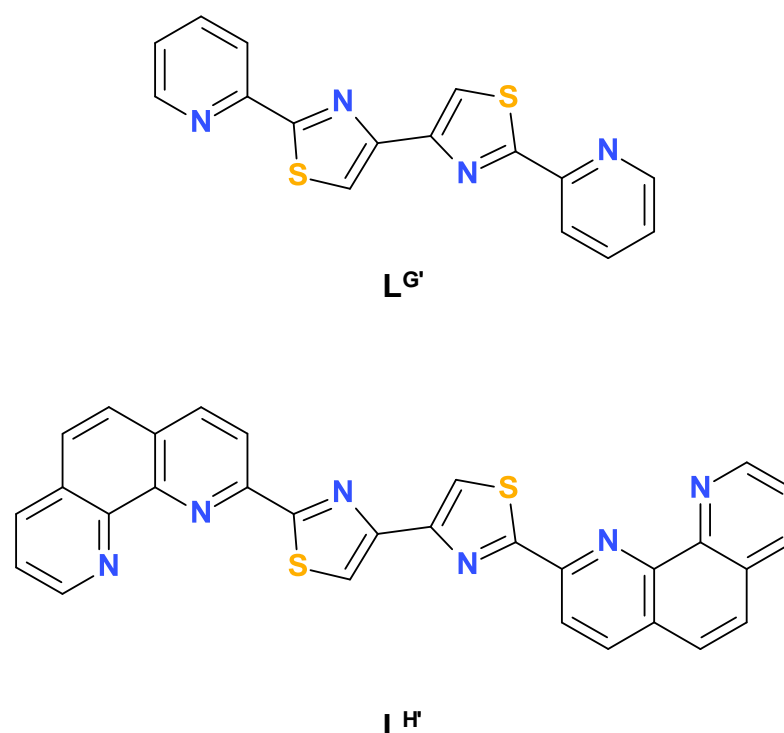


Figure 1.45 Thiazole-containing ligands which self-assemble into different helicates, $L^{G'}$ triple helicate and L^H double helicate, upon coordination to $Cu(II)$

As well as the examples shown here there are numerous others of programmed assemblies which display higher levels of control over the final architecture dependent on the design of the ligand and metal centres employed. As seen previously it is possible to produce circular helicates and the chirality of a helicate may also be controlled, in both linear and circular helicates, by incorporating chiral ligands.

1.9.2 Ligand recognition

The self-assembly of inorganic helicates is clearly an area of significant interest within supramolecular chemistry. This self-assembly has been linked to processes within biological systems in particular, in this case, the formation of the DNA double helix. The self-assembly of synthetic helical systems has thus received rigorous investigation. The basic features for their formation, in addition to the requirements of complementary molecular components, occur with positive cooperativity¹²⁶ and self-recognition.¹²⁷

Krämer *et al.* elegantly demonstrated this feature of self-recognition within helicate assembly. From a mixture of 6,6'- connected oligo(2,2'-bipyridine) ligands strands which contained a varying number of 2,2'-bipyridine subunits (between two and five) it was shown that coordination with copper(I) ions resulted in the formation of homostranded double helicates (figure 1.46) without significant crossover. All combinations of ligands tried gave the corresponding double helicates, indicating that helicate self-assembly occurs with self-recognition. This introduces the idea that ligands are able to discriminate between self and non-self; thus species with like ligands are strongly preferred over species with unlike ligands.¹²⁷

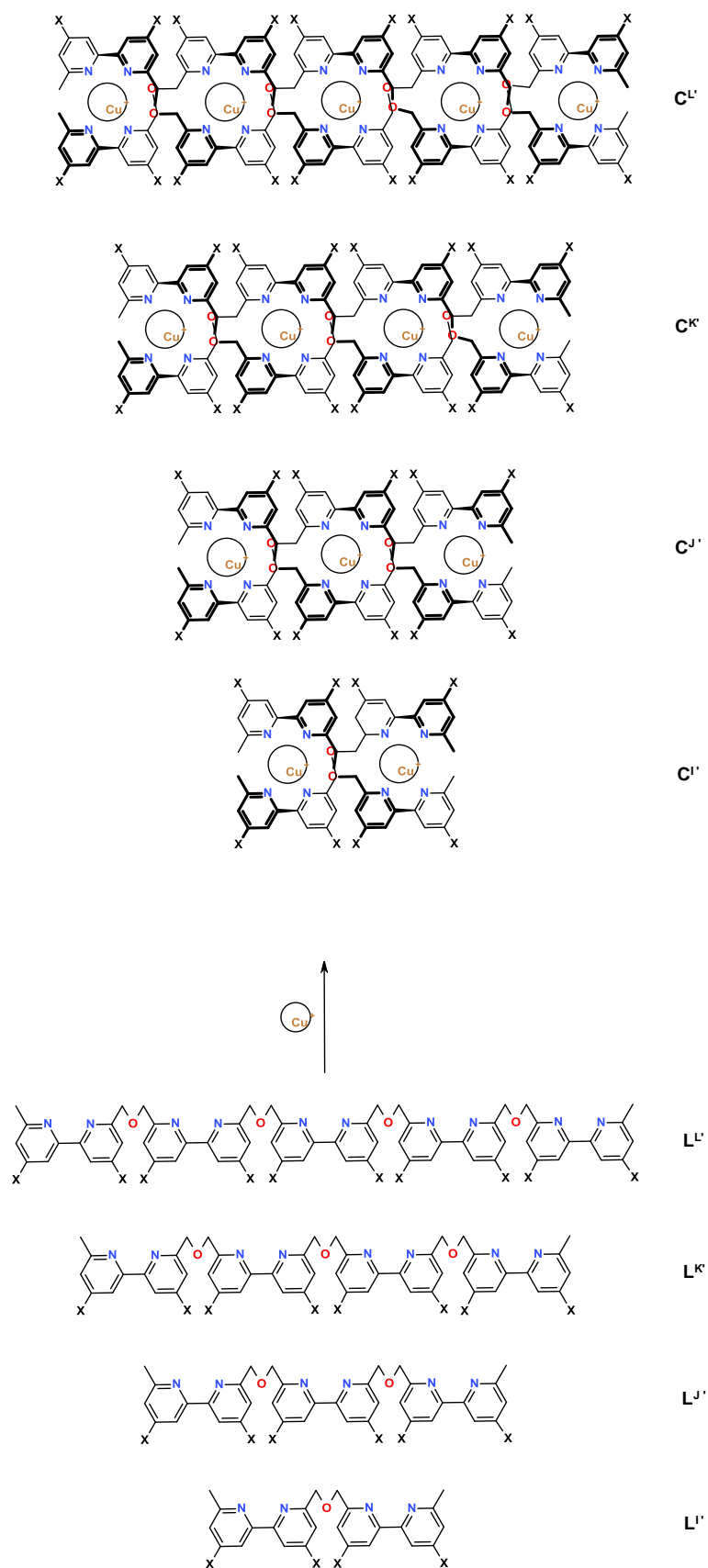


Figure 1.46 Self-recognition in the self-assembly of double helicates from a mixture of oligobipyridine ligand strands

In addition to the recognition of similar ligands a mixture of two tris-bipyridine ligands L^J and L^S (containing different bridging units) react with copper(I) and nickel(II) ions to form only the double helicate and the triple helicate (figure 1.47).¹²⁷ The previously reported 5,5'-disubstituted ligand strand (L^S) was shown to form a triple helicate with octahedrally-coordinated Ni(II) ions.¹²⁸ This architecture results from the steric programming of the ligand and the stereochemical information provided by the metal ion. This also applies to the double helicate produced from L^J and tetrahedral metal ions. Side-by-side operation of two programmed molecular systems led to the self-assembly of two discrete helical complexes from a mixture. As only discrete helicates resulted these systems are sufficiently instructed to produce programmed structures even with alteration of the parameters for self-assembly.

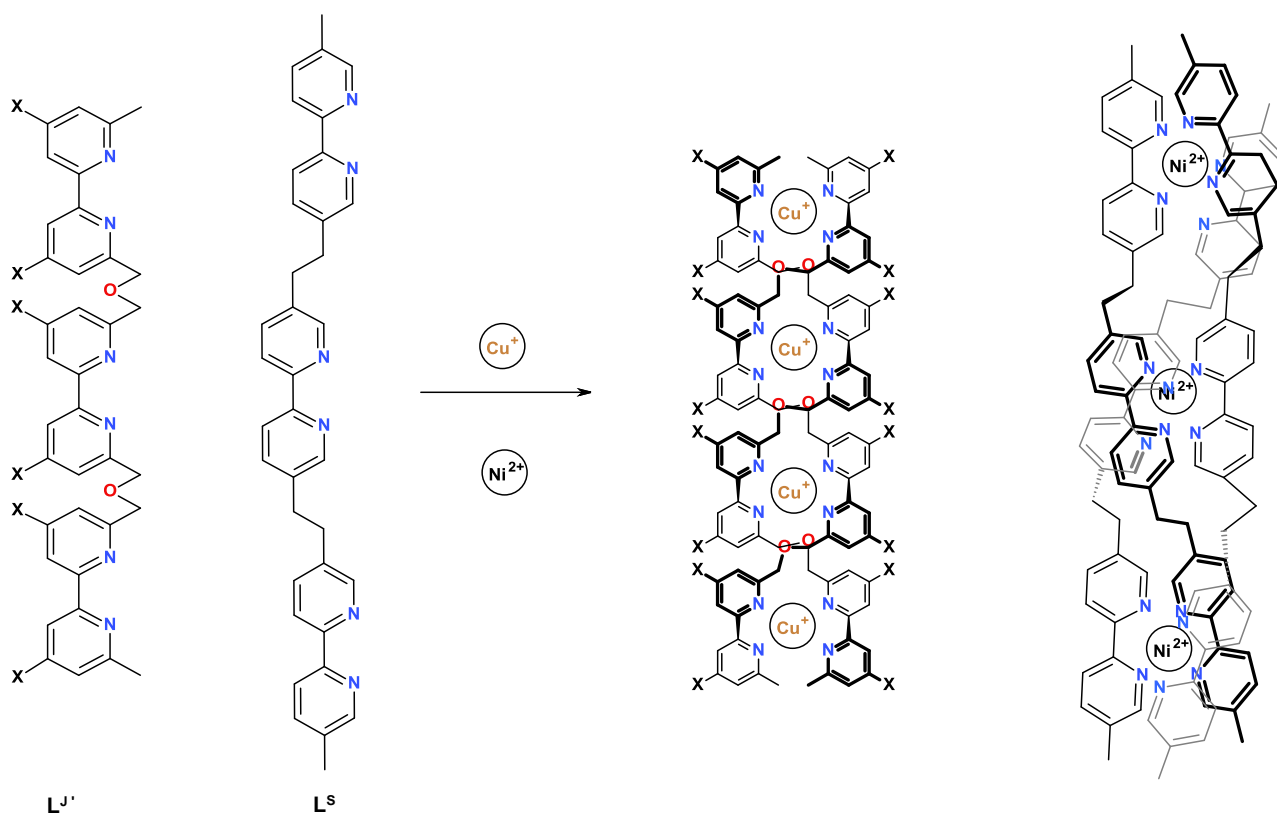


Figure 1.47 Self-recognition in the self-assembly of a double helicate and triple helicate from a mixture of oligobipyridine ligand strands (L^S , L^J) with Cu(I) and Ni(II)

Described in this work is the synthesis and coordination chemistry of 17 novel ligands. These ligands were designed in such a way as to direct the self-

assembly of the resulting supramolecular architecture. Chapter two exhibits an example of a pentanuclear circular helicate, similar to circular helicates mentioned previously. Chapter three illustrates how the interplay between ligand strand and metal ion size can control the formation of helicates and *meso*-helicate assemblies. Finally chapter four demonstrates how lanthanide metal ions can be incorporated within supramolecular systems; in this case providing dinuclear double stranded helicates.

2. Diastereoselective assembly of pentanuclear circular helicates

Described in this chapter is the synthesis and coordination chemistry of mixed N-donor and O-donor ligands which assemble into circular helicates upon exposure to zinc metal centres. These ligands contain two tridentate donor domains separated by a 1,3-phenylene spacer unit. The first ligand, L^1 , is a symmetrical ligand which can potentially act as a hexadentate donor; however, the 1,3-phenylene unit effectively partitions the ligand into two tridentate donor domains. The other ligands are essentially the same as L^1 with the difference being the terminal functional groups. For $L^2 - L^4$ variation of the terminal group led to the incorporation of amino acid esters and the potential to control the stereoselectivity of the resulting chiral supramolecular architectures (figure 2.1).

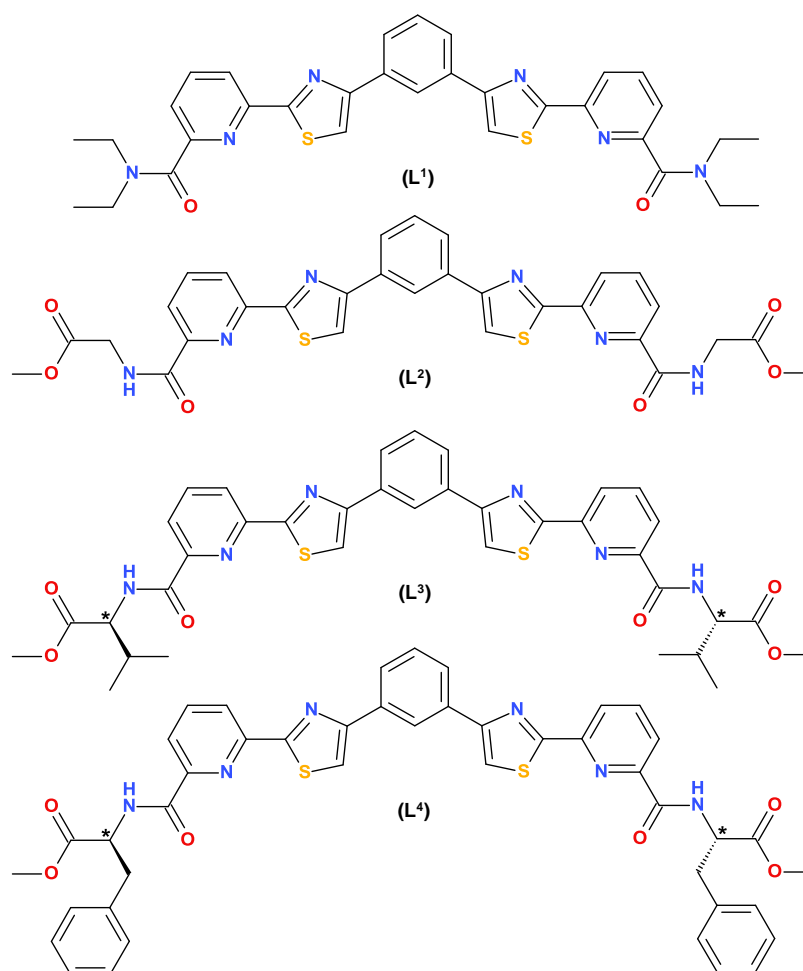


Figure 2.1 New class of helicates $L^1 - L^4$

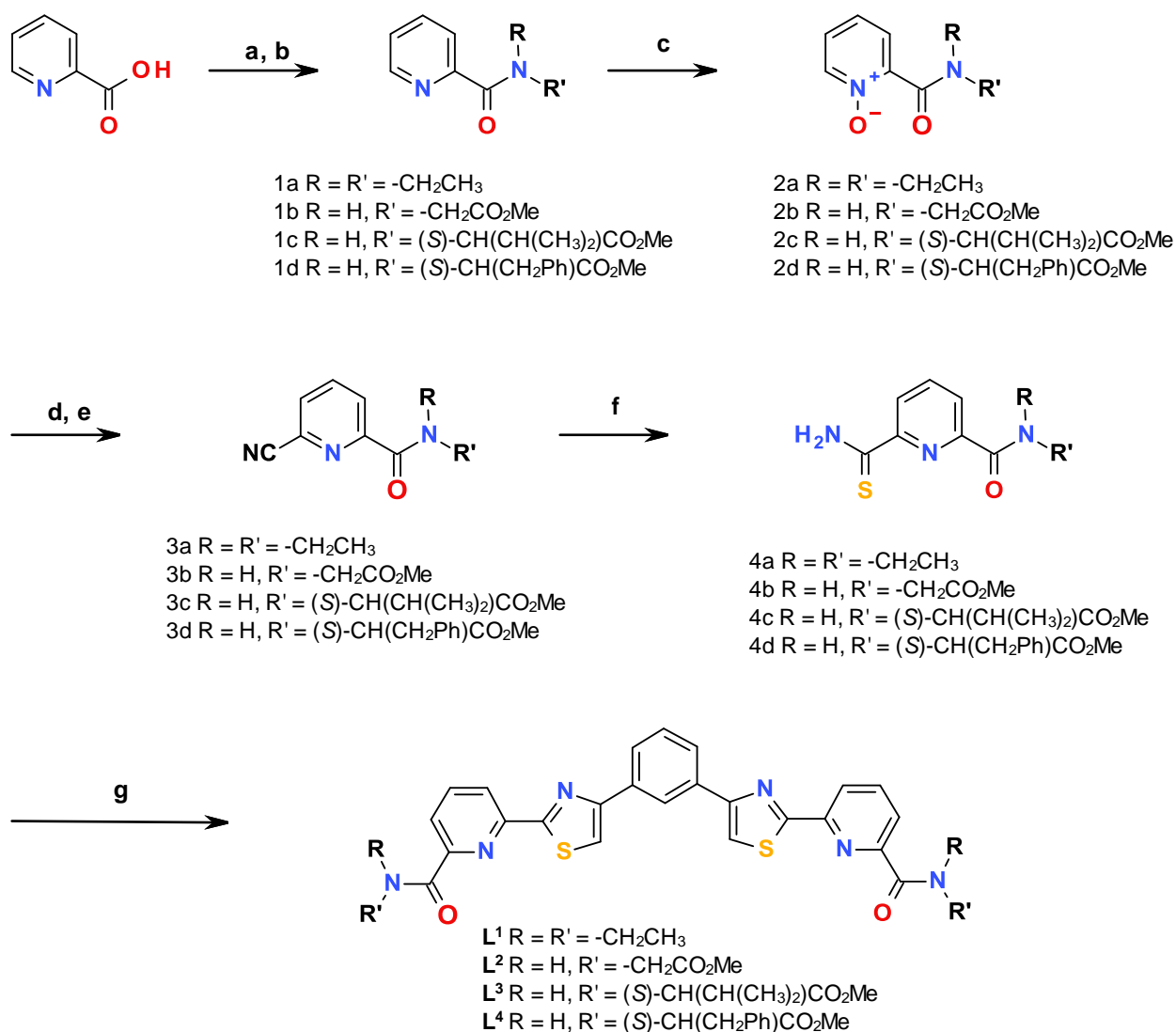
2.1 Ligand synthesis

The ligands, **L**¹ – **L**⁴, were synthesised in an analogous fashion via a multi-step synthetic process (Scheme 2.1).

2.1.1 Synthesis of **L**¹

The synthesis of the ligand, **L**¹, was achieved by activation of picolinic acid with oxalyl chloride followed by reaction with diethylamine to give, after liquid-liquid extraction, a crude product. By dissolving in ether and using decolourising charcoal the pure amide was obtained as a yellow oil (**1a**). Reaction of the amide with *m*CPBA in DCM was monitored by TLC, until all the amide was consumed. Purification by column chromatography gave the corresponding N-oxide as a white solid (**2a**). The ¹H NMR spectrum for the N-oxide should contain the same signals as those seen for **1a** (figure 2.2, 1a) as the compounds contain the same protons, however, the presence of the oxygen atom dramatically alters the aromatic region of the ¹H NMR spectrum for **2a** (figure 2.2, 2a). Methylation of the N-oxide was achieved by dissolving the solid in dimethyl sulfate and heating for 24 hours. After a wash with ether the resulting oil was dissolved in deionised water and neutralised with NaHCO₃. Addition of sodium cyanide and stirring at room temperature for five minutes gave a yellow oil; extraction into DCM gave the 6-cyanopicolinamide species, **3a**. Formation of the product was confirmed using ¹H NMR by the disappearance of one aromatic signal corresponding to the loss of a proton from the pyridine ring (figure 2.2, 3a). The corresponding thioamide, **4a**, was produced upon exposure of the cyanopicolinamide to hydrogen sulfide which was isolated upon filtration of the resulting yellow precipitate. Confirmation of the thioamide was obtained from the ¹H NMR spectrum which shows two new broad singlet peaks (9.31 and 7.67 ppm) corresponding to the -NH₂ protons (figure 2.2, 4a). A solution of the thioamide (**4a**) and 1,3-di(α-bromoacetyl)benzene (**6**) was refluxed for 3 hours in the final step of the synthesis. The resulting precipitate was isolated *via* filtration giving the ligand **L**¹ (figure 2.2) as a white solid which was subsequently characterized by ¹H NMR, ESI-MS and HR ESI-MS. The ¹H NMR spectrum showed a total of 7

aromatic signals as well as 4 aliphatic signals corresponding to the 8 ethyl and 12 methyl protons (figure 2.2, **L**¹). ESI-MS showed an ion at *m/z* 619 which is consistent with [**L**¹+Na]⁺.



Scheme 2.1 Synthesis of **L**¹ – **L**⁴.

Reagents and conditions: a) C₂O₂Cl₂, Et₃N, DCM 0 °C; b) RR'NH, Et₃N, DCM, RT; c) *m*CPBA, DCM, RT; d) (MeO)₂SO₂, 60 °C; e) NaHCO₃, NaCN, H₂O RT; f) H₂S, Et₃N, EtOH, RT; g) 1,3-di(α-bromoacetyl)benzene (**6**), EtOH, reflux.

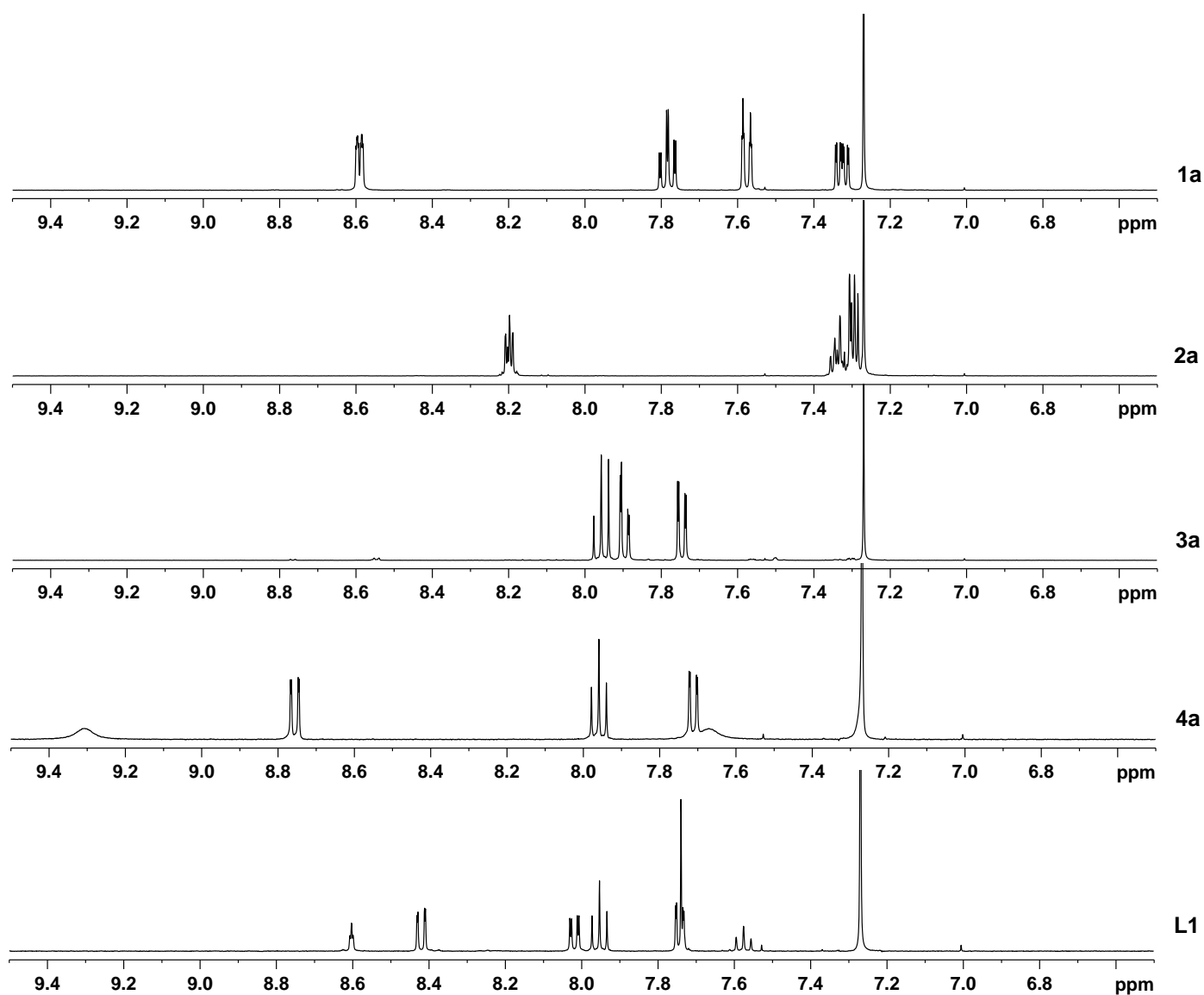


Figure 2.2 Aromatic regions in the ^1H NMR (400 MHz, CDCl_3) spectra of (1a) picolinamide derivative, (2a) picolinamide-*N*-oxide, (3a) 6-cyanopicolinamide, (4a) picolinamide-6-thioamide and Ligand 1 (L^1)

2.1.2 Synthesis of $\text{L}^2 - \text{L}^4$

For the synthesis of $\text{L}^2 - \text{L}^4$ methods analogous to that described for L^1 were employed. However, for L^2 , glycine methyl ester was used in place of diethylamine in step **b** of the synthesis (Scheme 2.1). For the two remaining ligands chiral methyl esters were used, for L^3 *S*-valine methyl ester and L^4 *S*-phenylalanine methyl ester substituted the diethylamine used for L^1 . This resulted in variation of the terminal functionality of the four ligands. For each subsequent ligand the structures were confirmed by ^1H NMR, ESI-MS and HR ESI-MS.

2.2 Coordination chemistry

2.2.1 Complexes of L^1 with zinc(II)

Reaction of L^1 with an equimolar amount of $Zn(CF_3SO_3)_2$ in acetonitrile gave a colourless solution. Analysis by ESI-MS gave an ion at m/z 2251 corresponding to the pentanuclear helicate complex $\{[Zn_5(L^1)_5](CF_3SO_3)_8\}^{2+}$ with some additional peaks observed likely due to fragmentation of the parent pentanuclear species. The 1H NMR spectrum shows 9 signals, with seven aromatic signals consistent with the helical wrapping of a helicate, as the signals have shifted with respect to the free ligand. Slow diffusion of ethyl acetate into the acetonitrile complex solution resulted in the formation of X-ray quality colourless crystals. The single crystal X-ray structure confirmed the formation of the pentanuclear species $[Zn_5(L^1)_5]^{10+}$ which crystallised in triclinic space group $P-1$ (figure 2.3).ⁱ

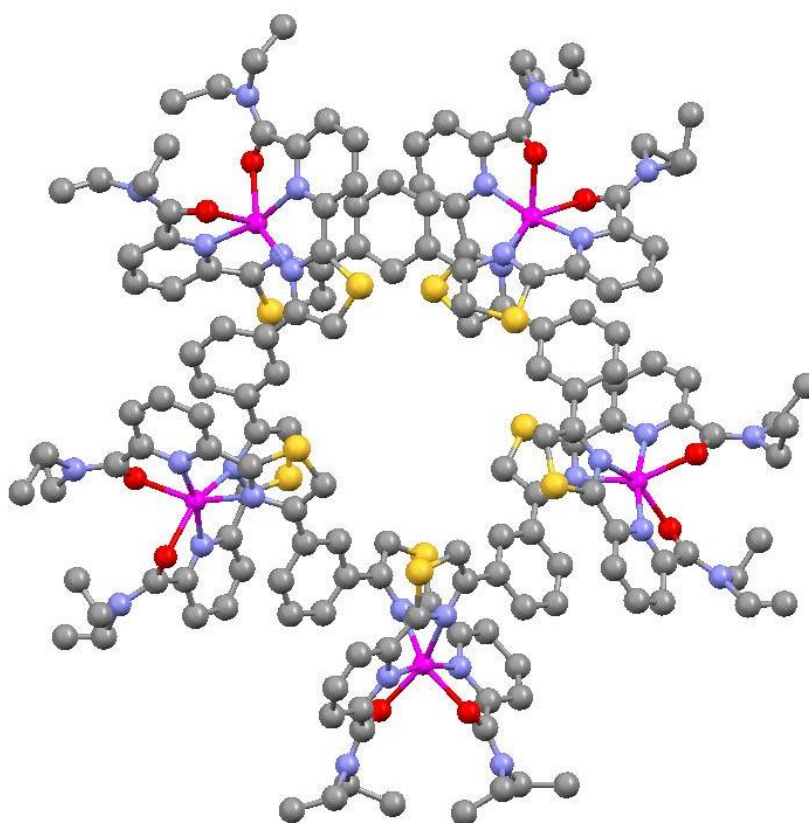


Figure 2.3 Solid state structure of the complex cation $[Zn_5(L^1)_5]^{10+}$

ⁱ X-ray data recorded by Professor Craig Rice with additional structure refinements contributed by Dr. Thomas Riis-Johannessen

The crystal structure confirms that in the solid state the ligand, L^1 , and Zn(II) ions self-assemble to form a pentanuclear circular helicate in which the ligand strand partitions into two tridentate donor domains, separated by the 1,3-phenylene spacer unit (figure 2.3). The two tridentate donor domains of each ligand coordinate two different metal ions. Each of the five Zn(II) ions is six-coordinate arising from the coordination of two tridentate N,N,O-domains (Zn–N distances: 2.029(7) – 2.261(7) Å ; Zn–O distances: 2.105(6) – 2.202(6) Å). The 1,3-phenylene spacers bridge the tridentate domains in an “over-and-under” conformation, giving rise to a helical cyclic oligomer in contrast to a “face-to-face” arrangement associated with grid-like arrays. Selected bond lengths and angles for the complex are shown in tables 2.1 and 2.2.

Bond	Bond Length (Å)	Bond	Bond Length (Å)
Zn(1)-N(130)	2.061(7)	Zn(3)-O(297)	2.160(8)
Zn(1)-N(150)	2.071(7)	Zn(3)-N(310)	2.214(7)
Zn(1)-O(137)	2.138(6)	Zn(3)-N(260)	2.223(8)
Zn(1)-O(157)	2.138(6)	Zn(4)-N(10)	2.062(6)
Zn(1)-N(124)	2.192(7)	Zn(4)-N(80)	2.071(6)
Zn(1)-N(174)	2.204(7)	Zn(4)-O(87)	2.143(6)
Zn(2)-N(200)	2.032(7)	Zn(4)-O(17)	2.175(5)
Zn(2)-N(220)	2.062(8)	Zn(4)-N(30)	2.209(6)
Zn(2)-O(227)	2.105(6)	Zn(4)-N(104)	2.261(7)
Zn(2)-O(207)	2.202(6)	Zn(5)-N(60)	2.029(7)
Zn(2)-N(240)	2.221(7)	Zn(5)-N(340)	2.065(7)
Zn(2)-N(194)	2.236(8)	Zn(5)-O(347)	2.146(6)
Zn(3)-N(270)	2.044(8)	Zn(5)-O(67)	2.171(5)
Zn(3)-N(290)	2.049(8)	Zn(5)-N(50)	2.204(6)
Zn(3)-O(277)	2.153(7)	Zn(5)-N(330)	2.222(6)

Table 2.1 Selected bond lengths (Å) for the complex cation $[Zn_5(L^1)_5]^{10+}$

Bond	Angle (°)	Bond	Angle (°)
N(130)-Zn(1)-N(150)	162.7(3)	O(277)-Zn(3)-N(310)	99.6(3)
N(130)-Zn(1)-O(137)	75.2(3)	O(297)-Zn(3)-N(310)	150.9(3)
N(150)-Zn(1)-O(137)	91.4(3)	N(270)-Zn(3)-N(260)	76.6(3)
N(130)-Zn(1)-O(157)	94.6(3)	N(290)-Zn(3)-N(260)	114.6(3)
N(150)-Zn(1)-O(157)	74.6(3)	O(277)-Zn(3)-N(260)	150.6(3)
O(137)-Zn(1)-O(157)	91.5(3)	O(297)-Zn(3)-N(260)	99.9(3)
N(130)-Zn(1)-N(124)	76.0(3)	N(310)-Zn(3)-N(260)	83.7(3)
N(150)-Zn(1)-N(124)	118.6(3)	N(10)-Zn(4)-N(80)	169.7(3)
O(137)-Zn(1)-N(124)	149.8(3)	N(10)-Zn(4)-O(87)	100.2(2)
O(157)-Zn(1)-N(124)	99.8(3)	N(80)-Zn(4)-O(87)	75.7(2)
N(130)-Zn(1)-N(174)	116.2(3)	N(10)-Zn(4)-O(17)	76.0(2)
N(150)-Zn(1)-N(174)	76.4(3)	N(80)-Zn(4)-O(17)	94.1(2)
O(137)-Zn(1)-N(174)	99.8(3)	O(87)-Zn(4)-O(17)	85.4(2)
O(157)-Zn(1)-N(174)	149.0(3)	N(10)-Zn(4)-N(30)	76.1(3)
N(124)-Zn(1)-N(174)	84.8(3)	N(80)-Zn(4)-N(30)	113.9(2)
N(200)-Zn(2)-N(220)	170.1(3)	O(87)-Zn(4)-N(30)	102.2(2)
N(200)-Zn(2)-O(227)	98.6(3)	O(17)-Zn(4)-N(30)	152.0(2)
N(220)-Zn(2)-O(227)	75.6(3)	N(10)-Zn(4)-N(104)	109.8(2)
N(200)-Zn(2)-O(207)	75.2(3)	N(80)-Zn(4)-N(104)	75.1(2)
N(220)-Zn(2)-O(207)	96.3(2)	O(87)-Zn(4)-N(104)	149.9(2)
O(227)-Zn(2)-O(207)	87.9(3)	O(17)-Zn(4)-N(104)	103.7(2)
N(200)-Zn(2)-N(240)	111.2(3)	N(30)-Zn(4)-N(104)	83.4(2)
N(220)-Zn(2)-N(240)	75.4(3)	N(60)-Zn(5)-N(340)	167.9(3)
O(227)-Zn(2)-N(240)	150.1(3)	N(60)-Zn(5)-O(347)	96.7(3)
O(207)-Zn(2)-N(240)	102.6(2)	N(340)-Zn(5)-O(347)	75.3(2)
N(200)-Zn(2)-N(194)	77.7(3)	N(60)-Zn(5)-O(67)	75.1(3)
N(220)-Zn(2)-N(194)	111.1(3)	N(340)-Zn(5)-O(67)	95.3(2)
O(227)-Zn(2)-N(194)	100.5(3)	O(347)-Zn(5)-O(67)	88.2(3)
O(207)-Zn(2)-N(194)	152.6(3)	N(60)-Zn(5)-N(50)	76.4(3)
N(240)-Zn(2)-N(194)	83.1(2)	N(340)-Zn(5)-N(50)	113.6(2)
N(270)-Zn(3)-N(290)	166.5(4)	O(347)-Zn(5)-N(50)	100.8(2)
N(270)-Zn(3)-O(277)	75.2(3)	O(967)-Zn(5)-N(50)	151.0(3)
N(290)-Zn(3)-O(277)	94.5(3)	N(60)-Zn(5)-N(330)	113.7(3)
N(270)-Zn(3)-O(297)	96.1(3)	N(340)-Zn(5)-N(330)	75.3(3)

Bond	Angle (°)	Bond	Angle (°)
N(290)-Zn(3)-O(297)	75.1(3)	O(347)-Zn(5)-N(330)	149.3(3)
O(277)-Zn(3)-O(297)	91.3(3)	O(67)-Zn(5)-N(330)	103.2(2)
N(270)-Zn(3)-N(310)	112.7(3)	N(50)-Zn(5)-N(330)	83.0(2)
N(290)-Zn(3)-N(310)	77.2(3)		

Table 2.2 Selected bond angles (°) for the complex cation $[\text{Zn}_5(\text{L}^1)_5]^{10+}$

The ligand, L^1 , contains two tridentate N-N-O donor domains separated by a phenylene spacer unit (figure 2.4). The incorporation of a 1,3-phenylene spacer unit has been shown to be a robust method for the successful synthesis of circular helicates.^{107, 108} The inter-ligand steric and/or electrostatic interactions between the protons present on the central phenylene units are an important factor which directs the assembly towards the formation of the more complex circular helicate instead of the thermodynamically more stable linear dinuclear helicate. The proximity of the phenylene protons is in turn controlled by the metal ion radii.

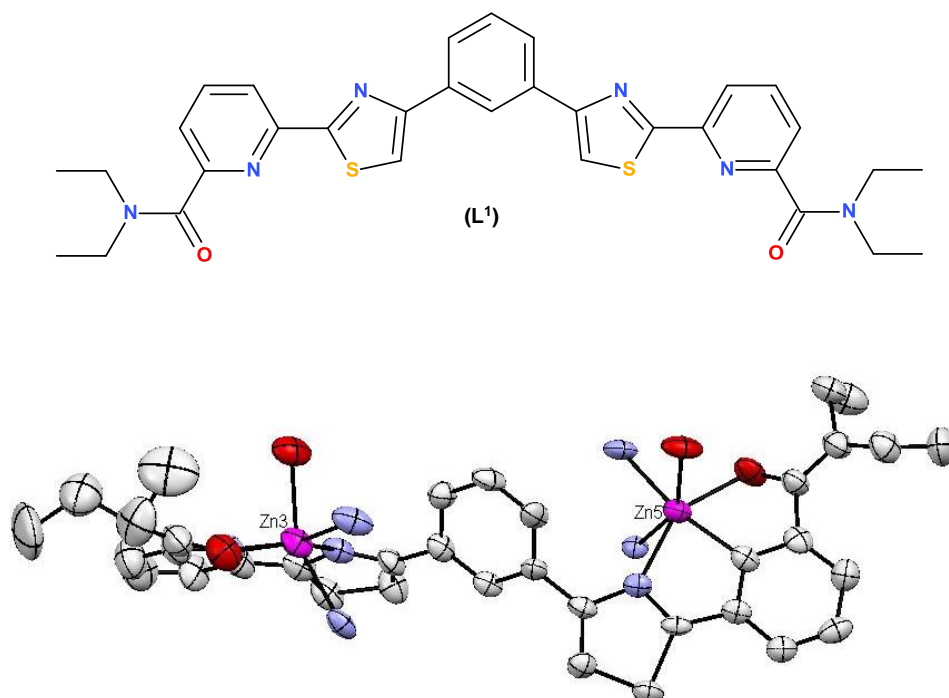


Figure 2.4 Structure of L^1 (i) diagram showing the two tridentate domains separated by the a 1,3-phenylene space unit and (ii) the partitioning seen within the crystal structure for L^1 .

As can be seen in the space-filling diagram (figure 2.5) of the pentanuclear helicate for L^1 there is a cavity within the complex cation; this is occupied by triflate anions. From previous research the anions have been shown to play major roles in the self-assembly and can influence the structure of the final complex. Recent research by Rice *et al.*, however, has shown there was no change to the ^1H NMR spectrum of a similar complex containing L^u (figure 1.36) upon addition of other anions, even when an excess of anion was added.

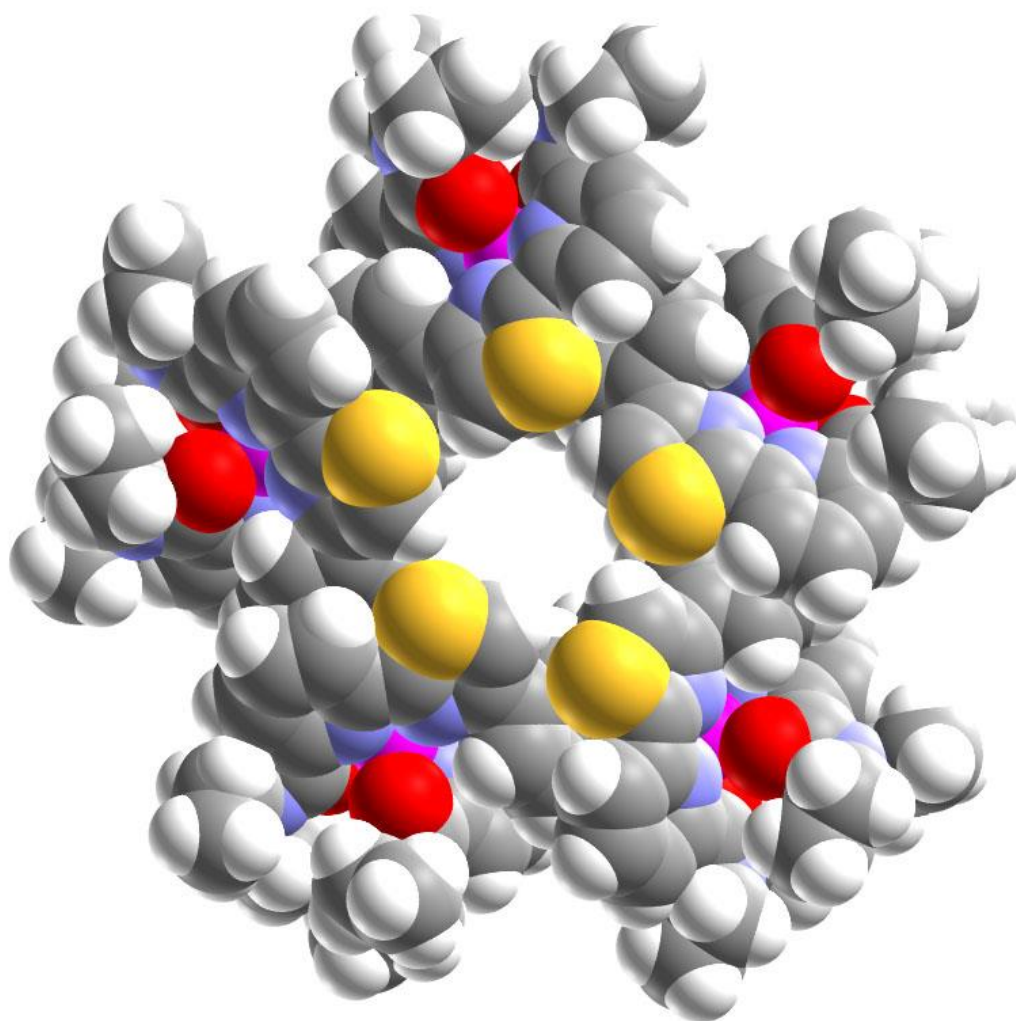


Figure 2.5 Space-filling picture of L^1 showing atoms with their van der Waal's radii

2.3 Solution studies

2.3.1 Solution state characterisation of $[\text{Zn}_5(\text{L}^1)_5]^{10+}$

The one-dimensional ^1H NMR spectrum of a CD_3NO_2 solution of $[\text{Zn}_5(\text{L}^1)_5]^{10+}$ shows the expected 9 resonances for a complex of D_5 symmetry (figure 2.6). Four of the seven aromatic signals, corresponding to the pyridyl and thiazole protons, are present between 7.0 and 8.4 ppm. The three protons of the bridging phenylene unit, however, resonate at much lower frequency (5.8–7.0 ppm). This has been observed previously in related circular helicates and has been ascribed to the close proximity of the central phenylene rings to the pyridyl-thiazole domains (average centroid---centroid distance of 3.87 Å). The protons of the phenylene spacer in the complex, $[\text{Zn}_5(\text{L}^1)_5]^{10+}$, are exposed to the shielding ring currents produced by the aromatic heterocycles of adjacent ligand strands, which explains the unusually low chemical shifts. This phenomenon is thus a useful diagnostic tool for the confirmation of helical wrapping in linear and circular helicates.

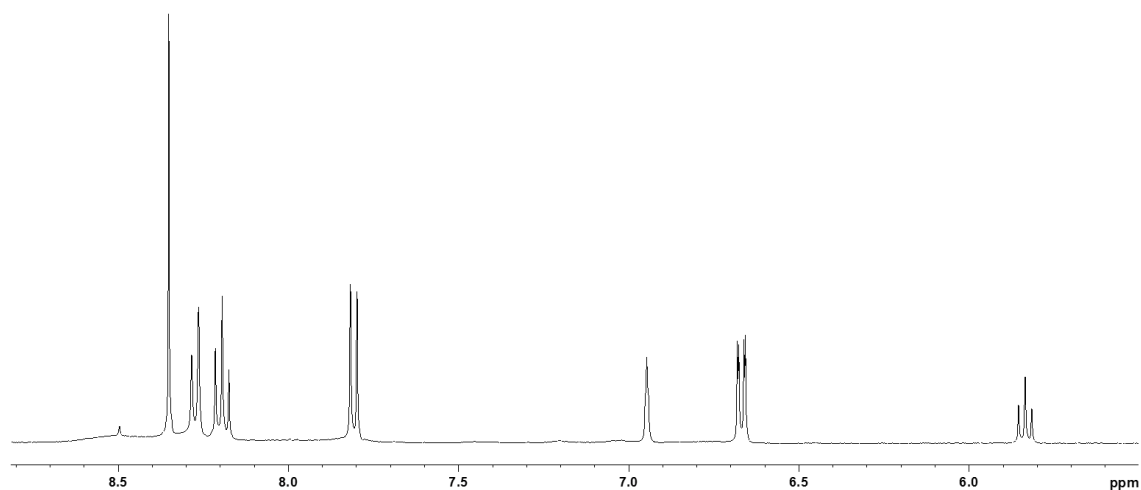


Figure 2.6 Aromatic region in the ^1H NMR (400 MHz, CD_3NO_2) spectrum of L^1 with $\text{Zn}(\text{II})$.

As stated briefly the ESI-mass spectrum of the L^1 complex with Zn(II) is also consistent with the formation of the pentanuclear species in the solution/gas phase showing ions at m/z 2251 corresponding to $\{[Zn_5(L^1)_5](CF_3SO_3)_8\}^{2+}$, as well as other ions at m/z 2732 and 1771 corresponding to $\{[Zn_3(L^1)_3](CF_3SO_3)_5\}^+$ and $\{[Zn_4(L^1)_4](CF_3SO_3)_6\}^{2+}$ respectively (figure 2.7). Other peaks observed corresponding to smaller di- or mononuclear species were also present; however, these species are likely due to fragmentation of the parent species.¹⁰⁸

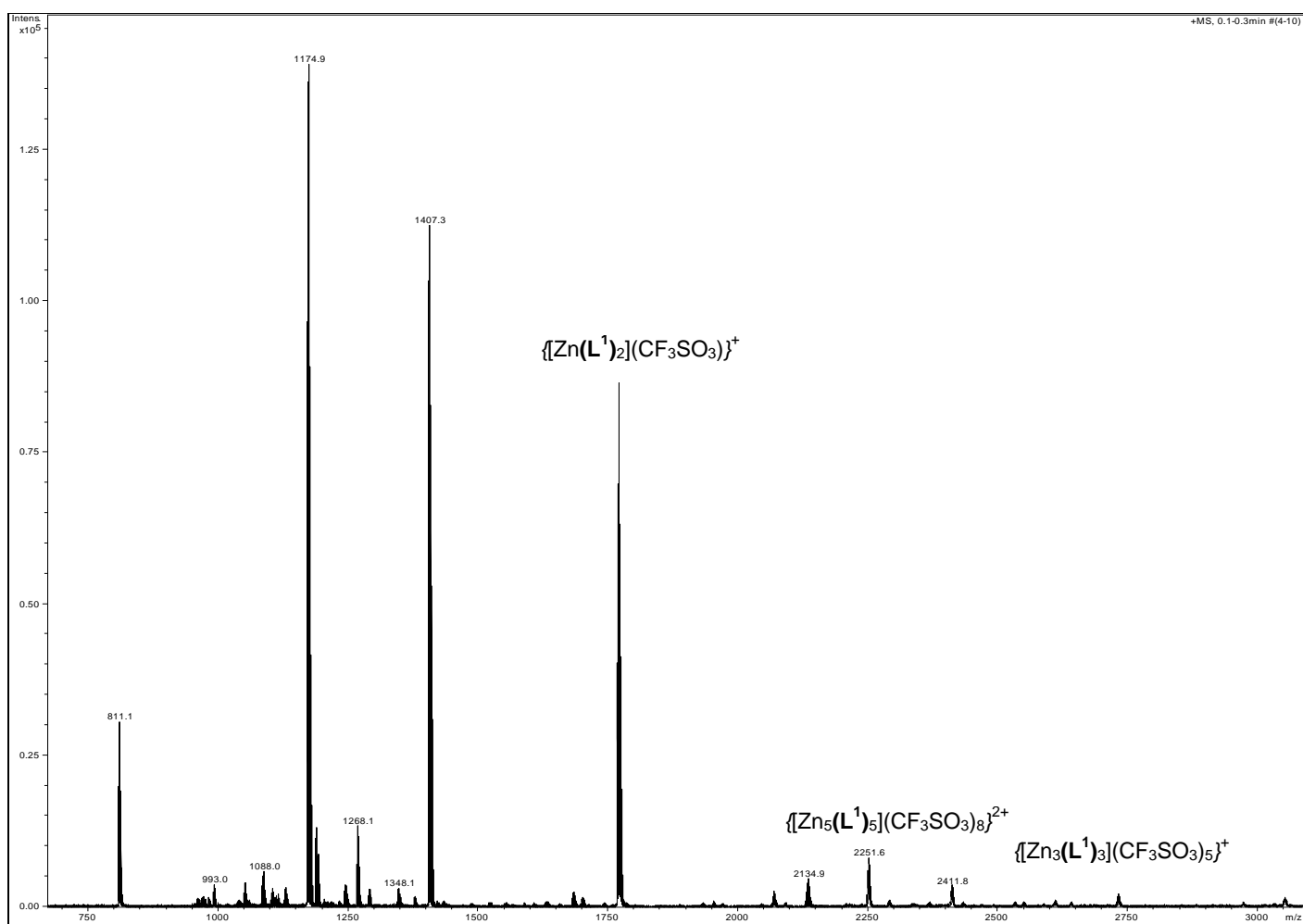


Figure 2.7 ESI-MS spectrum of $[Zn_5(L^1)_5](CF_3SO_3)_{10}$

2.3.2 Solution state characterisation of L^2-L^4

As the structure of the L^1 complex with Zn(II) has been successfully established as a system which assembles to give circular helicates the terminal groups of the ligand were varied to incorporate amino acid esters. This was in an attempt to control the enantio-selective assembly of the circular helicate. The same method employed for the crystallisation of L^1 was used to try and obtain solid state structures for L^2-L^4 , however, all attempts were unsuccessful in forming good quality crystals. The use of glycine methyl ester in the second step (step **b**) of the synthesis resulted in the production of a glycine-containing ligand, L^2 . Reaction of L^2 with $Zn(CF_3SO_3)_2$ in CD_3NO_2 gave a colourless solution for which the 1H NMR and ESI-MS were recorded. The ESI-MS showed a signal at m/z 2330 corresponding to $\{[Zn_5(L^2)_5](CF_3SO_3)_8\}^{2+}$. The 1H NMR showed a total of ten signals, seven aromatic signals, a signal corresponding to the amide –NH and two aliphatic signals (figure 2.8, b). Observed here are signals between 6.0–7.0 ppm, which are due to the protons present on the central phenylene spacer. This has been identified previously to be a characteristic of the protons of the phenylene spacer unit within similar helical structures. As can be seen this spectrum is very similar to that for the complex of L^1 ($[Zn_5(L^1)_5](CF_3SO_3)_{10}$) (figure 2.8 a). From these results it is suggested that the glycine-containing derivative, L^2 , forms an analogous pentanuclear species ($[Zn_5(L^2)_5](CF_3SO_3)_{10}$) as that observed for L^1 .

In addition to the glycine-containing derivative ligands L^3 , valine methyl ester ligand, and L^4 , phenylalanine methyl ester ligand, were produced to give two new ligands functionalised with enantiopure terminal amide groups. Reaction with $Zn(CF_3SO_3)_2$ in CD_3NO_2 , for both ligands, once again gave a colourless solution for which ESI-MS showed the expected peaks corresponding to a pentanuclear complex cation (m/z 2541 for $\{[Zn_5(L^3)_5](CF_3SO_3)_8\}^{2+}$ and m/z 2781 for $\{[Zn_5(L^4)_5](CF_3SO_3)_8\}^{2+}$). The 1H NMR spectra of the resulting solutions are again consistent with the formation of a helical structure (figure 2.8 c, d) as the phenylene protons are observed at a significantly lower frequency than the other aromatic signals. For ligands L^3 and L^4 , however, additional subsets of low intensity peaks are observed in the NMR spectra. These peaks are unlikely

to correspond to different nuclearity species, e.g. $[M_6L_6]^{12+}$ or $[M_4L_4]^{8+}$, as generally for these species the signals appear at significantly different chemical shifts ($\Delta\delta > 0.2$ ppm). Thus these additional peaks can be attributed to the possible minor diastereoisomer with some confidence.¹²⁹ To establish the diastereoisomer excess (d.e) the ratio of the integrated sets of peaks for $[Zn_5(L^3)_5]^{10+}$ gave a 9:1 ratio for the two diastereoisomers present. This demonstrates that the optically pure valine unit controls the self-assembly of the helicate and one isomer thus results giving an approximate 80% d.e. As for the phenylalanine-containing ligand the process appears to be less selective thus the self-assembly leads to a lower d.e. of ~ 70%.

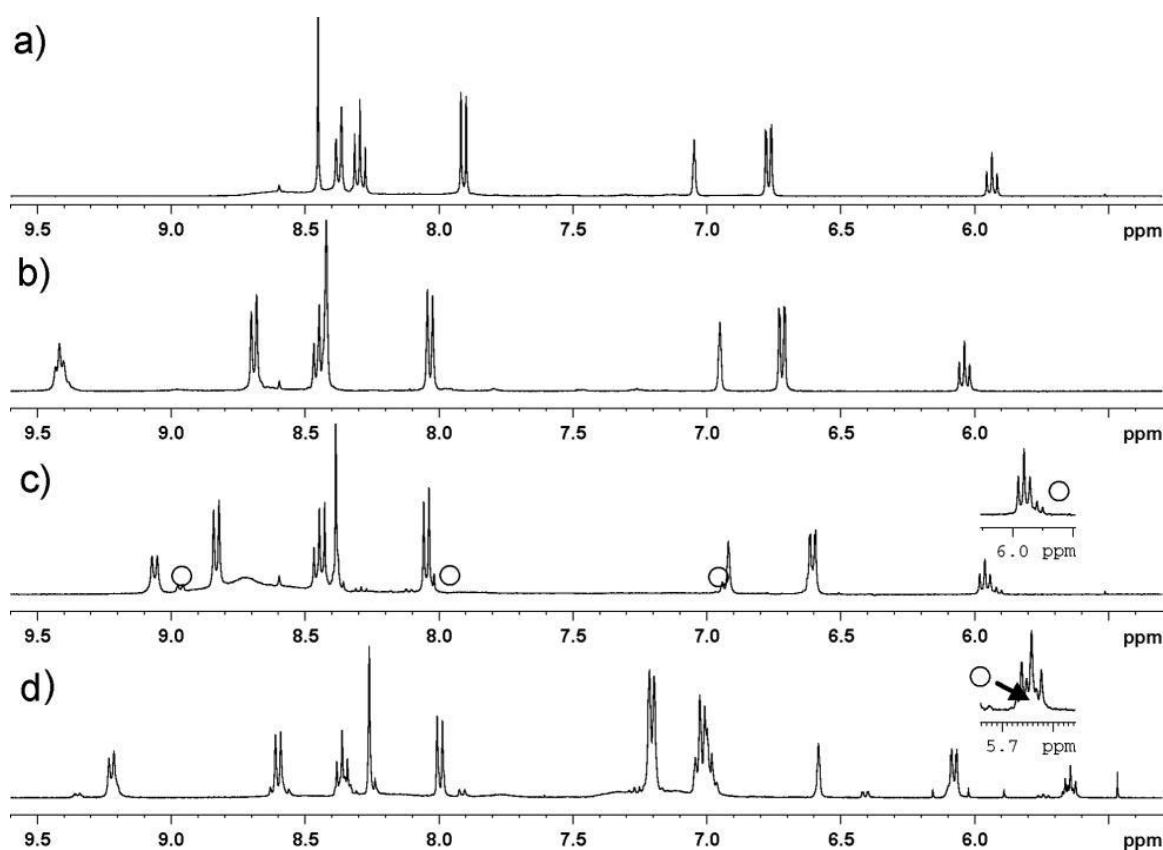


Figure 2.8 Aromatic region of the 1H NMR spectra of (a) $[Zn_5(L^1)_5]^{10+}(CD_3NO_2)$, (b) $[Zn_5(L^2)_5]^{10+}(CD_3NO_2)$, (c) $[Zn_5(L^3)_5]^{10+}(CD_3NO_2)$ and (d) $[Zn_5(L^4)_5]^{10+}(CD_3NO_2)$:

○ = selected peaks corresponding to the minor diastereoisomer.

Circular dichroism (CD) is the difference in the absorption of left-handed and right-handed circularly polarised light (CPL) which occurs when a molecule contains one or more chiral chromophores. CD spectroscopy is a technique where the CD of molecules is measured over a range of wavelengths. CD spectroscopy is used to study chiral molecules; its most important application is the study of the secondary structure of proteins. These structures are sensitive to changes in environment and as such CD spectroscopy can be used to observe how the structure changes as a result of alteration to environmental conditions or interaction with other molecules. For molecules that contain chiral components one circularly polarised light state will be absorbed to a greater extent than the other and the CD signal over the corresponding wavelength will be non-zero. The signal may be positive or negative depending on the difference in absorption between left-handed and right-handed circularly polarised light.

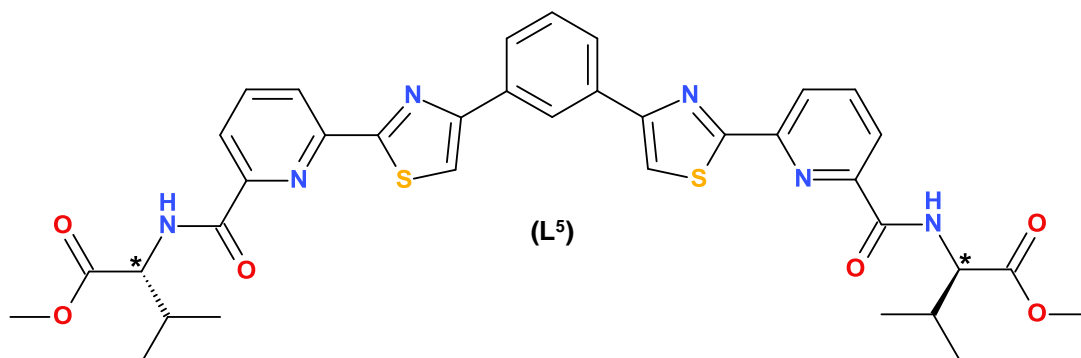


Figure 2.9 L^5 , (R,R)- enantiomer of ligand L^3

To conduct this type of analysis another ligand was required thus L^5 , (R,R)-enantiomer), was prepared. This was produced in an identical manner to the (S,S)-enantiomer, L^3 , apart from D-valine was used in the synthesis in place of L-valine. To all intents and purposes the NMR, ESI-MS data and yields of L^5 were identical to that obtained for L^3 . The CD spectra of ligands L^3 and L^5 (figure 2.9 a), opposite isomers, show a very weak equal and opposite bisignate Cotton effect relating to the higher energy $\pi-\pi^*$ transitions. These probably arise from a degree of exciton coupling between the two halves of the ligand. Addition of Zn(II) into the solution results in a considerable change to the observed CD spectrum of the free ligand (figure 2.9, b). As can be seen the signal around 355 nm has grown, although the intensity of the signals does not

dramatically increase, as had been anticipated. In addition to this the UV/vis absorption spectrum also shows a change in the large absorption at 264 nm which reduces in intensity and broadens. This is indicative of a strong exciton coupling assuming the complex adopts a similar configuration to that of \mathbf{L}^1 in the solid state structure of $[\text{Zn}_5(\mathbf{L}^1)_5]^{10+}$.

From this information it should be possible, in principle, to assign an overall sense of handedness to the dominant isomer by implementing exciton theoretical analysis.^{130, 131} The 330 nm absorption is assumed to relate to the $\pi-\pi^*$ transitions of the pyridyl-thiazole group. The complex derived from \mathbf{L}^3 demonstrates a negative signal at the lowest energy transitions in the CD spectrum in this region. Assuming a similar structure is adopted to that of ligand \mathbf{L}^1 , with a dihedral angle between the two chromophores of 70.8° , and the two chromophores at an angle of 59.8° relative to the perpendicular between them, then the resulting dominant complex can tentatively be assigned as having a D metal-centred configuration, and an overall M helicity. Extreme caution should be placed on this assignment given that the metal-centred exciton couplings will invariably be cancelled out by additional couplings in the structure as previously reported by Telfer and co-workers.¹³² In this particular case, it is observed in the structural analysis of $[\text{Zn}_5\mathbf{L}^1_5]^{10+}$ that inter-ligand phenyl-thiazole contacts possess the opposite sense of handedness with a separation of only 4.0 to 5.0 Å, whilst the metal-centred chromophores are longer (4.5–5.5 Å). Given that the strength of the observed exciton coupling is related by an inverse r^3 relationship these interactions cannot be ignored,^{130, 131} with the possibility that these conflicting bi-signate interactions could account for the surprisingly low observed Cotton effect, and could even lead to the mis-assignment of the overall helicity.

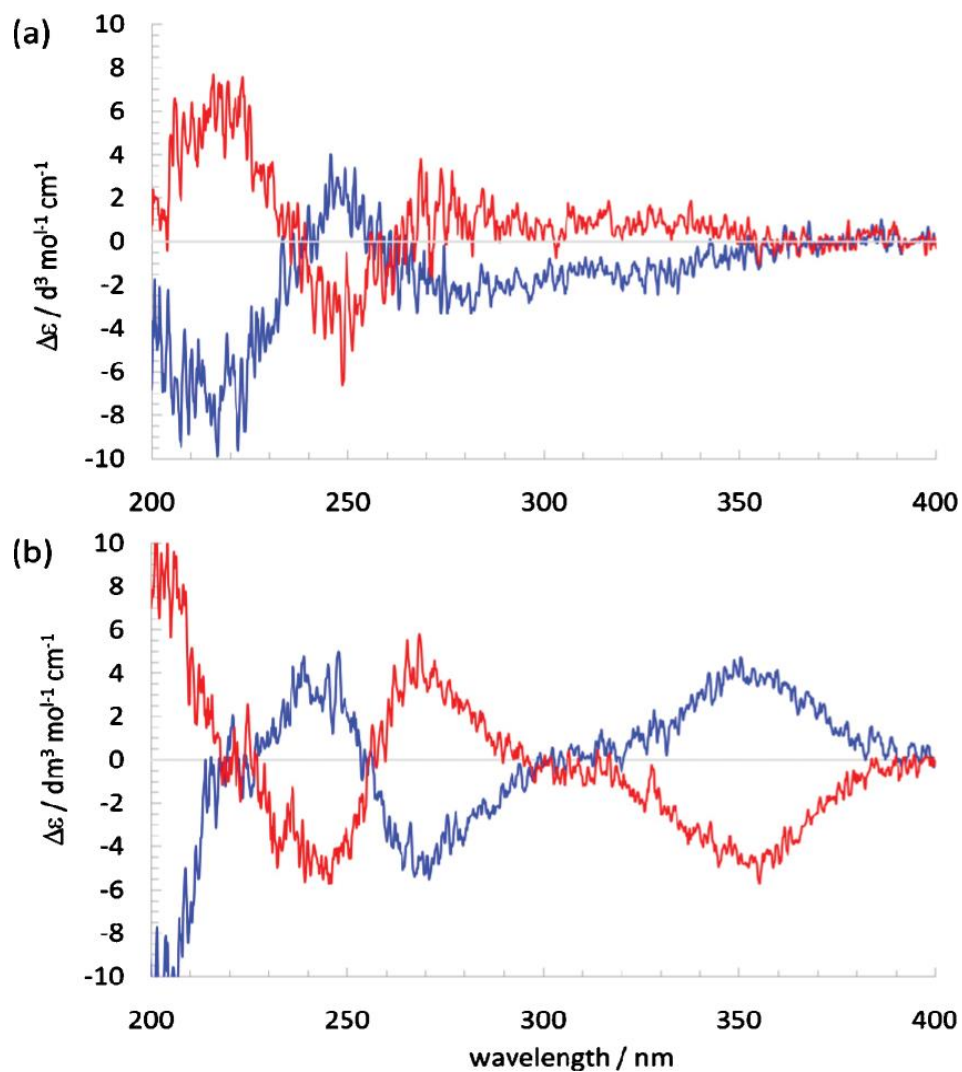


Figure 2.10 The CD spectra of (a) ligand L^3 (red) and L^5 (blue) and (b) the resulting complexes upon the addition of one equivalent of Zn (II) in acetonitrile (298 K, concentration of $2.5 \times 10^{-5} \text{ mol dm}^{-3}$)

2.4 Conclusion

In conclusion five ligands, **L**¹-**L**⁵, containing both N-donor and O-donor domains and a 1,3-phenylene spacer unit have been produced. **L**¹ has been shown to self-assemble into pentanuclear circular helicates upon reaction with Zn(II) ions and this structure persists in both the solid and solution state. This high nuclearity species forms as a result of unfavourable steric interactions between the phenyl units which destabilize the similar linear helicate, which in turn is governed by the size of the metal ion employed. Variation of the ligand allowed incorporation of enantiopure units within the strand leading to diastereoselective self-assembly giving up to 80% d.e.

3 Steric control over the formation of dinuclear double helicate and dinuclear *meso*-helicate assemblies

The term *meso*-helicate (mesocate or side-by-side helicate⁹⁸) has been introduced previously. These supramolecular complexes are closely related to helicates, but they differ in the manner by which the ligand strands are arranged. Taking an octahedral dinuclear double-stranded helicate, M_2L_2 as an example, each metal centre can either be left handed (Λ) or right handed (Δ) there are four possible configurations that may result: $\Lambda\Lambda$, $\Delta\Delta$, $\Delta\Lambda$ and $\Lambda\Delta$. The first two configurations represent the possible homochiral complexes, giving rise to left-handed (*M*-) and right-handed (*P*-) helicates, respectively, as the ligand strands would wrap helically around the metal centres. Alternatively, since the two heterochiral ($\Delta\Lambda$ or $\Lambda\Delta$) complex has two opposite chiral centres the strands would need to be in a side-by-side conformation generating a mirror plane within the structure thus giving an achiral structure known as a *meso*-helicate (figure 3.1). These systems can become more complicated as the number of metal ions and/or ligands employed within the assembly increases (e.g. M_2L_3 , figure 3.1).

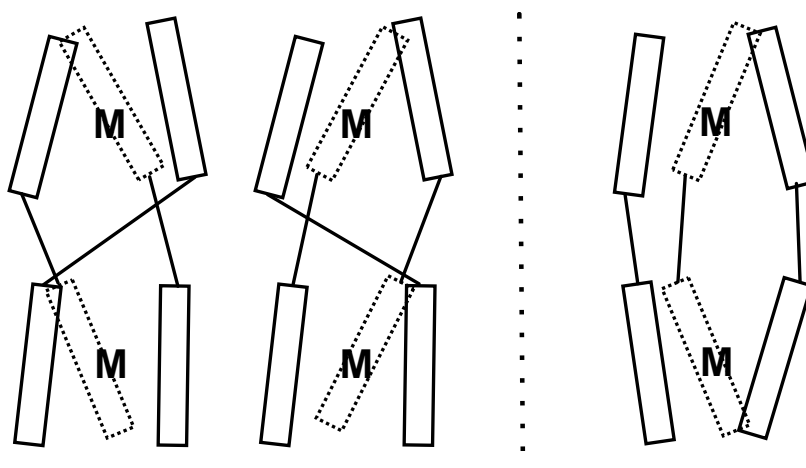


Figure 3.1 A schematic representation of the enantiomeric forms of a dinuclear triple helicate (left: $\Delta\Delta$, centre: $\Lambda\Lambda$) and the *meso*-helicate (right: $\Lambda\Delta$)⁽⁹⁹⁾

The assembly of dinuclear helicates is achieved with selection of appropriate ligand strands which can partition into two separate donor domains, allowing coordination to separate metal ions. This criterion is essentially the same as

that required for the formation of the *meso*-helicite assembly. Even though the field of helicates has expanded rapidly over the years, controlling the formation of helicate versus mesocate is still not fully understood.

The first mesocate was reported by Albrecht in 1995,¹³³ using the dicatechol ligand, $L^{M'}$ ($n=3$), (figure 3.2). Exposure to Ti(II) metal ions resulted in the assembly of a triple stranded mesocate. To determine the factors which direct the formation of the mesocate the group produced a number of dicatechol ligands with varying spacer length. It was determined that an odd number of methylene units produced the mesocate which was shown to exist in the solid state as well as in solution, while the compounds possessing even spacer length adopt a helicate structure. In the helicate the ligands show an “S”-type configuration while the ligands of the mesocate adopt a “C”-type configuration.^{100, 133-135}

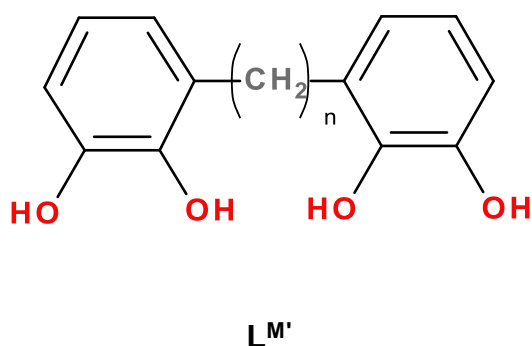


Figure 3.2 Dicatechol ligand, $L^{M'}$, employed to investigate the diastereoselectivity of helicates versus mesocate⁽¹⁰⁰⁾

Besides the dicatechol ligands, the *odd-even rule* was shown to be applicable to some other ligands with alkyl linkers. For instance, the bis(bipyridine) ligand, $L^{N'}$, led to a mesocate upon coordination with Fe(II) (figure 3.3).¹³⁵

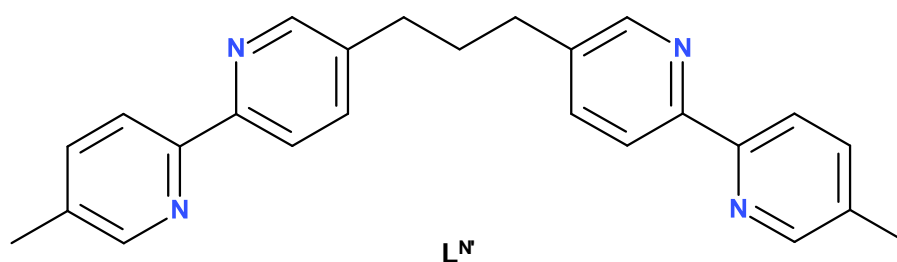


Figure 3.3 Bis(2,2'-bipyridine) ligand, L^N (135)

Raymond *et al.* report the synthesis and inversion mechanism of dinuclear biscatechol triple helicates.¹³⁶ To understand the racemisation of homochiral helicates the kinetics of inversion were investigated using NMR as a probe. This showed the inversion of the dinuclear complexes employed occurs *via* an intramolecular mechanism from the individual twisting of both metal centres. Thus the inversion of the $\Lambda\Lambda$ - and $\Delta\Delta$ - helicates was not achieved by the simultaneous inversion of both metal centres but *via* a stepwise inversion involving the heterochiral mesocate as an intermediate, with the intermediate being short-lived. Even though the mesocate intermediate was short-lived this study suggests the helicate and mesocate may interconvert under certain conditions.

This was elegantly demonstrated by Raymond *et al.* with the interconversion between helicate and mesocate driven by the formation of a host-guest complex.¹³⁷ Helical and *meso* complexes were formed from the same ligand strand, $L^{O'}$ (figure 3.4). Single crystal structural analysis confirms that in the solid state the $[Al_2(L^{O'})_3]$ complex is a helicate, while the $[Ga_2(L^{O'})_3]$ complex is a mesocate, with the helicate encapsulating a water molecule, with this host-guest complex being the most favourable thermodynamic product. NMR studies revealed for $[Ga_2(L^{O'})_3]$ and $[Al_2(L^{O'})_3]$ complexes in DMSO- d_6 both the helicate and mesocate are present, with the mesocate being enthalpically favoured. It was subsequently shown that the ratio of *meso* to helical complex is temperature dependent, with the stabilisation of helicate also being dependent on guest concentration.

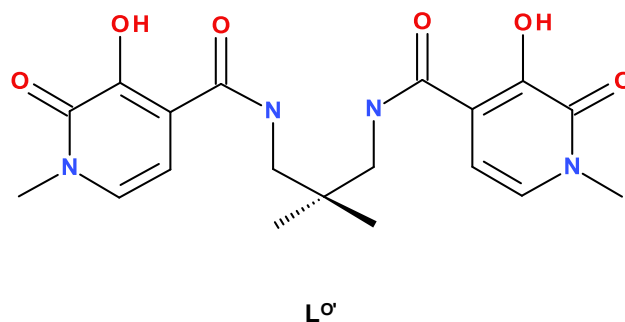


Figure 3.4 Chemical structure of ligand, $L^{O'}$ (137)

The formation of helicate *versus* mesocate has been an area of some interest. Different groups have reported different reasons as to why the mesocate forms in preference to the helicate. As proposed by Albrecht *et al.* the spacer length was one method to predict which assembly will result,^{100, 133-135} Wu and co-workers demonstrated that the self-assembly could be controlled based on anion size.¹³⁸ Hooley *et al.* have recently demonstrated similar stereochemical control over these self-assemblies using functionalised v-shaped ligands and Fe(II).¹³⁹

Hooley produced six pre-ligands, $L^{P'}$, these ligands being used to form the final complexes (figure 3.5). Combination of the pre-ligands with 2-formylpyridine and $Fe(ClO_4)_2$ in degassed acetonitrile resulted in the formation of iminopyridine complexes. The complexes, $(L^{P'(1-5)})_3Fe(ClO_4)_4$, were isolated as purple solids by precipitation with ether. The larger pre-ligand 6(adamantanamide) was incapable of forming the desired assembly and mostly formed insoluble coordination polymers. The complexes produced were mostly stable, but sensitive to air and moisture, meaning no X-ray quality crystals could be obtained. Therefore, assemblies were characterised by 1H NMR, 2D NMR, diffusion NMR and ESI-MS.

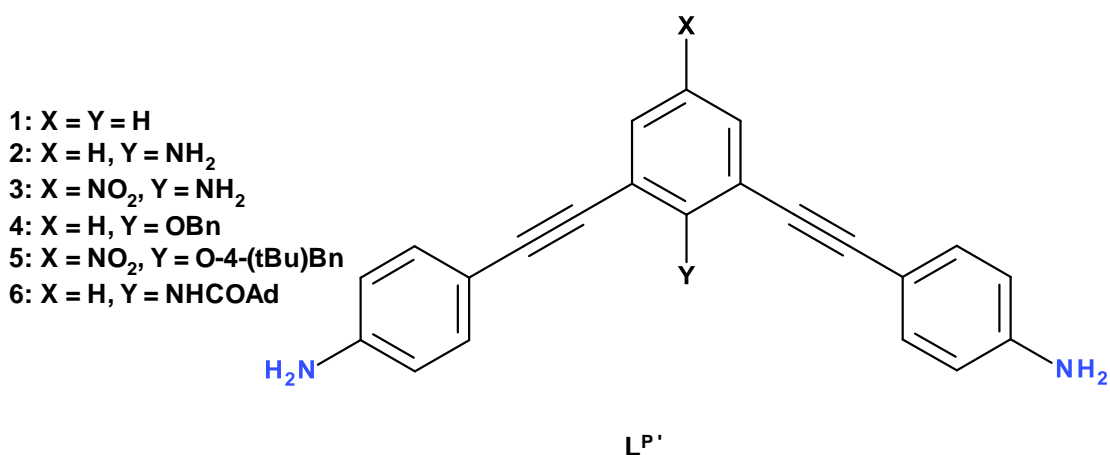


Figure 3.5 Chemical structure of pre-ligands, $L^{P'}$ (139)

An additional ligand, $L^{Q'}$, was also analysed alongside these complexes as a control (figure 3.6). $L^{Q'}$ is known to form the homotopic isomer, and the mesocate (heterotopic isomer) is not observed in solution. Comparison of the $L^{O'}$ complex ¹H NMR with that of $(L^{P'}(1-3))_3Fe(ClO_4)_4$ showed two sets of resonances, attributed to the homotopic and heterotopic species. This showed the longer more flexible ligands did not generate significant strain within the assembly, in comparison with $L^{O'}$, thus the additional freedom of the ligand allowed heterotopic species to form.

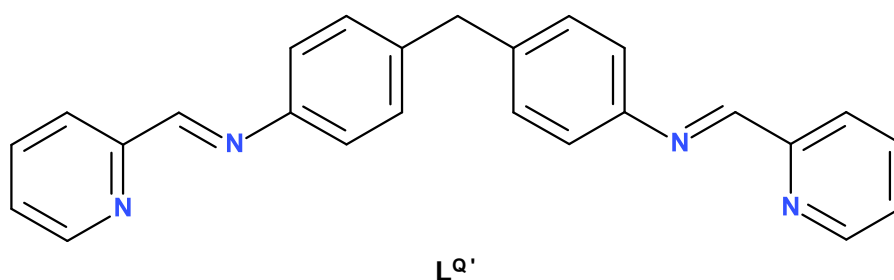
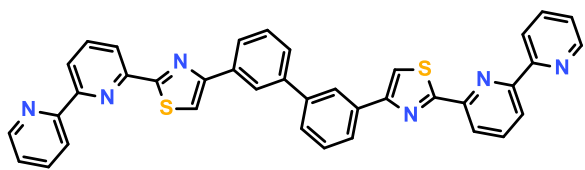


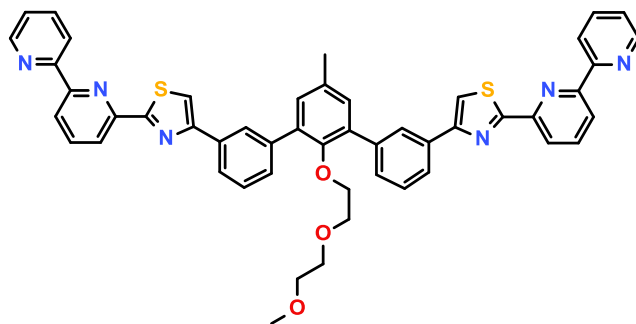
Figure 3.6 Chemical structure of ligand, $L^{Q'}$ (139)

$(L^{P'}(4-5))_3Fe(ClO_4)_4$ were shown to form only one isomer (homotopic matched isomer) which was due to the bulky groups limiting the flexibility of the ligand and preventing the formation of the *meso*-isomer.

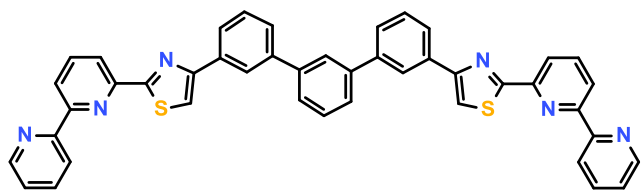
Described in this chapter is the synthesis and coordination chemistry of a number of N-donor ligands (L^6 - L^{14}) which assemble into dinuclear supramolecular arrays upon coordination to transition metal ions. These ligands contain two tridentate donor domains (pyridyl-pyridyl-thiazole) separated by different spacer units. The first ligand, L^6 , consists of two tridentate donor domains separated by a biphenyl spacer group. The spacer units of the remaining ligands each consist of three aromatic rings, with variation of the central ring of the spacer unit, in an effort to influence the final supramolecular architecture (figure 3.7).



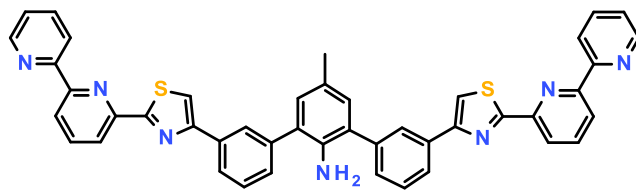
(L⁶)



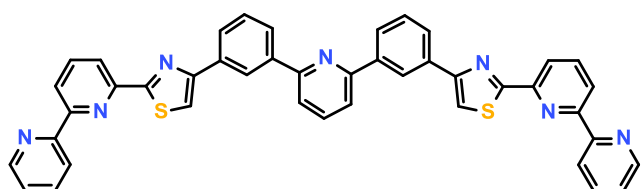
(L¹⁰)



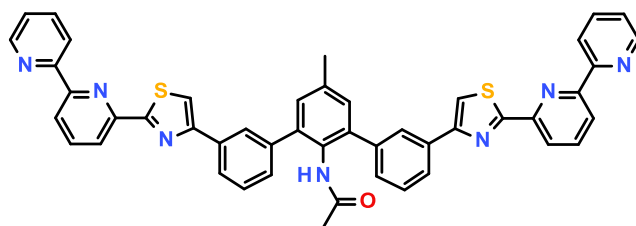
(L⁷)



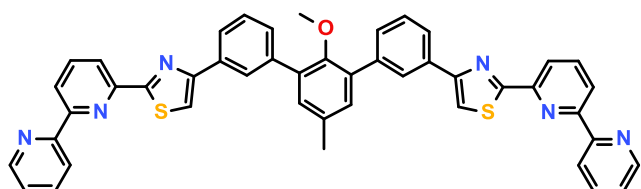
(L¹¹)



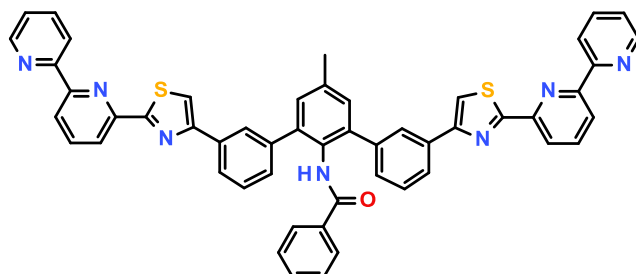
(L⁸)



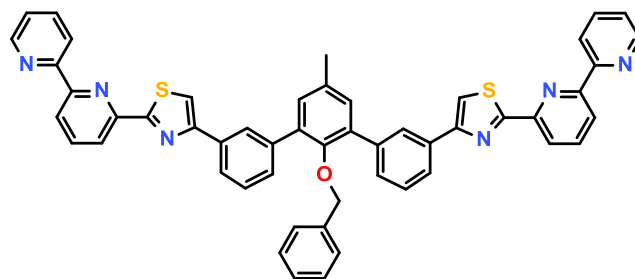
(L¹²)



(L⁹)



(L¹³)



(L¹⁴)

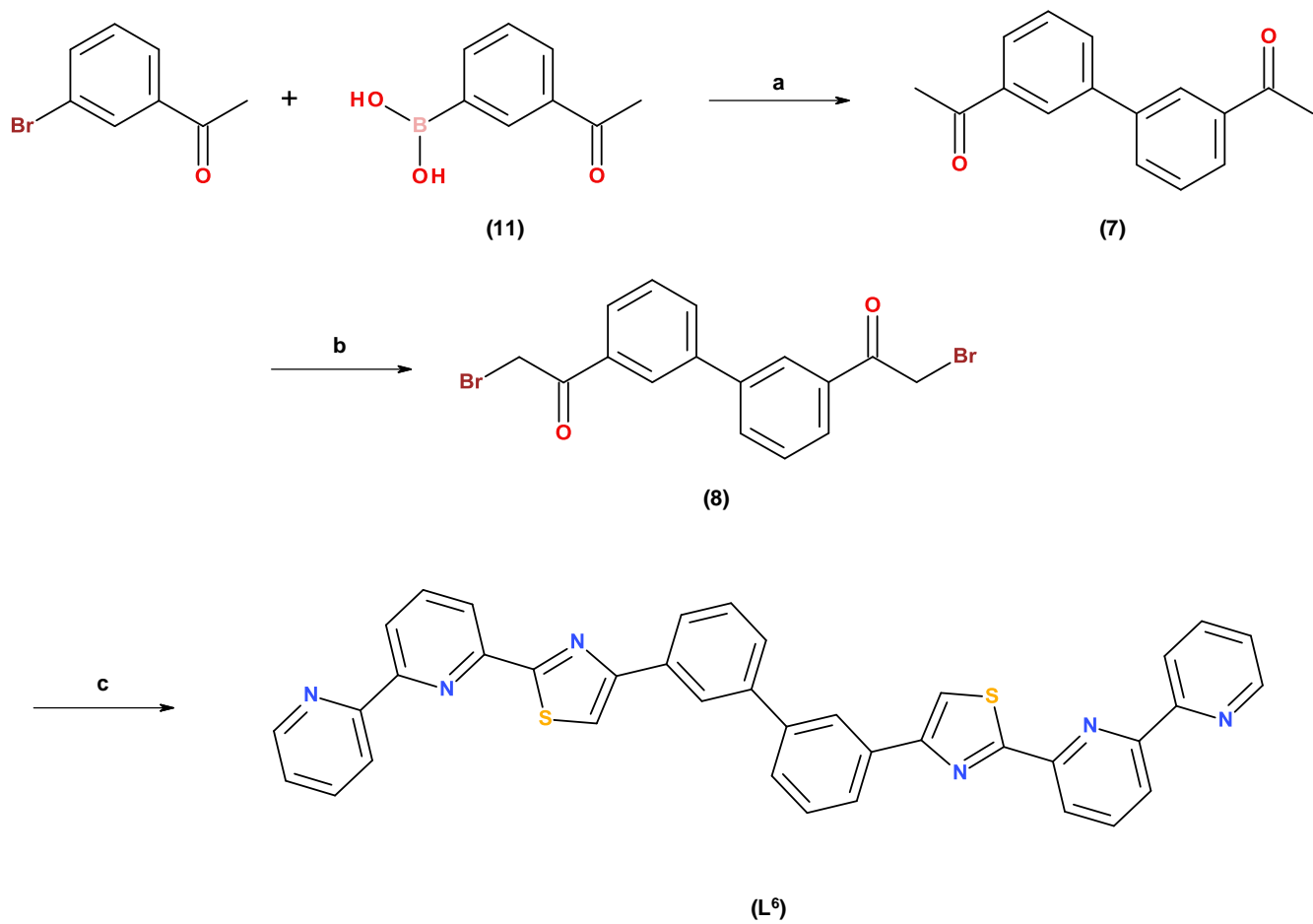
Figure 3.7 New class of ligands L⁶ – L¹⁴

3.1 Ligand synthesis

The ligands, $L^6 - L^{14}$, were synthesised *via* a multi-step synthetic process which differed in the initial stages of the synthesis and in the reagents employed. Further details regarding the synthesis of these ligands can be found within chapter 6 (section 6.2)

3.1.1 Synthesis of L^6

The synthesis of the ligand, L^6 , was achieved by a Suzuki cross-coupling reaction between 3-bromoacetophenone and 1,3-acetylphenyl boronic acid (**11**) following a procedure reported previously in the literature (scheme 3.1).¹⁴⁰ 3,3'-Diacetylbiaryl (**7**) upon exposure to bromine in acetic acid gave the di- α -bromoacetyl (**8**) after separation and purification *via* column chromatography. The aromatic region of the 1H NMR spectrum of the product is not significantly altered from that of the starting material, however the appearance of a singlet, corresponding to methylene protons, is observed at 4.52 ppm; along with the disappearance of the original methyl peak which was seen at 2.69 ppm for 3,3'-diacetylbiaryl (**7**). Reaction between the α -bromoacetyl (**8**) and 2,2'-bipyridine-6-thioamide (**9**) in ethanol was refluxed for several hours. The resulting precipitate was isolated *via* filtration giving the ligand, L^6 , as an off-white solid which was subsequently characterized by 1H NMR, ESI-MS and HR ESI-MS. The 1H NMR spectrum showed the expected 11 aromatic signals, with two signals overlapping. ESI-MS showed an ion at m/z 416 which is consistent with $[L^6+H]^+$.



Scheme 3.1 Synthesis of **L⁶**

Reagents and conditions: a) $[\text{Pd}(\text{PPh}_3)_2\text{Cl}_2]$, NaHCO_3 , $n\text{Bu}_4\text{NBr}$, H_2O , $70\text{ }^\circ\text{C}$ (71%); b) Br_2 , CH_3COOH , $80\text{ }^\circ\text{C}$ (37%); c) 2,2'-bipyridine-6-thioamide (**9**), EtOH , reflux (70%)

3.1.2 Synthesis of L^7 – L^{14}

The synthesis of these ligands is outlined in schemes 3.2 and 3.3 and was carried out in a similar manner to that of L^6 .

3.1.2.1 Synthesis of L^7

The synthesis of the ligand, L^7 , was achieved by a Suzuki cross-coupling reaction between 1,3-dibromobenzene (**10**) and 1,3-acetylphenyl boronic acid (**11**) following the same procedure employed for the synthesis of 3,3'-diacetyl biphenyl (**7**).¹⁴⁰ After purification *via* column chromatography the diacetyl (**12**) was obtained, the ^1H NMR spectrum confirms the formation of the desired compound (54 % yield). Exposure of the diacetyl to bromine in acetic acid gave the di- α -bromoacetyl (**13**) after column chromatography (63 % yield). Again the aromatic region of the ^1H NMR spectrum of the product is not significantly altered from that of the starting material; however the appearance of a singlet, corresponding to methylene protons, is observed at 4.53 ppm; along with the disappearance of the original methyl peak which was seen at 2.69 ppm for the starting material. Reaction between the α -bromoacetyl (**13**) and 2,2'-bipyridine-6-thioamide (**9**) in ethanol was refluxed for several hours. The resulting precipitate was isolated *via* filtration giving the ligand, L^7 , as a light brown powder which was subsequently characterized by ^1H NMR, ESI-MS and HR ESI-MS (71 % yield). The ^1H NMR spectrum showed the expected 15 aromatic signals, with two signals overlapping. ESI-MS showed an ion at m/z 705 which is consistent with $[\text{L}^7+\text{H}]^+$.

3.1.2.2 Synthesis of L^8

L^8 also consists of a spacer unit containing three aromatic rings similar to L^7 , except the central ring of the spacer unit contains a heteroatom, nitrogen. Thus this spacer unit has a central pyridyl ring and two phenyl rings. This ligand was produced by following a synthesis scheme identical to that employed for L^7 (scheme 3.2, b) with 2,6-dibromopyridine (**14**) employed in the first step of the synthesis for L^8 .

3.1.2.3 Synthesis of L^9

L^9 was also produced in an analogous fashion to L^7 , with the difference being a variation of the central aromatic ring of the spacer unit (scheme 3.2, c). L^9 is a ligand possessing two tridentate donor domains separated by a spacer unit which consists of two phenyl groups and a methoxytoluene-type aromatic ring as the central component of the spacer. This was achieved using 1,3-dibromo-2-methoxy-5-methylbenzene (**17**) for the Suzuki cross-coupling reaction in the first step of ligand synthesis.

3.1.2.4 Synthesis of L^{10}

L^{10} may be seen as an extension of L^9 , as the ligands are similar except a glycol ether chain is present on the central aromatic ring for L^{10} . Once again the synthesis for this ligand follows the same multistep scheme employed for the other ligands described here (scheme 3.2, d).

3.1.2.5 Synthesis of L^{11}

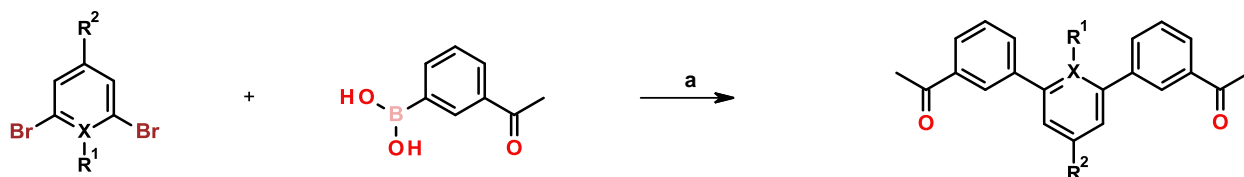
The synthesis for L^{11} is outlined in scheme 3.2, e. As with previous ligands the synthesis of this ligand was carried out in a similar manner to that of L^7 with the incorporation of different starting materials for the Suzuki cross-coupling reaction further variation of the spacer unit was achieved. The central aromatic ring of the spacer group for L^{11} is a p-toluidine (aminotoluene) functionality.

3.1.2.6 Synthesis of L^{12} and L^{13}

The synthesis schemes for L^{12} and L^{13} are outlined in scheme 3.2, f and g respectively. As with previous ligands the synthesis for this ligand was carried out in a similar manner to that of L^7 . The central aromatic ring of the spacer unit for L^{12} is essentially acetyl amino toluene. L^{13} is similar to that of L^{12} , except the central aromatic group possesses a benzoyl pendant group from the amino toluene central aromatic ring, giving a larger pendant group.

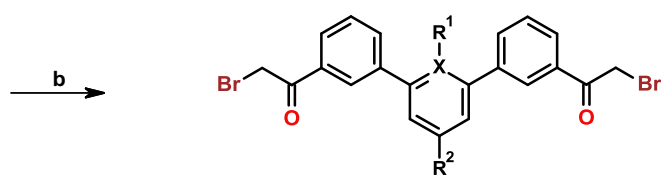
3.1.2.7 Synthesis of L^{14}

The initial synthesis for this ligand follows the same procedure as employed for the other ligands seen herein, with the difference in starting material allowing variation of the triphenyl spacer (scheme 3.3). However, in this case an additional synthesis step was required to produce a ligand containing a benzyl pendant group on the central aromatic ring.

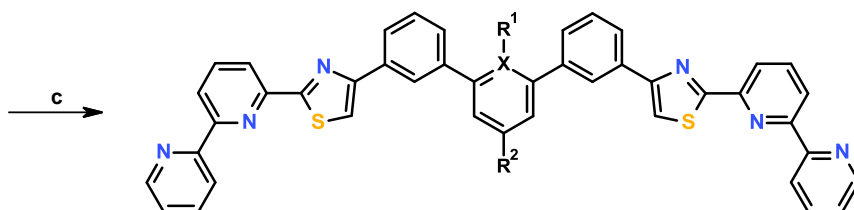


- a) X = C, R¹ = R² = H (10)
- b) X = N, R¹ = N/A, R² = H (14)
- c) X = C, R¹ = OCH₃, R² = CH₃ (18)
- d) X = C, R¹ = O(CH₂CH₂)O(CH₂CH₂)OCH₃, R² = CH₃ (24)
- e) X = C, R¹ = NH₂, R² = CH₃ (27)
- f) X = C, R¹ = NH(COCH₃), R² = CH₃ (30)
- g) X = C, R¹ = NH(COPh), R² = CH₃ (33)

- a) X = C, R¹ = R² = H (12)
- b) X = N, R¹ = N/A, R² = H (15)
- c) X = C, R¹ = OCH₃, R² = CH₃ (19)
- d) X = C, R¹ = O(CH₂CH₂)O(CH₂CH₂)OCH₃, R² = CH₃ (25)
- e) X = C, R¹ = NH₂, R² = CH₃ (28)
- f) X = C, R¹ = NH(COCH₃), R² = CH₃ (31)
- g) X = C, R¹ = NH(COPh), R² = CH₃ (34)



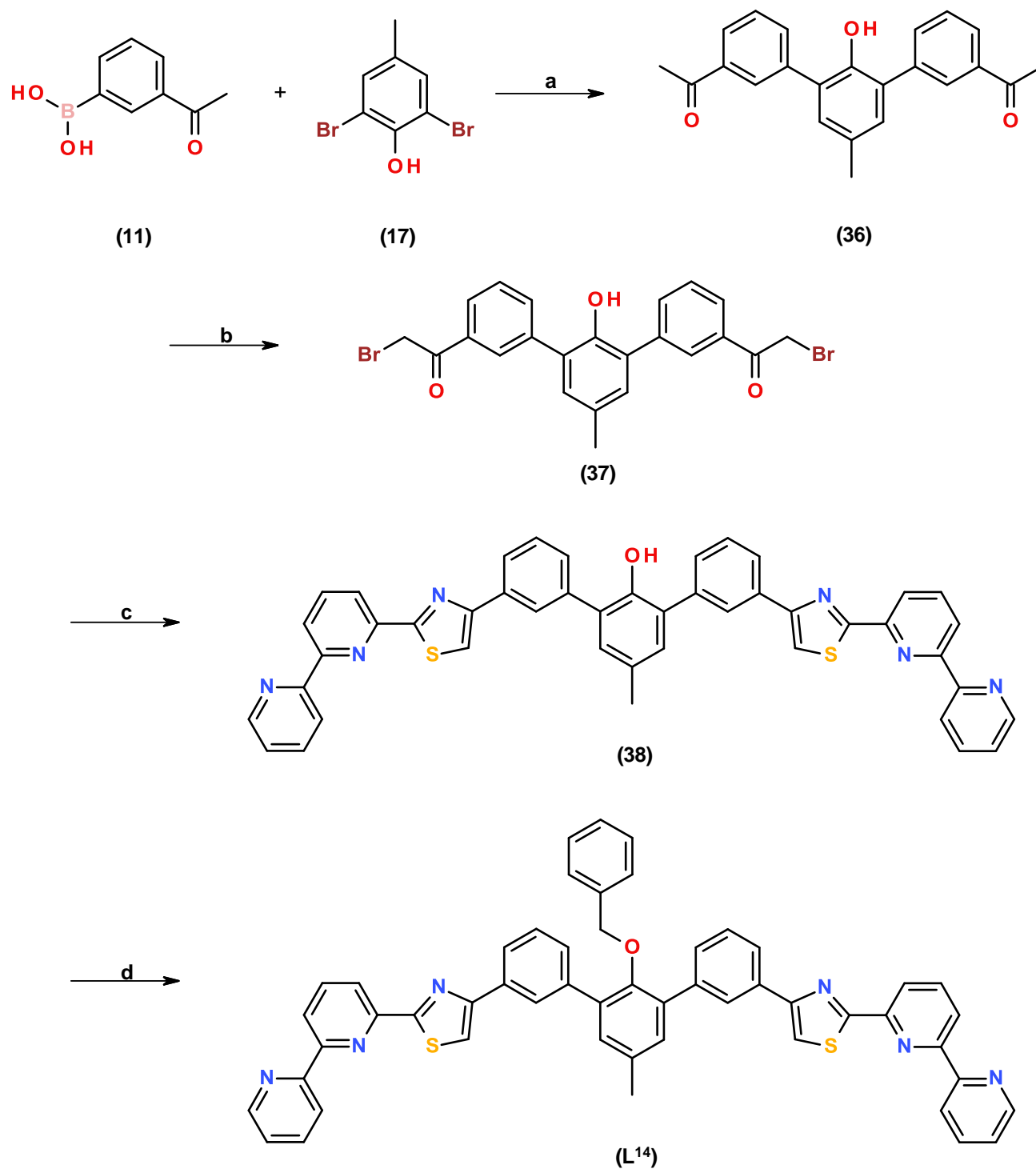
- a) X = C, R¹ = R² = H (13)
- b) X = N, R¹ = N/A, R² = H (16)
- c) X = C, R¹ = OCH₃, R² = CH₃ (20)
- d) X = C, R¹ = O(CH₂CH₂)O(CH₂CH₂)OCH₃, R² = CH₃ (26)
- e) X = C, R¹ = NH₂, R² = CH₃ (29)
- f) X = C, R¹ = NH(COCH₃), R² = CH₃ (32)
- g) X = C, R¹ = NH(COPh), R² = CH₃ (35)



- a) X = C, R¹ = R² = H (L⁷)
- b) X = N, R¹ = N/A, R² = H (L⁸)
- c) X = C, R¹ = OCH₃, R² = CH₃ (L⁹)
- d) X = C, R¹ = O(CH₂CH₂)O(CH₂CH₂)OCH₃, R² = CH₃ (L¹⁰)
- e) X = C, R¹ = NH₂, R² = CH₃ (L¹¹)
- f) X = C, R¹ = NH(COCH₃), R² = CH₃ (L¹²)
- g) X = C, R¹ = NH(COPh), R² = CH₃ (L¹³)

Scheme 3.2 Synthesis of L⁷-L¹³

Reagents and conditions: a) [Pd(PPh₃)₂Cl₂], NaHCO₃, nBu₄NBr, EtOH, H₂O, 70 °C; b) Br₂, CH₃COOH; c) 2,2'-bipyridine-6-thioamide (**9**), EtOH, reflux



Scheme 3.3 Synthesis of L¹⁴

Reagents and conditions: a) [Pd(PPh₃)₂Cl₂], NaHCO₃, nBu₄NBr, EtOH, H₂O, 70 °C (65%); b) Br₂, CH₃COOH (89%); c) 2,2'-bipyridine-6-thioamide (9), EtOH, reflux (79%); d) NaH, DMF, N₂ (g), benzyl bromide, 80 °C (56%)

3.2 Coordination chemistry

3.2.1 Complexes of L^6 with copper(II)

Reaction of L^6 with an equimolar quantity of $Cu(ClO_4)_2$ in acetonitrile gave a light green solution, which upon analysis by ESI-MS showed ions at m/z 1683 and 792 corresponding to $\{[Cu_2(L^6)_2](ClO_4)_3\}^+$ and $\{[Cu_2(L^6)_2](ClO_4)_2\}^{2+}$. Slow diffusion of ether into the acetonitrile complex solution resulted in the formation of X-ray quality green crystals. Single crystal X-ray structure determination showed crystallisation in the triclinic space group $P-1$ and confirmed the formation of the dinuclear species $[Cu_2(L^6)_2]^{4+}$ (figure 3.8).

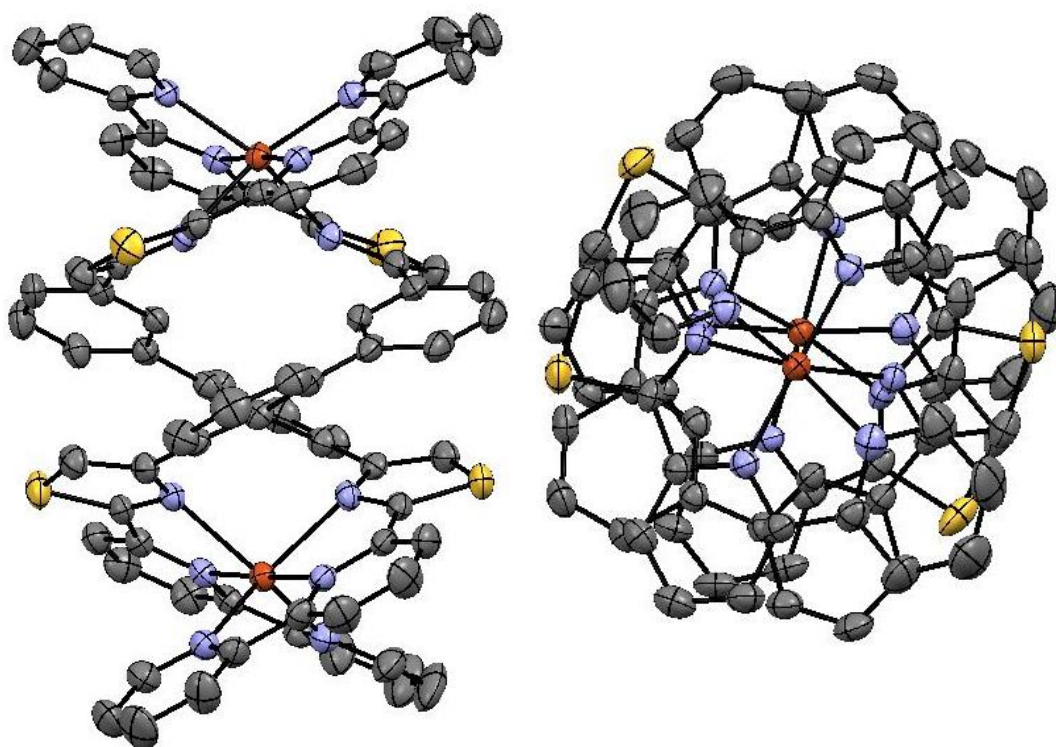


Figure 3.8 Two views for the solid state structure of the complex cation $[Cu_2(L^6)_2]^{4+ii}$

The crystal structure confirms that in the solid state the ligand, L^6 , and $Cu(II)$ ions self-assemble to form a dinuclear double helicate, in which the ligand strand partitions into two tridentate donor domains, separated by the bi-phenylene spacer unit (figure 3.8). The bi-phenyl spacer bridges the tridentate domains in an “over-and-under” conformation giving a helical structure. Each

ⁱⁱ All X-ray crystallography data for this chapter was recorded by Professor Craig Rice.

ligand twists and adopts an S-type arrangement resulting in the two metal ions having the same chirality which leads to a “true” helicate. The two tridentate donor domains of each ligand coordinate both of the metal ions. The two Cu(II) ions (Cu–Cu distance: 7.955(1) Å) are six-coordinate arising from coordination with two tridentate N,N,N-domains (Cu–N distances: 1.954(3) – 2.358(3) Å). Selected bond lengths and angles for the complex are shown in tables 3.1 and 3.2.

Bond	Bond Length (Å)	Bond	Bond Length (Å)
Cu(1)-N(8)	1.968(3)	Cu(2)-N(5)	1.954(3)
Cu(1)-N(2)	1.968(3)	Cu(2)-N(11)	1.964(3)
Cu(1)-N(7)	2.138(3)	Cu(2)-N(6)	2.109(3)
Cu(1)-N(1)	2.141(3)	Cu(2)-N(12)	2.167(3)
Cu(1)-N(9)	2.304(3)	Cu(2)-N(4)	2.290(3)
Cu(1)-N(3)	2.358(3)	Cu(2)-N(10)	2.356(3)

Table 3.1 Selected bond lengths (Å) for the complex cation $[\text{Cu}_2(\text{L}^6)_2]^{4+}$

Bond	Angle (°)	Bond	Angle (°)
N(8)-Cu(1)-N(2)	176.53(12)	N(5)-Cu(2)-N(11)	178.49(13)
N(8)-Cu(1)-N(7)	78.76(12)	N(5)-Cu(2)-N(6)	79.07(13)
N(2)-Cu(1)-N(7)	101.76(11)	N(11)-Cu(2)-N(6)	102.33(13)
N(8)-Cu(1)-N(1)	104.20(12)	N(5)-Cu(2)-N(12)	101.77(13)
N(2)-Cu(1)-N(1)	78.83(13)	N(11)-Cu(2)-N(12)	78.31(13)
N(7)-Cu(1)-N(1)	112.27(12)	N(6)-Cu(2)-N(12)	110.06(13)
N(8)-Cu(1)-N(9)	76.34(12)	N(5)-Cu(2)-N(4)	77.30(12)
N(2)-Cu(1)-N(9)	102.75(12)	N(11)-Cu(2)-N(4)	101.25(12)
N(7)-Cu(1)-N(9)	154.43(11)	N(6)-Cu(2)-N(4)	155.81(13)
N(1)-Cu(1)-N(9)	79.74(11)	N(12)-Cu(2)-N(4)	79.96(12)
N(8)-Cu(1)-N(3)	100.89(12)	N(5)-Cu(2)-N(10)	103.58(12)
N(2)-Cu(1)-N(3)	75.90(12)	N(11)-Cu(2)-N(10)	76.14(12)
N(7)-Cu(1)-N(3)	79.67(11)	N(6)-Cu(2)-N(10)	82.70(12)
N(1)-Cu(1)-N(3)	153.86(12)	N(12)-Cu(2)-N(10)	153.41(12)
N(9)-Cu(1)-N(3)	99.35(11)	N(4)-Cu(2)-N(10)	97.87(11)

Table 3.2 Selected bond angles (°) for the complex cation $[\text{Cu}_2(\text{L}^6)_2]^{4+}$

3.2.2 Complexes of L^7 with iron(II)

Reaction of L^7 with an equimolar amount of $Fe(ClO_4)_2$ in nitromethane gave a deep purple solution. Analysis by ESI-MS showed an ion at m/z 1819 corresponding to $\{[Fe_2(L^7)_2](ClO_4)_3\}^+$ indicating a dinuclear species has formed. Slow diffusion of ether into the nitromethane complex solution resulted in the formation of X-ray quality purple crystals. Single crystal X-ray structure determination showed crystallisation in the orthorhombic space group $Cmca$ and confirmed the formation of the dinuclear species $[Fe_2(L^7)_2]^{4+}$ (figure 3.9).

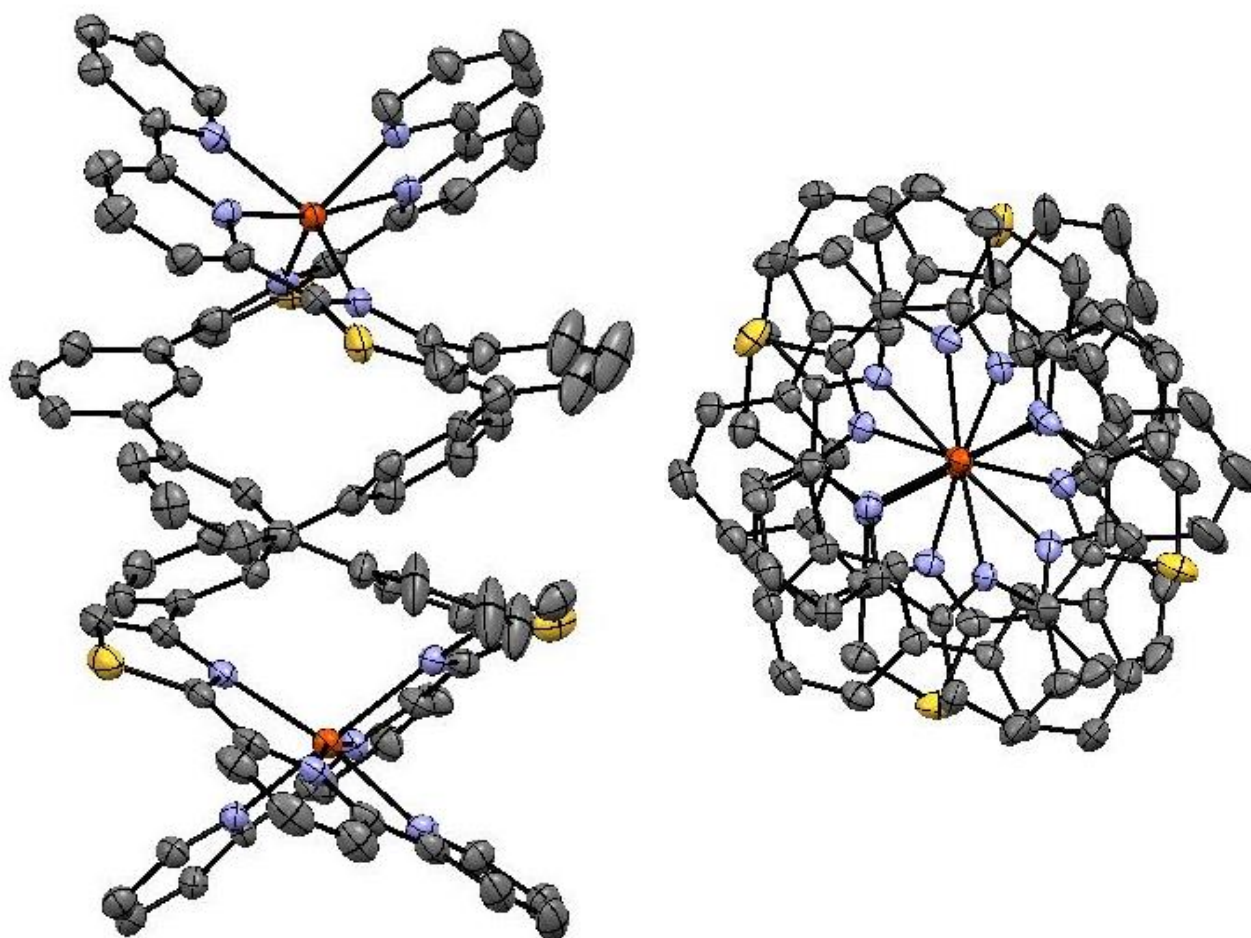


Figure 3.9 Two views for the solid state structure of the complex cation $[Fe_2(L^7)_2]^{4+}$

The crystal structure confirms in the solid state the ligand, L^7 , and Fe(II) ions self-assemble to form a dinuclear double helicate, in a similar manner seen for the previous ligand, L^6 . This ligand strand partitions into two tridentate donor

domains due to the central phenylene spacer group; the two tridentate donor domains of each ligand coordinate both of the metal ions. The Fe(II) ions (Fe–Fe distance: 8.8746(7) Å) are six coordinate arising from coordination with two tridentate N,N,N-domains (Fe–N distances: 2.142(3) – 2.270(3) Å). Selected bond lengths and angles for the complex are shown in tables 3.3 and 3.4.

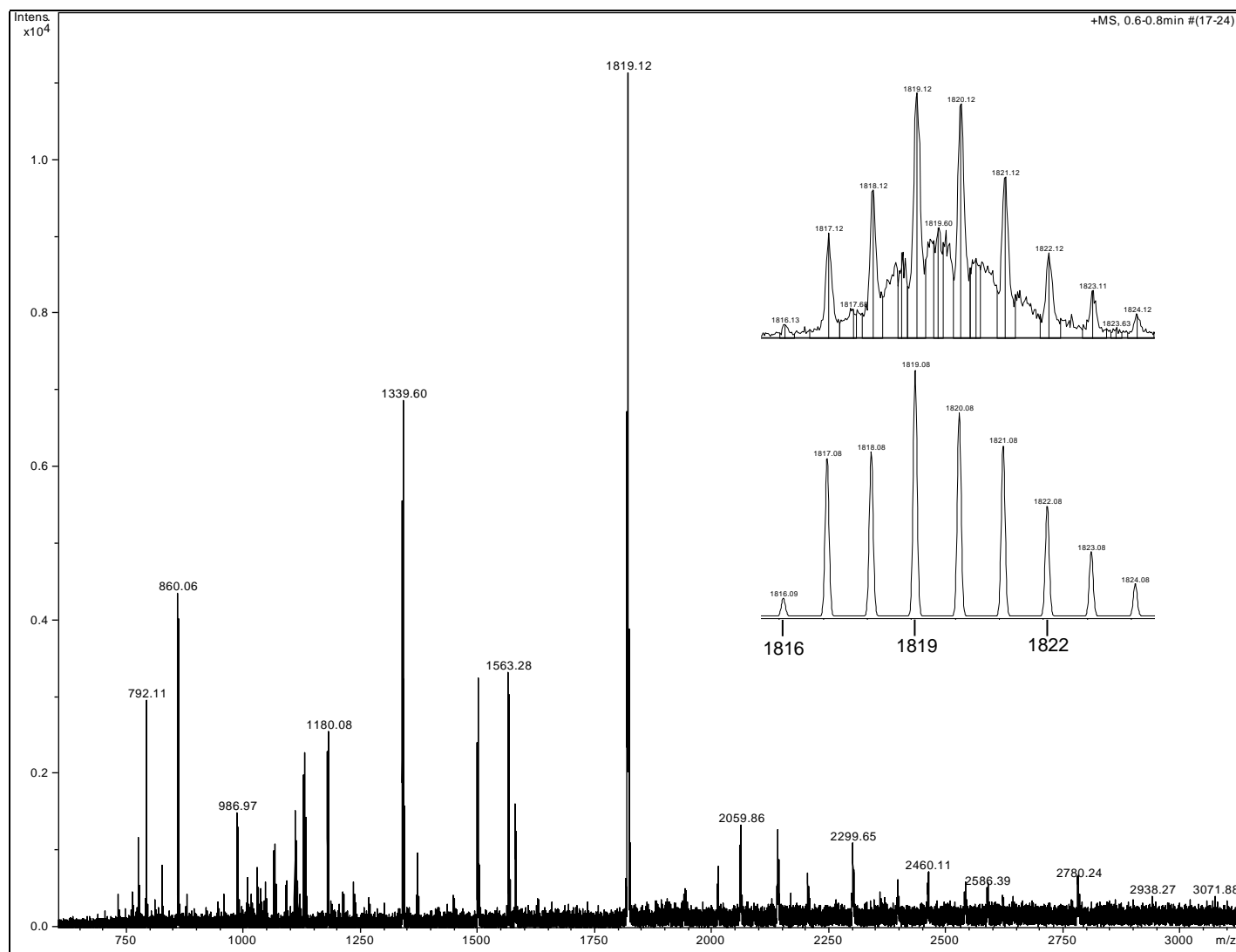


Figure 3. 10 ESI-MS of $[Fe_2(L^7)_2](ClO_4)_4$ with the found (top) and predicted (bottom) isotopic distribution pattern of $\{[Fe_2(L^7)_2](ClO_4)_3\}^+$ (inset)

Bond	Bond Length (Å)
Fe(1)-N(5)	2.142(3)
Fe(1)-N(2)	2.148(3)
Fe(1)-N(4)	2.215(3)
Fe(1)-N(1)	2.216(3)
Fe(1)-N(3)	2.221(3)
Fe(1)-N(6)	2.270(3)

Table 3.3 Selected bond lengths (Å) for the complex cation $[\text{Fe}_2(\text{L}^7)_2]^{4+}$

Bond	Angle (°)
N(5)-Fe(1)-N(2)	165.65(11)
N(5)-Fe(1)-N(4)	73.59(11)
N(2)-Fe(1)-N(4)	103.18(11)
N(5)-Fe(1)-N(1)	93.90(10)
N(2)-Fe(1)-N(1)	73.06(11)
N(4)-Fe(1)-N(1)	103.73(10)
N(5)-Fe(1)-N(3)	118.99(11)
N(2)-Fe(1)-N(3)	73.70(11)
N(4)-Fe(1)-N(3)	82.71(10)
N(1)-Fe(1)-N(3)	146.74(11)
N(5)-Fe(1)-N(6)	73.78(11)
N(2)-Fe(1)-N(6)	109.48(11)
N(4)-Fe(1)-N(6)	147.10(10)
N(1)-Fe(1)-N(6)	82.51(10)
N(3)-Fe(1)-N(6)	109.89(10)

Table 3.4 Selected bond angles (°) for the complex cation $[\text{Fe}_2(\text{L}^7)_2]^{4+}$

3.2.3 Complexes of L^8 with mercury(II)

Reaction of L^8 with an equimolar amount of $Hg(ClO_4)_2$ in nitromethane gave a pale yellow solution, which upon analysis by ESI-MS showed an ion at m/z 2111 corresponding to $\{[Hg_2(L^8)_2](ClO_4)_3\}^+$. Slow diffusion of diisopropyl ether into the nitromethane complex solution resulted in the formation of X-ray quality colourless crystals. X-ray crystal structure determination showed crystallisation in the monoclinic space group $P2(1)/c$ and confirmed the formation of the dinuclear species $[Hg_2(L^8)_2]^{4+}$ (figure 3.10).

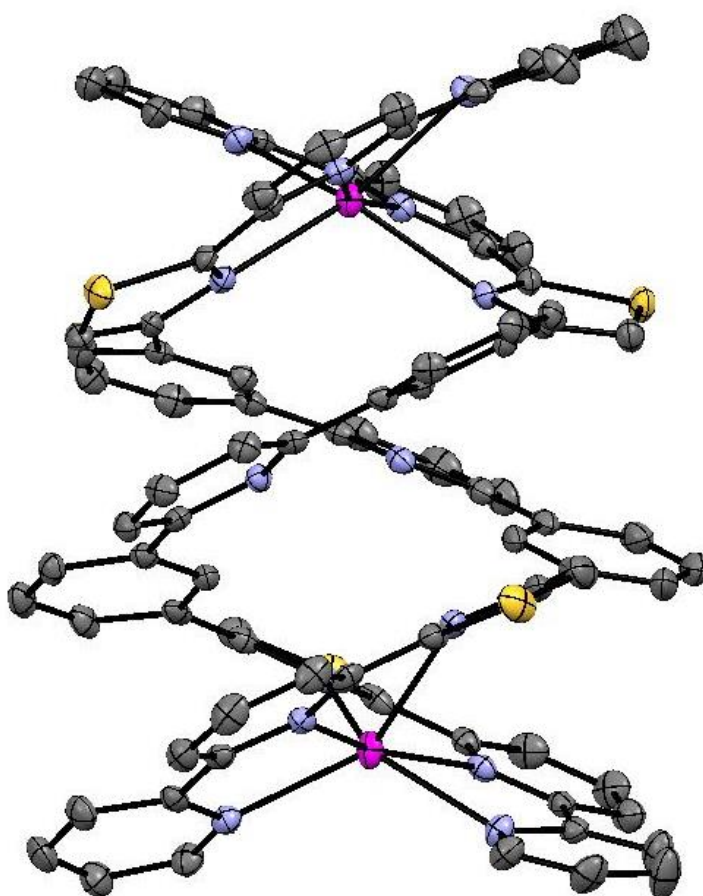


Figure 3.11 Solid state structure of the complex cation $[Hg_2(L^8)_2]^{4+}$

The crystal structure confirms in the solid state this ligand, L^8 , and $Hg(II)$ ions self-assemble to form a dinuclear double helicate. The $Hg(II)$ ions ($Hg-Hg$ distance: 8.1526(3) Å) are six coordinate arising from coordination with two tridentate N,N,N -domains from two different ligands ($Hg-N$ distances:

2.273(3)– 2.578(3)Å). Selected bond lengths and angles for the complex are shown in tables 3.5 and 3.6.

Bond	Bond Length (Å)	Bond	Bond Length (Å)
Hg(1)-N(9)	2.333(3)	Hg(2)-N(5)	2.273(3)
Hg(1)-N(11)	2.333(3)	Hg(2)-N(2)	2.311(3)
Hg(1)-N(7)	2.383(3)	Hg(2)-N(4)	2.364(3)
Hg(1)-N(10)	2.411(3)	Hg(2)-N(1)	2.388(3)
Hg(1)-N(8)	2.454(3)	Hg(2)-N(3)	2.438(3)
Hg(1)-N(12)	2.490(3)	Hg(2)-N(6)	2.578(3)

Table 3.5 Selected bond lengths (Å) for the complex cation $[\text{Hg}_2(\text{L}^8)_2]^{4+}$

Bond	Angle (°)	Bond	Angle (°)
N(9)-Hg(1)-N(11)	162.96(10)	N(5)-Hg(2)-N(2)	160.68(10)
N(9)-Hg(1)-N(7)	126.06(10)	N(5)-Hg(2)-N(4)	71.42(10)
N(11)-Hg(1)-N(7)	70.67(10)	N(2)-Hg(2)-N(4)	126.43(10)
N(9)-Hg(1)-N(10)	68.89(10)	N(5)-Hg(2)-N(1)	122.16(9)
N(11)-Hg(1)-N(10)	120.71(10)	N(2)-Hg(2)-N(1)	70.60(10)
N(7)-Hg(1)-N(10)	83.49(10)	N(4)-Hg(2)-N(1)	86.59(10)
N(9)-Hg(1)-N(8)	69.88(9)	N(5)-Hg(2)-N(3)	96.38(10)
N(11)-Hg(1)-N(8)	102.14(9)	N(2)-Hg(2)-N(3)	69.19(10)
N(7)-Hg(1)-N(8)	112.38(9)	N(4)-Hg(2)-N(3)	119.28(10)
N(10)-Hg(1)-N(8)	137.14(10)	N(1)-Hg(2)-N(3)	139.74(10)
N(9)-Hg(1)-N(12)	95.17(10)	N(5)-Hg(2)-N(6)	68.49(10)
N(11)-Hg(1)-N(12)	68.20(10)	N(2)-Hg(2)-N(6)	95.19(10)
N(7)-Hg(1)-N(12)	138.77(10)	N(4)-Hg(2)-N(6)	137.93(9)
N(10)-Hg(1)-N(12)	115.51(10)	N(1)-Hg(2)-N(6)	104.13(9)
N(8)-Hg(1)-N(12)	79.29(9)	N(3)-Hg(2)-N(6)	77.85(9)

Table 3.6 Selected bond angles (°) for the complex cation $[\text{Hg}_2(\text{L}^8)_2]^{4+}$

3.2.4 Complexes of L^9

3.2.4.1 Complex of L^9 cobalt(II)

Reaction of L^9 with an equimolar amount of $Co(BF_4)_2$ in nitromethane gave an orange solution which gave an ion in the ESI-MS at m/z 1876 corresponding to $\{[Co_2(L^9)_2](BF_4)_3\}^+$ indicating the formation of a dinuclear assembly. Slow diffusion of chloroform into the nitromethane complex solution resulted in the formation of X-ray quality orange crystals. The X-ray structure determination showed crystallisation in the triclinic space group $P-1$ and confirmed the formation of the dinuclear species $[Co_2(L^9)_2]^{4+}$ (figure 3.11).

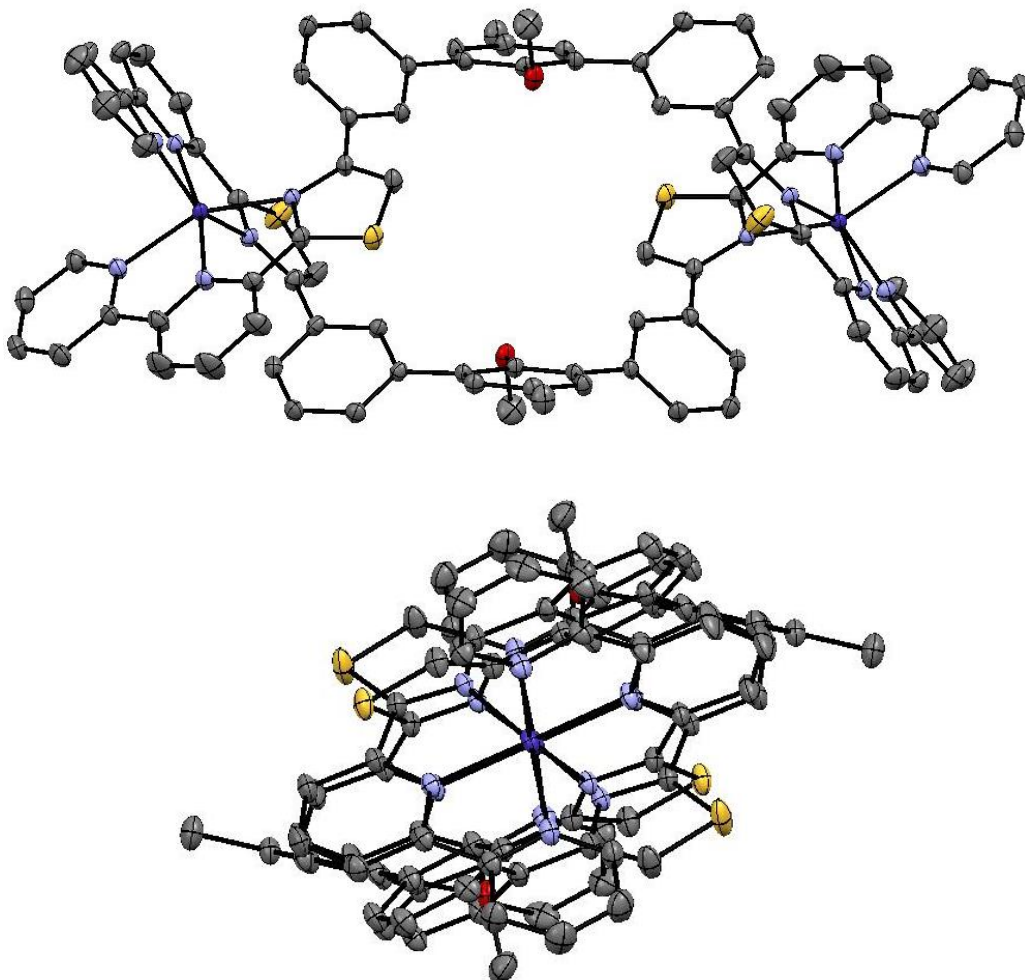


Figure 3.12 Two views for the solid state structure of the complex cation $[Co_2(L^9)_2]^{4+}$

Figure 3.11 shows the solid state structure which results upon complex formation between cobalt and \mathbf{L}^9 . This self-assembly results in the formation of a dinuclear double *meso*-helicate, in which the two tridentate domains of each ligand coordinate two different metal ions in a ‘side by side’ conformation. Each of the ligands coordinates *via* a C-type arrangement giving rise to metal centres of opposite chirality which leads to a dinuclear double *meso*-helicate, as opposed to a “true” helicate where the ligand twists and adopts an S-type arrangement resulting in the two metal ions having the same chirality. The cobalt metal ions (Co–Co distance: 14.0996(3) Å) display an octahedral geometry from coordination with six nitrogen atoms from two coordination sites (Co–N distances: 2.059(3) – 2.213(2) Å). Selected bond lengths and angles for the complex are shown in tables 3.7 and 3.8.

Bond	Bond Length (Å)
Co(1)-N(1)	2.191(3)
Co(1)-N(2)	2.059(3)
Co(1)-N(3)	2.213(2)
Co(1)-N(4)	2.157(3)
Co(1)-N(5)	2.069(3)
Co(1)-N(6)	2.153(3)

Table 3.7 Selected bond lengths (Å) for the complex cation $[\text{Co}_2(\mathbf{L}^9)_2]^{4+}$

Bond	Angle
N(2)-Co(1)-N(5)	167.44(10)
N(2)-Co(1)-N(6)	111.90(11)
N(5)-Co(1)-N(6)	76.57(10)
N(2)-Co(1)-N(4)	97.52(11)
N(5)-Co(1)-N(4)	75.39(10)
N(6)-Co(1)-N(4)	150.07(10)
N(2)-Co(1)-N(1)	75.53(10)
N(5)-Co(1)-N(1)	94.54(10)
N(6)-Co(1)-N(1)	97.47(10)
N(4)-Co(1)-N(1)	94.98(10)
N(2)-Co(1)-N(3)	76.26(10)
N(5)-Co(1)-N(3)	114.33(10)
N(6)-Co(1)-N(3)	86.62(9)
N(4)-Co(1)-N(3)	95.49(10)
N(1)-Co(1)-N(3)	150.94(10)

Table 3.8 Selected bond angles (°) for the complex cation $[\text{Co}_2(\text{L}^9)_2]^{4+}$

3.2.4.1 Complex of L^9 cadmium(II)

Reaction of L^9 with an equimolar amount of $Cd(ClO_4)_2$ in acetonitrile gave a pale yellow solution and analysis by ESI-MS showed ions corresponding to $\{[Cd(L^9)]ClO_4\}^+$ and $\{[Cd_2(L^9)_2](ClO_4)_3\}^+$ (m/z 961 and 2022 respectively). Layering of the acetonitrile complex solution with diethyl ether resulted in the formation of X-ray quality crystals. The X-ray crystal structure showed crystallisation in the triclinic space group $P-1$ and confirmed the formation of the dinuclear species $[Cd_2(L^9)_2]^{4+}$.

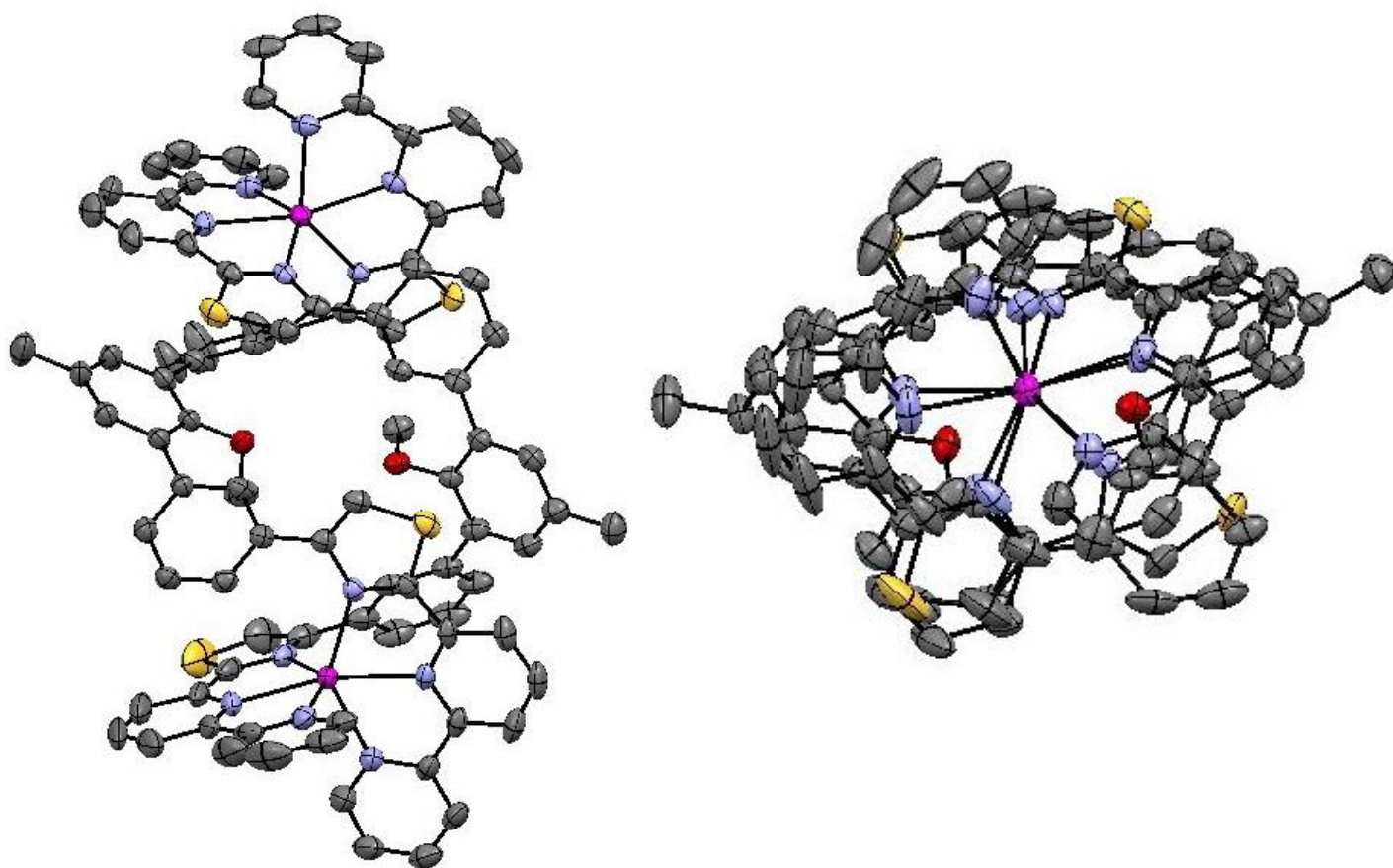


Figure 3.13 Two views for the solid state structure of the complex cation $[Cd_2(L^9)_2]^{4+}$

Figure 3.12 shows the solid state structure which results upon complex formation between cadmium(II) and L^9 . This self-assembly allows the formation of a dinuclear double helicate, in contrast with the previous complex observed for this ligand with cobalt(II). Each metal ion (Cd–Cd distance: 11.0466(6) Å)

displays an octahedral geometry from coordination with six nitrogen atoms from two coordination sites (Cd–N distances: 2.295(3) – 2.422(3) Å). The “over-and-under” conformation of the ligand giving a helical structure may be seen more clearly in figure 3.13 in which only one of the ligands of the dinuclear species is shown. Selected bond lengths and angles for the complex are shown in tables 3.9 and 3.10.

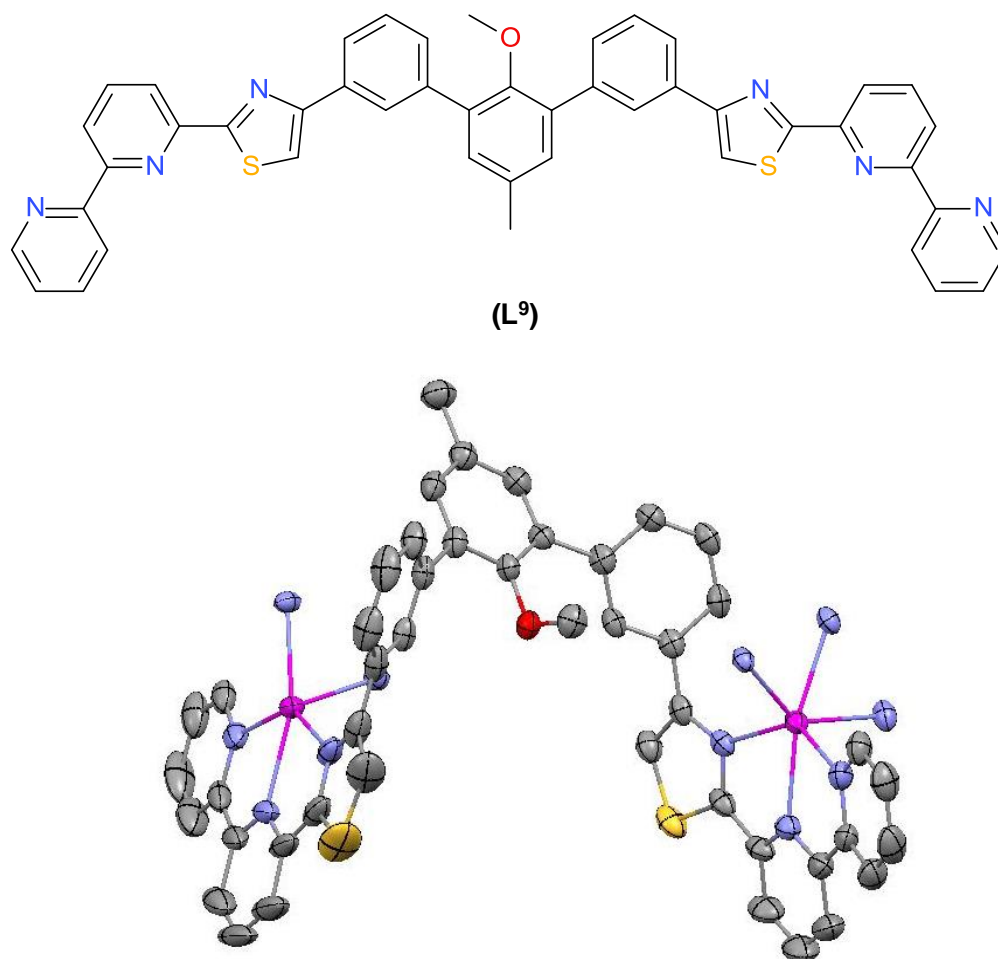


Figure 3.14 (i) Structure of L^9 , (ii) ligand coordination within the complex cation $[Cd_2(L^9)_2]^{4+}$

Bond	Bond Length (Å)	Bond	Bond Length (Å)
Cd(1)-N(11)	2.295(3)	Cd(2)-N(2)	2.313(3)
Cd(1)-N(5)	2.312(3)	Cd(2)-N(8)	2.326(4)
Cd(1)-N(4)	2.336(3)	Cd(2)-N(1)	2.352(4)
Cd(1)-N(12)	2.383(4)	Cd(2)-N(9)	2.352(4)
Cd(1)-N(6)	2.385(3)	Cd(2)-N(7)	2.386(4)
Cd(1)-N(10)	2.422(3)	Cd(2)-N(3)	2.395(3)

Table 3.9 Selected bond lengths (Å) for the complex cation $[\text{Cd}_2(\text{L}^9)_2]^{4+}$

Bond	Angle (°)	Bond	Angle (°)
N(11)-Cd(1)-N(5)	161.90(12)	N(2)-Cd(2)-N(8)	160.80(14)
N(11)-Cd(1)-N(4)	127.66(11)	N(2)-Cd(2)-N(1)	69.47(12)
N(5)-Cd(1)-N(4)	70.38(11)	N(8)-Cd(2)-N(1)	102.86(13)
N(11)-Cd(1)-N(12)	69.57(13)	N(2)-Cd(2)-N(9)	125.32(13)
N(5)-Cd(1)-N(12)	113.65(12)	N(8)-Cd(2)-N(9)	71.08(16)
N(4)-Cd(1)-N(12)	88.54(12)	N(1)-Cd(2)-N(9)	91.31(12)
N(11)-Cd(1)-N(6)	92.80(12)	N(2)-Cd(2)-N(7)	94.31(13)
N(5)-Cd(1)-N(6)	69.19(12)	N(8)-Cd(2)-N(7)	68.74(15)
N(4)-Cd(1)-N(6)	138.38(12)	N(1)-Cd(2)-N(7)	97.63(12)
N(12)-Cd(1)-N(6)	98.69(12)	N(9)-Cd(2)-N(7)	139.82(14)
N(11)-Cd(1)-N(10)	70.82(12)	N(2)-Cd(2)-N(3)	70.30(12)
N(5)-Cd(1)-N(10)	108.54(11)	N(8)-Cd(2)-N(3)	116.76(12)
N(4)-Cd(1)-N(10)	104.55(11)	N(1)-Cd(2)-N(3)	139.53(12)
N(12)-Cd(1)-N(10)	137.79(12)	N(9)-Cd(2)-N(3)	108.43(11)
N(6)-Cd(1)-N(10)	97.20(11)	N(7)-Cd(2)-N(3)	89.57(12)

Table 3.10 Selected bond angles (°) for the complex cation $[\text{Cd}_2(\text{L}^9)_2]^{4+}$

For this ligand, L^9 , two different self-assembled structures have been shown to form. This demonstrates well how subtle changes within such a reaction, i.e. different metal ion, can influence the resulting supramolecular architecture. In contrast with the previous ligand, L^7 , the inclusion of a more bulky pendant group on the central aromatic ring sufficiently prevents the formation of the more compact double helicate, when first row transition metals are employed, resulting in a *meso*-helicate structure.

3.2.5 Complexes of L^{10} with iron(II)

Reaction of L^{10} with an equimolar amount of $Fe(ClO_4)_2$ in acetonitrile gave a deep purple solution which upon analysis by ESI-MS showed ions at m/z 2084 and 992 corresponding to $\{[Fe_2(L^{10})_2](ClO_4)_3\}^+$ and $\{[Fe_2(L^{10})_2](ClO_4)_2\}^{2+}$ respectively, indicating the formation of a dinuclear species. Slow diffusion of chloroform into the acetonitrile complex solution resulted in the formation of X-ray quality purple crystals. The X-ray crystal structure showed crystallisation in the triclinic space group $P-1$ and confirmed the formation of the dinuclear species $[Fe_2(L^{10})_2]^{4+}$ (figure 3.14).

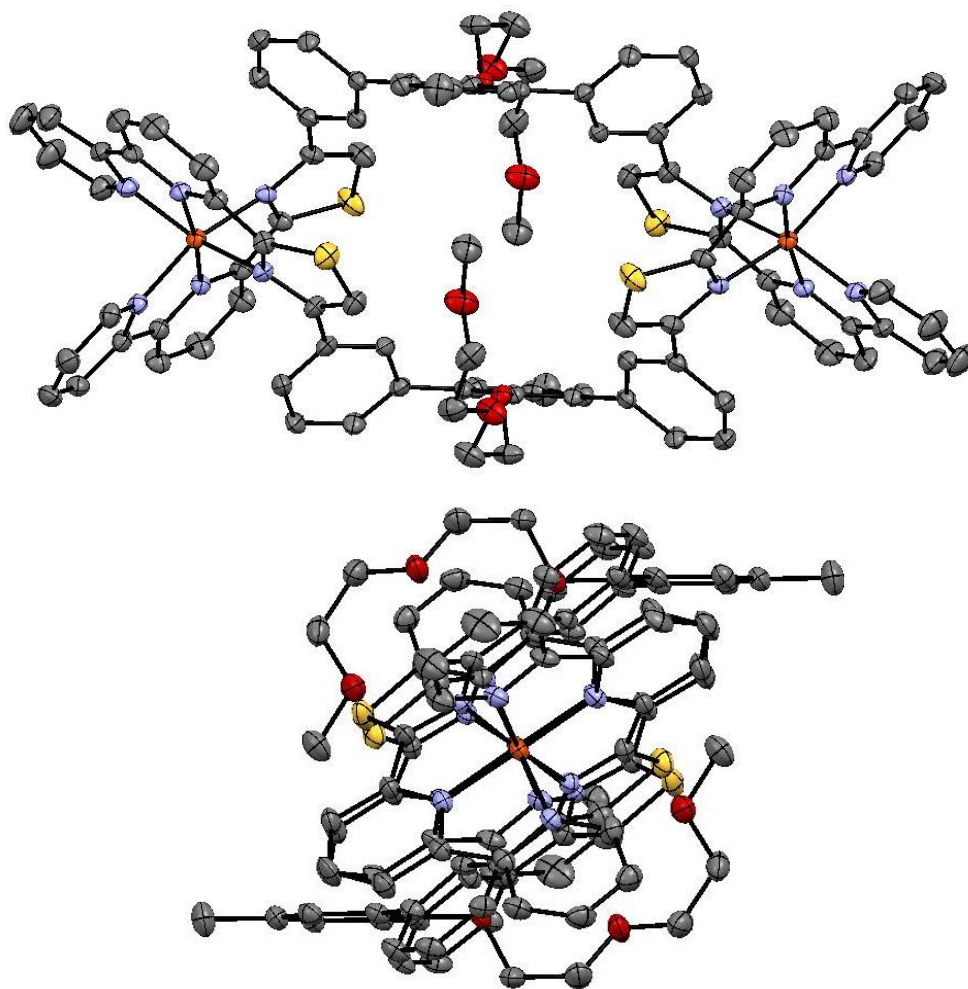


Figure 3.15 Two views for the solid state structure of the complex cation $[Fe_2(L^{10})_2]^{4+}$

The solid state structure of the complex cation $[Fe_2(L^{10})_2]^{4+}$ (figure 3.14) confirms the formation of a dinuclear species, as is expected for a ligand

possessing tridentate domains, separated by a spacer unit preventing coordination to a single metal ion. In the structure the two Fe(II) ions (Fe–Fe distance: 13.0506(9) Å) are six-coordinate from coordination by two thiazole-pyridyl-pyridyl donor domains from each ligand (Fe–N distances: 1.897(3) – 2.040(3) Å). However in this case the spacers bridge the tridentate domains in a “side-by-side” conformation not an “over-and-under” conformation as seen for helicates, for this structure a mesocate is produced (figure 3.15). Selected bond lengths and angles for the complex are shown in tables 3.11 and 3.12.

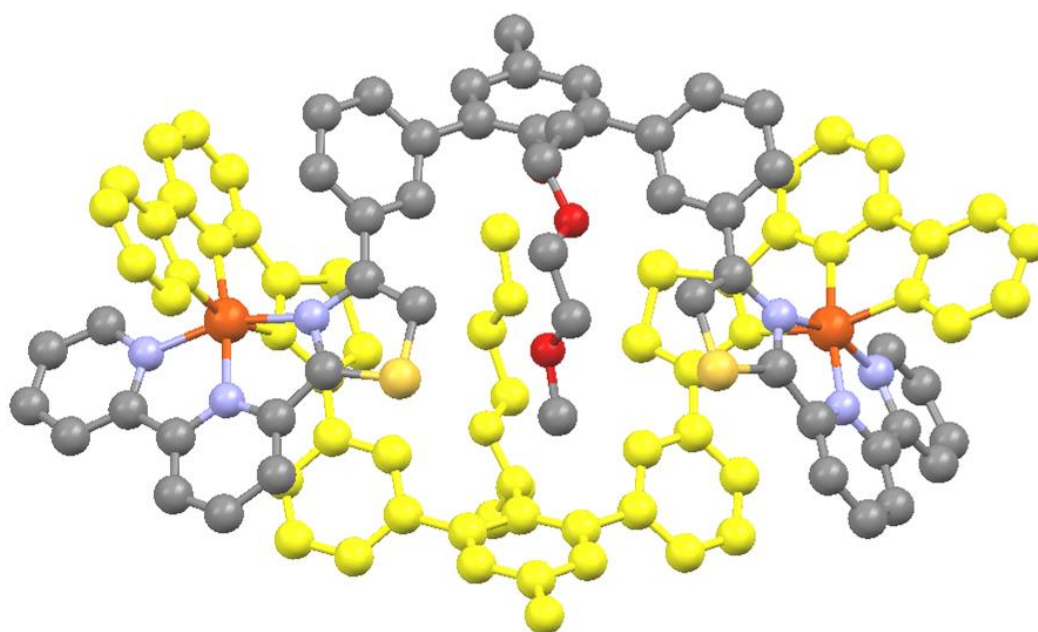


Figure 3.16 solid state structure of the complex cation $[\text{Fe}_2(\text{L}^{10})_2]^{4+}$. One ligand shown in yellow to better illustrate the “side-by-side” conformation of the ligand strands

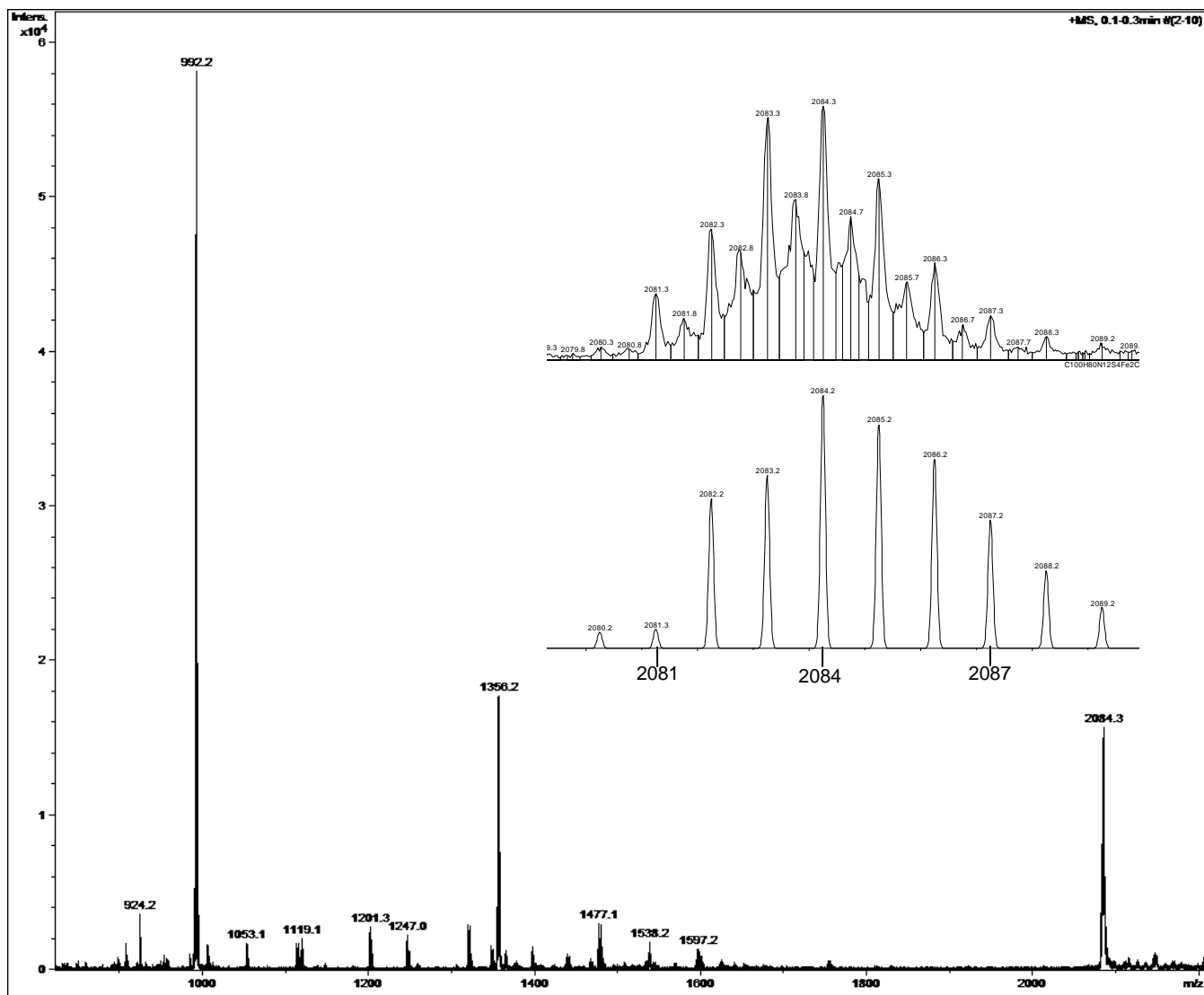


Figure 3. 17 ESI-MS of $[\text{Fe}_2(\text{L}^{10})_2](\text{ClO}_4)_4$ with the found (top) and predicted (bottom) isotopic distribution pattern of $\{[\text{Fe}_2(\text{L}^{10})_2](\text{ClO}_4)_3\}^+$ (inset)

Bond	Bond Length (Å)
Fe(1)-N(5)	1.897(3)
Fe(1)-N(2)	1.904(3)
Fe(1)-N(4)	1.966(3)
Fe(1)-N(1)	1.983(3)
Fe(1)-N(6)	2.038(3)
Fe(1)-N(3)	2.040(3)

Table 3.11 Selected bond lengths (Å) for the complex cation $[\text{Fe}_2(\text{L}^{10})_2]^{4+}$

Bond	Angle (°)
N(5)-Fe(1)-N(2)	172.35(12)
N(5)-Fe(1)-N(4)	80.50(12)
N(2)-Fe(1)-N(4)	95.46(12)
N(5)-Fe(1)-N(1)	93.30(12)
N(2)-Fe(1)-N(1)	80.12(12)
N(4)-Fe(1)-N(1)	89.65(12)
N(5)-Fe(1)-N(6)	79.70(12)
N(2)-Fe(1)-N(6)	104.95(12)
N(4)-Fe(1)-N(6)	159.12(12)
N(1)-Fe(1)-N(6)	98.03(12)
N(5)-Fe(1)-N(3)	106.64(12)
N(2)-Fe(1)-N(3)	80.03(12)
N(4)-Fe(1)-N(3)	94.28(12)
N(1)-Fe(1)-N(3)	160.04(12)
N(6)-Fe(1)-N(3)	85.12(11)

Table 3.12 Selected bond angles (°) for the complex cation $[\text{Fe}_2(\text{L}^{10})_2]^{4+}$

3.2.6 Complexes of L^{11} with cadmium(II)

Reaction of L^{11} with an equimolar amount of $Cd(ClO_4)_2$ in nitromethane gave a colourless solution, which upon analysis by ESI-MS showed ions at m/z 1990 and 946 corresponding to $\{[Cd_2(L^{11})_2](ClO_4)_3\}^+$ and $\{[Cd_2(L^{11})_2](ClO_4)_2\}^{2+}$ indicating a dinuclear species. Camphorsulfonic acid (1 equivalent per ligand for protonation of the amine groups) was added to the solution and upon slow diffusion of dichloromethane into the nitromethane complex solution X-ray quality colourless crystals were obtained. The structural determination showed crystallisation in the triclinic space group $P-1$ and confirmed the formation of the dinuclear species $[Cd_2(L^{11})(L^{11}-H)]^{5+}$ (figure 3.16).

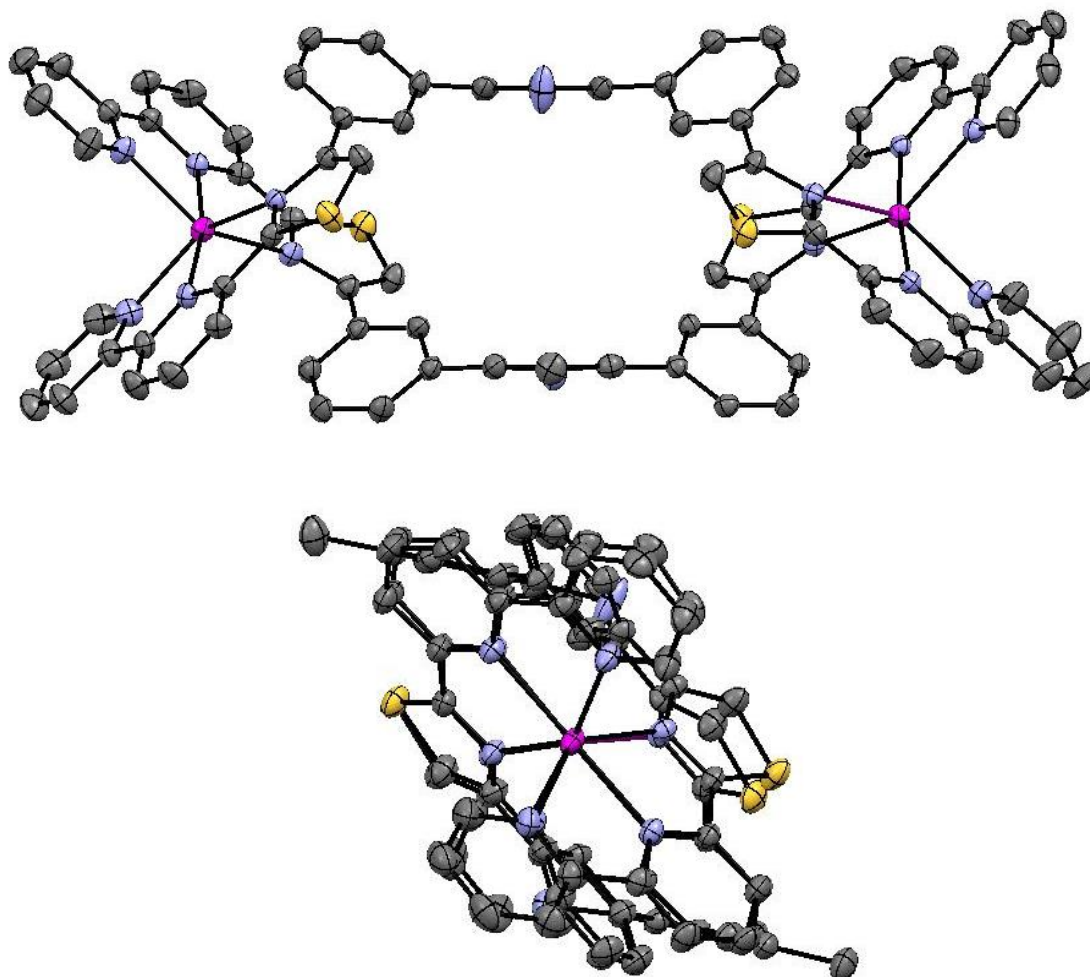


Figure 3.18 Solid state structure of the complex cation $[Cd_2(L^{11})(L^{11}-H)]^{5+}$

The solid state structure of the complex cation $[\text{Cd}_2(\text{L}^{11})(\text{L}^{11}\text{-H})]^{5+}$ confirms the formation of a dinuclear species. In the structure Cd(II) metal ions (Cd–Cd distance: 14.3905(6) Å) coordinate two thiazole-pyridyl-pyridyl donor domains giving a six-coordinate geometry (Cd–N distances: 2.301(3) – 2.396(3) Å). Selected bond lengths and angles for the complex are shown in tables 3.13 and 3.14. Again in this case the spacers bridge the tridentate domains in a “side-by-side” conformation giving a *meso*-helicite (figure 3.16). As can be seen from the formula for this complex cation there are five perchlorate counter anions ($[\text{Cd}_2(\text{L}^{11})(\text{L}^{11}\text{-H})](\text{ClO}_4)_5$) and as the crystals were grown in the presence of camphorsulfonic acid it is assumed that one of the amine nitrogen atoms has been protonated. In the central cavity a water molecule is present and this is able to act as a hydrogen bond acceptor to the protonated amine (2.850(6) Å) and a donor to the other, unprotonated, amine (3.254(6) Å) (figure 3.17). Selected bond lengths and angles for the complex are shown in tables 3.13 and 3.14.

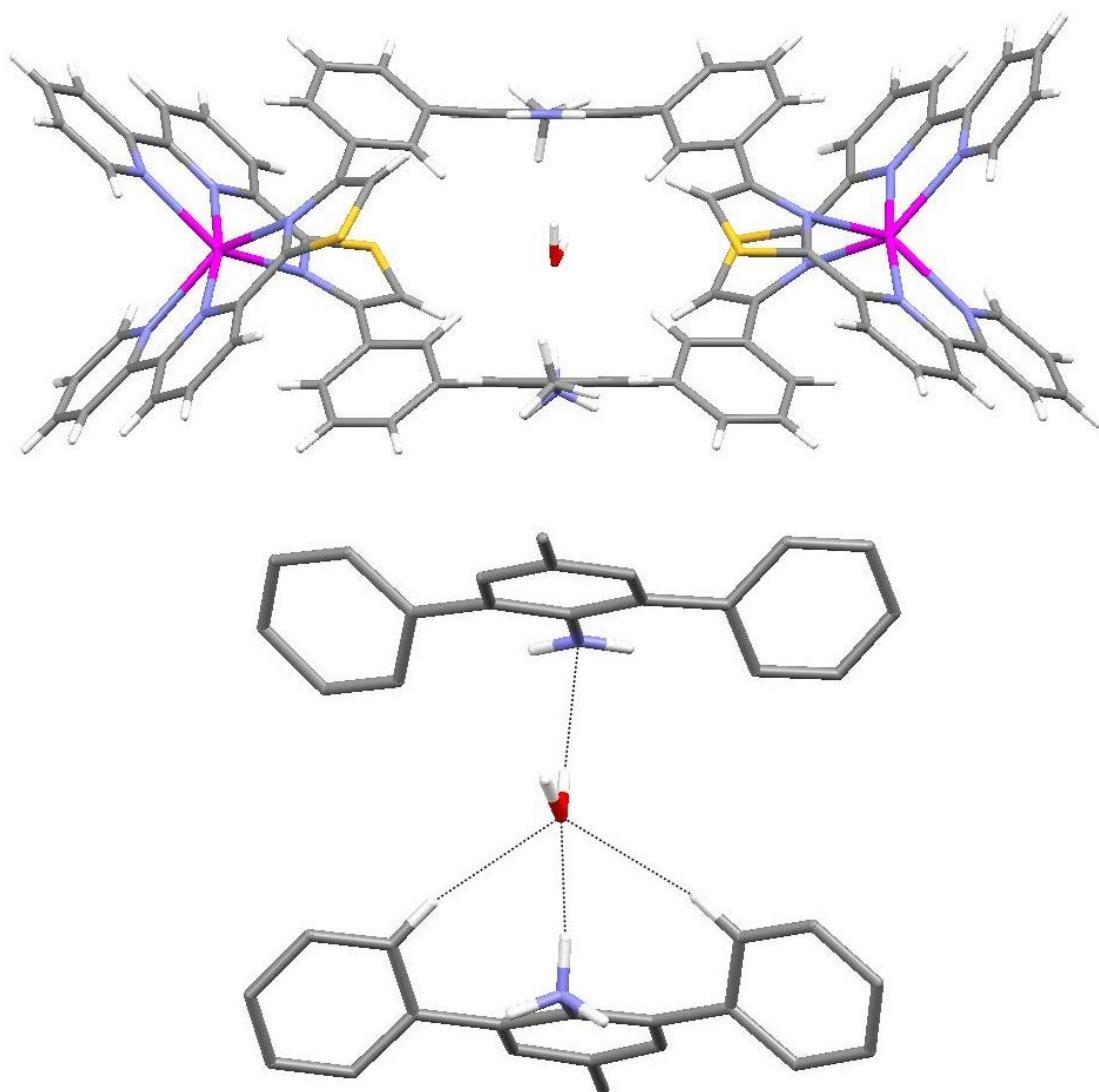


Figure 3.19 Two views of the complex cation $[\text{Cd}_2(\text{L}^{11})(\text{L}^{11}\text{-H})]^{5+}$ (i) Solid state structure including the water molecule within the cavity; (ii) Solid state structure showing hydrogen bonding.

Bond	Bond Length (Å)	Bond	Bond Length (Å)
Cd(1)-N(6)	2.301(3)	Cd(2)-N(9)	2.308(3)
Cd(1)-N(13)	2.309(3)	Cd(2)-N(2)	2.313(3)
Cd(1)-N(12)	2.335(3)	Cd(2)-N(8)	2.352(3)
Cd(1)-N(7)	2.339(3)	Cd(2)-N(3)	2.373(3)
Cd(1)-N(5)	2.342(3)	Cd(2)-N(1)	2.378(3)
Cd(1)-N(14)	2.351(4)	Cd(2)-N(10)	2.396(3)

Table 3.13 Selected bond lengths (Å) for the complex cation $[\text{Cd}_2(\text{L}^{11})(\text{L}^{11}\text{-H})]^{5+}$

Bond	Angle (°)	Bond	Angle (°)
N(6)-Cd(1)-N(13)	169.09(11)	N(9)-Cd(2)-N(2)	173.25(11)
N(6)-Cd(1)-N(12)	117.50(11)	N(9)-Cd(2)-N(8)	69.25(11)
N(13)-Cd(1)-N(12)	70.95(11)	N(2)-Cd(2)-N(8)	107.30(11)
N(6)-Cd(1)-N(7)	69.58(12)	N(9)-Cd(2)-N(3)	115.10(11)
N(13)-Cd(1)-N(7)	102.84(12)	N(2)-Cd(2)-N(3)	71.17(11)
N(12)-Cd(1)-N(7)	100.84(11)	N(8)-Cd(2)-N(3)	105.05(11)
N(6)-Cd(1)-N(5)	71.45(11)	N(9)-Cd(2)-N(1)	105.06(11)
N(13)-Cd(1)-N(5)	117.04(11)	N(2)-Cd(2)-N(1)	69.00(11)
N(12)-Cd(1)-N(5)	88.73(11)	N(8)-Cd(2)-N(1)	93.69(12)
N(7)-Cd(1)-N(5)	139.89(11)	N(3)-Cd(2)-N(1)	139.46(11)
N(6)-Cd(1)-N(14)	102.47(11)	N(9)-Cd(2)-N(10)	70.54(11)
N(13)-Cd(1)-N(14)	69.68(11)	N(2)-Cd(2)-N(10)	113.56(11)
N(12)-Cd(1)-N(14)	139.98(11)	N(8)-Cd(2)-N(10)	138.89(11)
N(7)-Cd(1)-N(14)	94.55(12)	N(3)-Cd(2)-N(10)	84.47(11)
N(5)-Cd(1)-N(14)	102.78(12)	N(1)-Cd(2)-N(10)	104.62(11)

Table 3.14 Selected bond angles (°) for the complex cation $[\text{Cd}_2(\text{L}^{11})(\text{L}^{11}\text{-H})]^{5+}$

3.2.7 Complexes of L^{12} with zinc(II)

Reaction of L^{12} with an equimolar quantity of $Zn(ClO_4)_2$ in nitromethane gave a colourless solution which gave ions in the ESI-MS at m/z 1981 and 940 corresponding to $\{[Cd_2(L^{12})_2](ClO_4)_3\}^+$ and $\{[Cd_2(L^{12})_2](ClO_4)_2\}^{2+}$ indicating the formation of a dinuclear assembly. Slow diffusion of dichloromethane into the nitromethane complex solution resulted in the formation of X-ray quality colourless crystals. The X-ray crystal structure determination showed crystallisation in the triclinic space group $P-1$ and confirmed the formation of the dinuclear species $[Zn_2(L^{12})_2]^{4+}$ (figure 3.18).

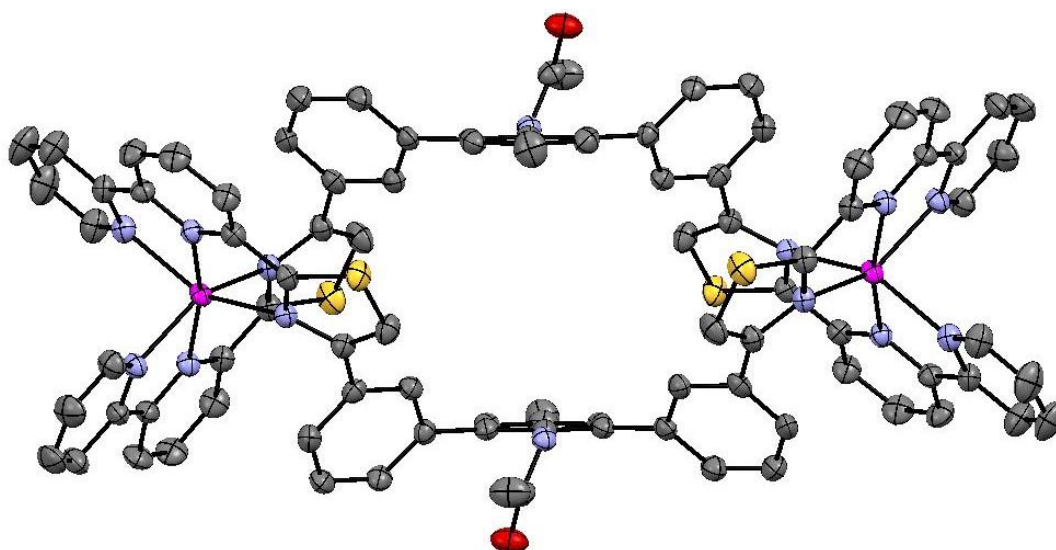


Figure 3.20 Solid state structure of the complex cation $[Zn_2(L^{12})_2]^{4+}$

The solid state structure of the complex cation $[Zn_2(L^{12})_2]^{4+}$ shows the formation of a dinuclear species. In the structure Zn(II) metal ions are coordinated by two thiazole-pyridyl-pyridyl donor domains giving a six-coordinate geometry; again in this case the spacers bridge the tridentate domains in a “side-by-side” conformation giving a *meso*-helicate. The data obtained for this particular structure, however, was not of the highest quality due to the loss of solvent. As a result the data should be interpreted with caution; however, the structure does provide enough information about the gross molecular connectivity within the self-assembly.

3.2.8 Complexes of L^{13} with zinc(II)

Reaction of L^{13} with an equimolar amount of $Zn(ClO_4)_2$ in nitromethane gave a colourless solution, which upon analysis by ESI-MS showed ions at m/z 2105 and 1002 corresponding to $\{[Zn_2(L^{13})_2](ClO_4)_3\}^+$ and $\{[Zn_2(L^{13})_2](ClO_4)_2\}^{2+}$ respectively, indicating a dinuclear species has formed. Slow diffusion of dichloromethane into the nitromethane complex solution resulted in the formation of X-ray quality colourless crystals. The X-ray crystal structure determination showed crystallisation in the triclinic space group $P-1$ and confirmed the formation of the dinuclear species $[Zn_2(L^{13})_2]^{4+}$ (figure 3.19).

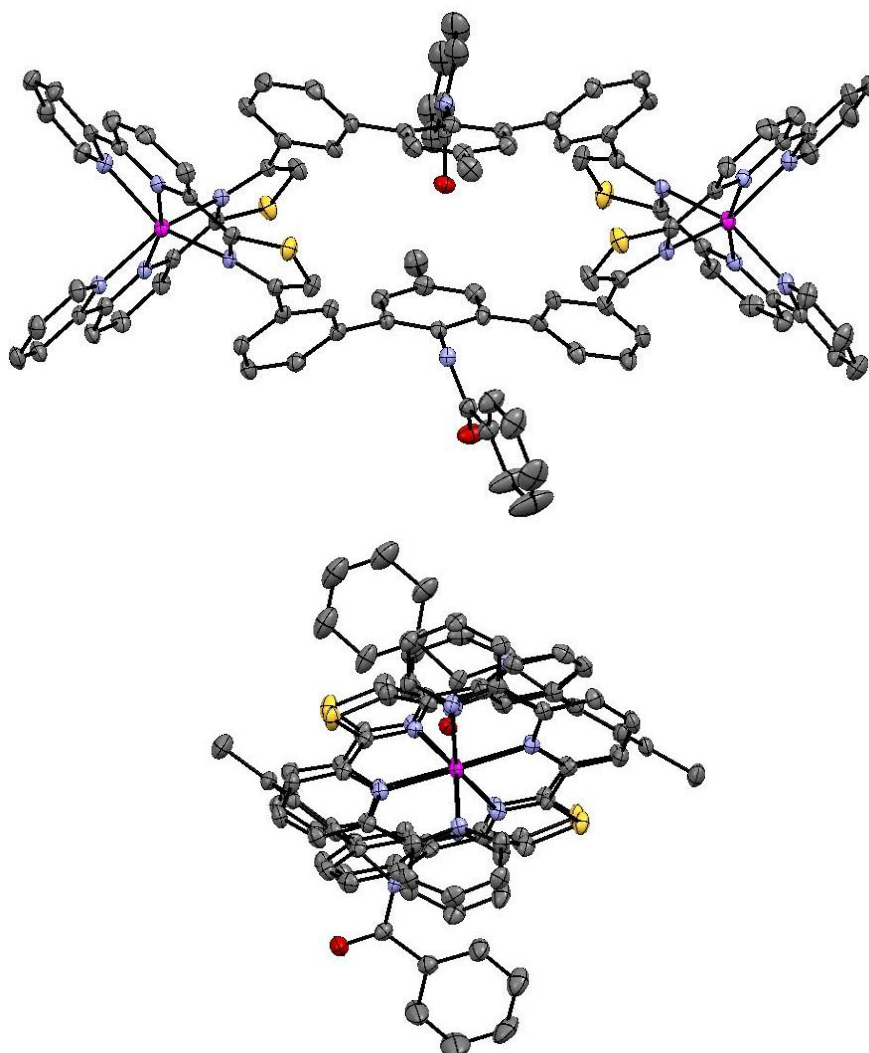


Figure 3.21 Two views for the solid state structure of the complex cation $[Zn_2(L^{13})_2]^{4+}$, solvent molecule omitted for clarity.

The crystal structure confirms that in the solid state the ligand, L^{13} , and Zn(II) ions self-assemble to form a dinuclear double *meso*-helicate, in which the ligand strand partitions into two tridentate donor domains, separated by the tri-phenylene spacer unit (figure 3.19). The two tridentate donor domains of each ligand coordinate both of the metal ions; the two Zn(II) ions (Zn–Zn distance: 14.1821(5) Å) are six coordinate arising from coordination with two tridentate N,N,N-domains (Zn–N distances: 2.073(3) – 2.214(4) Å).

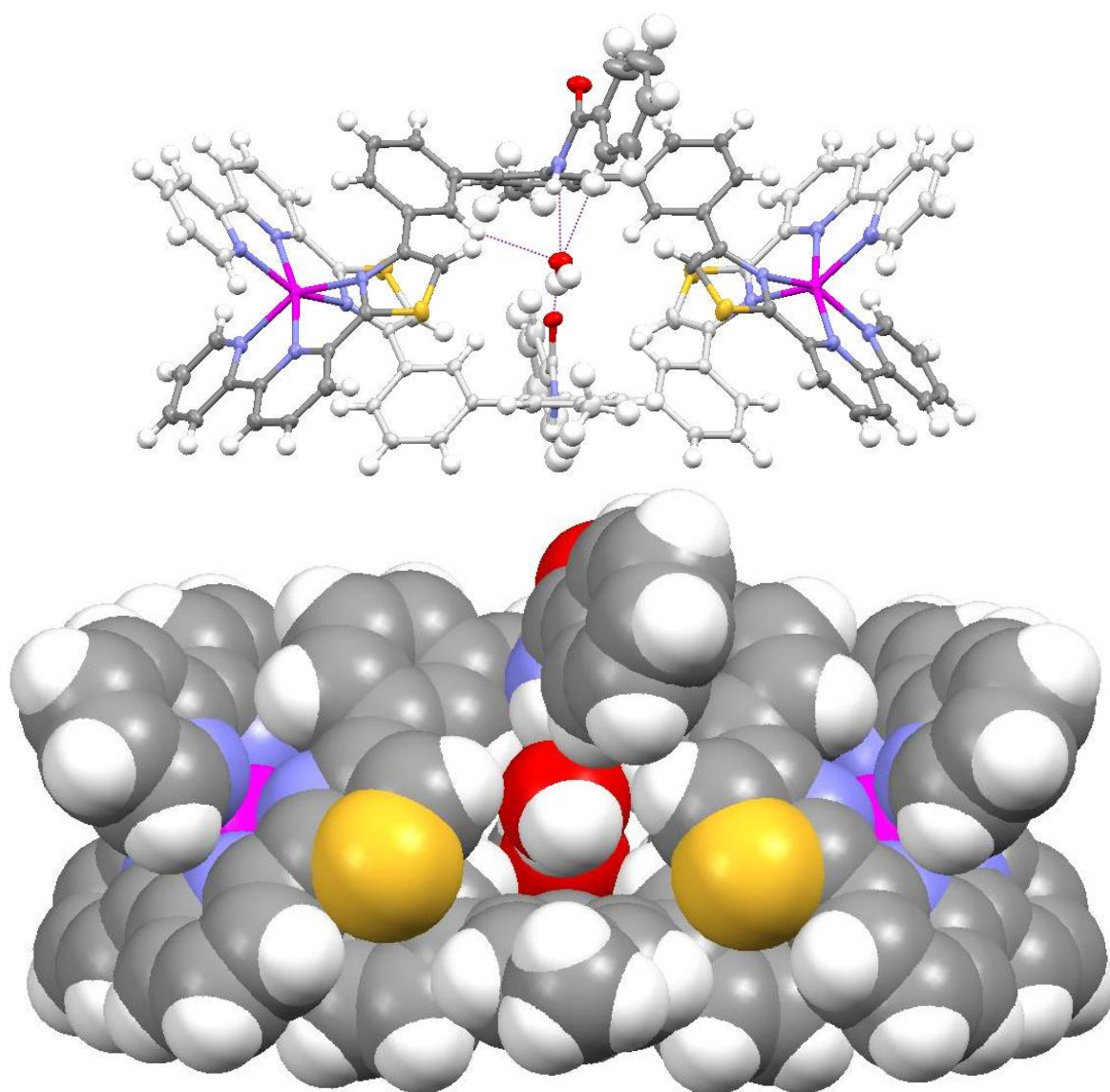


Figure 3.22 Two views of the complex cation $[Zn_2(L^{13})_2]^{4+}$ (i) Solid state structure; (ii) a space-filling picture showing all atoms and their van der Waal's radii

Within the cavity of the *meso*-helicate there is a water molecule present, this fits well between the two ligands (figure 3.20). This is held in place through hydrogen bonding, where the water is able to act as a hydrogen bond acceptor (2.1288(1) – 2.5589(1) Å) as well as a donor (1.8811(1) Å). Selected bond lengths and angles for the complex are shown in tables 3.15 and 3.16.

Bond	Bond Length (Å)	Bond	Bond Length (Å)
Zn(1)-N(1)	2.195(3)	Zn(2)-N(4)	2.196(3)
Zn(1)-N(2)	2.073(3)	Zn(2)-N(5)	2.076(3)
Zn(1)-N(3)	2.198(3)	Zn(2)-N(6)	2.214(4)
Zn(1)-N(8)	2.198(4)	Zn(2)-N(11)	2.197(3)
Zn(1)-N(9)	2.078(3)	Zn(2)-N(12)	2.090(4)
Zn(1)-N(10)	2.195(3)	Zn(2)-N(13)	2.171(4)

Table 3.15 Selected bond lengths (Å) for the complex cation $[\text{Zn}_2(\text{L}^{13})_2]^{4+}$

Bond	Angle (°)	Bond	Angle (°)
N(2)-Zn(1)-N(1)	75.35(13)	N(5)-Zn(2)-N(4)	77.03(13)
N(3)-Zn(1)-N(1)	149.42(13)	N(6)-Zn(2)-N(4)	150.83(13)
N(3)-Zn(1)-N(2)	76.44(13)	N(6)-Zn(2)-N(5)	74.94(14)
N(8)-Zn(1)-N(1)	93.17(13)	N(11)-Zn(2)-N(4)	87.59(13)
N(8)-Zn(1)-N(2)	94.88(13)	N(11)-Zn(2)-N(5)	114.89(14)
N(8)-Zn(1)-N(3)	100.75(13)	N(11)-Zn(2)-N(6)	96.93(13)
N(9)-Zn(1)-N(1)	94.08(13)	N(12)-Zn(2)-N(4)	115.69(14)
N(9)-Zn(1)-N(2)	165.14(13)	N(12)-Zn(2)-N(5)	164.67(14)
N(9)-Zn(1)-N(3)	115.71(13)	N(12)-Zn(2)-N(6)	93.27(14)
N(9)-Zn(1)-N(8)	75.01(13)	N(12)-Zn(2)-N(11)	75.69(14)
N(10)-Zn(1)-N(1)	93.47(13)	N(13)-Zn(2)-N(4)	96.44(13)
N(10)-Zn(1)-N(2)	114.13(13)	N(13)-Zn(2)-N(5)	95.53(14)
N(10)-Zn(1)-N(3)	87.43(13)	N(13)-Zn(2)-N(6)	94.11(14)
N(10)-Zn(1)-N(8)	150.98(13)	N(13)-Zn(2)-N(11)	149.39(13)
N(10)-Zn(1)-N(9)	76.36(13)	N(13)-Zn(2)-N(12)	75.25(14)

Table 3.16 Selected bond angles (°) for the complex cation $[\text{Zn}_2(\text{L}^{13})_2]^{4+}$

3.2.9 Complexes of L^{14} with cadmium(II)

Reaction of L^{14} with an equimolar amount of $Cd(ClO_4)_2$ in acetonitrile gave a colourless solution, which upon analysis by ESI-MS showed ions at m/z 1037 and 2173 corresponding to $\{[Cd(L^{14})]ClO_4\}^+$ and $\{[Cd_2(L^{14})_2](ClO_4)_3\}^+$. Slow diffusion of dichloromethane into the acetonitrile complex solution resulted in the formation of X-ray quality colourless crystals. The X-ray crystal structure showed crystallisation in the monoclinic space group $P 1 21/c$ and confirmed the formation of the dinuclear species $[Cd_2(L^{14})_2]^{4+}$ (figure 3.21).

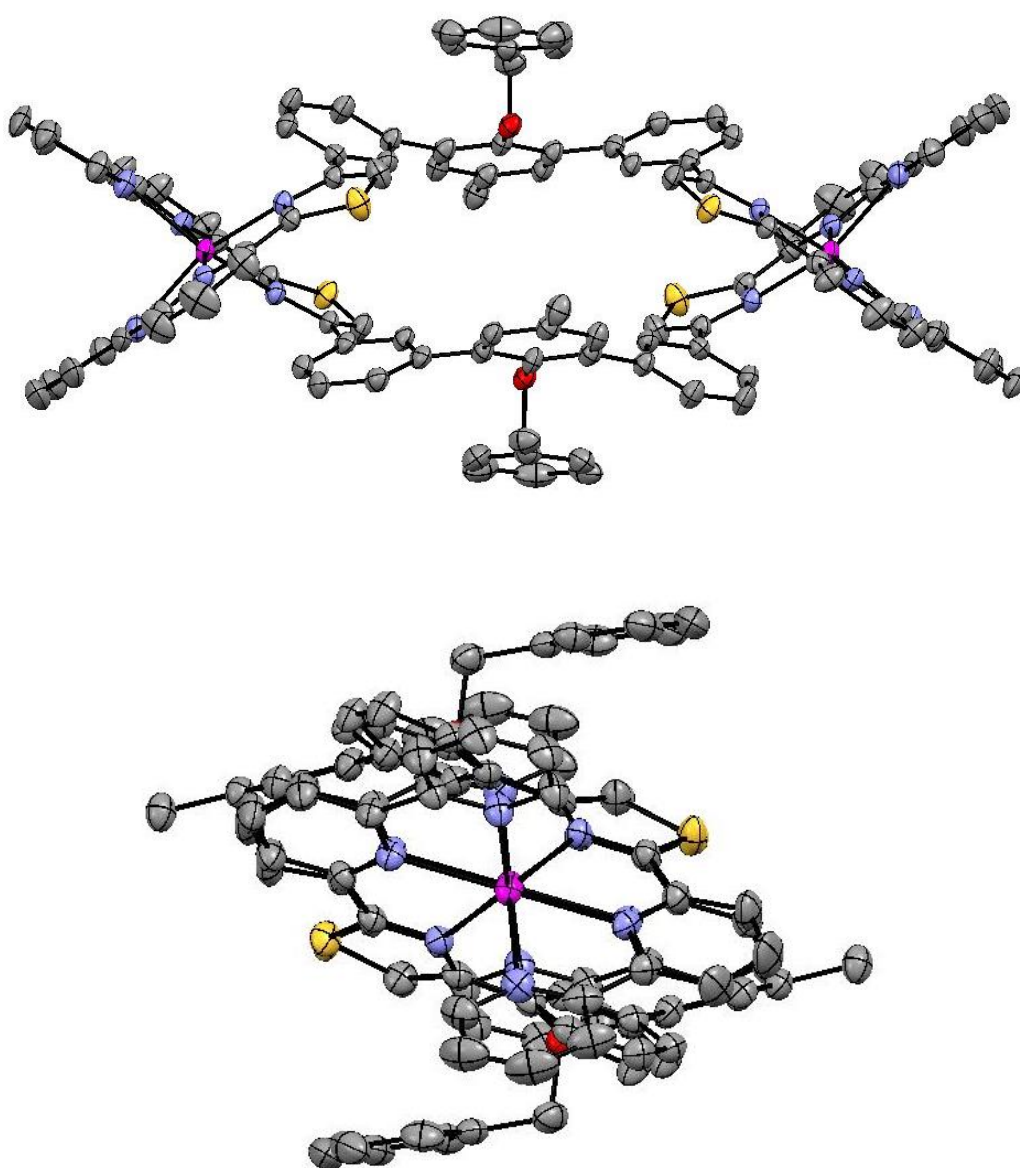


Figure 3.23 Two views for the solid state structure of the complex cation $[Cd_2(L^{14})_2]^{4+}$

The crystal structure confirms that in the solid state the ligand, L^{14} , and Cd(II) ions self-assemble to form a dinuclear double *meso*-helicate, in which the ligand strand partitions into two tridentate donor domains, separated by the tri-phenylene spacer unit (figure 3.21). The space-filling structure is shown in figure 3.22. The two tridentate donor domains of each ligand coordinate each of the two metal ions; the two Cd(II) ions (Cd–Cd distance: 14.1958(6) Å) are six-coordinate arising from coordination by two tridentate N,N,N-domains (Cd–N distances: 2.301(4) – 2.379(4) Å). Selected bond lengths and angles for the complex are shown in tables 3.16 and 3.17.

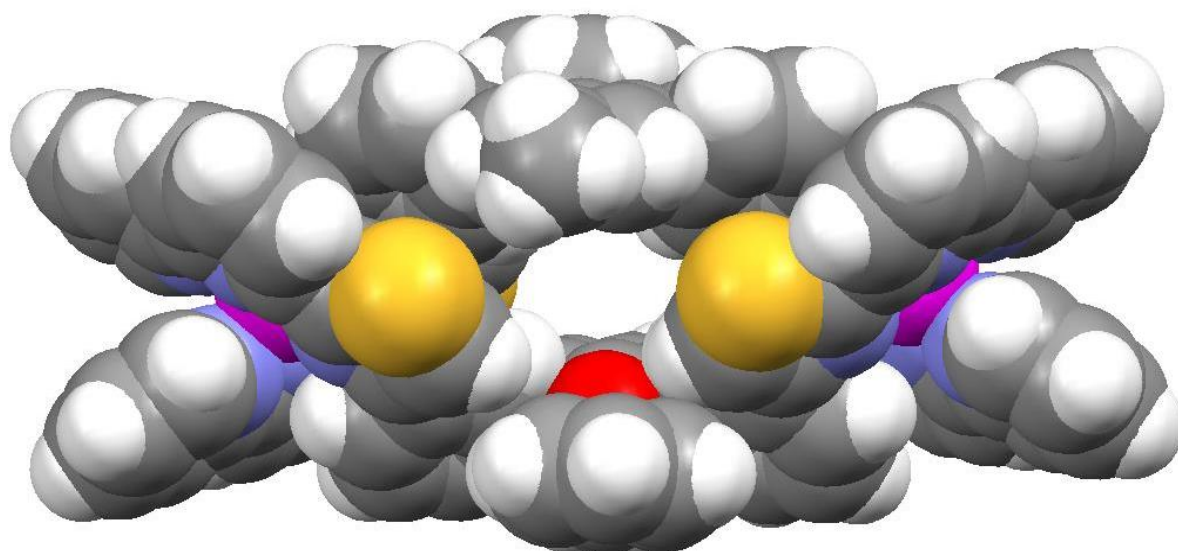


Figure 3.24 Space-filling picture of the complex cation $[Cd_2(L^{14})_2]^{4+}$ showing all atoms and their van der Waal's radii

Bond	Bond Length (Å)
Cd(1)-N(2)	2.301(4)
Cd(1)-N(5)	2.314(4)
Cd(1)-N(6)	2.333(3)
Cd(1)-N(1)	2.355(3)
Cd(1)-N(3)	2.374(3)
Cd(1)-N(4)	2.379(4)

Table 3.17 Selected bond lengths (Å) for the complex cation $[Cd_2(L^{14})_2]^{4+}$

Bond	Angle (°)
N(2)-Cd(1)-N(5)	165.97(12)
N(2)-Cd(1)-N(6)	119.33(13)
N(5)-Cd(1)-N(6)	71.27(13)
N(2)-Cd(1)-N(1)	70.13(12)
N(5)-Cd(1)-N(1)	98.70(13)
N(6)-Cd(1)-N(1)	106.65(13)
N(2)-Cd(1)-N(3)	71.05(12)
N(5)-Cd(1)-N(3)	120.36(12)
N(6)-Cd(1)-N(3)	88.47(12)
N(1)-Cd(1)-N(3)	140.92(13)
N(2)-Cd(1)-N(4)	101.82(14)
N(5)-Cd(1)-N(4)	68.57(14)
N(6)-Cd(1)-N(4)	138.79(13)
N(1)-Cd(1)-N(4)	88.32(13)
N(3)-Cd(1)-N(4)	103.86(13)

Table 3.18 Selected bond angles (°) for the complex cation $[\text{Cd}_2(\text{L}^{14})_2]^{4+}$

3.3 Solution studies

3.3.1 Solution state characterisation of complexes of \mathbf{L}^9

The zinc containing species, $[\text{Zn}_2(\mathbf{L}^9)_2]^{4+}$, is iso-structural to the cobalt complex seen previously (figure 3.8); mesocates are formed in both cases. This gives a better species for direct comparison with the cadmium complex, i.e. both have d^{10} electronic configuration.

3.3.1.1 Solution state characterisation of $[\text{Zn}_2(\mathbf{L}^9)_2]^{4+}$

The ^1H NMR spectrum of a CD_3NO_2 solution of $[\text{Zn}_2(\mathbf{L}^9)_2](\text{CF}_3\text{SO}_3)_4$ is an interesting spectrum. Some of the signals are coincident; even with this it is clear there are two species present (figure 3.23, a). It has been shown previously with such complexes that typically the less symmetrical mismatched species are disfavoured in solution, in this case the mesocate, which is seen as the lower percentage of the equilibrium mixture.¹⁴¹ Here the minor set of signals observed correspond to the mesocate while the major set corresponds to the helicate.

3.3.1.2 Solution state characterisation of $[\text{Cd}_2(\mathbf{L}^9)_2]^{4+}$

The one-dimensional ^1H NMR spectrum of $[\text{Cd}_2(\mathbf{L}^9)_2](\text{ClO}_4)_4$ in CD_3NO_2 shows the 13 aromatic signals expected for such an assembly, in this case showing only one species is present (figure 3.23, b). Seen in the spectrum are a number of broad peaks, cooling of the NMR sample only resulted in further broadening of the peaks, thus the broad peaks have been attributed to restricted rotation of the ligand framework.

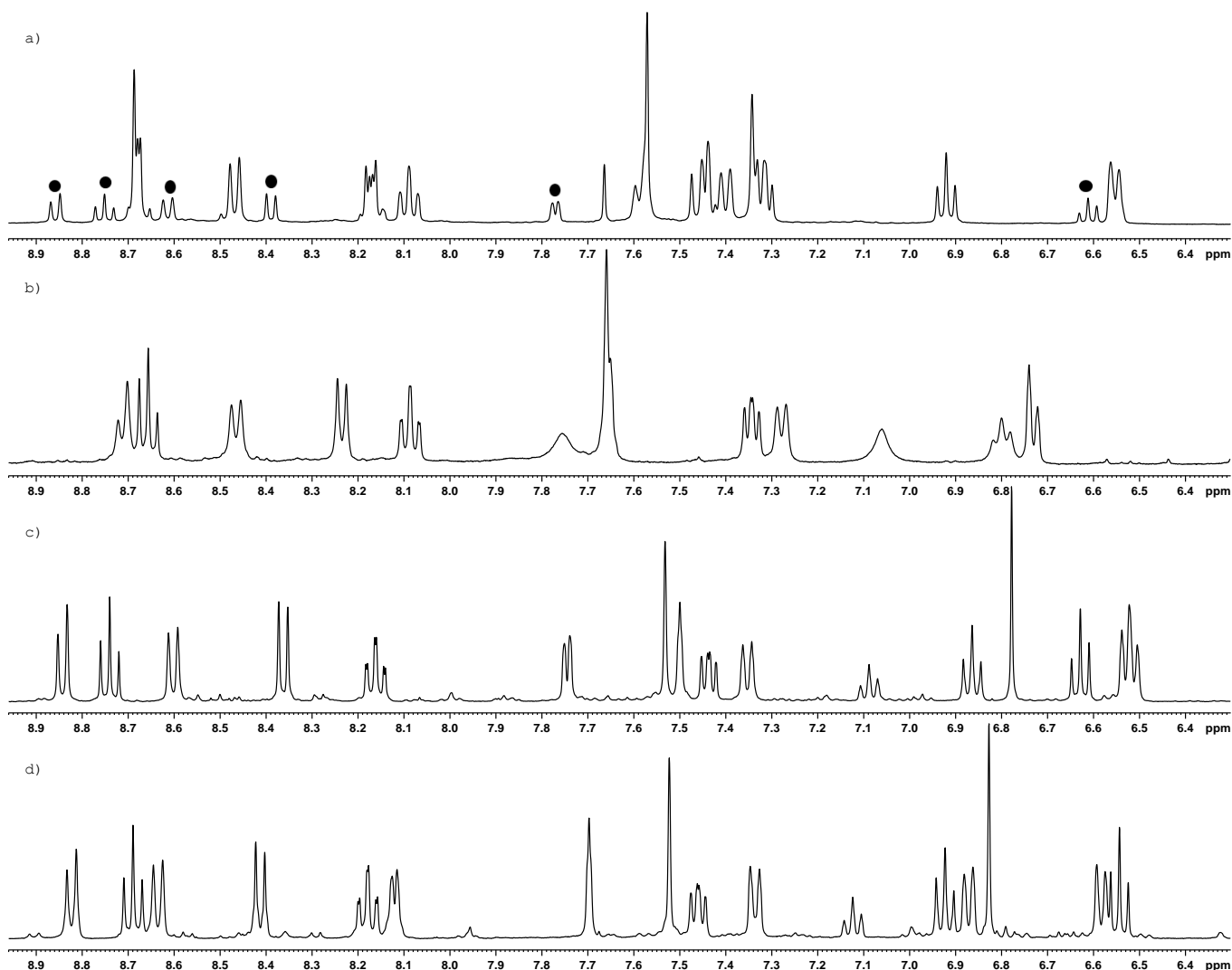


Figure 3.25 Aromatic region of the ^1H NMR spectra (CD_3NO_2) of a) $[\text{Zn}_2(\text{L}^9)_2]^{4+}$ (● = mesocate), b) $[\text{Cd}_2(\text{L}^9)_2]^{4+}$, c) $[\text{Zn}_2(\text{L}^{14})_2]^{4+}$ and d) $[\text{Cd}_2(\text{L}^{14})_2]^{4+}$

3.3.2 Solution state characterisation of complexes of L^{14}

The one-dimensional ^1H NMR spectrum of $[\text{Cd}_2(\text{L}^{14})_2](\text{ClO}_4)_4$ in CD_3NO_2 shows the expected 16 aromatic signals, in this case showing one species is present (figure 3.23, d), which is consistent with formation of the mesocate assembly. In addition the $[\text{Zn}_2(\text{L}^{14})_2](\text{CF}_3\text{SO}_3)_4$ complex in CD_3NO_2 shows only one set of signals, which it is reasonable to assume is the mesocate species (figure 3.23, c). The ^1H - ^1H COSY NMR spectrum shows the coupling between protons allowing identification of which signals correspond to which proton (figure 3.24).

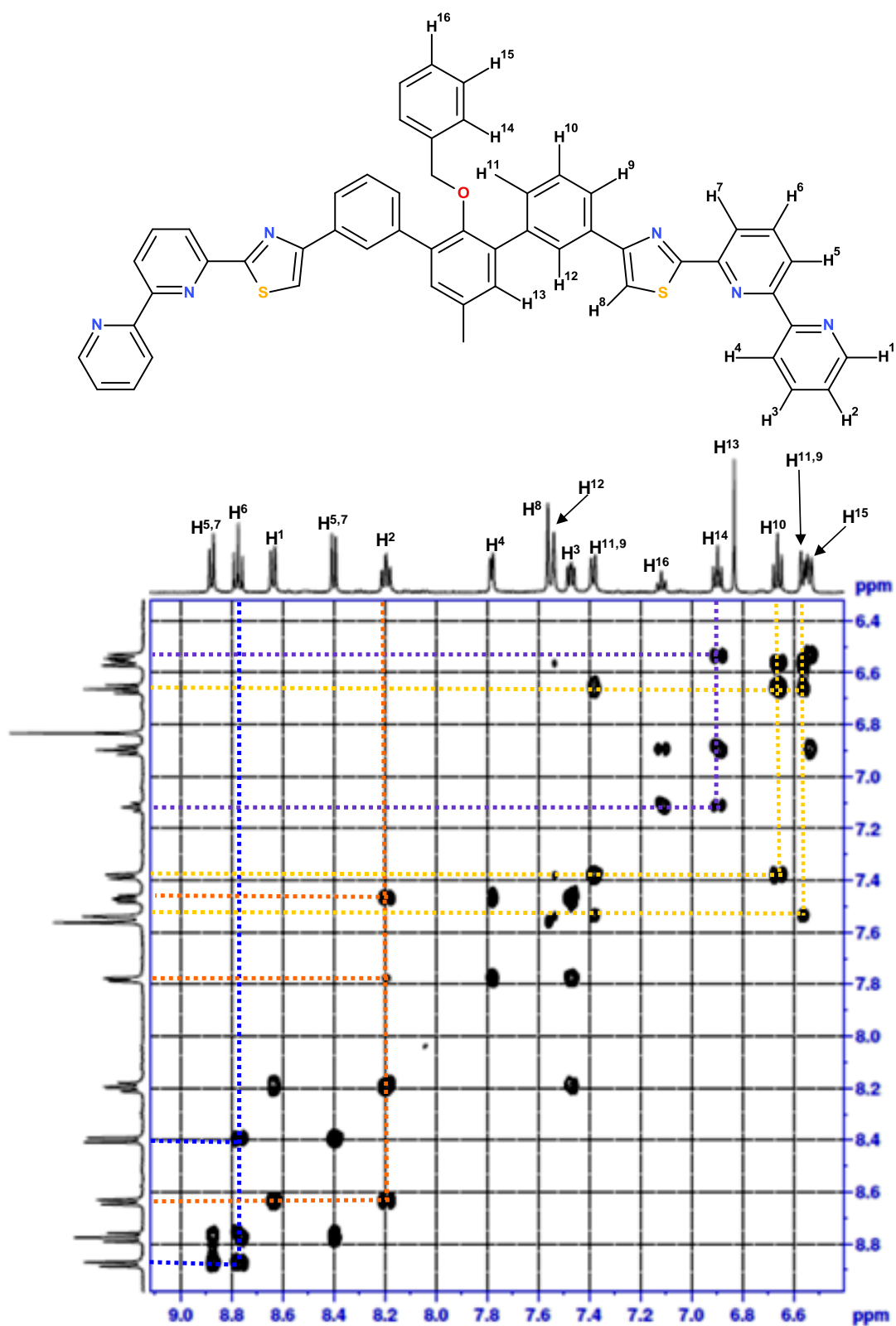


Figure 3.26 Aromatic region of the ¹H-¹H COSY spectrum of [Zn₂(L¹⁴)₂]⁴⁺ in CD₃NO₂

From the ^1H - ^1H COSY spectrum of $[\text{Zn}_2(\text{L}^{14})_2]^{4+}$ it is possible to identify which signals correspond to the benzyl group (Bn), this functional group essentially being the structural difference between L^{14} and L^9 . Therefore, if the signals for this group (Bn) are not taken into consideration, the remaining signals represent what would be expected for L^9 if only the mesocate species was present in solution. Comparison of the ^1H NMR spectrum of $[\text{Zn}_2(\text{L}^{14})_2]^{4+}$ with $[\text{Zn}_2(\text{L}^9)_2]^{4+}$ reveals several of the minor peaks seen in $[\text{Zn}_2(\text{L}^9)_2]^{4+}$ directly correspond to those present in the complex solution of L^{14} which is known to be the mesocate. This demonstrates it is reasonable to assume that the minor peaks seen in the ^1H NMR spectrum of $[\text{Zn}_2(\text{L}^9)_2]^{4+}$ are indeed due to the mesocate assembly.

3.4 Discussion

The ligands L^6 , L^7 and L^8 have been shown to form dinuclear double helicates in the solid state upon complexation with selected transition metals; in addition L^9 gives a similar assembly with cadmium(II). In the self-assembly of the helicate (cadmium(II) and L^9) the oxygen atoms of each ligand are brought into close proximity (3.644 Å) and examination of the van der Waal's radii shows minimal space between the inward facing atoms. Cobalt(II) is smaller than cadmium(II), giving smaller metal to ligand bond lengths. It is likely that steric and/or electrostatic repulsion between the ligands would be significantly amplified in an isostructural dicobalt(II) helicate. Thus an alternative species forms, where the two methoxy groups are not within such close proximity, giving the *meso*-helicate. The zinc containing assembly ($[\text{Zn}_2(\text{L}^9)_2]^{4+}$) for L^9 is isostructural with that observed for the cobalt(II) assembly i.e. a double *meso*-helicate.

This shows how an assembly can be destabilized due to subtle changes in metal-ligand bond distances, which in turn influences inter-ligand interactions and contributes significantly to the resulting self-assembly. This steric control is further supported by L^{14} , this ligand consisting of the same basic ligand chain as L^9 but containing the more sterically demanding benzyl unit in place of the

methyl group. L^{14} provides the expected dinuclear species upon reaction with cadmium(II), in this case the mesocate, demonstrating how increasing the steric bulk of the central unit is significant in directing the self-assembly.

Inspection of the space-filling structures shows that in the helicate there is extensive π -stacking from the aromatic groups (figure 3.25). Comparison of the complexes of L^7 and L^9 illustrate this well. To define a close interaction between aromatic units as $\leq 5\text{\AA}$ and essentially co-planar ($\leq 30^\circ$ interannular angle) then in the helicate (figure 3.25, a) there are 23 close interactions whereas only 14 in the *meso*-species (figure 3.25, b). These interactions arise in the helicate structure as the tridentate pyridyl-pyridyl-thiazole domains are closely aligned to the central triphenylene spacer. This type of interaction is not observed in the mesocate ($[\text{Co}_2(L^2)_2]^{4+}$ or $[\text{Zn}_2(L^2)_2]^{4+}$) and it is the π -interaction that must favour the formation of the helicate species.

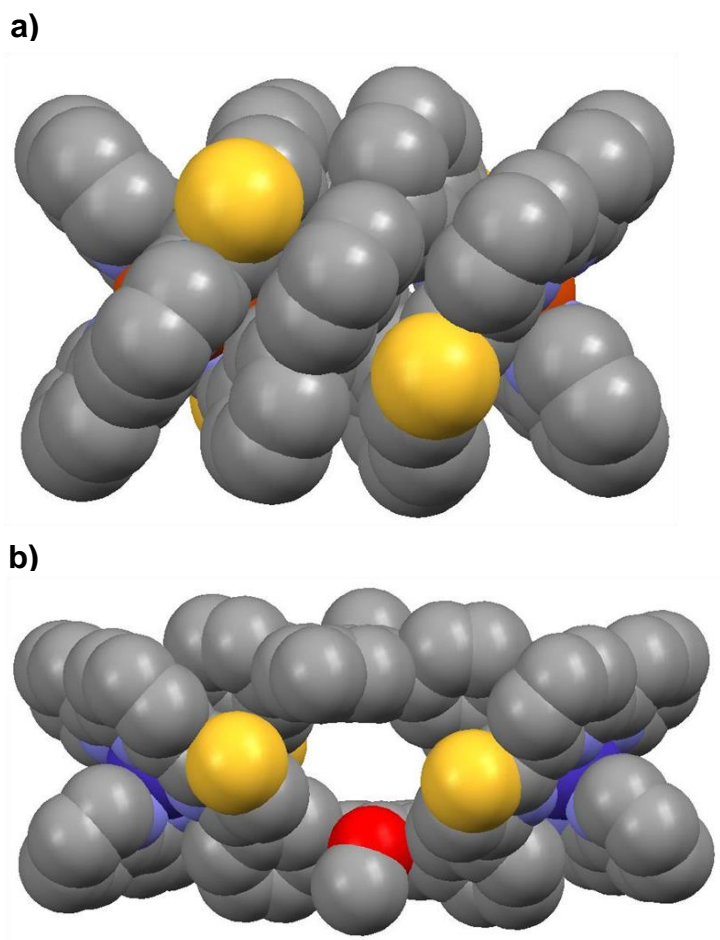


Figure 3.27 Space-filling view of the crystal structures of a) $[\text{Fe}_2(L^7)_2]^{4+}$, b) $[\text{Co}_2(L^9)_2]^{4+}$

Reaction between L^{10} , which possesses an ethylene glycol chain on the central phenyl spacer, and Fe(II) gives a *meso*-helicite complex ($[Fe_2(L^{10})_2]^{4+}$). This structure is observed as the ligands coordinate the metal ions *via* a C-type arrangement giving metal ions of opposite chirality which leads to a dinuclear double *meso*-helicite. This is observed due to the ethylene glycol chain within the ligand strand which would be brought into close proximity preventing the formation of a “true” helicite, where the ligand twists and adopts an S-type arrangement and giving metal ions of the same chirality. Reaction of L^{11} with Cd(II) again gives a dinuclear *meso*-helicite with the ligand partitioning into two tridentate donor units, each of which coordinates a different metal ion. In the solid-state each of the helicite assemblies has five perchlorate counter anions associated with it ($[Cd_2(L^{11})_2](ClO_4)_5$), as the crystals were grown in the presence of camphorsulfonic acid it is assumed that one of the amine nitrogen atoms has been protonated giving $[Cd_2(L^{11})(L^{11}-H)]^{5+}$. In the central cavity a water molecule is present and this acts as a hydrogen bond acceptor to the protonated amine and a donor to the other unprotonated amine. It is unclear why only one of the amine groups is protonated even though enough acid was used to protonate both. It is possible that the ability of the mono-protonated complex to act as both a hydrogen bond acceptor and donor offers some stability compared to the di-protonated species.

Reaction of L^{10} , L^{11} , $Cd(ClO_4)_2 \cdot 6(H_2O)$ and camphorsulfonic acid in nitromethane (in the ratio 1:1:2:1) gave a colourless solution. Slow diffusion of dichloromethane into the nitromethane complex solution resulted in the formation of large colourless crystals. Analysis by X-ray crystallographyⁱⁱⁱ showed that in the solid state both the dinuclear *meso*-helicite containing Cd(II) and L^{10} and L^{11} were present (figure 3.28). The complex with L^{10} (e.g. $[Cd_2(L^{10})_2]^{4+}$, figure 3.26) is very similar to the iron-containing structure ($[Fe_2(L^{10})_2]^{4+}$, figure 3.14) the ligand coordinates different metal ions *via* its tridentate, thiazole-pyridyl-pyridyl, donor units separated by the triphenylene unit bearing an ethylene glycol group on the central phenyl spacer. The metal-nitrogen bond lengths are similar to those observed for the Fe(II) complex,

ⁱⁱⁱ Some structural refinements for the complex cation $[Cd_2(L^{10})_2][Cd_2(L^{12}-H)_2]^{10+}$ were provided by Dr. Michaele Hardie.

$[\text{Fe}_2(\text{L}^{10})_2]^{4+}$, one major difference observed between the two structures is that in $[\text{Cd}_2(\text{L}^{10})_2]^{4+}$ complex the two glycol arms do not curl around the complex but extend away from the assembly with the two outer oxygen atoms pointing away from the complex. This cannot be an effect of the different metal ions, Cd(II) vs. Fe(II), as the metal ions are remote to the glycol arms.

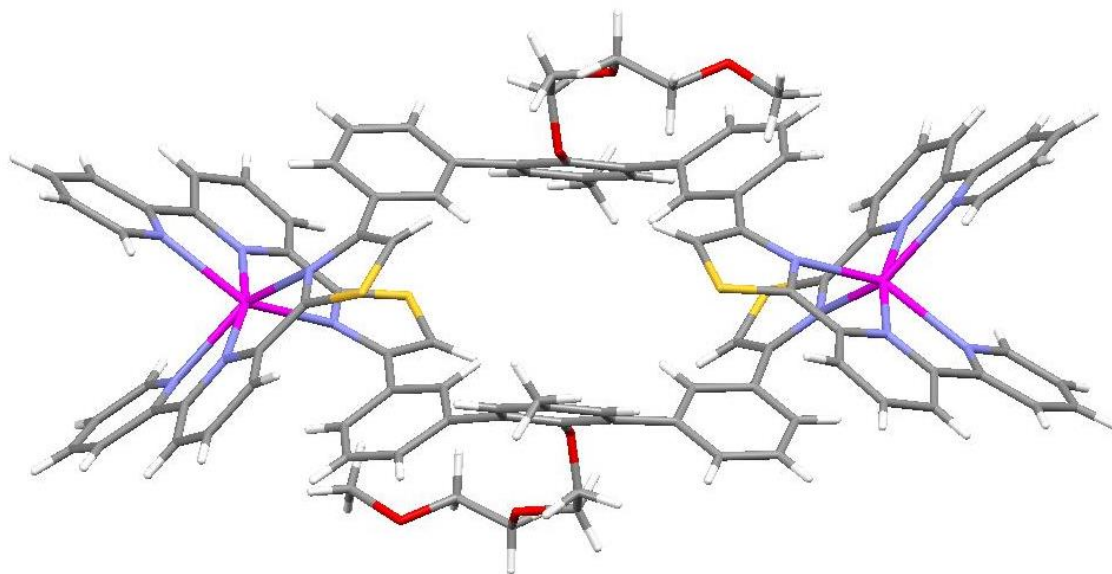


Figure 3.28 The $[\text{Cd}_2(\text{L}^{10})_2]^{4+}$ section of the one-dimensional $([\text{Cd}_2(\text{L}^{10})_2][\text{Cd}_2(\text{L}^{11}\text{-H})_2]^{10+})_n$ heteroleptic chain assembly.

A similar *meso*-helicite species for L^{11} and Cd(II) is also observed and again this is almost identical to the complex isolated by the reaction of L^{11} with Cd(II). However, due to the number of perchlorate counter ions present it is assumed that in this case both the amine groups are protonated giving the complex $[\text{Cd}_2(\text{L}^{11}\text{-H})_2]^{6+}$. In the central cavity there are two water molecules which act as hydrogen bond acceptors from the protonated amine (N–O 2.763(1) Å) (figure 3.27). The Cd^{2+} metal ions adopt a six-coordinate pseudo-octahedral geometry arising from coordination of a thiazole-pyridyl-pyridyl domain from each ligand. The metal-nitrogen bond lengths range from 2.309(8) to 2.356(8) Å similar to those observed for the complex of just L^{11} with Cd(II), $[\text{Cd}_2(\text{L}^{11})(\text{L}^{11}\text{-H})]^{5+}$.

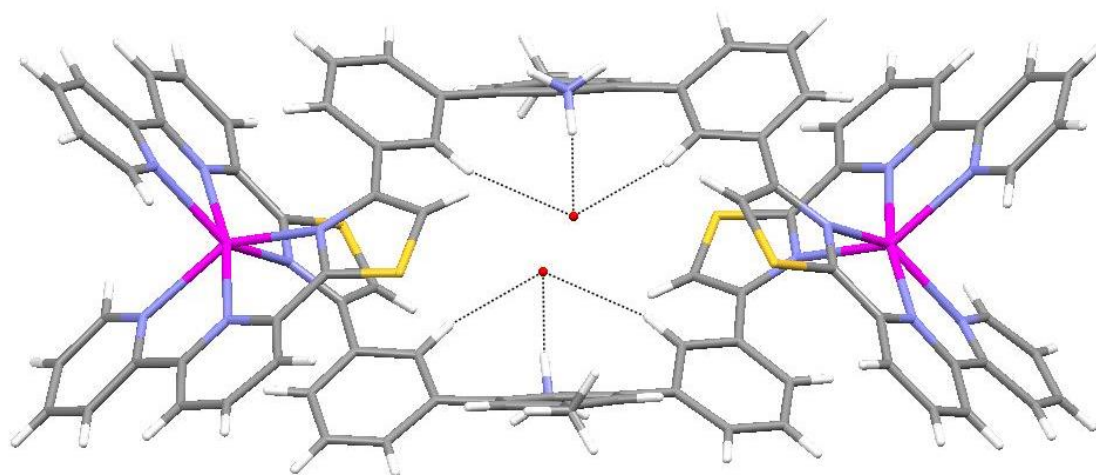


Figure 3.29 The $[\text{Cd}_2(\text{L}^{11}\text{-H})_2]^{6+}$ section of the one-dimensional chain $([[\text{Cd}_2(\text{L}^{10})_2][\text{Cd}_2(\text{L}^{11}\text{-H})_2]]^{10+})_n$ assembly containing the two hydrogen-bond acceptor water molecules

Thus upon reaction of Cd(II) with both L^{10} and L^{11} , in the presence of acid, an infinite one-dimensional chain containing units of $[\text{Cd}_2(\text{L}^{10})_2]^{4+}$ and $[\text{Cd}_2(\text{L}^{11}\text{-H})_2]^{6+}$ is observed. In the solid state each of the *meso*-helicate assemblies interact with one another *via* the protonated amine of L^{11} and the glycol chains from L^{10} such that the two oxygen atoms at the end of the glycol chain hydrogen bond to the $-\text{NH}_3^+$ unit (average O-N distance 2.947 Å, figure 3.28). This results in a structure which contains both of these *meso*-helicate structures in an extended one-dimensional system $(([\text{Cd}_2(\text{L}^{10})_2][\text{Cd}_2(\text{L}^{12}\text{-H})_2])(\text{ClO}_4)_{10})_n$.

Even though identical stoichiometry of acid was used in the crystallisation of L^{11} and Cd^{2+} , when just this ligand and cadmium were crystallised only one of the ligands in the helicite system is protonated but for the mixed ligand system $(([\text{Cd}_2(\text{L}^{10})_2][\text{Cd}_2(\text{L}^{11}\text{-H})_2])(\text{ClO}_4)_{10})_n$ each ligand in the *meso*-helicite assembly is protonated. As mentioned previously mono-protonation (e.g. $[\text{Cd}_2(\text{L}^{11})(\text{L}^{11}\text{-H})]^{5+}$) may be stabilised due to a water molecule within the mesocate cavity as this can act as a hydrogen-bond acceptor/donor. In the case of the mixed ligand system $([\text{Cd}_2(\text{L}^{11}\text{-H})_2]^{6+})$ it is conceivable that diprotonation is stabilised, in the solid state, by interaction with the ethylene glycol chain on the neighbouring helicite assemblies.

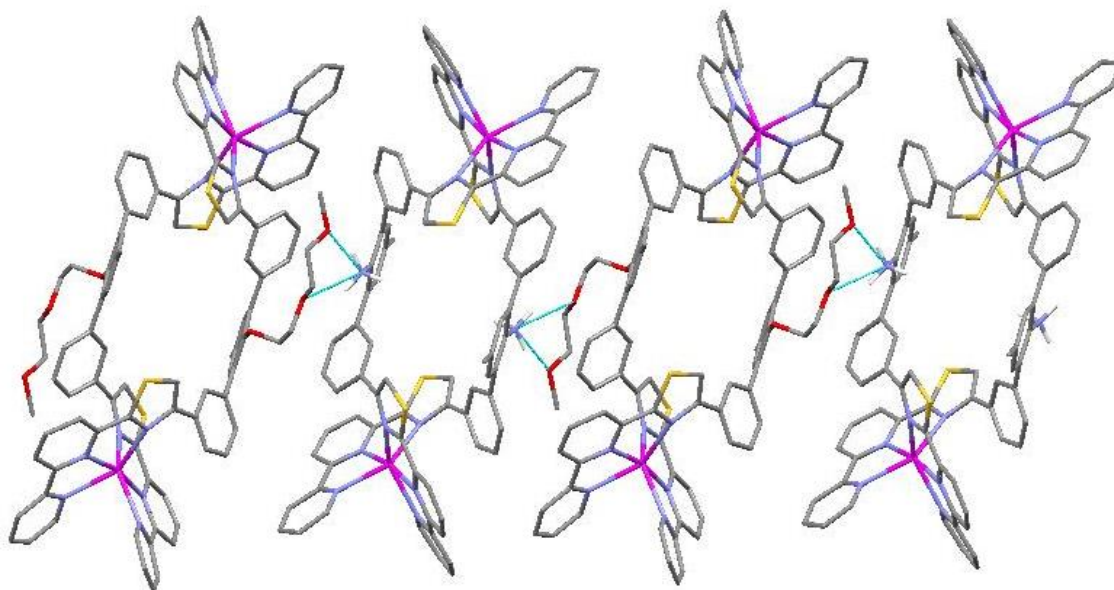


Figure 3.30 The X-ray crystal structure of the mesocate-containing one-dimensional chain $([\text{Cd}_2(\text{L}^{10})_2][\text{Cd}_2(\text{L}^{11}\text{-H})_2])^{10+}_n$ showing the hydrogen-bonding interaction

This is the first example where *meso*-helicite assemblies form a one-dimensional chain *via* interaction between an ammonium and glycol chain unit resulting in a heteroleptic system. One-dimensional helicite-containing chains have been reported previously, such as the example by Ward *et al.* where infinite chains are produced due to $\text{Ag}\cdots\text{Ag}$ interactions, giving a triple helical braid.¹⁴² Hannon *et al.* also report a hydroxyl substituted helicite which forms a chain *via* hydrogen bonding either with itself or chloride anions.¹⁴³ However, in both these cases only one type of helicite is present in the chains i.e. a homoleptic system.

3.5 Conclusion

In conclusion, nine novel ligands L^6 - L^{14} , consisting of two tridentate N-donor domains separated by various phenyl spacer units were successfully synthesised. It has been demonstrated here that if possible the ligands prefer to form the helicate assembly; this preferential formation of the helicate has been attributed to increased π -stacking interactions. However, inclusion of sterically demanding groups leading to unfavourable inter-ligand interactions (which in turn is governed by ion size) can destabilise this assembly resulting in a *meso*-helicate.

Additionally a mixture of two ligands, L^{10} and L^{11} , react with cadmium(II) ions to form two discrete *meso*-helicate complexes. This architecture results due to the steric programming of the ligand and the stereochemical information provided by the metal ion. Further to this, favourable interactions of the ethylene glycol chain (L^{10}) with the ammonium functionality (L^{11}) direct the assembly towards a one-dimensional chain of the two *meso*-helicates. This is the first example where *meso*-helicate assemblies form a one-dimensional chain *via* interaction between an ammonium and glycol chain unit resulting in a heteroleptic system.

4. Emissive lanthanide-containing dinuclear double stranded helicates

As previously stated a metallo-helicate is a supramolecular complex composed of one or more covalent organic strands coordinated to at least two metal ions defining the helical axis.⁷² So far most examples discussed have focused on the use of transition metal ions; however it is possible to employ lanthanide metal ions to play the same role within the supramolecular assembly. The use of these metal ions has expanded rapidly since the first lanthanide-containing helicate reported by Piguet *et al.* in 1992.¹⁴⁴

The chemistry of the lanthanides is different from the transition metals; these ions are larger and prefer higher coordination numbers, normally observed as 8- or 9- coordinate, with the favoured oxidation state being 3⁺. The bonding between metal and ligand is mostly electrostatic bonding (ionic), thus directionality of the bonding is not as easily predicted as with the transition metals (generally tetrahedral or octahedral). They are known to interact strongly with ligands containing oxygen atoms i.e. they are oxophilic.¹⁴⁵ However, a weakness of the lanthanides is that the f - f transitions are Laporte forbidden, thus direct luminescent excitation is difficult to achieve. This problem may be overcome *via* the indirect luminescent excitation of the lanthanide ion by an 'antenna', this is a sensitising chromophore which could be an organic system (containing aromatic chromophores or conjugated components) or may be an inorganic coordination complex (containing other metal ions to sensitize the lanthanide ions).

So what has made the lanthanide ions desirable for use in supramolecular coordination chemistry? The main interest stems from their potential applications due to their unique photophysical and magnetic properties, leading to the production of sensors^{146, 147}, switches and molecular probes¹⁴⁸ to name a few. The interest of incorporating lanthanide ions within helicates is thus to provide functional applications for such assemblies. However, due to the

chemistry of the lanthanide orbitals, as stated the bonding is significantly less covalent than the transition metals, as such the lanthanides exhibit no pronounced stereochemical preferences. Consequently the lanthanide assemblies rely almost exclusively on the programming of the ligand strands and as such there are fewer examples of such assemblies.

Despite these drawbacks there are now numerous examples of supramolecular assemblies containing lanthanide metal centres from various research groups, including those of Piguet,^{149, 150} Albrecht^{151, 152} and Gunnlaugsson.¹⁵³ The pioneering studies by Piguet and Bünzli focusing on helicate assembly have led to some fascinating architectures. By developing ligand systems based on $L^{R'}$ (figure 4.1) and related derivatives Piguet *et al.* have created numerous helicate assemblies possessing lanthanide metal centres.

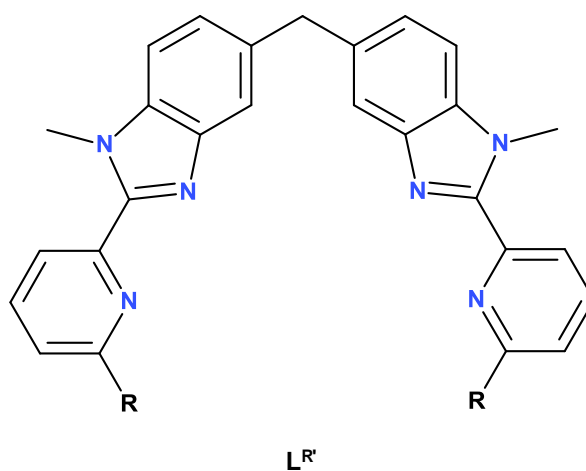


Figure 4.1 Basic ligand, $L^{R'}$, employed to investigate lanthanide-containing helicates¹⁵⁴⁻¹⁵⁸

Incorporation of this basic motif, $L^{R'}$, within several ditopic ligands resulted in the self-assembly of helicates containing lanthanide and/or transition metals to give 4f-4f, 4f-4f' or 3d-4f bimetallic complexes.¹⁵⁵⁻¹⁵⁸ Two segmental ligands were produced, $L^{S'}$, which possesses a bidentate 2-(benzimidazolyl)pyridine unit and a tridentate 2,6-bis-(benzimidazolyl)pyridine unit coded for coordination with octahedral transition metal ions and nine-coordinate lanthanide metal ions

respectively, and L^T which possesses similar functionality except for a terminal carboxamide group within the tridentate unit (figure 4.2).^{159, 160} For ligand $L^{S'}$ the heterodinuclear d-f complexes were investigated in solution (f = La and d = Zn). Spectroscopic titrations of the ligand gave a mixture with the heterodimetallic species being the predominant product when the ligand and metal ions ($La(ClO_4)_3 \cdot 7H_2O$ and $Zn(ClO_4)_2 \cdot 6H_2O$) were mixed in a stoichiometric ratio (3:1:1). It was rationalised that the tridentate domains considerable affinity for the transition metals limited the selectivity of domains and thus for the formation of the heterodimetallic helicate.¹⁵⁹

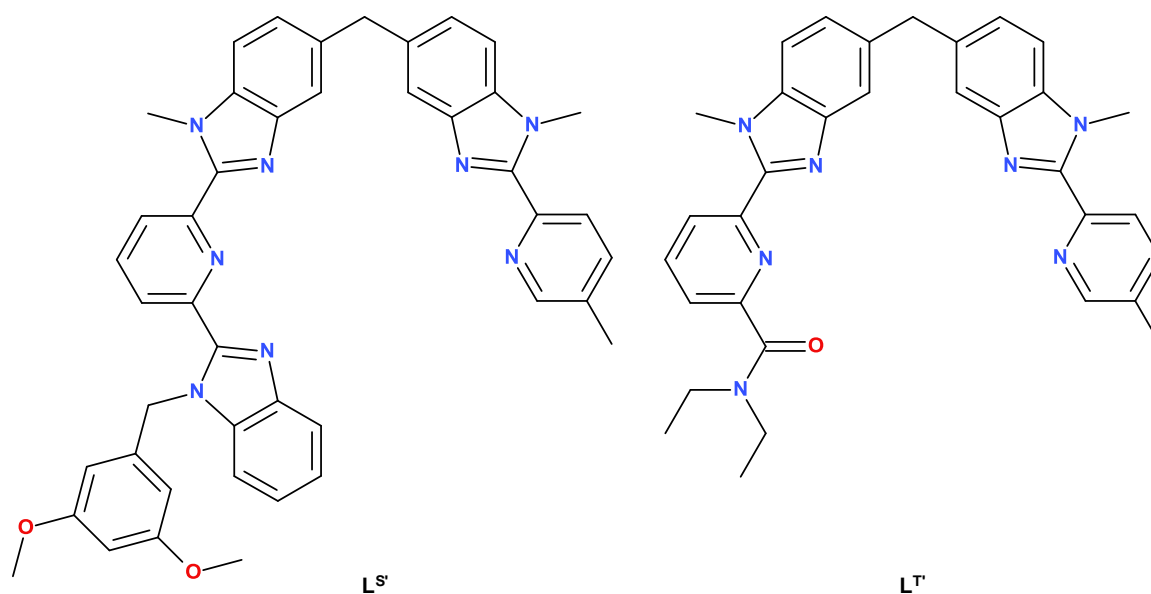


Figure 4.2 Ligands, $L^{S'}$ and L^T , employed for the self-assembly of heterodinuclear d-f helicates⁽¹⁶⁰⁾

For the second ligand, L^T , the incorporation of a carboxamide terminal group was shown to improve the selectivity of the assembly process. The 1H NMR spectrum of $[EuZn(L^T)_3]^{5+}$ showed one species in solution consistent with three equivalent head-to-head ligands wrapped about the Eu-Zn axis.¹⁶⁰ Due to unsuitable crystals the assembly with $L^{S'}$ could not be structurally characterised by X-ray diffraction. For L^T slow diffusion of diethyl ether into a concentrated acetonitrile solution of the ligand and metal ions allowed isolation of a polycrystalline aggregate. Colourless single crystals suitable for X-ray diffraction were subsequently obtained upon diffusion of diisopropyl ether into

an acetonitrile solution of the isolated polycrystalline material containing 30 equivalents of $\text{NBu}_4\text{CF}_3\text{SO}_3$. The Eu(III) is coordinated by the tridentate domains of three ligands giving a slightly distorted tricapped trigonal prism with three nitrogen atoms of the benzimidazole units and the three oxygen atoms occupying the vertices of the prism. Coordination of the bidentate site of the three ligands gives an octahedral Zn(II) centre which is severely distorted. This results in the Zn-N bond lengths for the pyridine nitrogen being longer than what is generally observed for such interactions.

Subsequent analysis of the complexes showed the heterodinuclear complex $[\text{EuZn}(\text{L}^{\text{T}})_3]^{5+}$ possesses a lifetime which is indicative of an ion which is well protected from quenching processes. Quantum yield data of the two complexes ($[\text{EuZn}(\text{L}^{\text{S}})_3]^{5+}$ and $[\text{EuZn}(\text{L}^{\text{T}})_3]^{5+}$) in acetonitrile show that the heterodinuclear complex of L^{T} is more luminescent than the corresponding L^{S} complex, this increase in luminescence being attributed to a more efficient antenna effect associated with L^{T} . Further to this L^{T} has been employed within a number of triple-stranded helicates using different combinations of transition metals and lanthanide ions. For a given transition metal (Fe , Co or Zn) a triple-stranded helicate was obtained for all lanthanides with the structure being confirmed by NMR analysis, with these types of systems displaying potential as luminescent probes.⁸⁹

Piguet and co-workers have also skilfully produced a ligand which is capable of selectively forming a heterodimetallic helicate consisting of different lanthanide metal ions, assuming there is sufficient size difference between the metals selected.¹⁶¹ Other groups have reported similar heterometallic helicate assemblies.^{151, 162} Not only have lanthanide helicates been produced there are now other assemblies incorporating lanthanide metals; for example, circular helicates^{149,163} and cage complexes¹⁶⁴ have recently been reported.

Described in this chapter is the synthesis and coordination chemistry of three mixed N-donor and O-donor ligands, L^{15} - L^{17} , which possess the same central *p*-cresol unit. Reaction of these ligands with selected lanthanide metal ions results in the formation of dinuclear double helicates. All three ligands are symmetrical, L^{15} contains thiazole-hydroxyquinoline, L^{16} possesses thiazole-pyridine-pyridine binding domains and L^{17} consists of thiazole-pyridine-pyridine-*N*-oxide binding domains (Figure 4.3).

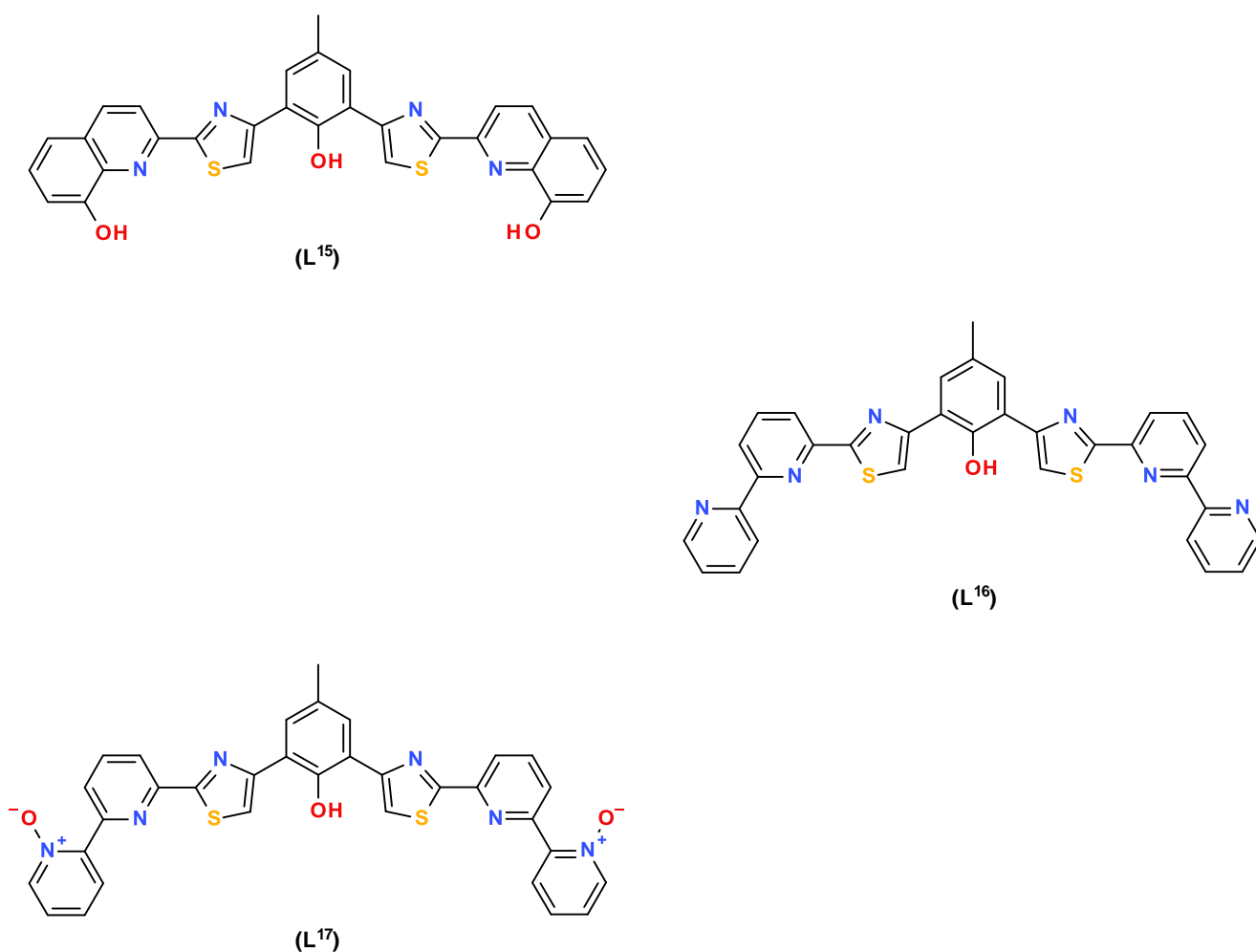


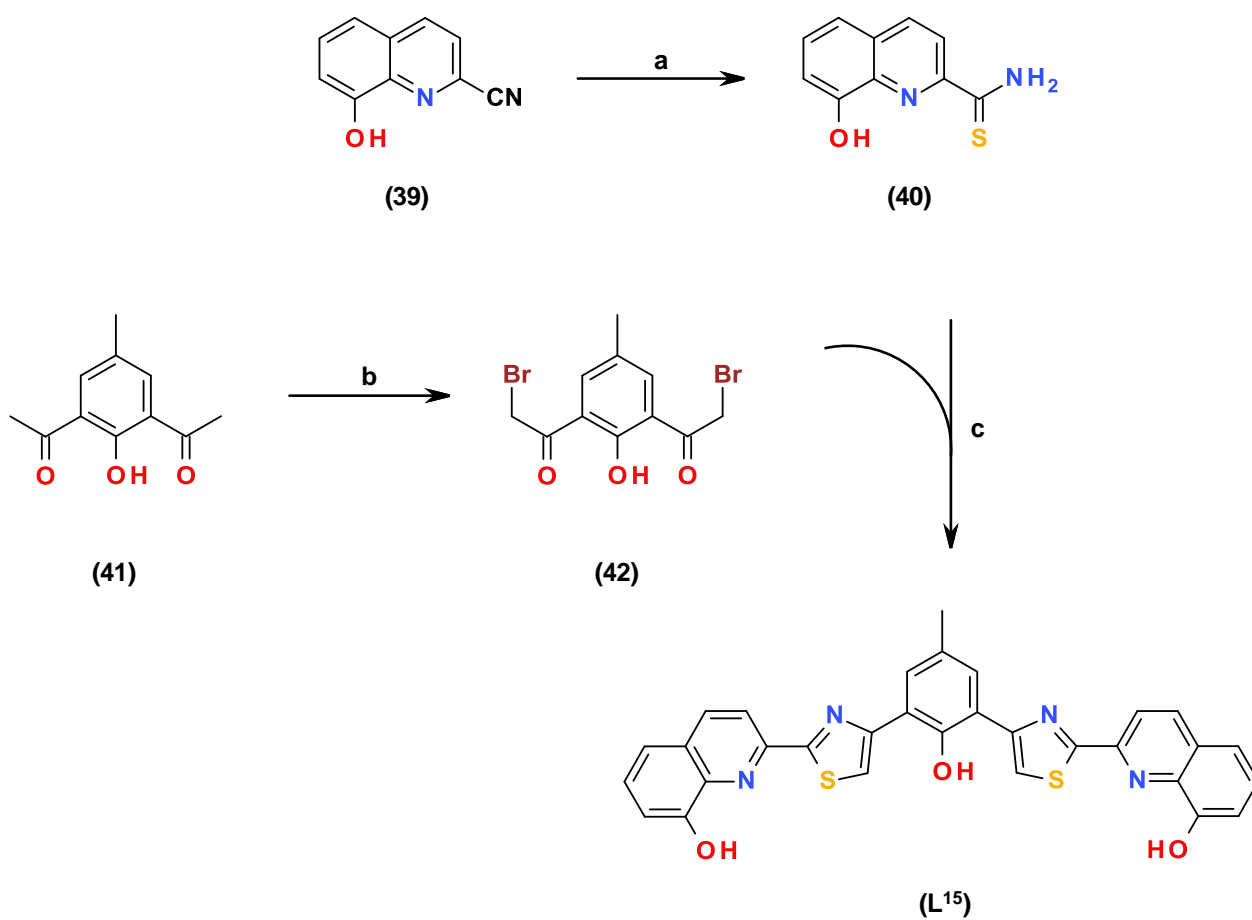
Figure 4.3 A new group of multidentate ligands L^{15} – L^{17}

4.1 Ligand synthesis

The ligands, L^{15} – L^{17} , were synthesised *via* multi-step synthetic processes (Schemes 4.1 and 4.2); for further details regarding the synthesis of L^{15} – L^{17} see chapter 6 section 6.3.

4.1.1 Synthesis of L^{15}

The synthesis of the ligand, L^{15} , was achieved following a three step synthesis route (Scheme 4.1). Starting with 8-hydroxyquinoline-2-carbonitrile (**39**) and triethylamine in ethanol, H_2S was slowly bubbled through the solution which turned the solution yellow after a few minutes, on standing for 48 hours a precipitate was produced. Filtration gave 8-hydroxyquinoline-2-carbothioamide (**40**) as a yellow powder. The 1H NMR spectrum confirms the formation of the desired compound with the presence of two broad singlets (9.21 and 7.76 ppm) corresponding to the $-NH_2$ protons. Reaction of diacetyl cresol¹⁶⁵ (**41**) with bromine in acetic acid gave the desired dibrominated species (**42**) after separation and purification *via* column chromatography. 1H NMR analysis of the product shows the appearance of a singlet at 4.60 ppm corresponding to methylene protons, along with the disappearance of the original methyl peak seen for the starting material. Reaction of the 8-hydroxyquinoline-2-carbothioamide (**40**) with the dibromocresol (**42**) in ethanol at reflux afforded L^{15} as a pale yellow solid. Confirmation of the successful formation of the ligand was obtained by 1H NMR analysis which showed 9 aromatic signals, with overlapping multiplets corresponding to the protons of the terminal phenol ring. Furthermore an ion in the ESI-MS was observed at m/z 583 which is consistent with $[L^{15}+Na]^+$.

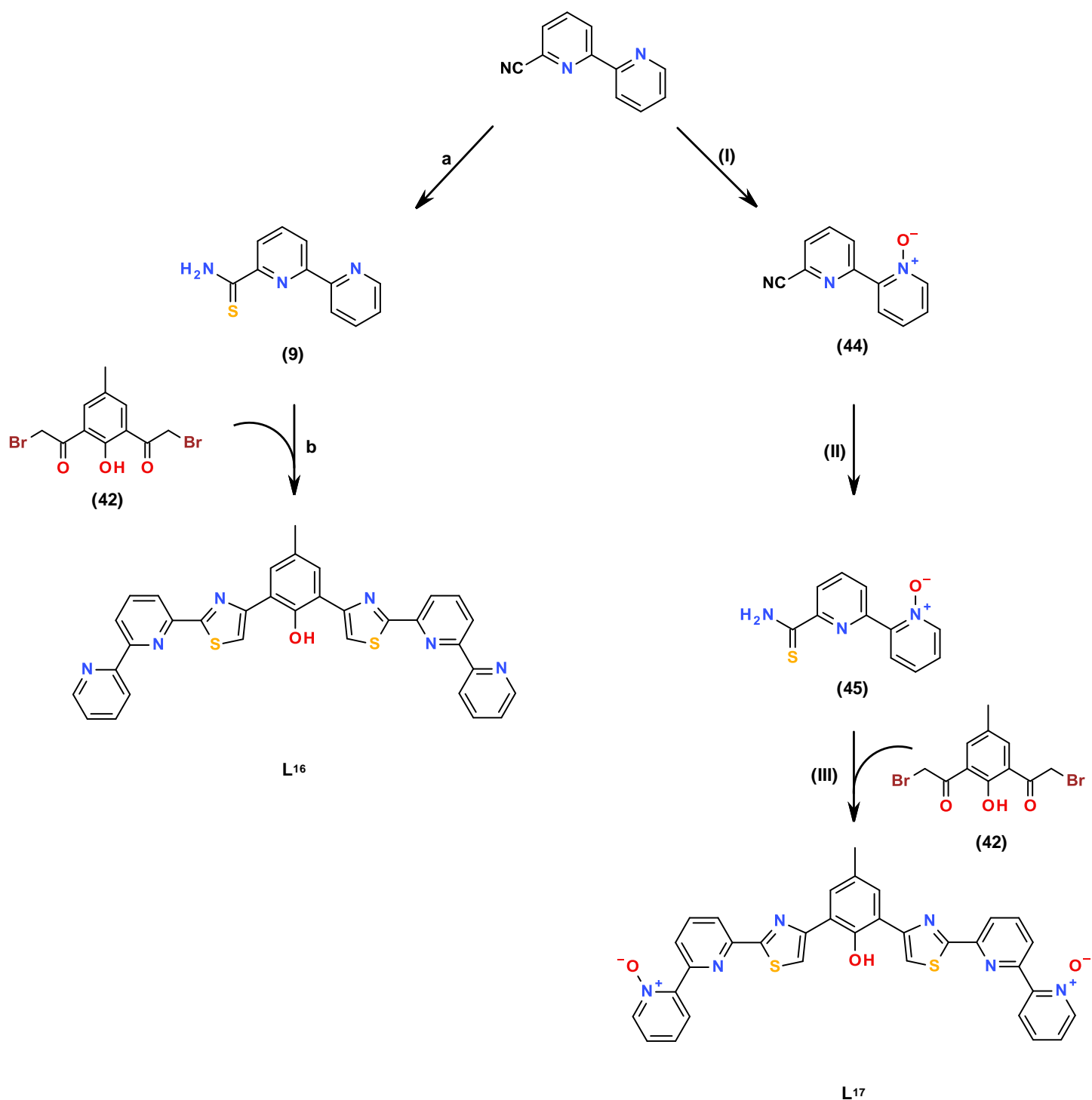


Scheme 4.1 Synthesis of L¹⁵

Reagents and conditions: a) H₂S, Et₃N, EtOH, RT (91 %); b) Br₂, CH₃COOH, 60°C (41 %); c) EtOH, reflux (78 %).

4.1.2 Synthesis of **L**¹⁶ and **L**¹⁷

The synthesis of ligands **L**¹⁶ and **L**¹⁷ was achieved following a multi-step synthesis route (Scheme 4.2). These two ligands have the same central ring as **L**¹⁵, however, the thioamides employed are different to the one used for **L**¹⁵. The synthesis of 2,2'-bipyridine-6-thioamide was achieved following methods already reported in the literature.^{166, 167} Reaction of 2,2'-bipyridine-6-thioamide (**9**) with the α -dibromoacetyl (**42**) in DMF gave **L**¹⁶ after deprotonation. Confirmation of the successful formation of the ligand was obtained by ¹H NMR analysis which showed 10 aromatic signals, two signals overlapping, including two signals expected for the hydroxyl and methyl groups. Furthermore an ion in the ESI-MS was observed at m/z 605 which is consistent with [**L**¹⁶+Na]⁺. The synthesis of **L**¹⁷ is essentially the same procedure used for **L**¹⁶ except *N*-oxide-2,2'-bipyridine-6'-thioamide was used in place of 2,2'-bipyridine-6-thioamide. For **L**¹⁶, 6-cyano-2,2'-bipyridine (**43**) was reacted with *m*CPBA in DCM to give 6'-cyano-2,2'-bipyridine-*N*-oxide (**44**). The corresponding thioamide (**45**) was produced upon exposure of the *N*-oxide to hydrogen sulphide which was isolated upon filtration of the resulting yellow precipitate. Reaction of 2,2'-bipyridine-6-thioamide-*N*-oxide (**45**) with the α -dibromoacetyl (**42**) in DMF gave **L**¹⁷ after deprotonation. Confirmation of the formation of the ligand was not obtained by ¹H NMR spectrometry due to poor solubility in organic solvents.



Scheme 4. 2 Syntheses of L¹⁶ and L¹⁷

Reagents and conditions: a) H₂S, Et₃N, EtOH, RT; b) DMF, 80 °c (84 %). I) *m*CPBA, DCM, RT (78 %); II) H₂S, Et₃N, EtOH, RT (88 %); III) DMF, 80 °C (62 %).

4.2 Coordination chemistry

4.2.1 Complex of L^{15} with europium(III)

Reaction of L^{15} with an equimolar quantity of $Eu(CF_3SO_3)_3$ in nitromethane gave a yellow solution. Analysis by ESI-MS showed an ion at m/z 1869 which corresponds to $\{[(L^{15})_2Eu_2](CF_3SO_3)_3\}^+$ indicating that a dinuclear species had formed and the ligand was acting as a monoanionic species. Slow diffusion of chloroform into the nitromethane complex solution resulted in the formation of X-ray quality yellow crystals. . The X-ray crystal structure showed crystallisation in the monoclinic space group $C2/c$ and confirmed the formation of the dinuclear species $[(L^{15})_2Eu_2]^{4+}$ (figure 4.4)^{iv}.

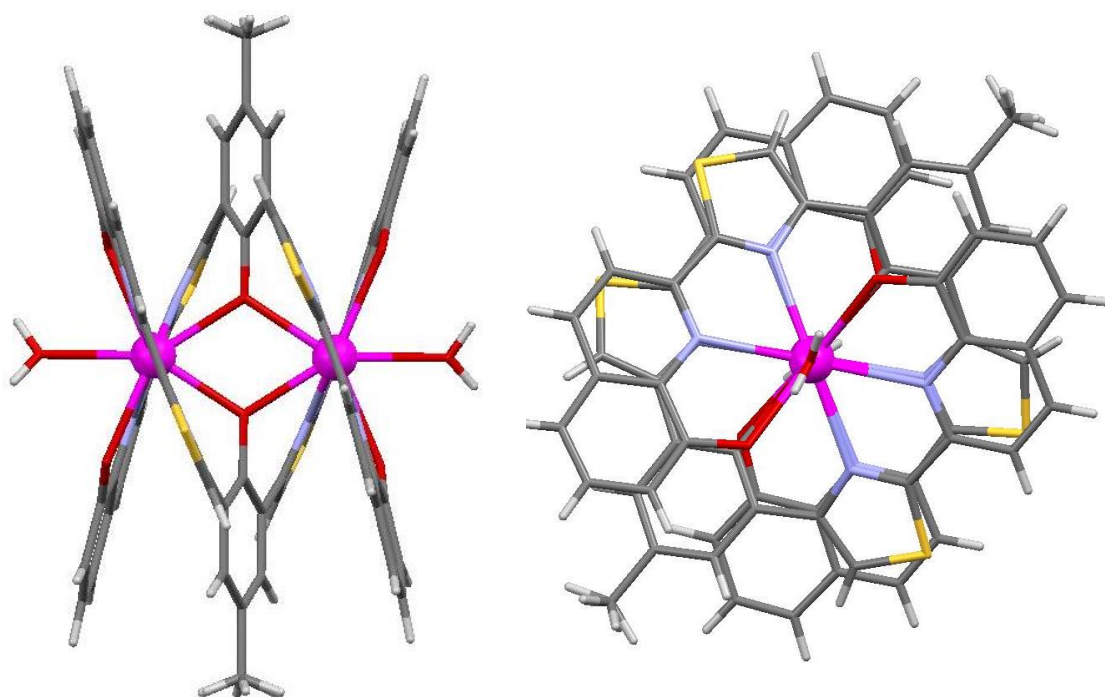


Figure 4.4 Two views for the solid state structure of the complex cation $[(L^{15})_2Eu_2(H_2O)_2]^{4+}$

The crystal structure confirms that in the solid state the ligand, L^{15} , and $Eu(III)$ ions self-assemble to form a dinuclear double helicate. The binding domains of the ligand strand partition into two tridentate donor domains due to the *p*-cresol

^{iv} All X-ray crystallography data for this chapter was recorded by Professor Craig Rice.

central bridging unit. However in this case, as the bridging group possesses an O-donor, this *p*-cresol unit also coordinates both metal ions (figure 4.4). The two Eu(III) ions (Eu–Eu distance: 3.9275(1) Å) are nine coordinate arising from coordination of two tridentate N,N,O-domains, the O-donor from the central *p*-cresol unit of both ligands and one water molecule (Eu–N distances: 2.591(3) – 2.605(3) Å, Eu–O distances: 2.3332(18) – 2.521(3) Å). Selected bond lengths and angles are shown in tables 4.1 and 4.2.

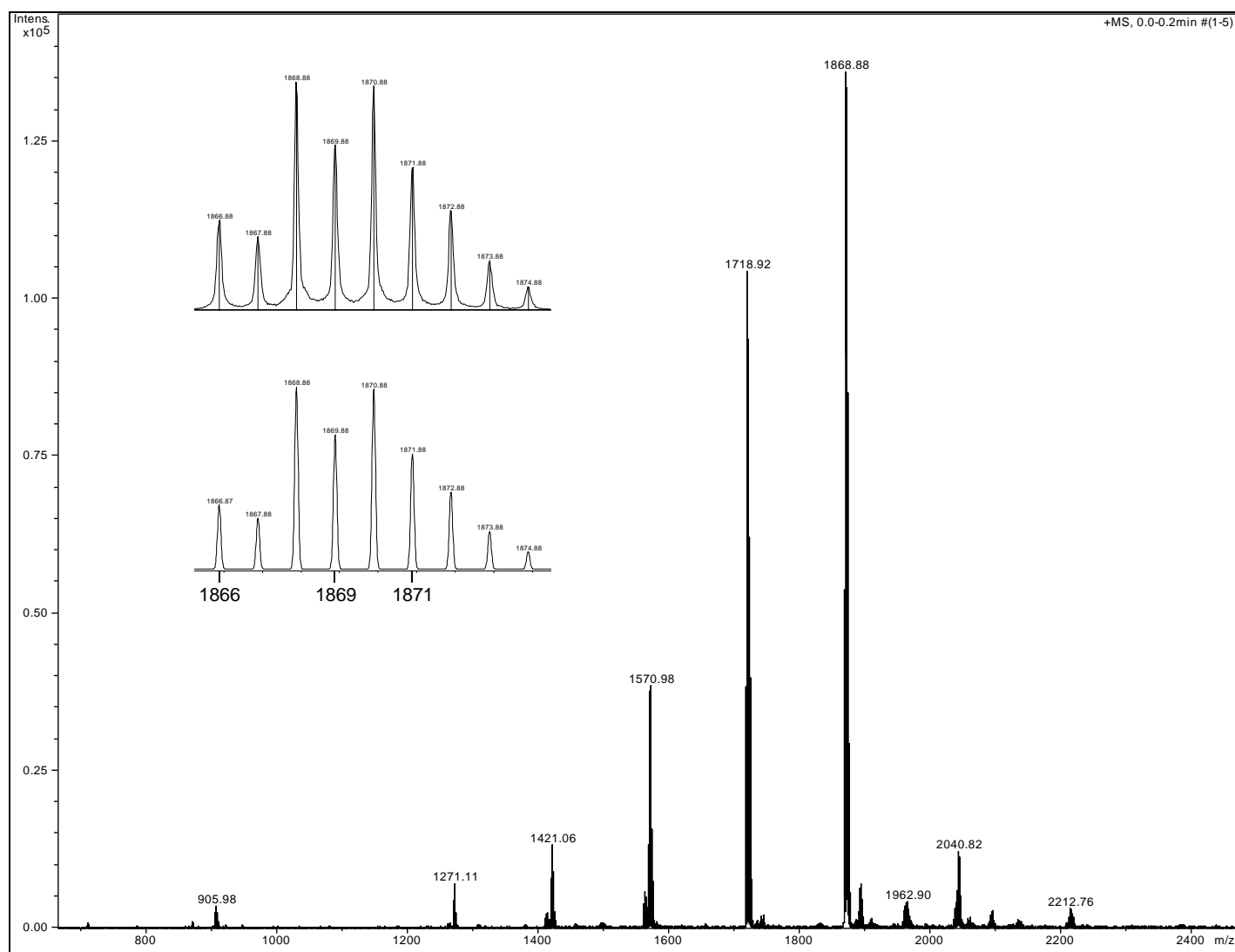


Figure 4. 5 ESI-MS of $[(L^{15})_2Eu_2](CF_3SO_3)_4$ with the found (top) and predicted (bottom) isotopic distribution pattern of $\{[(L^{15})_2Eu_2](CF_3SO_3)_3\}^+$ (inset)

Bond	Bond Length (Å)	Bond	Bond Length (Å)
Eu(1)-O(4)	2.513(3)	Eu(1)-N(3)	2.604(3)
Eu(1)-N(1)	2.604(3)	Eu(1)-O(2)	2.3369(18)
Eu(1)-O(3)	2.3332(18)	Eu(1)-N(2)	2.591(3)
Eu(1)-O(11)	2.471(3)	Eu(1)-N(4)	2.605(3)
Eu(1)-O(1)	2.521(3)		

Table 4.1 Selected bond lengths (Å) for the complex cation $[(L^{15})_2Eu_2(H_2O)_2]^{4+}$

Bond	Angle (°)	Bond	Angle (°)
N(1)-Eu(1)-O(4)	109.34(9)	O(2)-Eu(1)-O(11)	146.89(10)
O(3)-Eu(1)-O(4)	80.72(9)	O(2)-Eu(1)-O(1)	80.21(10)
O(3)-Eu(1)-N(1)	114.15(8)	O(2)-Eu(1)-N(3)	112.43(8)
O(11)-Eu(1)-O(4)	66.87(9)	N(2)-Eu(1)-O(4)	66.61(9)
O(11)-Eu(1)-N(1)	78.50(11)	N(2)-Eu(1)-N(1)	62.55(10)
O(11)-Eu(1)-O(3)	147.59(10)	N(2)-Eu(1)-O(3)	64.04(7)
O(1)-Eu(1)-O(4)	133.58(9)	N(2)-Eu(1)-O(11)	101.20(10)
O(1)-Eu(1)-N(1)	62.02(10)	N(2)-Eu(1)-O(1)	124.56(9)
O(1)-Eu(1)-O(3)	145.66(10)	N(2)-Eu(1)-N(3)	122.04(10)
O(1)-Eu(1)-O(11)	66.73(10)	N(2)-Eu(1)-O(2)	95.82(8)
N(3)-Eu(1)-O(4)	61.94(10)	N(4)-Eu(1)-O(4)	124.08(10)
N(3)-Eu(1)-N(1)	160.45(10)	N(4)-Eu(1)-N(1)	122.32(11)
N(3)-Eu(1)-O(3)	82.76(8)	N(4)-Eu(1)-O(3)	95.51(8)
N(3)-Eu(1)-O(11)	81.95(11)	N(4)-Eu(1)-O(11)	102.29(10)
N(3)-Eu(1)-O(1)	109.92(10)	N(4)-Eu(1)-O(1)	65.82(10)
O(2)-Eu(1)-O(4)	146.20(9)	N(4)-Eu(1)-N(3)	62.24(11)
O(2)-Eu(1)-N(1)	84.63(8)	N(4)-Eu(1)-O(2)	63.60(8)
O(2)-Eu(1)-O(3)	65.51(10)	N(4)-Eu(1)-N(2)	156.50(10)

Table 4.2 Selected bond angles (°) for the complex cation $[(L^{15})_2Eu_2(H_2O)_2]^{4+}$

4.2.2 Complex of L^{16} with lanthanum(III)

Reaction of L^{16} with an equimolar amount of $La(CF_3SO_3)_3$ in nitromethane gave a light yellow solution. ESI-MS analysis gave an ion at m/z 1887 corresponding to $\{[(L^{16})_2La_2](CF_3SO_3)_3\}^+$ again with the ligand acting as a monoanionic species. Slow diffusion of diisopropyl ether into the nitromethane complex solution resulted in the formation of X-ray quality crystals. The X-ray crystal structure showed crystallisation in the triclinic space group $P-1$ and confirmed the formation of the dinuclear double helicate $[(L^{16})_2La_2(H_2O)_2(CF_3SO_3)_2]^{2+}$ (figure 4.5).

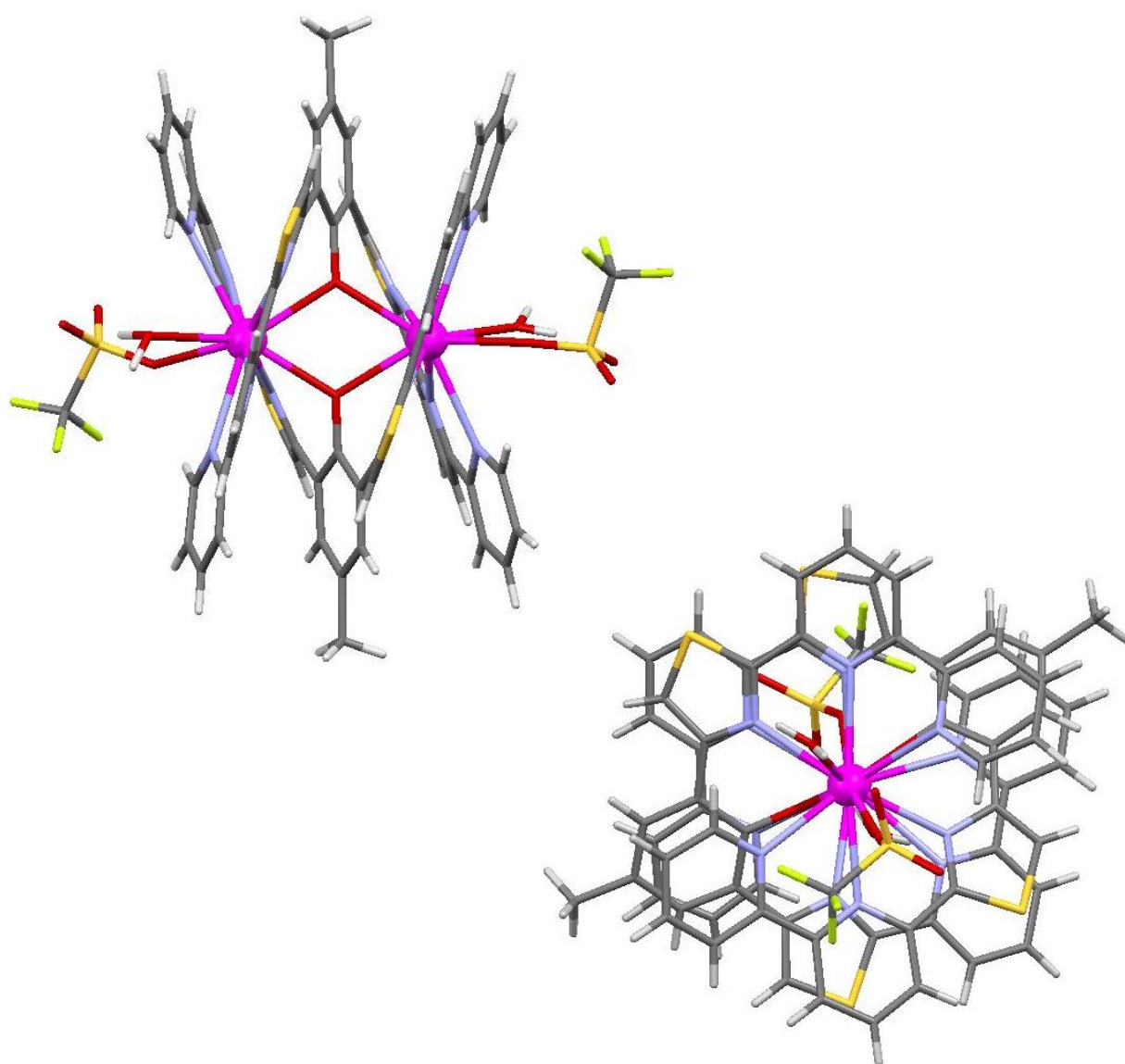


Figure 4.6 Two views for the solid state structure of the complex cation $[(L^{16})_2La_2(H_2O)_2(CF_3SO_3)_2]^{2+}$

The crystal structure confirms that in the solid state the ligand, L^{16} , and La(III) ions form a dinuclear double helicate. The coordination of this ligand is similar to that seen for the previous ligand, L^{15} . The phenolic central unit deprotonates and bridges the two lanthanide ions contributing to the coordination sphere of the metal ions (figure 4.7). The two La(III) ions (La–La distance: 4.2111(4) Å) are ten-coordinate arising from coordination of two tridentate N,N,N-domains, the O-donor of the *p*-cresol central units, one water molecule and a triflate anion (La–N distances: 2.698(5) – 2.846(6) Å, La–O distances: 2.462(4) – 2.689(5) Å). Selected bond lengths and angles are shown in tables 4.3 and 4.4.

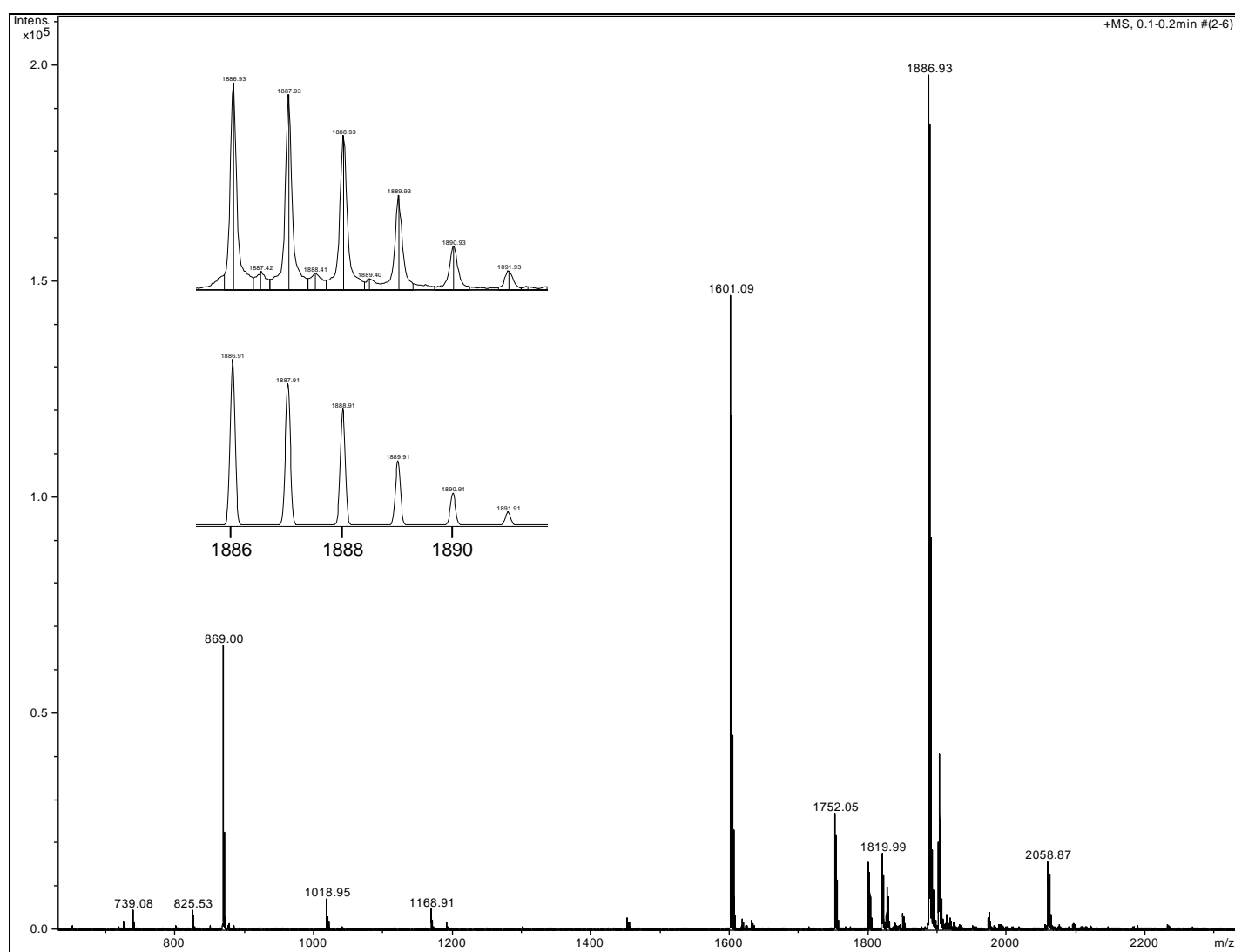


Figure 4. 7 ESI-MS of $[(L^{16})_2La_2](CF_3SO_3)_4$ with the found (top) and predicted (bottom) isotopic distribution pattern of $\{[(L^{16})_2La_2](CF_3SO_3)_3\}^+$ (inset)

Bond	Bond Length (Å)	Bond	Bond Length (Å)
La(1)-O(2)	2.482(4)	La(2)-O(2)	2.462(4)
La(1)-O(1)	2.488(4)	La(2)-O(1)	2.484(4)
La(1)-O(3)	2.575(4)	La(2)-O(5)	2.588(4)
La(1)-O(8)	2.684(4)	La(2)-O(4)	2.689(5)
La(1)-N(3)	2.698(5)	La(2)-N(10)	2.748(5)
La(1)-N(9)	2.726(5)	La(2)-N(12)	2.761(5)
La(1)-N(1)	2.740(5)	La(2)-N(4)	2.763(5)
La(1)-N(7)	2.773(5)	La(2)-N(6)	2.802(5)
La(1)-N(2)	2.801(5)	La(2)-N(5)	2.822(5)
La(1)-N(8)	2.818(5)	La(2)-N(11)	2.846(6)

Table 4.3 Selected bond lengths (Å) for the complex cation
 $[(L^{16})_2La_2(H_2O)_2(CF_3SO_3)_2]^{2+}$

Bond	Angle (°)	Bond	Angle (°)
O(2)-La(1)-O(1)	63.28(13)	O(2)-La(1)-N(2)	103.84(14)
O(2)-La(1)-O(3)	139.96(15)	O(1)-La(1)-N(2)	78.66(14)
O(1)-La(1)-O(3)	130.57(16)	O(3)-La(1)-N(2)	115.38(16)
O(2)-La(1)-O(8)	135.31(13)	O(8)-La(1)-N(2)	60.37(14)
O(1)-La(1)-O(8)	137.11(13)	N(3)-La(1)-N(2)	59.87(16)
O(3)-La(1)-O(8)	65.52(15)	N(9)-La(1)-N(2)	127.34(16)
O(2)-La(1)-N(3)	60.30(14)	N(1)-La(1)-N(2)	59.06(16)
O(1)-La(1)-N(3)	93.97(14)	N(7)-La(1)-N(2)	114.64(16)
O(3)-La(1)-N(3)	134.86(17)	O(2)-La(1)-N(8)	77.09(14)
O(8)-La(1)-N(3)	76.98(14)	O(1)-La(1)-N(8)	107.98(14)
O(2)-La(1)-N(9)	88.96(14)	O(3)-La(1)-N(8)	62.98(15)
O(1)-La(1)-N(9)	61.97(15)	O(8)-La(1)-N(8)	113.76(14)
O(3)-La(1)-N(9)	74.05(17)	N(3)-La(1)-N(8)	115.59(15)
O(8)-La(1)-N(9)	134.86(14)	N(9)-La(1)-N(8)	59.76(16)
N(3)-La(1)-N(9)	148.07(15)	N(1)-La(1)-N(8)	124.75(15)
O(2)-La(1)-N(1)	139.92(15)	N(7)-La(1)-N(8)	58.06(15)
O(1)-La(1)-N(1)	77.31(14)	N(2)-La(1)-N(8)	172.65(16)
O(3)-La(1)-N(1)	72.55(16)	O(2)-La(1)-La(2)	31.45(10)
O(8)-La(1)-N(1)	71.34(14)	O(1)-La(1)-La(2)	32.10(9)
N(3)-La(1)-N(1)	118.85(16)	O(3)-La(1)-La(2)	149.34(13)
N(9)-La(1)-N(1)	78.29(15)	O(8)-La(1)-La(2)	144.90(9)
O(2)-La(1)-N(7)	83.54(14)	N(3)-La(1)-La(2)	72.77(11)
O(1)-La(1)-N(7)	146.66(14)	N(9)-La(1)-La(2)	76.24(11)
O(3)-La(1)-N(7)	73.43(16)	N(1)-La(1)-La(2)	108.57(11)
O(8)-La(1)-N(7)	69.62(14)	N(7)-La(1)-La(2)	114.95(10)
N(3)-La(1)-N(7)	70.50(15)	N(2)-La(1)-La(2)	88.77(11)
N(9)-La(1)-N(7)	117.48(16)	N(8)-La(1)-La(2)	95.34(10)
N(1)-La(1)-N(7)	136.01(15)		

Table 4.4 Selected bond angles (°) for the complex cation
 $[(L^{16})_2La_2(H_2O)_2(CF_3SO_3)_2]^{2+}$

4.2.3 Complex of L^{17} with terbium(III)

Reaction of L^{17} with an equimolar amount of $Tb(CF_3SO_3)_3$ in nitromethane gave a yellow solution. Again the formation of a dinuclear species was demonstrated by ESI-MS with an ion at m/z 1991 corresponding to $\{[(L^{17})_2Tb_2](CF_3SO_3)_3\}^+$. Slow diffusion of diethyl ether into the nitromethane complex solution resulted in the formation of X-ray quality crystals. The X-ray crystal structure showed crystallisation in the monoclinic space group $P2(1)/n$ and confirmed the formation of the dinuclear species $[(L^{17})_2Tb_2]^{4+}$ (figure 4.6)

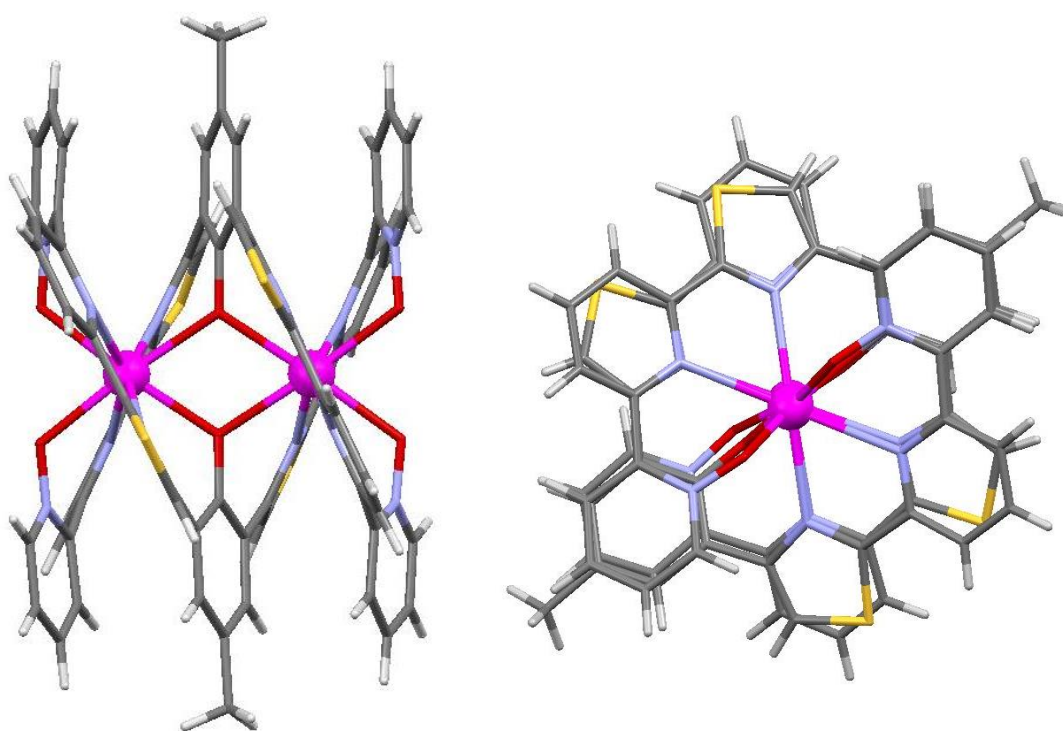


Figure 4.8 Two views for the solid state structure of the complex cation $[(L^{17})_2Tb_2]^{4+}$

The crystal structure confirms this ligand and Tb(III) ions form a dinuclear double helicate. The binding of this ligand, L^{17} , is similar to that seen for the previous ligand, L^{15} . The central p -cresol again acts as a bridging bidentate donor coordinating both terbium cations (figure 4.6). The two Tb(III) ions (Tb–Tb distance: 3.8501(2) Å) are eight-coordinate arising from coordination of two tridentate N,N,O-domains and the O-donor from the p -cresol central units (Tb–

N distances: 2.543(4) – 2.642(5) Å, Tb–O distances: 2.278(4) – 2.314(4) Å.
Selected bond lengths and angles are shown in tables 4.5 and 4.6.

Bond	Bond Length (Å)	Bond	Bond Length (Å)
Tb(1)-O(4)	2.279(4)	Tb(2)-O(6)	2.278(4)
Tb(1)-O(1)	2.295(4)	Tb(2)-O(2)	2.290(4)
Tb(1)-O(2)	2.304(4)	Tb(2)-O(5)	2.296(4)
Tb(1)-O(5)	2.314(4)	Tb(2)-O(3)	2.300(4)
Tb(1)-N(9)	2.543(4)	Tb(2)-N(10)	2.573(5)
Tb(1)-N(3)	2.557(4)	Tb(2)-N(4)	2.581(5)
Tb(1)-N(8)	2.590(5)	Tb(2)-N(11)	2.634(5)
Tb(1)-N(2)	2.601(5)	Tb(2)-N(5)	2.642(5)

Table 4.5 Selected bond lengths (Å) for the complex cation $[(L^{17})_2Tb_2]^{4+}$.

Bond	Angle (°)	Bond	Angle (°)
O(4)-Tb(1)-O(1)	72.76(10)	O(6)-Tb(2)-O(2)	173.47(10)
O(4)-Tb(1)-O(2)	174.37(10)	O(6)-Tb(2)-O(5)	108.92(10)
O(1)-Tb(1)-O(2)	111.06(10)	O(2)-Tb(2)-O(5)	66.70(10)
O(4)-Tb(1)-O(5)	110.53(10)	O(6)-Tb(2)-O(3)	77.02(11)
O(1)-Tb(1)-O(5)	173.24(10)	O(2)-Tb(2)-O(3)	107.75(10)
O(2)-Tb(1)-O(5)	66.14(10)	O(5)-Tb(2)-O(3)	172.67(11)
O(4)-Tb(1)-N(9)	120.74(10)	O(6)-Tb(2)-N(10)	122.04(11)
O(1)-Tb(1)-N(9)	76.16(10)	O(2)-Tb(2)-N(10)	64.05(11)
O(2)-Tb(1)-N(9)	64.71(10)	O(5)-Tb(2)-N(10)	96.77(11)
O(5)-Tb(1)-N(9)	97.16(10)	O(3)-Tb(2)-N(10)	76.19(12)
O(4)-Tb(1)-N(3)	76.92(10)	O(6)-Tb(2)-N(4)	76.23(11)
O(1)-Tb(1)-N(3)	122.09(11)	O(2)-Tb(2)-N(4)	97.32(10)
O(2)-Tb(1)-N(3)	97.46(10)	O(5)-Tb(2)-N(4)	64.23(10)
O(5)-Tb(1)-N(3)	64.66(10)	O(3)-Tb(2)-N(4)	122.25(11)
N(9)-Tb(1)-N(3)	159.35(11)	N(10)-Tb(2)-N(4)	158.36(12)
O(4)-Tb(1)-N(8)	67.75(10)	O(6)-Tb(2)-N(11)	67.53(11)
O(1)-Tb(1)-N(8)	92.60(10)	O(2)-Tb(2)-N(11)	115.89(11)
O(2)-Tb(1)-N(8)	115.50(10)	O(5)-Tb(2)-N(11)	84.82(11)
O(5)-Tb(1)-N(8)	83.48(10)	O(3)-Tb(2)-N(11)	93.79(12)

Bond	Angle (°)	Bond	Angle (°)
N(9)-Tb(1)-N(8)	64.69(10)	N(10)-Tb(2)-N(11)	64.16(12)
N(3)-Tb(1)-N(8)	119.36(11)	N(4)-Tb(2)-N(11)	120.59(11)
O(4)-Tb(1)-N(2)	91.75(11)	O(6)-Tb(2)-N(5)	92.95(11)
O(1)-Tb(1)-N(2)	68.40(11)	O(2)-Tb(2)-N(5)	84.97(10)
O(2)-Tb(1)-N(2)	86.03(11)	O(5)-Tb(2)-N(5)	115.46(10)
O(5)-Tb(1)-N(2)	116.77(11)	O(3)-Tb(2)-N(5)	67.66(11)
N(9)-Tb(1)-N(2)	121.13(11)	N(10)-Tb(2)-N(5)	121.57(11)
N(3)-Tb(1)-N(2)	64.50(11)	N(4)-Tb(2)-N(5)	63.77(11)
N(8)-Tb(1)-N(2)	155.92(12)	N(11)-Tb(2)-N(5)	156.21(12)
O(4)-Tb(1)-Tb(2)	143.61(7)	O(6)-Tb(2)-Tb(1)	142.07(8)
O(1)-Tb(1)-Tb(2)	143.56(7)	O(2)-Tb(2)-Tb(1)	33.26(7)
O(2)-Tb(1)-Tb(2)	32.96(7)	O(5)-Tb(2)-Tb(1)	33.45(7)
O(5)-Tb(1)-Tb(2)	33.19(7)	O(3)-Tb(2)-Tb(1)	140.90(8)
N(9)-Tb(1)-Tb(2)	78.99(8)	N(10)-Tb(2)-Tb(1)	79.48(8)
N(3)-Tb(1)-Tb(2)	80.37(8)	N(4)-Tb(2)-Tb(1)	78.89(8)
N(8)-Tb(1)-Tb(2)	100.40(8)	N(11)-Tb(2)-Tb(1)	102.58(9)
N(2)-Tb(1)-Tb(2)	103.66(8)	N(5)-Tb(2)-Tb(1)	101.20(8)

Table 4.6 Selected bond angles (°) for the complex cation $[(L^{17})_2Tb_2]^{4+}$.

4.3 Photophysical measurements

Since both the metal ion coordination and second sphere proximity of solvent molecules (particularly protic solvents and water) are known to quench the excited states of lanthanide ions, complexes based upon L^{17} were selected for further study; through the crystallographic structural studies, it was deduced that these species revealed the most effective encapsulation of the coordinated lanthanide ion. Additionally analysis by ESI-MS demonstrated that L^{17} has analogous reactivity with all the lanthanide ions, for example reaction with $Nd(CF_3SO_3)_3$ gave an ion at m/z 1963 corresponding to $\{[(L^{17})_2Nd_2](CF_3SO_3)_3\}^+$. The ESI-MS of $[(L^{17})_2Gd_2](CF_3SO_3)_4$ shows ions at m/z = 1989, 1384 and 920 corresponding to $\{[(L^{17})_2Gd_2](CF_3SO_3)_3\}^+$, $\{[(L^{17})_2Gd]\}^+$ and $\{[(L^{17})_2Gd_2](CF_3SO_3)_2\}^{2+}$ respectively (figure 4.7).

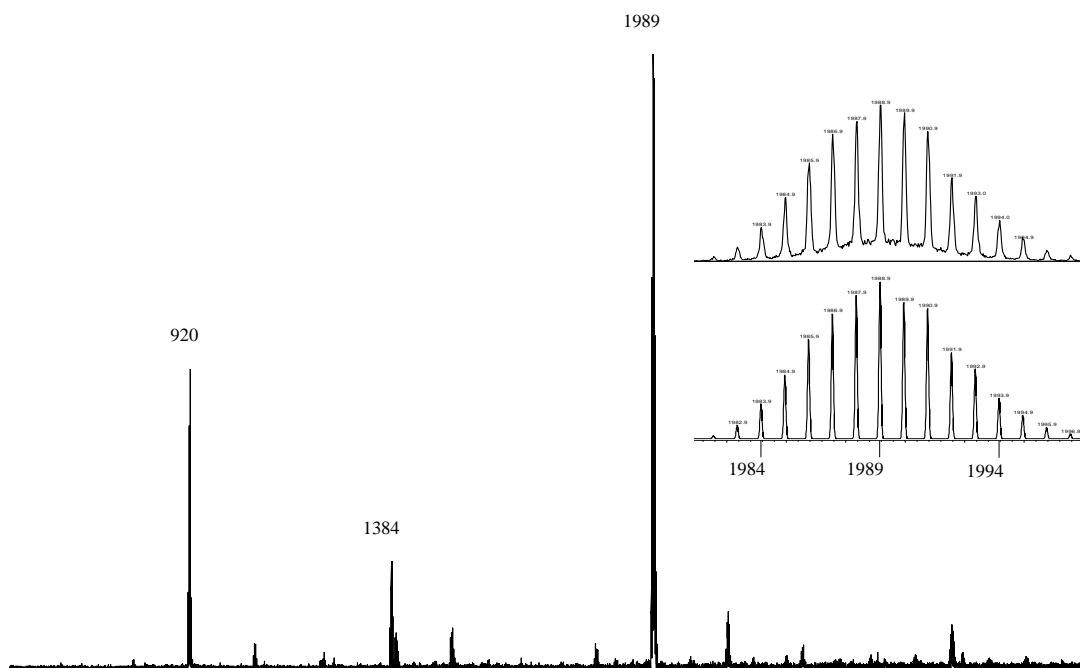


Figure 4.9 ESI-MS of $[(L^{17})_2Gd_2](CF_3SO_3)_4$ with the found (top) and predicted (bottom) isotopic distribution pattern of $\{[(L^{17})_2Gd_2](CF_3SO_3)_3\}^+$ (inset)

Firstly, the dimetallic Gd(III) complex was assessed in aerated solution (acetonitrile) revealing that the ligand itself was fluorescent at 440 nm ($\lambda_{ex} = 380$ nm). Since the ${}^6P_{7/2}$ excited state of Gd(III) lies at approximately 32000 cm^{-1} an ethanolic glass of $[(L^{17})_2Gd_2]^{4+}$ was formed at 77K and the resultant emission spectrum obtained, revealing that the corresponding excited triplet level, obtained from the onset of the peak, of the coordinated ligand was at *ca.* 19300 cm^{-1} . This energy level is insufficient for populating the accepting excited state of Tb(III) (5D_4 at *ca.* 20430 cm^{-1}). Preliminary measurements on $[(L^{17})_2Eu_2]^{4+}$ using $\lambda_{ex} = 340$ nm, revealed significant ligand-based fluorescence at 426 nm (*cf.* free ligand at 440 nm), but negligible Eu(III)-based peaks, suggesting that energy transfer to Eu(III) is relatively inefficient, where the 5D_1 and 5D_0 accepting states lie at *ca.* 19020 and 17250 cm^{-1} respectively. However, using a shorter excitation wavelength ($\lambda_{ex} = 290$ nm), which would be sufficient to excite the bridging phenolate chromophoric unit, did subsequently reveal both ligand-based and characteristic Eu(III)-centred emission lines between 580-730 nm (figure 4.8), the latter corresponding to ${}^5D_0 - {}^7F_J$.

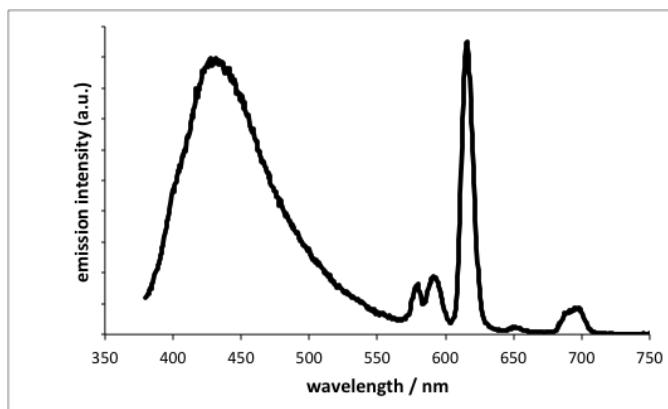


Figure 4.10 Total emission spectrum of $[(L^{17})_2Eu_2]^{2+}$ recorded in acetonitrile ($\lambda_{ex} = 290$ nm).

The relatively low-lying triplet state of L^{17} was advantageously utilised by incorporating the near-IR-emitting Ln(III) ions, Nd(III), Er(III) and Yb(III), since these possess lower energy excited $4f$ states. Firstly, emission lifetime measurements were obtained on room temperature acetonitrile solutions of the near-IR-emitting complexes utilising pulsed 355 nm excitation. Each of the dimetallic species (Ln(III) = Nd, Er and Yb) revealed mono-exponential decay profiles (figure 4.9), consistent with the existence of a single Ln(III) coordination environment within the complex in solution. The magnitude of the life time for $[(L^{17})_2Eu_2]^{4+}$ ($\tau = 21.0 \mu s$) was particularly notable, suggesting that both Yb(III) ions are not only well shielded from quenching solvent and typical of an anhydrous environment, but that the ligand structure and conformation induces a rigid architecture that limits the non-radiative deactivation pathways available through vibrational modes. The measured lifetime for the Yb(III) dimer compares very favourably with those reported for hetero-bimetallic complexes based upon benzoxazole-substituted 8-hydroxyquinolines,¹⁶⁸ albeit in dichloromethane solution. However, such enhancements in lifetime were not as pronounced for the Nd(III) ($\tau = 0.362 \mu s$) and Er(III) ($\tau = 1.45 \mu s$) analogues.

The corresponding steady state spectra were also obtained for these complexes; for $[(L^{17})_2Nd_2]^{4+}$ ($\lambda_{ex} = 370$ nm) this revealed the characteristic ${}^4F_{3/2} - {}^4I_{9/2}$, ${}^4F_{3/2} - {}^4I_{11/2}$ and ${}^4F_{3/2} - {}^4I_{13/2}$ transitions between 880-1350 nm (figure 4.9, a). For $[(L^{17})_2Yb_2]^{4+}$ the spectrum displayed a very sharp transition at 971 nm

(${}^2F_{5/2} - {}^2F_{7/2}$) with minor features to low energy of this peak, often attributed to ligand-field-induced splitting of the ${}^2F_{7/2}$ manifold.

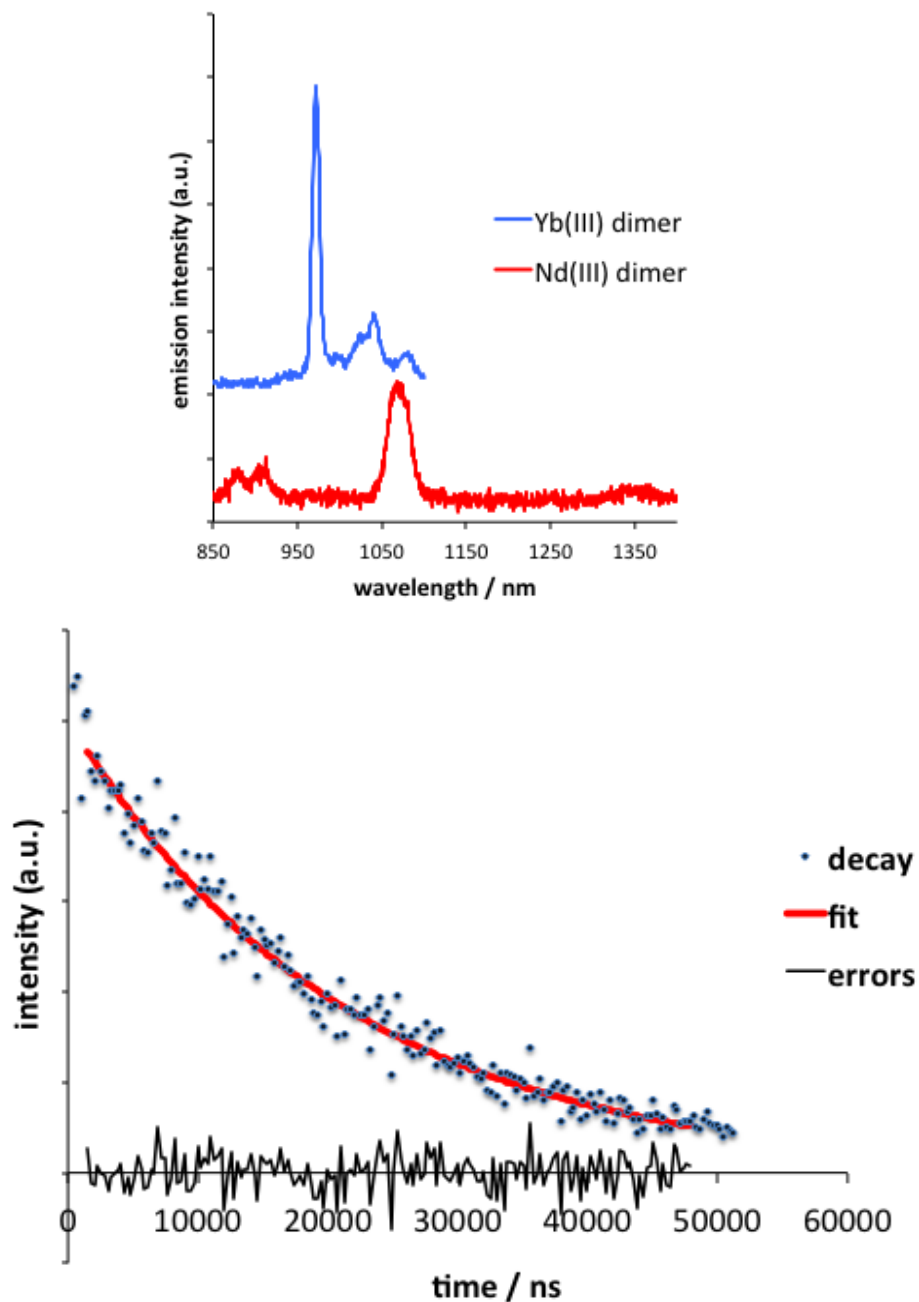


Figure 4.11 a) Steady state emission spectrum of $[(L^{17})_2Yb_2]^{2+}$ and $[(L^{17})_2Nd_2]^{2+}$ recorded in acetonitrile ($\lambda_{ex} = 370$ nm); b) fitted decay profile for $[(L^{17})_2Yb_2]^{2+}$ ($\lambda_{ex} = 355$ nm)

4.4 Discussion

All three structures are very similar; each ligand partitions into two tetradentate domains (comprising of four nitrogen or three nitrogen and one oxygen donor atoms) and these units coordinate different metal ions. The central phenolic unit deprotonates and bridges the two lanthanide metal ions (figure 4.10).

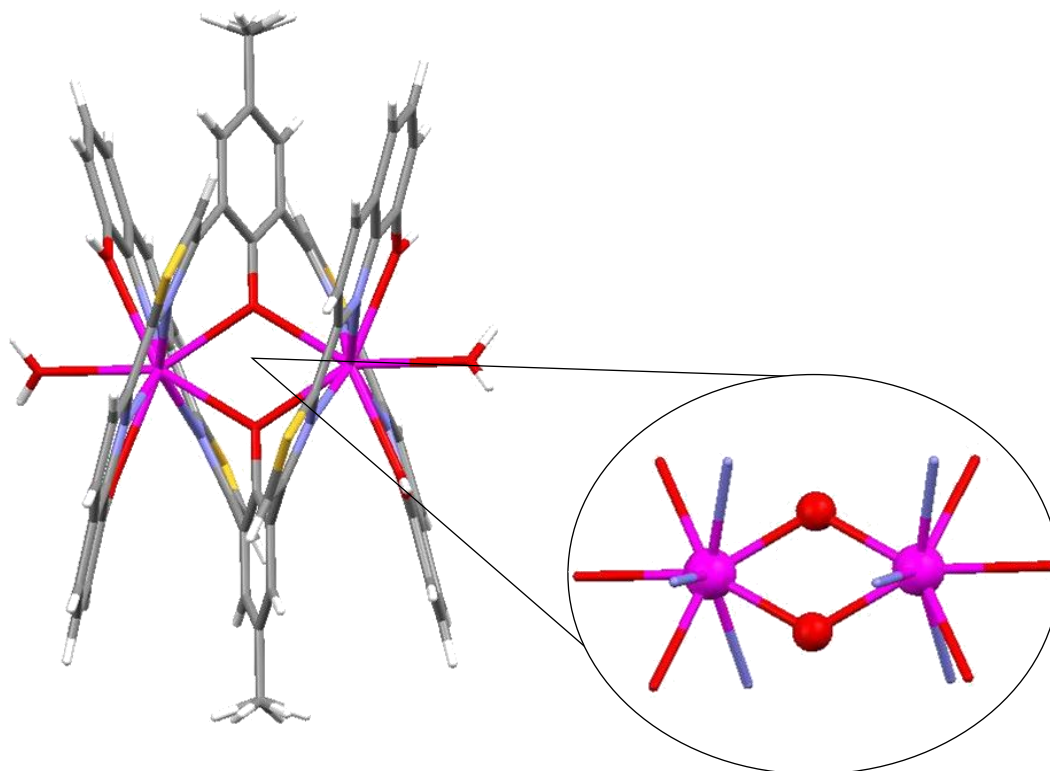


Figure 4.12 Structure of the complex cation $[(\mathbf{L}^{15})_2\text{Eu}_2(\text{H}_2\text{O})_2]^{4+}$ showing the $\{\text{Eu}(\mu\text{-O}_2)\text{Eu}\}$ core

The only major difference is the supplementation of the coordination sphere by either solvents or anions i.e. the metal centre in $[(\mathbf{L}^{15})_2\text{Eu}_2]^{4+}$ is coordinated by a molecule of water and $[(\mathbf{L}^{16})_2\text{La}_2]^{4+}$ is coordinated by both a molecule of water and a triflate anion. However, in the *N*-oxide containing complex $[(\mathbf{L}^{17})_2\text{Tb}_2]^{4+}$ there are no additional species which coordinate the metal ion; this behaviour is attributed to the shape of the ligand strands. With both \mathbf{L}^{15} and \mathbf{L}^{16} the linear nature of the ligand strands leaves some of the metal exposed (figure 3.11), allowing coordination of solvent molecules. However, due to the shape of the

N-oxide-containing ligand L^{17} the lanthanide ion is totally encompassed by the ligand strand, minimising solvent access (fig. 4.11).

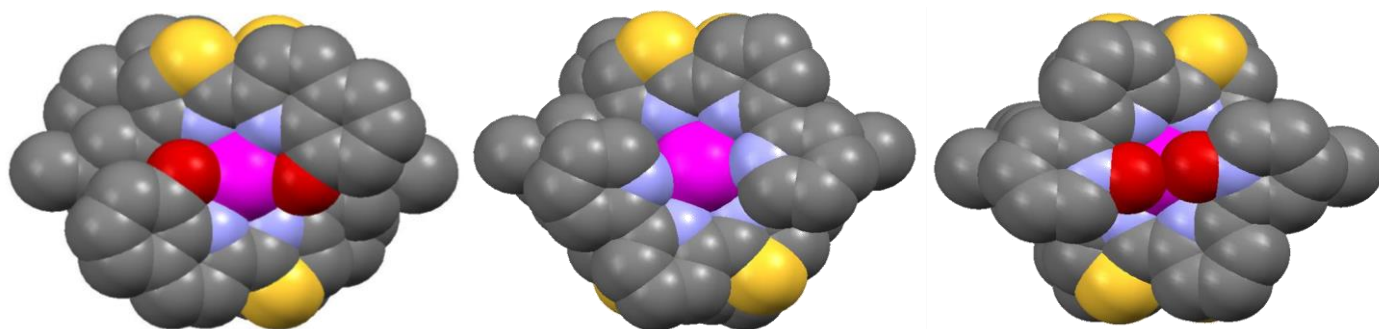


Figure 4.13 End-on view of the space-filled X-ray structures of complexes a) $[(L^{15})_2Eu_2]^{4+}$, b) $[(L^{16})_2La_2]^{4+}$ and c) $[(L^{17})_2Tb_2]^{4+}$ (c). Coordinated anions/water molecules omitted for clarity

4.5 Conclusion

In conclusion, three novel ligands L^{15} - L^{17} , consisting of two tetradentate domains (comprising nitrogen and oxygen donor atoms) were successfully synthesised. It has been demonstrated here that if the ligand does not effectively encapsulate the lanthanide ion supplementation of the coordination sphere will result. As L^{17} successfully encompasses the lanthanide ion non-radiative deactivation pathways available through vibrational modes are limited.

5. Conclusion

In conclusion 17 novel ligands, L^1 - L^{17} , have been successfully synthesised and where possible the coordination chemistry of these ligands has been investigated in the solid state and in solution. L^{17} has recently been reported, however this research was focused on the influence of N-oxide within self-assembly rather than lanthanide ions and luminescence.¹⁶⁹

The potentially hexadentate ligands, L^1 - L^5 , contain both N-donor and O-donor domains separated by a 1,3-phenylene spacer unit, the incorporation of this space group with careful selection of the metal ion has been shown to be a robust method for the successful formation of circular helicates.^{107, 108} These higher nuclearity species form due to destabilization of the similar linear helicate. Reaction of L^1 with Zn(II) results in the self-assembly of a pentanuclear circular helicate which persists in both the solution and solid state. Variation of the terminal functional group of the ligand allowed incorporation of enantiopure units which were shown to selectively direct the self-assembly. These ligands, L^2 - L^5 , led to the diastereoselective control of the resulting supramolecular architecture upon coordination with selected metal ions giving up to 80% diastereomeric excess.

The potentially hexadentate symmetrical ligands, L^6 - L^{14} , partition into two tridentate pyridyl-pyridyl-thiazolyl domains due to separation by various aromatic space-units allowing coordination with two different metal ions. Reaction of L^9 with Cd(II) results in the formation of a dinuclear double helicate $[Cd_2(L^9)_2]^{4+}$, the two tridentate donor domains of each ligand coordinate both of the metal ions with the triphenyl space group bridging the tridentate domains in an “over-and-under” conformation giving a helical structure. However, reaction of this same ligand with Co(II) results in the formation of a dinuclear double mesocate $[Co_2(L^9)_2]^{4+}$, where the two metal ions again adopt an octahedral coordination geometry arising from the coordination of the two tridentate domains from two different ligand strands, in this case the triphenyl space

group bridges the tridentate domains in a “side by side” conformation in the solid state. This difference in structure is attributed to unfavourable steric and/or electrostatic repulsion which prevent the ligands forming the dicobalt(II) helicate with these unfavourable interactions not present within the complex employing the larger Cd(II) ion. Further to this L^{14} , which consists of the same basic ligand chain as L^9 , contains the more sterically demanding benzyl functionality, results in the self-assembly of the mesocate species even upon coordination with the larger second row transition metal ions.

The final class of symmetrical ligands described here, L^{15} - L^{17} , possess tridentate donor domains separated by a central phenol unit. The tridentate domains of these ligands consist of either a thiazole-hydroxyquinoline, thiazole-pyridine-pyridine or thiazole-pyridine-pyridine-*N*-oxide units. All three of these ligands form dinuclear double helicates with trivalent lanthanide metal ions, with the central phenol unit deprotonating and bridging the two lanthanide cations. Depending on how effective the ligand is at surrounding the metal ion, the complex may also coordinate anions and/or solvent molecules. L^{17} , which possesses the pyridine-*N*-oxide as the terminal group, effectively encompasses the cations minimising access for the coordination of any anions or solvent molecules. Photophysical measurements show that this ligand forms emissive complexes with a number of lanthanide ions, with the magnitude of the lifetime for $[(L^{17})_2Yb_2]^{4+}$ ($\tau = 21.0 \mu s$) suggesting both the Yb(III) ions are well shielded from quenching solvent and typical of an anhydrous environment. In addition the ligand structure and conformation induces a rigid architecture which limits the non-radiative deactivation pathways available through vibrational modes.

It has been shown in this thesis that judicious programming and matching of the components (i.e. the metal ions and ligands) provides control over the self-assembly process. For example the diastereoselectivity of circular helicates can be governed by the incorporation of chiral units within the ligand strand. Also shown here is the preferential assembly of *meso*-helicates; controlled by the inclusion of sterically demanding substituents within the ligand strand. A mixture of two ligands and metal ions resulted in the self-assembly of discrete

meso-helicates, due to the correct matching of the components, which led to the assembly of a heteroleptic one-dimensional chain through hydrogen bond donor and acceptor groups. Finally it has been shown that dimetallic lanthanide-containing double helicates can be formed and by employing the correct donor units within the ligand gives emissive self-assembled species.

Supplementary to the work presented herein it may be interesting to investigate some of these ligands further. For example **L**¹ possesses terminal N,N'-diethylcarboxamido functionalities which have been shown previously to coordinate well with trivalent lanthanide metal ions. Additionally new ligands could be synthesised with variation in coordination domains of the ligand strands to see the influence on the assemblies. For example incorporation of alternative domains (e.g. thiazole-pyridine-pyridine-*N*-oxide) within the ligands presented in chapter three, e.g. **L**⁹, may provide new ligands which behave differently upon coordination and within the resulting assemblies. As the ligands throughout this work have been symmetrical, i.e. homotopic, it would be interesting to investigate some systems which are heterotopic. One possibility could be the alteration of **L**¹⁷ to incorporate a thiazole-pyridine-pyridine domain (as seen within ligand **L**¹⁶) while keeping the same central *p*-cresol unit and a thiazole-pyridine-pyridine-*N*-oxide domain.

6. Experimental

Chemicals were purchased and used without further purification. ^1H NMR spectra were recorded on a 400MHz Bruker Avance DP X400 or on a 500MHz Bruker Avance 500. Mass spectra were obtained on a Bruker MicroTOF-q LC mass spectrometer.

The following compounds were prepared using literature methods:

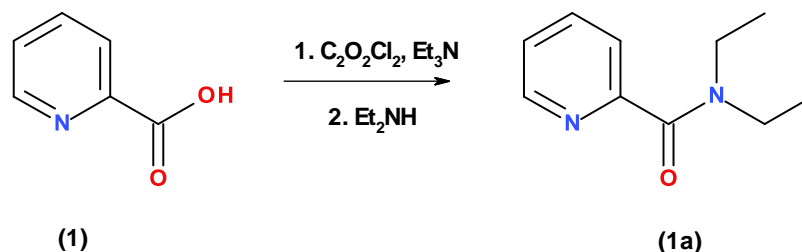
3,3'-Diacetylbiphenyl (**7**)¹⁴⁰

Bipythioamide (**9**)^{166, 167}

Acetyl cresol (**39**)¹⁶⁵

6.1 Preparation of diastereoselective ligands (L^1 - L^4)

6.1.1 Synthesis of picolinamide derivative **1a** ¹⁷⁰

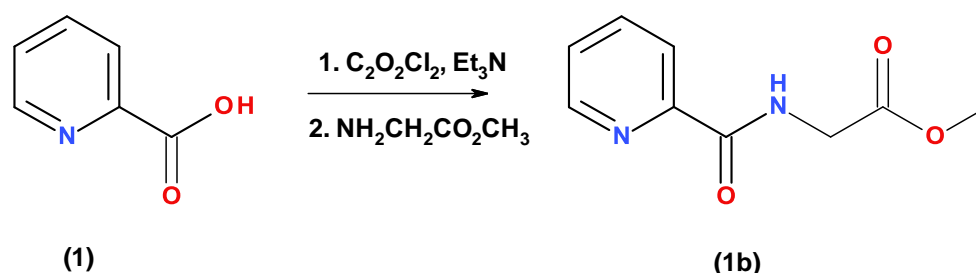


To a two necked round bottom flask charged with picolinic acid (**1**) (1.5 g, 0.012 mol), anhydrous DCM was added and the reaction stirred under an atmosphere of dinitrogen at 0°C. To this was then added oxalyl chloride (2M, 8.5 ml, 0.017 mol) and the solution left to stir for 10 minutes. After this time triethylamine (2.4 g, 0.024 mol) was slowly added and the reaction was left at room temperature for 3 h. The solvent was removed by rotary evaporation giving a black solid. This was redissolved in anhydrous DCM, stirred at 0°C and triethylamine (1.9 g, 0.019 mol) and diethylamine (0.73 g, 0.010 mol) were added and the reaction stirred at room temperature for 2 h. The solution was poured into $NaHCO_3$ (aq) (30ml) and extracted into DCM (3 x 50 ml), then the combined organic layers were dried ($MgSO_4$) and concentrated. The crude product was dissolved in ether (100 ml) and decolourising charcoal (0.1 g) added; filtration followed by removal of solvent gave the pure product as a light brown oil (**1a**) (0.6 g, 60% yield).

1H NMR [400 MHz, $CDCl_3$]: δ_H = 8.59 (ddd, J = 4.8, 1.6, 1.0, 1H, Py), 7.78 (dt, J = 7.7, 1.7, 1H, Py), 7.58 (dt, J = 7.8, 1.0, 1H, Py), 7.33 (ddd, J = 7.6, 4.9, 1.2, 1H, Py), 3.58 (q, J = 7.2, 2H, $-CH_2CH_3$), 3.39 (q, J = 7.1, 2H, $-CH_2CH_3$), 1.28 (t, J = 7.1, 3H, $-CH_2CH_3$), 1.16 (t, J = 7.1 Hz, 3H, $-CH_2CH_3$).

ESI-MS m/z 201.1 ($[M+Na]^+$), HR ESI-MS found 201.1002 $C_{10}H_{14}N_2NaO$ requires 201.0998 (error 2.03 ppm).

6.1.2 Synthesis of picolinamide derivative **1b**

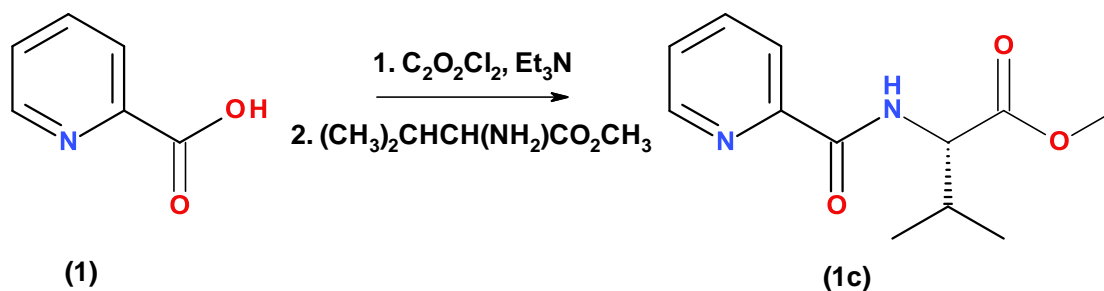


This compound was prepared in an identical manner to **1a**, except glycine methyl ester was used in place of diethylamine and the resulting compound was purified *via* column chromatography (Al_2O_3 , 5% MeOH in DCM) giving **1b** as a brown oil (42% yield).

^1H NMR [400 MHz, CDCl_3]: δ_{H} = 8.60 (ddd, J = 4.8, 1.6, 0.9, 1H, Py), 8.49 (br s, 1H, -CONH), 8.19 (dt, J = 7.8, 1.0, 1H, Py), 7.86 (dt, J = 7.8, 1.7, 1H, Py), 7.46 (ddd, J = 7.6, 4.8, 1.2, 1H, Py), 4.29 (d, J = 5.7 Hz, 2H, - NHCH_2CO_2), 3.80 (s, 3H, - CO_2CH_3).

ESI-MS m/z 217 ($[\text{M}+\text{Na}]^+$), HR ESI-MS found 217.0590 $\text{C}_9\text{H}_{10}\text{N}_2\text{NaO}_3$ requires 217.0584 (error 3.11 ppm).

6.1.3 Synthesis of picolinamide derivative **1c**



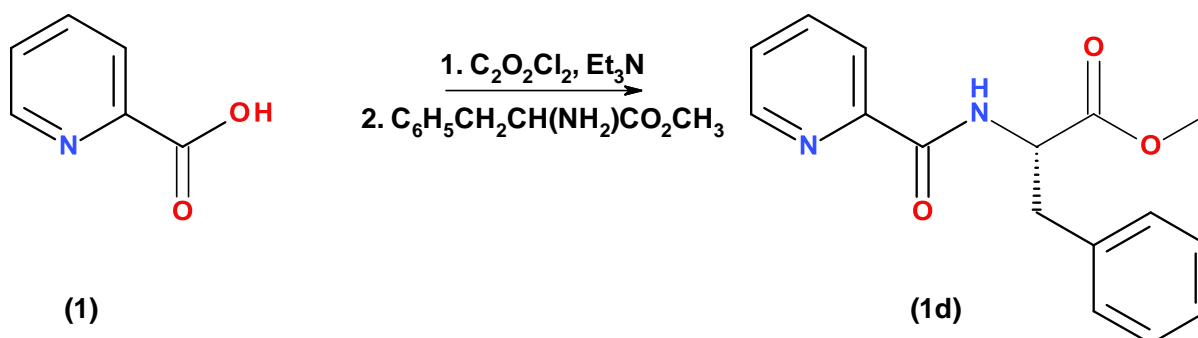
This compound was prepared in an identical manner to **1a**, except *S*-valine

methyl ester was used in place of diethylamine giving **1c** as a yellow oil (37% yield).

^1H NMR [400 MHz, CDCl_3]: δ_{H} = 8.61 (ddd, J = 4.8, 1.6, 0.9, 1H, Py), 8.53 (br d, J = 8.9, 1H, -CONH), 8.19 (dt, J = 7.8, 1.0, 1H, Py), 7.86 (dt, J = 7.7, 1.7, 1H, Py), 7.45 (ddd, J = 7.6, 4.8, 1.2, 1H, Py), 4.75 (dd, J = 9.3, 5.2, 1H, -NHCH), 3.78 (s, 3H, - CO_2CH_3), 2.33 (m, 1H, - $\text{CH}(\text{CH}_3)_2$), 1.03 (d, J = 6.9, 3H, - $\text{CH}(\text{CH}_3)_2$), 1.02 (d, J = 6.9 Hz, 3H, - $\text{CH}(\text{CH}_3)_2$).

ESI-MS m/z 259 ($[\text{M}+\text{Na}]^+$), HR ESI-MS found 259.1051 $\text{C}_{12}\text{H}_{16}\text{N}_2\text{NaO}_3$ requires 259.1053 (error 0.98 ppm)

6.1.4 Synthesis of picolinamide derivative **1d**



This compound was prepared in an identical manner to **1a**, except *S*-phenylalanine methyl ester was used in place of diethylamine giving **1d** as a brown oil (54 % yield).

^1H NMR [400 MHz, CDCl_3]: δ_{H} = 8.56 (ddd, J = 4.8, 1.6, 0.9, 1H, Py), 8.50 (br d, J = 8.2, 1H, -CONH), 8.17 (dt, J = 7.8, 1.0, 1H, Py), 7.85 (dt, J = 7.7, 1.7, 1H, Py), 7.44 (ddd, J = 7.6, 4.8, 1.2, 1H, Py), 7.31-7.20 (m, overlap, 5H, Ph), 5.08 (dt, J = 8.4, 6.1, 1H, - CHCH_2Ph), 3.74 (s, 3H, - CO_2CH_3), 3.28 (dd, J = 13.8, 6.0, 1H, - CH_2Ph), 3.23 (dd, J = 13.8, 6.2 Hz, 1H, - CH_2Ph).

ESI-MS m/z 307 ($[M+Na]^+$), HR ESI-MS found 307.1047 $C_{16}H_{16}N_2NaO_3$ requires 307.1053 (error 1.95 ppm).

6.1.5 Synthesis of picolinamide-N-oxide derivative **2a**

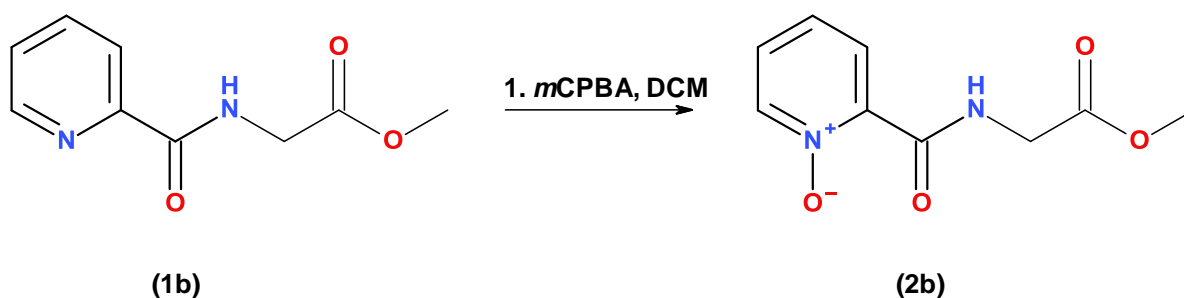


To a solution of **1a** (0.3 g, 1.7 mmol) in DCM (25 ml) *m*CPBA (70%, 0.89 g, 3.7 mmol) was slowly added over 30 minutes, while the solution stirred at room temperature. The reaction was monitored *via* TLC and upon completion (~ 8 h) the reaction was carefully evaporated (Caution: N-oxides are potentially explosive). Purification by column chromatography (Al_2O_3 , 2% MeOH in DCM) gave the N-oxide **2a** as a white solid (0.3 g, 91% yield).

1H NMR [400 MHz, $CDCl_3$]: δ_H = 8.32 (d, J = 6.2, 1H, Py), 7.35- 7.28 (m, overlap, 3H, Py), 3.65 (m, 1H, $-CH_2CH_3$), 3.54 (m, 1H, $-CH_2CH_3$), 3.20 (m, 2H, $-CH_2CH_3$), 1.29 (t, J = 7.2, 3H, $-CH_2CH_3$), 1.13 (t, J = 7.2 Hz, 3H, $-CH_2CH_3$).

ESI-MS m/z 217 ($[M+Na]^+$), HR ESI-MS found 217.0958 $C_{10}H_{14}N_2NaO_2$ requires 217.0947 (error 4.91 ppm).

6.1.6 Synthesis of picolinamide-N-oxide derivative **2b**

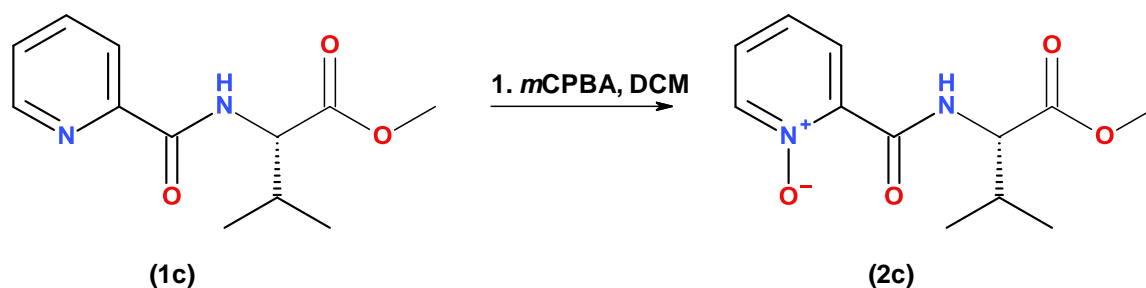


This compound was prepared in an identical manner to **2a**, except **1b** was used instead of **1a**. Purification *via* column chromatography (Al_2O_3 , 1 % MeOH in DCM) gave the N-oxide **2b** as a fine white powder (85 % yield).

^1H NMR [400 MHz, CDCl_3]: δ_{H} = 11.72 (br s, 1H, -CONH), 8.43 (dd, J = 7.8, 2.3, 1H, Py), 8.29 (dd, J = 6.4, 1.2, 1H, Py), 7.47 (dt, J = 7.7, 1.3, 1H, Py), 7.42 (dt, J = 6.4, 2.3, 1H, Py), 4.29 (d, J = 5.6 Hz, 2H, -NHCH₂CO₂), 3.80 (s, 3H, -CO₂CH₃).

ESI-MS m/z 233 ($[\text{M}+\text{Na}]^+$), HR ESI-MS found 233.0538 $\text{C}_9\text{H}_{10}\text{N}_2\text{NaO}_4$ requires 233.0533 (error 2.25 ppm).

6.1.7 Synthesis of picolinamide-N-oxide derivative **2c**



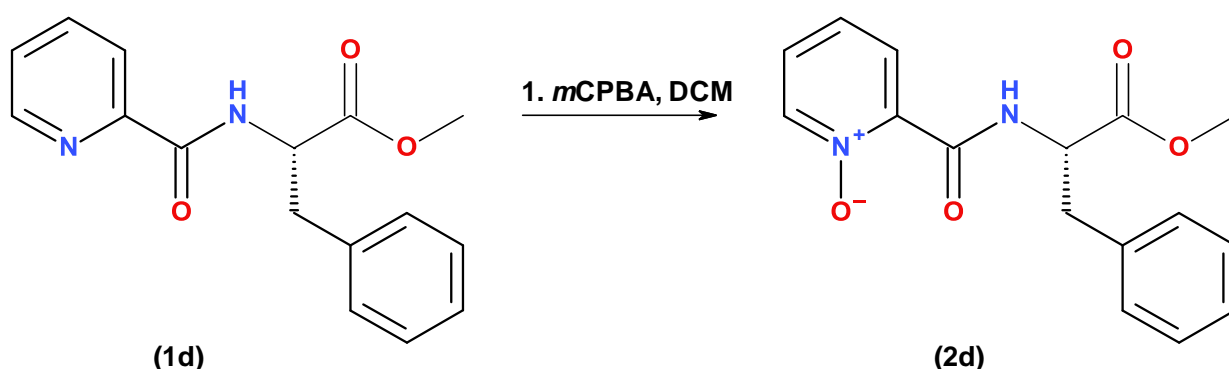
This compound was prepared in an identical manner to **2a**, except **1c** was used instead of **1a**. Purification *via* column chromatography (Al_2O_3 , 2 % MeOH in

DCM) gave the N-oxide **2c** as a white solid (88 % yield).

^1H NMR [400 MHz, CDCl_3]: δ_{H} = 11.82 (br d, J = 7.9, 1H, -CONH), 8.42 (dd, J = 7.9, 2.2, 1H, Py), 8.28 (dd, J = 6.3, 0.9, 1H, Py), 7.47 (dt, J = 7.8, 1.0, 1H, Py), 7.42 (dt, J = 6.4, 2.3, 1H, Py), 4.70 (dd, J = 8.0, 4.9, 1H, -NHCH), 3.77 (s, 3H, - CO_2CH_3), 2.36 (m, 1H, - $\text{CH}(\text{CH}_3)_2$), 1.05 (d, J = 6.8, 3H, - $\text{CH}(\text{CH}_3)_2$), 1.04 (d, J = 6.9 Hz, 3H, - $\text{CH}(\text{CH}_3)_2$).

ESI-MS m/z 275 ($[\text{M}+\text{Na}]^+$), HR ESI-MS found 275.1008 $\text{C}_{12}\text{H}_{16}\text{N}_2\text{NaO}_4$ requires 275.1002 (error 2.24 ppm).

6.1.8 Synthesis of picolinamide-N-oxide derivative **2d**



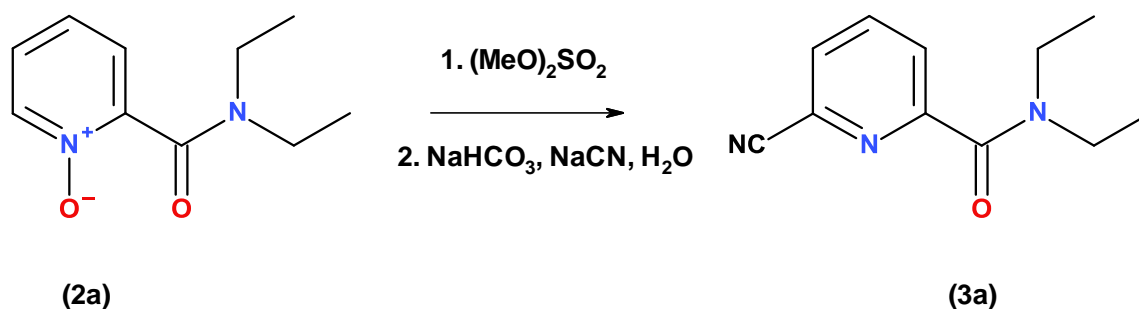
This compound was prepared in an identical manner to **2a**, except **1d** was used instead of **1a**. Purification *via* column chromatography (Al_2O_3 , 2 % MeOH in DCM) gave the N-oxide **2d** (80 % yield).

^1H NMR [400 MHz, CDCl_3]: δ_{H} = 11.75 (br d, J = 5.5, 1H, -CONH), 8.38 (dd, J = 7.9, 2.3, 1H, Py), 8.25 (dd, J = 6.3, 1.2 1H, Py), 7.44 (dt, J = 7.6, 1.4, 1H, Py), 7.39 (dt, J = 6.3, 2.4, 1H, Py), 7.34-7.23 (m, overlap, 5H, Ph), 5.00 (dt, J = 7.5, 5.5, 1H, - CHCH_2Ph), 3.74 (s, 3H, - CO_2CH_3), 3.28 (dd, J = 13.9, 5.5, 1H, - CH_2Ph), 3.19 (dd, J = 13.9, 7.6 Hz, 1H, - CH_2Ph).

ESI-MS m/z 323 ($[\text{M}+\text{Na}]^+$), HR ESI-MS found 323.1013 $\text{C}_{16}\text{H}_{16}\text{N}_2\text{NaO}_4$

requires 323.1002 (error 3.32 ppm).

6.1.9 Synthesis of 6-cyanopicolinamide derivative **3a**

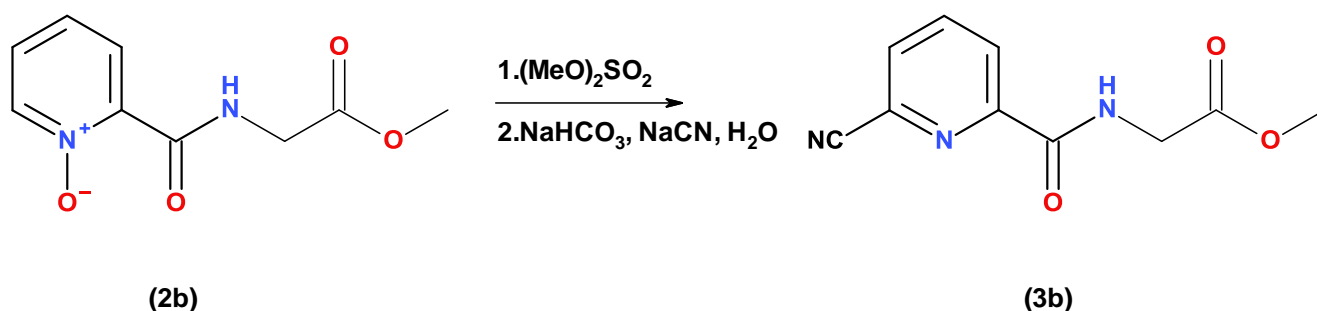


To a 50 ml round bottom flask containing **2a** (0.2 g, 1.00 mmol) dimethyl sulfate (3 ml) was added and the reaction was placed under nitrogen and heated at 60°C for 24 h with stirring. The reaction was allowed to cool to room temperature then ether (25 ml) was added and left to stir for 1 h. The reaction was left to settle for 12 h. The ether was decanted off and the remaining oil was washed with ether and decanted again and any remaining solvent removed by rotary evaporation. Distilled water was added (10 ml) and the solution neutralised with NaHCO₃, to this was then added NaCN (0.1g, 2.00 mmol) and the reaction stirred for 5 mins, during which time a yellow oil was produced. Extraction into DCM (3 x 30 ml), followed by drying (MgSO₄) and evaporation produced the nitrile derivative **3a** as a light purple solid (0.16 g, 77% yield).

¹H NMR [400 MHz, CDCl₃]: δ_H = 7.96 (t, *J* = 7.9, 1H, Py), 7.90 (dd, *J* = 8.0, 1.3, 1H, Py), 7.75 (dd, *J* = 7.9, 1.3, 1H, Py), 3.58 (q, *J* = 7.1, 2H, -CH₂CH₃), 3.40 (q, *J* = 7.1, 2H, -CH₂CH₃), 1.29 (t, *J* = 7.1, 3H, -CH₂CH₃), 1.32 (t, *J* = 7.1 Hz, 3H, -CH₂CH₃).

ESI-MS *m/z* 226 ([M+Na]⁺), HR ESI-MS found 226.0951 C₁₁H₁₃NaN₃O requires 226.0951 (error 0.06 ppm).

6.1.10 Synthesis of 6-cyanopicolinamide derivative **3b**

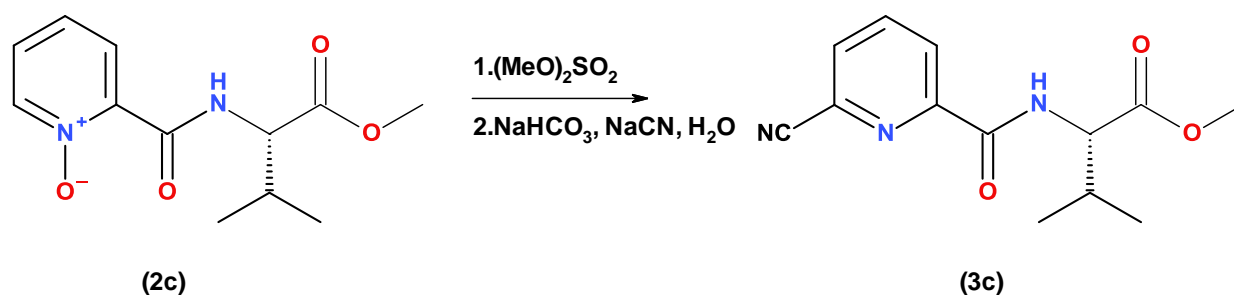


This compound was prepared in an identical manner to **3a**, except **2b** was used instead of **2a** giving **3b** as a white solid (76 % yield).

$^1\text{H NMR}$ [400 MHz, CDCl_3]: $\delta_{\text{H}} = 8.43$ (dd, $J = 8.9, 1.0$, 1H, Py), 8.28 (br s, 1H, -CONH), 8.06 (t, $J = 7.9$, 1H, Py), 7.87 (dd, $J = 7.9, 1.0$, 1H, Py), 4.30 (d, $J = 5.8$, 2H, $-\text{NHCH}_2\text{CO}_2$), 3.82 (s, 3H, $-\text{CO}_2\text{CH}_3$).

ESI-MS m/z 242 ($[\text{M}+\text{Na}]^+$), HR ESI-MS found 242.0529 $\text{C}_{10}\text{H}_9\text{N}_3\text{NaO}_3$ requires 242.0536 (error 2.80 ppm).

6.1.11 Synthesis of 6-cyanopicolinamide derivative **3c**



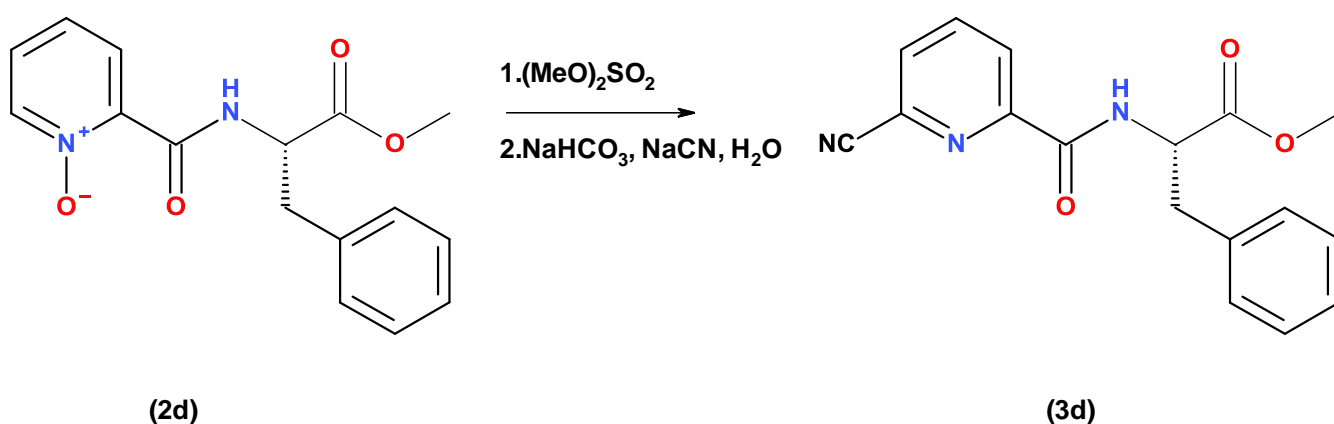
This compound was prepared in an identical manner to **3a**, except **2c** was used instead of **2a** giving **3c** as a white solid (77 % yield).

$^1\text{H NMR}$ [400 MHz, CDCl_3]: $\delta_{\text{H}} = 8.42$ (dd, $J = 8.0, 1.1$, 1H, Py), 8.25 (br d, $J =$

8.9, 1H, -CONH), 8.05 (t, $J = 7.9$, 1H, Py), 7.87 (dd, $J = 7.7$, 1.1, 1H, Py), 4.73 (dd, $J = 9.2$, 5.1, 1H, -NHCH), 3.97 (s, 3H, -CO₂CH₃), 2.34 (m, 1H, -CH(CH₃)₂), 1.04 (d, $J = 1.7$, 3H, -CH(CH₃)₂), 1.03 (d, $J = 1.7$ Hz, 3H, -CH(CH₃)₂).

ESI-MS m/z 284 ([M+Na]⁺), HR ESI-MS found 284.1017 C₁₃H₁₅N₃NaO₃ requires 284.1006 (error 3.96 ppm).

6.1.12 Synthesis of 6-cyanopicolinamide derivative **3d**

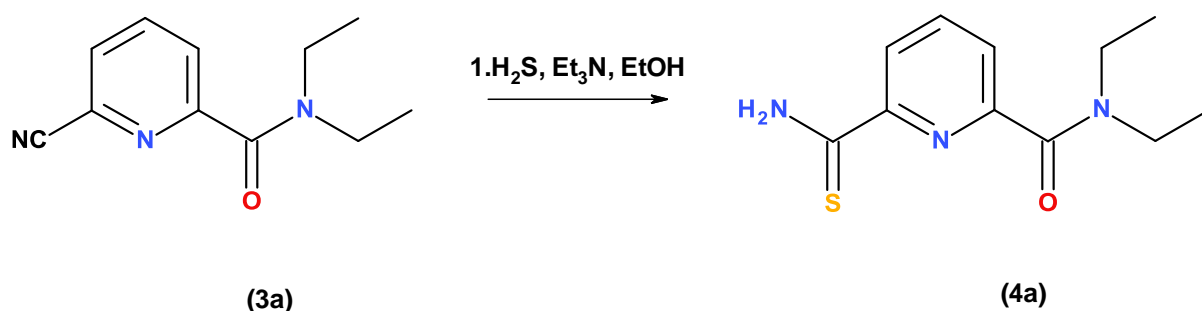


This compound was prepared in an identical manner to **3a**, except **2d** was used instead of **2a** giving **3d** as a colourless oil (74 % yield).

¹H NMR [400 MHz, CDCl₃]: δ_H = 8.38 (dd, $J = 8.0$, 1.1, 1H, Py), 8.22 (br d, $J = 8.2$, 1H, -CONH), 8.03 (t, $J = 7.9$, 1H, Py), 7.84 (dd, $J = 7.8$, 1.1, 1H, Py), 7.35-7.19 (m, overlap, 5H, Ph), 5.05 (dt, $J = 8.3$, 5.9, 1H, -CHCH₂Ph), 3.77 (s, 3H, -CO₂CH₃), 3.29 (dd, $J = 13.9$, 5.9, 1H, -CH₂Ph), 3.23 (dd, $J = 13.9$, 5.8 Hz, 1H, -CH₂Ph).

ESI-MS m/z 332 ([M+Na]⁺), HR ESI-MS found 332.0991 C₁₇H₁₅N₃NaO₃ requires 332.1006 (error 4.35 ppm).

6.1.13 Synthesis of picolinamide-6-thioamide derivative **4a**

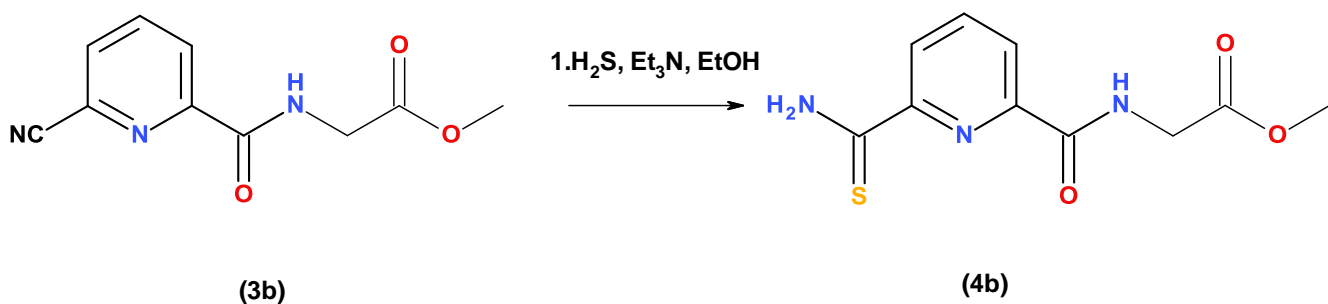


To a solution of the nitrile derivative **3a** (0.1 g, 0.49 mmol) in ethanol (20 ml), triethylamine (1.0 g, 9.9 mmol) was added and H₂S slowly bubbled through the solution which turned yellow after a few minutes. The solution was then left to stand at room temperature for 48 h during which time a precipitate was produced. Filtration gave the thioamide **4a** as a light yellow powder (0.9 g, 78% yield).

¹H NMR [400 MHz, CDCl₃]: δ_H = 9.31 (br s, 1H, -NH₂), 8.76 (dd, *J* = 7.8, 1.0, 1H, Py), 7.96 (t, *J* = 7.8, 1H, Py), 7.71 (dd, *J* = 7.8, 1.0, 1H, Py), 7.67 (br s, 1H, -NH₂), 3.60 (q, *J* = 7.1, 2H, -CH₂CH₃), 3.30 (q, *J* = 7.1, 2H, -CH₂CH₃), 1.30 (t, *J* = 7.1, 3H, -CH₂CH₃), 1.18 (t, *J* = 7.1 Hz, 3H, -CH₂CH₃).

ESI-MS *m/z* 260.1 ([M+Na]⁺), HR ESI-MS found 260.0820 C₁₁H₁₅N₃NaOS requires 260.0828 (error 2.92 ppm).

6.1.14 Synthesis of picolinamide-6-thioamide derivative **4b**

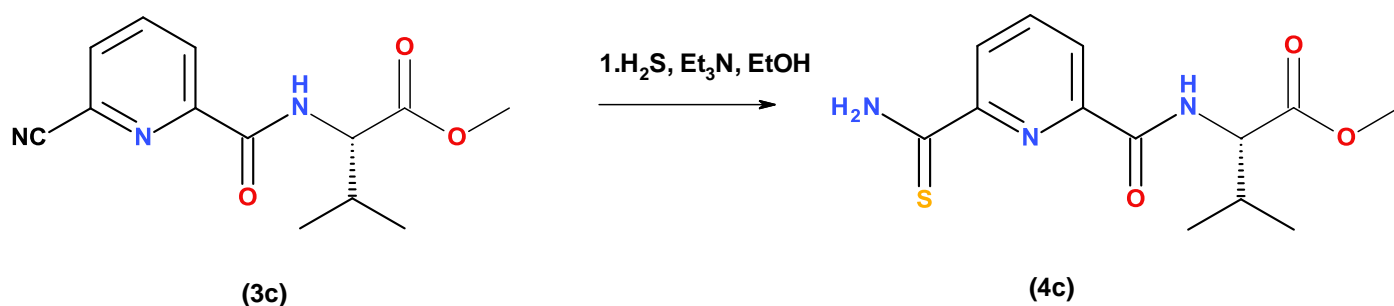


This compound was prepared in an identical manner to **4a**, except **3b** was used instead of **3a** giving **4b** as a yellow powder (92 % yield).

¹H NMR [400 MHz, CDCl₃]: δ_H = 9.08 (br s, 1H, -NH₂), 8.89 (dd, *J* = 7.9, 1.0, 1H, Py), 8.39 (dd, *J* = 7.9, 1.0, 1H, Py), 8.12 (br s, 1H, -CONH), 8.04 (t, *J* = 7.9, 1H, Py), 7.71 (brs, 1H, -NH₂), 4.31 (d, *J* = 5.4 Hz, 2H, -NHCH₂CO₂), 3.84 (s, 3H, -CO₂CH₃).

ESI-MS *m/z* 253 ([M+H]⁺), HR ESI-MS found 253.0510 C₁₀H₁₁N₃O₃S requires 253.0516 (error 2.37 ppm).

6.1.15 Synthesis of picolinamide-6-thioamide derivative **4c**

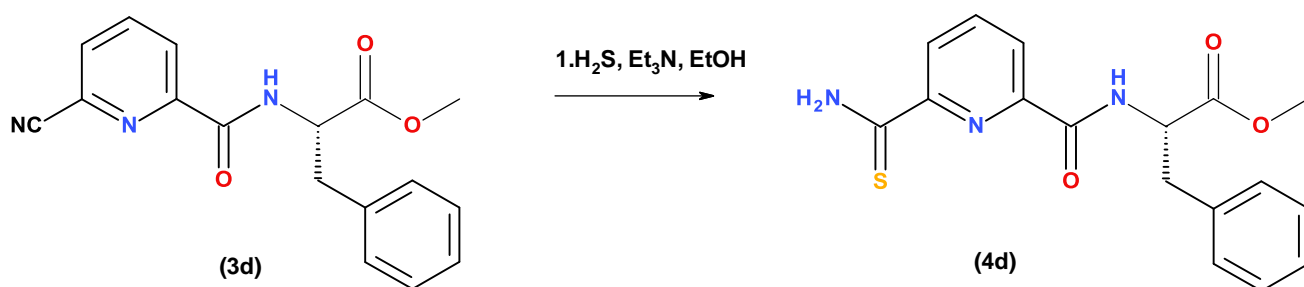


This compound was prepared in an identical manner to **4a**, except **3c** was used instead of **3a** giving **4c** as a yellow powder (60 % yield).

^1H NMR [400 MHz, CDCl_3]: δ_{H} = 9.06 (br s, 1H, $-\text{NH}_2$), 8.88 (dd, J = 7.9, 1.1, 1H, Py), 8.38 (dd, J = 7.8, 1.1, 1H, Py), 8.16 (br d, J = 8.8, 1H, $-\text{CONH}$), 8.04 (t, J = 7.8, 1H, Py), 7.76 (br s, 1H, $-\text{NH}_2$), 4.77 (dd, J = 8.8, 5.0, 1H, $-\text{NHCH}$), 3.81 (s, 3H, $-\text{CO}_2\text{CH}_3$), 2.34 (m, 1H, $-\text{CH}(\text{CH}_3)_2$), 1.03 (d, J = 7.0 Hz, 3H, $-\text{CH}(\text{CH}_3)_2$), 1.02 (d, J = 7.0 Hz, 3H, $-\text{CH}(\text{CH}_3)_2$).

ESI-MS m/z 318 ($[\text{M}+\text{Na}]^+$), HR ESI-MS found 318.0893 $\text{C}_{13}\text{H}_{17}\text{N}_3\text{NaO}_3\text{S}$ requires 318.0883 (error 3.21 ppm).

6.1.16 Synthesis of picolinamide-6-thioamide derivative **4d**

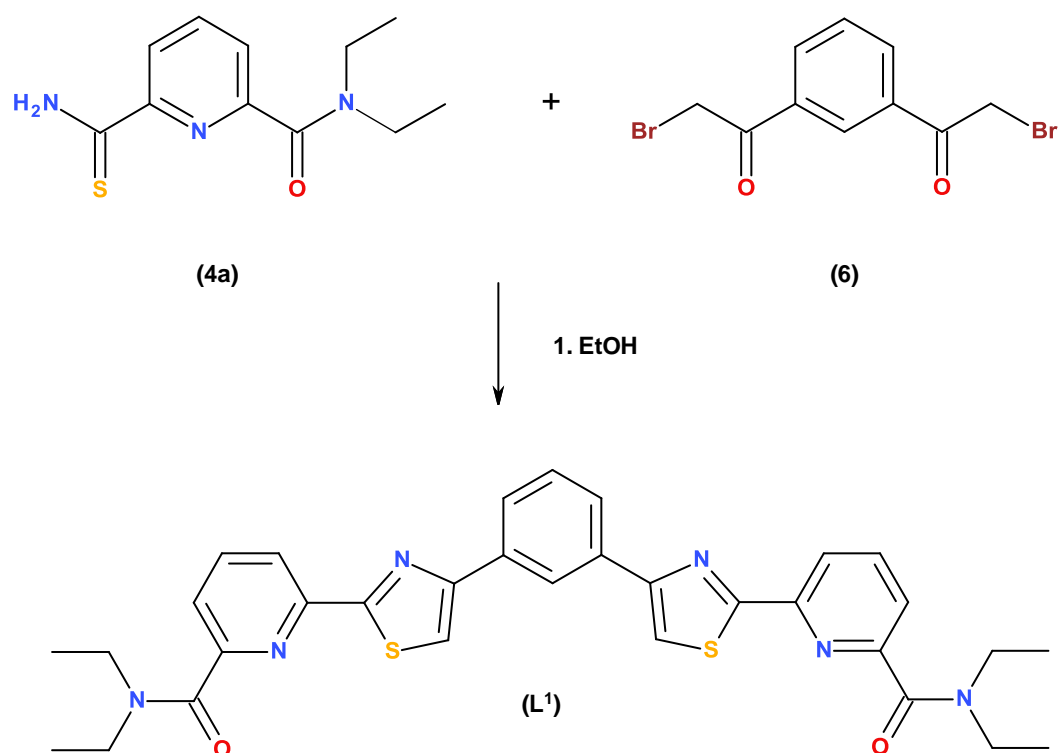


This compound was prepared in an identical manner to **4a**, except **3d** was used instead of **3a** giving **4d** as a yellow powder (87 % yield).

^1H NMR [400 MHz, CDCl_3]: δ_{H} = 8.86 (dd, J = 7.8, 1.1, 1H, Py), 8.75 (br s, 1H, $-\text{NH}_2$), 8.36 (dd, J = 7.8, 1.1, 1H, Py), 8.03 (t, J = 7.8, 1H, Py), 7.99 (br d, J = 8.2, 1H, $-\text{CONH}$), 7.53 (br s, 1H, $-\text{NH}_2$), 7.26-7.10 (m, overlap, 5H, Ph), 5.10 (dt, J = 8.1, 5.2, 1H, $-\text{CHCH}_2\text{Ph}$), 3.80 (s, 3H, $-\text{CO}_2\text{CH}_3$), 3.34 (dd, J = 13.8, 5.2, 1H, $-\text{CH}_2\text{Ph}$), 3.27 (dd, J = 13.8, 5.2 Hz, 1H, $-\text{CH}_2\text{Ph}$).

ESI-MS m/z 366 ($[\text{M}+\text{Na}]^+$), HR ESI-MS found 366.0870 $\text{C}_{17}\text{H}_{17}\text{N}_3\text{NaO}_3\text{S}$ requires 366.0883 (error 3.41 ppm).

6.1.17 Synthesis of L¹



To a solution of 1,3-di(α -dibromoacetyl)benzene (**6**) (0.05 g, 0.16 mmol) in ethanol (25 ml) was added the thioamide **4a** (0.08 g, 0.34 mmol) and the reaction refluxed for 3 h. On cooling a white precipitate formed, which was isolated by filtration, followed by washing with EtOH (2 x 2 ml) and Et₂O (2 x 2 ml) (0.064 g, 67 % yield).

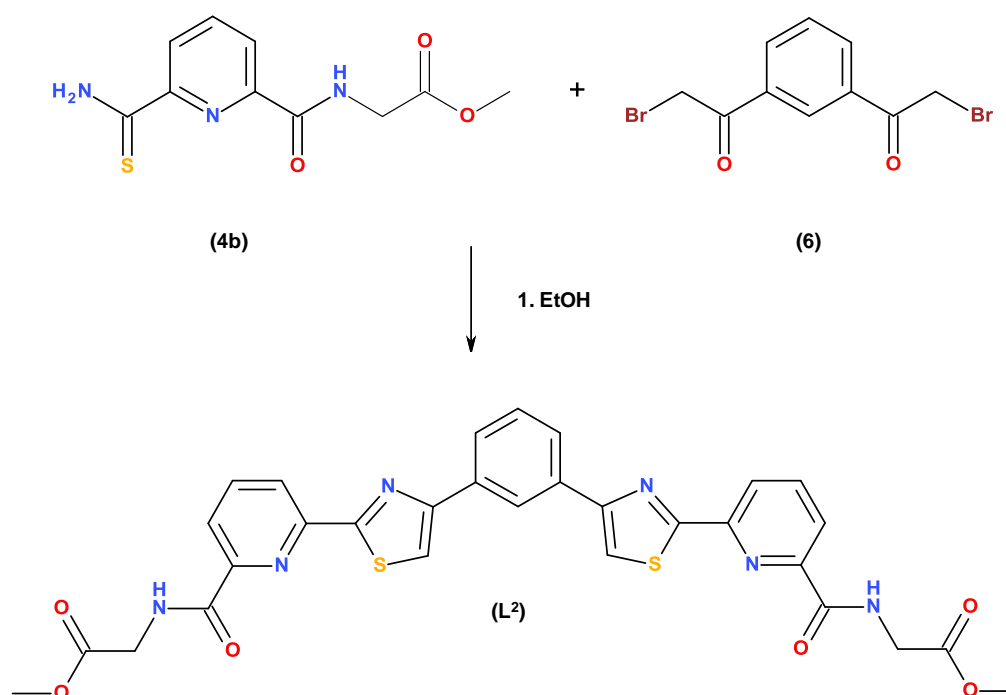
¹H NMR [400 MHz, CDCl₃]: δ_{H} = 8.60 (t, J = 1.6, 1H, Ph), 8.42 (dd, J = 7.8, 1.0, 2H, Py), 8.02 (dd, J = 7.7, 1.6, 2H, Ph), 7.95 (t, J = 7.8, 2H, Py), 7.75 (dd, J = 7.8, 1.0, 2H, Py), 7.74 (s, 2H, tz), 7.58 (t, J = 7.7, 1H, Ph), 3.63 (q, J = 7.1, 4H, -CH₂CH₃), 3.51 (q, J = 7.0, 4H, -CH₂CH₃), 1.38 (t, J = 7.0, 6H, -CH₂CH₃), 1.32 (t, J = 7.0 Hz, 6H, -CH₂CH₃).

¹³C NMR [100 MHz, CDCl₃]: δ_{C} = 168.5 (Q), 167.6 (Q), 156.5 (Q), 154.7 (Q), 149.7 (Q), 138.1 (CH), 134.9 (Q), 129.3 (CH), 126.3 (CH), 124.7 (CH), 124.3 (CH), 120.4 (CH), 116.1 (CH), 43.6 (CH₂), 40.6 (CH₂), 14.6 (CH₃), 12.8 (CH₃).

IR (solid, ν/cm^{-1}) 3086, 2976, 2932, 1620, 1569, 1489, 1476, 1465, 1444, 1426, 1377, 1320, 1116, 1081, 1028, 828, 776, 758.

ESI-MS m/z 619 ($[\text{M}+\text{Na}]^+$), HR ESI-MS found 619.1932 $\text{C}_{32}\text{H}_{32}\text{N}_6\text{NaO}_2\text{S}_2$ requires 619.1920 (error 1.88 ppm).

6.1.18 Synthesis of L^2



This compound was prepared in an identical manner to L^1 , except **4b** was used instead of **4a** giving L^2 as a cream powder (66 % yield).

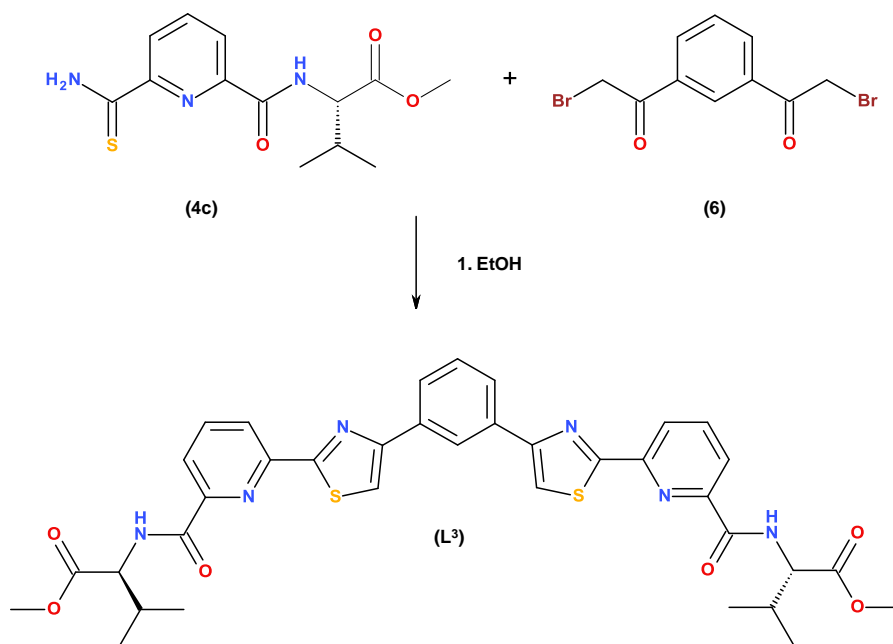
^1H NMR (400 MHz, CDCl_3): δ_{H} = 8.62 (t, J = 1.6, 1H, Ph), 8.55 (dd, J = 7.7, 1.0, 2H, Py), 8.51 (br t, J = 5.4, 2H, -CONH), 8.26 (dd, J = 7.7, 1.0, 2H, Py), 8.05 (m, overlap, 4H, Py, Ph), 7.79 (s, 2H, tz), 7.59 (t, J = 7.8, 1H, Ph), 4.36 (d, J = 5.4 Hz, 4H, $-\text{CH}_2-$), 3.86 (s, 6H, $-\text{CO}_2\text{CH}_3$).

^{13}C NMR [100 MHz, CDCl_3]: δ_{C} = 170.2 (Q), 167.6 (Q), 163.8 (Q), 156.7 (Q), 150.2 (Q), 148.9 (Q), 138.7 (CH), 134.8 (Q), 129.4 (CH), 126.4 (CH), 124.3 (CH), 123.2 (CH), 122.6 (CH), 116.2 (CH), 52.6 (CH_3), 41.4 (CH_2).

IR (solid, ν/cm^{-1}) 3385, 3108, 2954, 1747, 1679, 1590, 1568, 1521, 1446, 1374, 1281, 1215, 1089, 1026, 998, 939, 833, 786, 773, 762, 754, 732, 664.

ESI-MS m/z 629 ($[\text{M}+\text{H}]^+$), HR ESI-MS found 629.1282 $\text{C}_{30}\text{H}_{25}\text{N}_6\text{O}_6\text{S}_2$ requires 629.1272 (error 1.74 ppm).

6.1.19 Synthesis of L^3



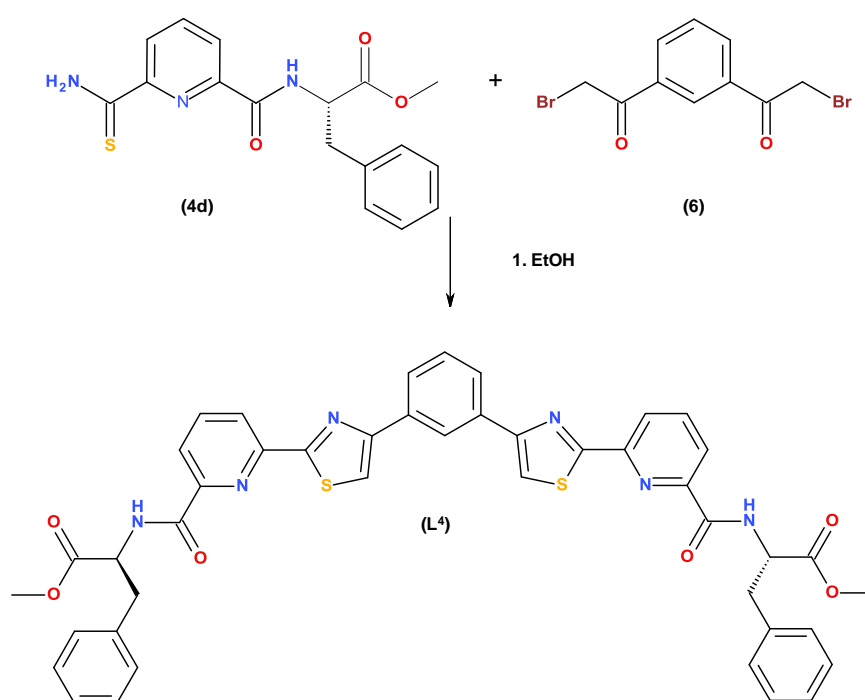
This compound was prepared in an identical manner to L^1 , except **4c** was used instead of **4a**. The reaction was monitored *via* TLC until the starting material was consumed. Purification *via* column chromatography (Al_2O_3 , 1% MeOH in DCM) gave L^3 as a yellow solid (42 % yield).

^1H NMR [400 MHz, CDCl_3]: δ_{H} = 8.63 (t, J = 1.0, 1H, Ph), 8.59 (br d, J = 8.9, 2H, -CONH), 8.54 (dd, J = 7.8, 1.0, 2H, Ph), 8.24 (dd, J = 7.6, 1.0, 2H, Py), 8.05 (t, J = 7.6, 2H, Py), 8.04 (dd, J = 7.6, 1.0, 2H, Py), 7.78 (s, 2H, tz), 7.60 (t,

$J = 7.8$, 1H, Ph), 4.78 (dd, $J = 8.9$, 4.7, 2H, -NHCH), 3.83 (s, 6H, -CO₂CH₃), 2.41 (m, 2H, -CH(CH₃)₂), 1.11 (d, $J = 1.6$, 6H, -CH(CH₃)₂), 1.09 (d, $J = 1.5$ Hz, 6H, -CH(CH₃)₂).

ESI-MS m/z 735 ([M+Na]⁺), HR ESI-MS found 735.2027 C₃₆H₃₆N₆NaO₆S₂ requires 735.2030 (error 0.39 ppm).

6.1.20 Synthesis of L⁴



This compound was prepared in an identical manner to L¹, except **4d** was used instead of **4a** giving L⁴ as a white powder (67 % yield).

¹H NMR [400 MHz, CDCl₃]: δ_H = 8.62 (t, $J = 1.6$, 1H, Ph), 8.53 (dd, $J = 7.8$, 1.0, 2H, Py), 8.47 (br d, $J = 8.0$, 2H, -CONH), 8.23 (dd, $J = 7.8$, 1.0, 2H, Py), 8.05 (t, $J = 7.8$, 2H, Py), 8.04 (dd, $J = 7.7$, 1.6, 2H, Ph), 7.78 (s, 2H, tz), 7.59 (t, $J = 7.7$, 1H, Ph), 7.38-7.29 (m, overlap, 10H, Ph), 5.09 (dt, $J = 8.0$, 5.9, 2H, -CHCH₂Ph), 3.80 (s, 6H, -CO₂CH₃), 3.32 (d, $J = 5.9$ Hz, 4H, -CH₂Ph).

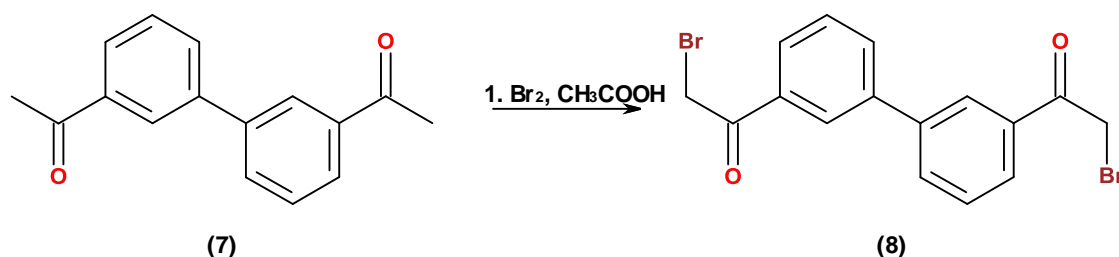
^{13}C NMR [100 MHz, CDCl_3]: δ_{C} = 171.8 (Q), 167.7 (Q), 163.3 (Q), 156.7 (Q), 150.1 (Q), 149.0 (Q), 138.7 (CH), 135.9 (Q), 134.9 (Q), 129.4 (CH), 129.4 (CH), 128.8 (CH), 127.3 (CH), 126.4 (CH), 124.3 (CH), 123.1 (CH), 122.5 (CH) 116.2 (CH), 53.4 (CH) 52.5 (CH_3), 38.2 (CH_2).

IR (solid, v/cm^{-1}) 3393, 3061, 2952, 1742, 1683, 1607, 1588, 1568, 1516, 1454, 1441, 1366, 1280, 1202, 1179, 1103, 1073, 1026, 997, 767, 744, 702.

ESI-MS m/z 831 ($[\text{M}+\text{Na}]^+$), HR ESI-MS found 831.2029 $\text{C}_{44}\text{H}_{36}\text{N}_6\text{NaO}_6\text{S}_2$ requires 831.2030 (error 0.10 ppm).

6.2 Preparation of phenyl-spacer ligands (L^6 - L^{14})

6.2.1 Synthesis of 3, 3'-Bis (2-bromoacetyl) biphenyl (**8**)

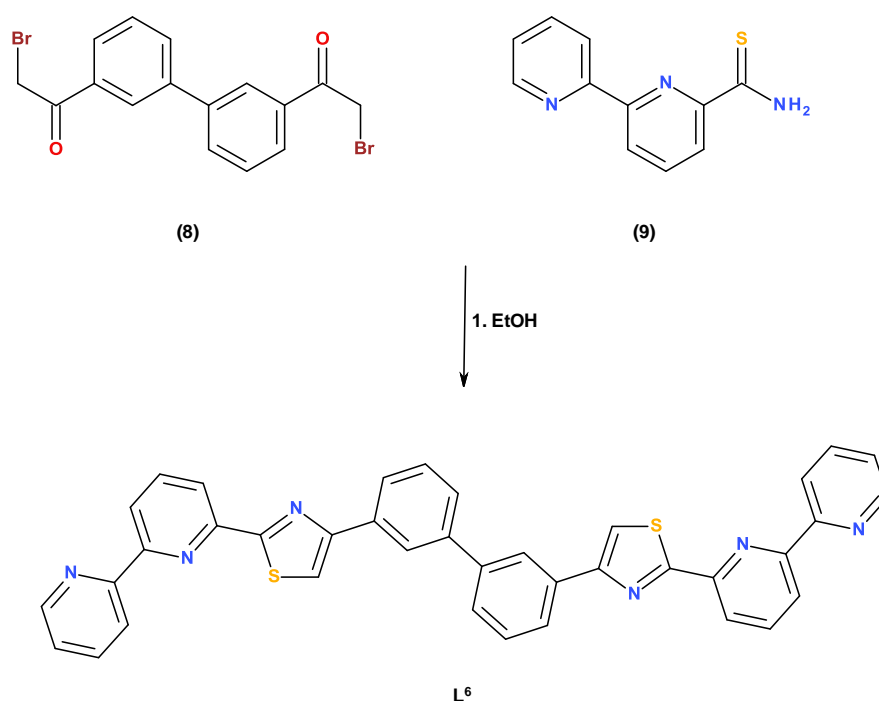


3,3'- Diacetylbiphenyl (**7**) (0.24 g, 1.0 mmol) was dissolved in acetic acid (25 ml) and set to stir at 80 °C under an atmosphere of dinitrogen. Bromine (0.32 g, 2.0 mmol) was diluted using acetic acid to give approximately 1 ml (approx. 0.9 ml acetic acid) to allow slow addition to the reaction over 1 h. The reaction was monitored *via* TLC (SiO_2 , 1% MeOH in DCM); once the starting material was consumed the reaction was allowed to cool then poured over deionised water (30 ml) and NaHCO_3 (0.1 g) was added to neutralise the reaction. The product was extracted into DCM (3 x 30 ml) and the combined organic layers dried (MgSO_4). Removal of solvent left a crude product as a yellow-orange oil. Purification *via* column chromatography (SiO_2 , DCM) gave **8** as an off-white solid (145 mg, 37 % yield).

^1H NMR [400 MHz, CDCl_3]: δ_{H} = 8.24 (br t, J = 1.7, 2H), 8.02 (dt, J = 7.8, 1.4, 2H), 7.88 (dq, J = 7.7, 1.8, 1.1, 2H), 7.63 (t, J = 7.7 Hz, 2H), 4.52 (s, 4H, $-\text{CH}_2-\text{Br}$).

ESI-MS m/z 416 ($[\text{M}+\text{Na}]^+$), HR ESI-MS found 416.9099 $\text{C}_{16}\text{H}_{12}\text{Br}_2\text{NaO}_2$ requires 416.9096 (error 0.89 ppm).

6.2.2 Synthesis of L^6



To a solution of 2,2'-bipyridine-6-thioamide (**9**) (0.072 g, 0.33 mmol) in ethanol (25 ml) was added the α -bromoacetyl (**8**) (0.06 g, 0.15 mmol) and the reaction refluxed for 8 h, during which time a precipitate was produced. This was isolated by filtration, whilst hot, followed by washing with EtOH and Et_2O (2 x 2 ml). The compound was isolated as the H.Br salt; to obtain the free ligand the product was suspended in concentrated ammonia (0.88 S.G., 10 ml) for 24 h. Filtration and washing with $\text{d.H}_2\text{O}$, EtOH and Et_2O (2 x 2 ml) gave the ligand, L^6 , as a cream powder (0.066 g, 70 % yield).

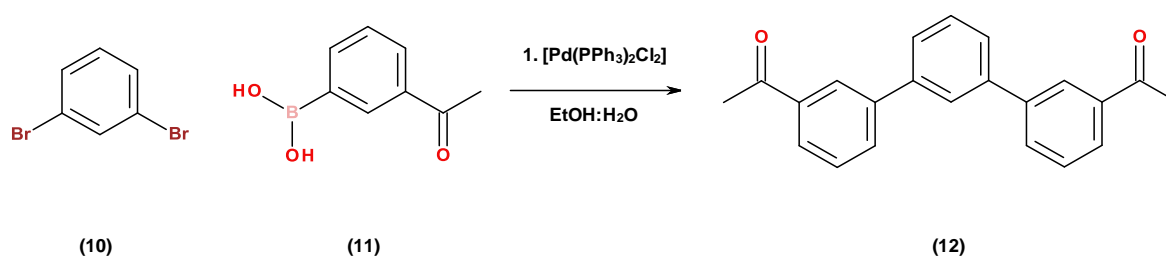
^1H NMR [400 MHz, DMSO- d_6]: δ_{H} = 8.77 (dt, J = 4.7, 0.7, 2H, Py^{term}), 8.57 (s, 2H, Tz), 8.52 (m, overlap, 4H, Py^{term}, Py), 8.47 (s, 2H, Ph), 8.49 (dd, J = 7.7, 0.8, 2H, Py), 8.18 (m, overlap, 4H, Py, Ph), 8.10 (dt, J = 7.7, 1.7, 2H, Py^{term}), 7.83 (d, J = 7.9, 2H, Ph), 7.67 (t, J = 7.7, 2H, Ph), 7.57 (ddd, J = 7.4, 4.8, 1.0 Hz, 2H, Py^{term}).

^{13}C NMR [100 MHz, CDCl₃]: δ_{C} = 169.3 (Q), 156.6 (Q), 155.7 (Q), 155.4 (Q), 150.7 (Q), 149.2 (CH), 141.8 (Q), 138.1 (CH), 137.0 (CH), 135.1 (Q), 129.3 (CH), 127.3 (CH), 125.5 (CH), 125.4 (CH), 124.1 (CH), 121.8 (CH), 121.3 (CH), 119.8 (CH), 115.7 (CH).

IR (solid, ν/cm^{-1}) 3060, 2360, 2337, 1601, 1581, 1562, 1475, 1454, 1431, 1080, 1013, 776, 738, 732, 717, 693, 637.

ESI-MS m/z 629 ($[\text{M}+\text{H}]^+$), HR ESI-MS found 629.1577 C₃₈H₂₅N₆S₂ requires 629.1577 (error 0.01ppm).

6.2.3 Synthesis of **12**



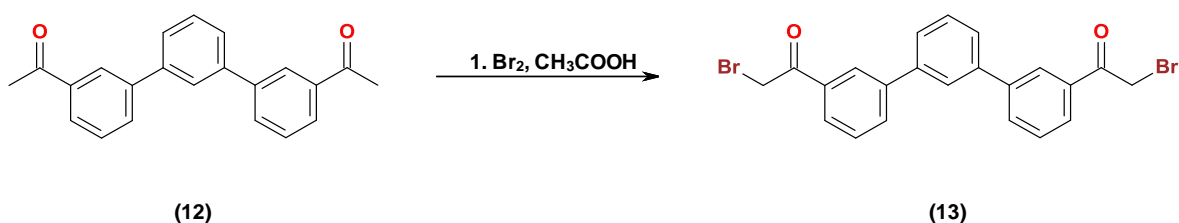
To a 50 ml round bottom flask 1,3-dibromobenzene (**10**) (0.17 g, 0.7 mmol), 3-acetyl phenylboronic acid (**11**) (0.3 g, 2.0 mmol), sodium carbonate (0.08 g, 0.76 mmol), nBu₄NBr (0.03 g, 0.09 mmol) and bis(triphenylphosphine) palladium chloride (0.01 g, 2 mol %) was suspended in deionised water (10 ml) and ethanol (10 ml). The reaction was left to stir at 70 °C for 20 h, and was monitored *via* TLC (SiO₂, 1% MeOH in DCM). The ethanol was removed by rotary evaporation to allow extraction into DCM (3 x 30ml); the combined organic layers were dried over MgSO₄. Filtration and evaporation provided a

crude product that was purified *via* column chromatography (SiO₂, 1% MeOH in DCM) producing the desired product, **12**, as a cream solid (0.12 g, 54 % yield).

¹H NMR [400 MHz, CDCl₃]: δ_H = 8.24 (t, *J*= 1.7, 2H, Ph), 7.98 (dt, *J*=7.8, 1.2, 2H, Ph), 7.87 (dq, *J*=7.7, 1.2, 2H, Ph), 7.84 (t, *J*= 1.7 1H, Ph^{cent}), 7.65 (dt, *J*= 7.6, 2H, Ph^{cent}), 7.59 (t, *J*=7.7, 2H, Ph), 7.58 (t, *J*=7.5 Hz, 1H, Ph^{cent}), 2.69 (s, 6H, -CH₃).

ESI-MS *m/z* 337 ([M+Na]⁺), HR ESI-MS found 337.1199 C₂₂H₁₈NaO₂ requires 337.1199 (error 0.07ppm).

6.2.4 Synthesis of **13**

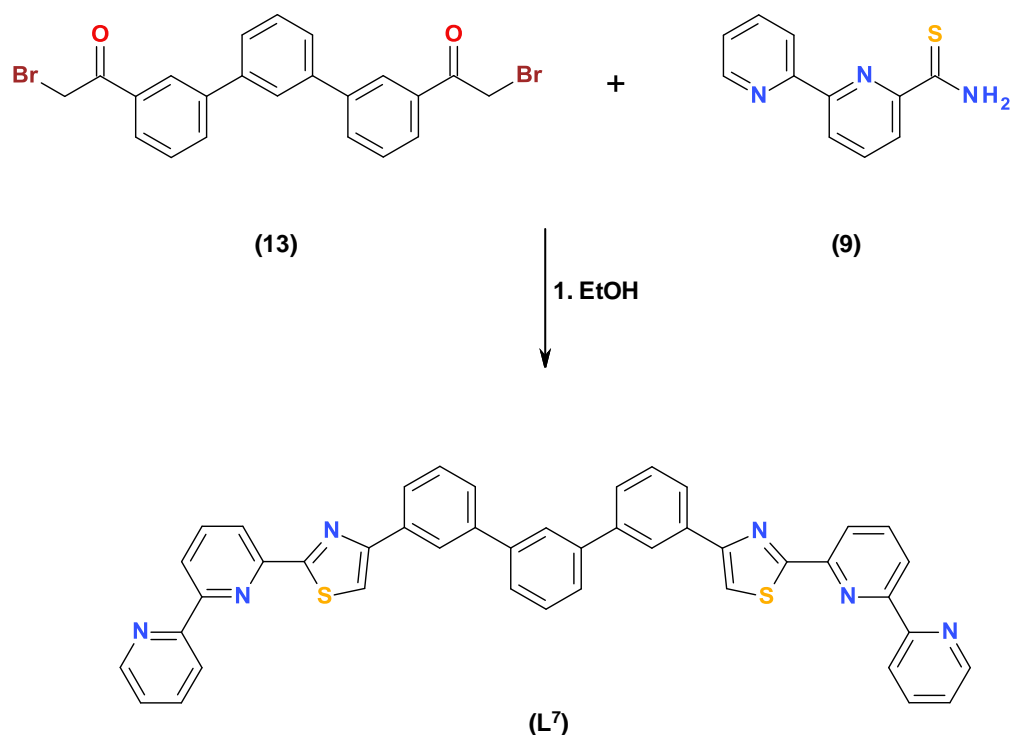


This compound was produced in a similar manner to 3,3'-bis(2-bromoacetyl)biphenyl (**8**), except **12** was used in place of 3,3'- diacetylbiphenyl (**7**). The reaction was monitored *via* TLC (SiO₂, 1% MeOH in DCM). Purification *via* column chromatography (SiO₂, DCM) gave the desired product, **13**, as an orange solid (63 % yield).

¹H NMR [400 MHz, CDCl₃]: δ_H = 8.27 (t, *J*= 1.7, 2H, Ph), 8.01 (dq, *J*= 7.8, 1.6, 1.2, 2H, Ph), 7.91 (dq, *J*= 7.8, 1.8, 1.1, 2H, Ph), 7.83 (t, *J*= 1.1, 1H, Ph^{cent}), 7.66 (dt, *J*= 7.8, 1.2 Hz, 2H, Ph^{cent}), 7.63-7.59 (m, overlap, 3H, Ph, Ph^{cent}), 4.53 (s, 4H, -CH₂-Br).

ESI-MS *m/z* 493 ([M+Na]⁺), HR ESI-MS found 492.9419 C₂₂H₁₆Br₂NaO₂ requires 492.9409 (error 1.97 ppm).

6.2.5 Synthesis of L⁷



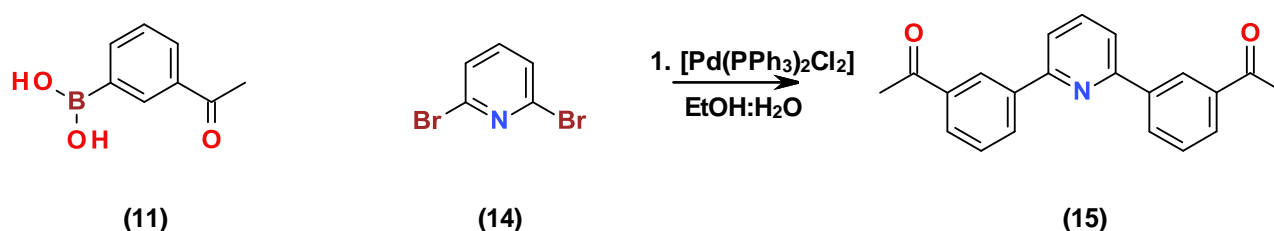
To a solution of 2,2'-bipyridine-6-thioamide (**9**) (0.075 g, 0.35 mmol) in ethanol (25 ml) was added the α -bromoacetyl (**13**) (0.075 g, 0.16 mmol) and the reaction refluxed for 8 h, during which time a precipitate was produced. This was isolated by filtration, whilst hot, followed by washing with EtOH and Et₂O (2 x 2 ml). The compound was isolated as the H.Br salt; to obtain the free ligand the product was suspended in concentrated ammonia (0.88 S.G., 10 ml) for 24 h. Filtration and washing with d.H₂O, EtOH and Et₂O (2 x 2 ml) gave the desired ligand, L⁷, as a light brown powder (0.08 g, 71 % yield).

¹H NMR [400 MHz, CDCl₃]: δ_{H} = 8.71 (dq, J = 4.8, 1.7, 0.9, 2H, Py^{term}), 8.61 (d, J = 8.0, 2H, Py^{term}), 8.49 (dd, J = 7.8, 0.9, 2H, Py), 8.37 (dd, J = 7.8, 0.9, 2H, Py), 8.35 (t, J = 1.6, 2H, Ph), 8.05 (dt, J = 7.8, 1.4, 2H, Ph), 8.01 (t, J = 1.6, 1H, Ph^{cent}), 7.96 (t, J = 7.8, 2H, Py), 7.90 (dt, J = 7.7, 1.8, 2H, Py^{term}), 7.74 (s, 2H, Tz), 7.73 (dd, J = 7.3, 1.7, 2H, Ph^{cent}), 7.70 (dt, J = 8.0, 1.2, 2H, Ph), 7.64-7.58 (m, overlap, 3H, Ph^{cent}, Ph), 7.37 (ddd, J = 7.5, 4.8, 1.2 Hz, 2H, Py^{term}).

^{13}C NMR [125 MHz, CDCl_3]: δ_{C} = 169.3 (quaternary, Q), 156.6 (Q), 155.6 (Q), 155.3 (Q), 150.7 (Q), 149.0 (CH), 141.9 (Q), 141.8 (Q), 138.0 (CH), 137.1 (CH), 135.2 (Q), 129.2 (CH), 127.2 (CH), 126.5 (CH), 126.4 (CH), 125.4 (CH), 124.0 (CH), 121.8 (CH), 121.3 (CH), 119.8 (CH), 115.6 (CH).

ESI-MS m/z 705 ($[\text{M}+\text{H}]^+$), HR ESI-MS found 705.1894 $\text{C}_{44}\text{H}_{29}\text{N}_6\text{S}_2$ requires 705.1890 (error 0.55 ppm).

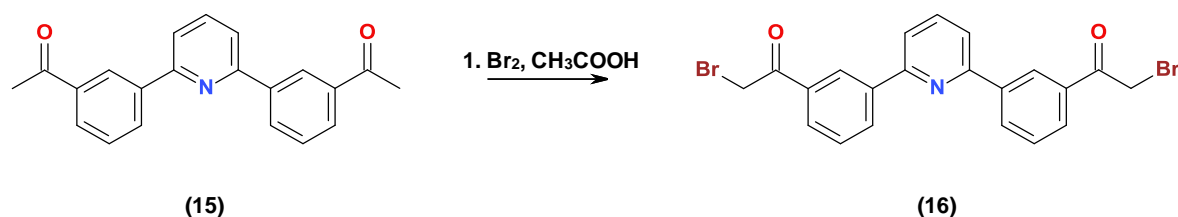
6.2.6 Synthesis of **15**



This compound was produced in an analogous fashion to compound **12**, except 2,6-dibromopyridine (**14**) was used in place of 1,3-dibromobenzene (**10**). The reaction was monitored *via* TLC (SiO_2 , 1 % MeOH in DCM). Purification *via* column chromatography (SiO_2 , 1 % MeOH in DCM) gave **15** as a yellow oil (95 % yield).

^1H NMR [400 MHz, CDCl_3]: δ_{H} = 8.74 (t, J = 1.7, 2H, Ph), 8.41 (dq, J = 7.8, 1.6, 1.3, 2H, Ph), 8.05 (dt, J = 7.7, 1.3, 2H, Ph), 7.92 (t, J = 7.8, 1H, Py), 7.82 (d, J = 7.8, 2H, Py), 7.64 (t, J = 7.7 Hz, 2H, Ph), 2.73 (s, 6H, $-\text{CH}_3$).

6.2.7 Synthesis of **16**

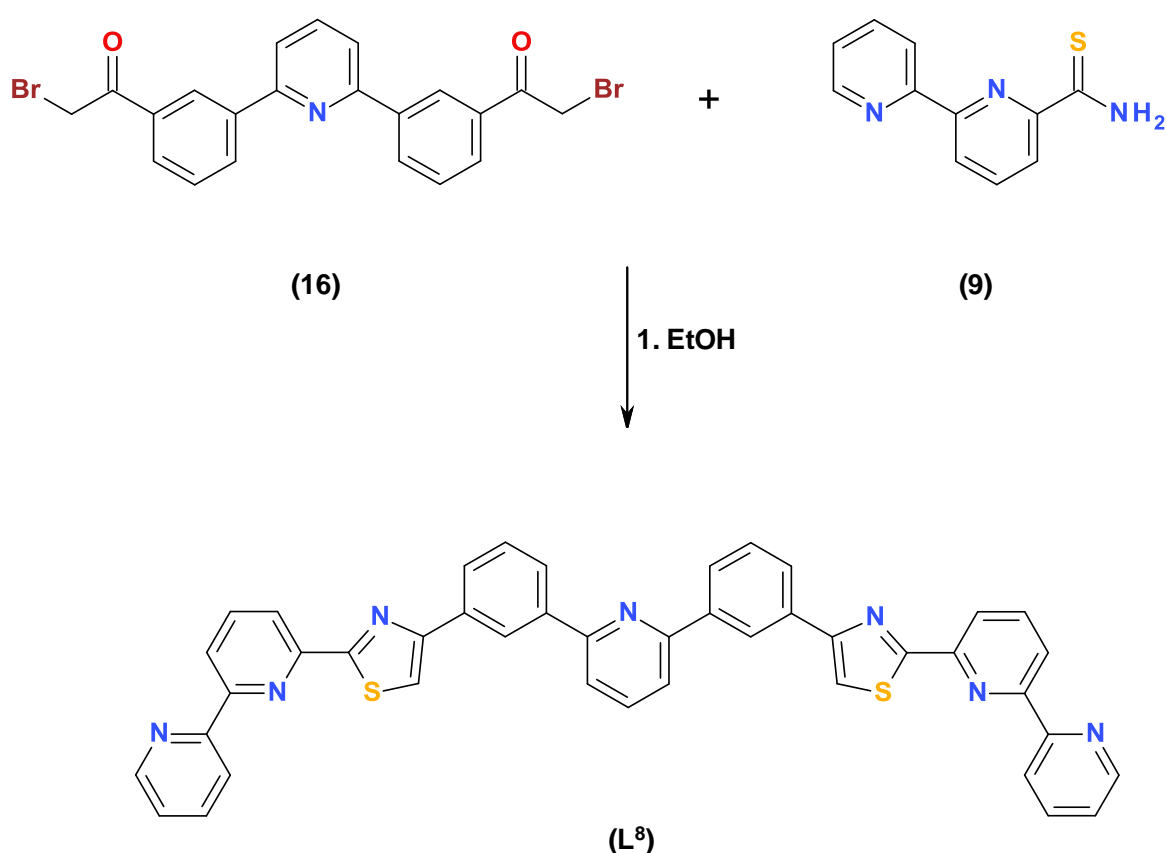


This compound was produced in an identical manner to 3,3'-bis(2-bromoacetyl)biphenyl (**8**), except **15** was used in place of 3,3'-diacetylbiphenyl

(7). The reaction was monitored *via* TLC (SiO₂, DCM). Purification *via* column chromatography (SiO₂, DCM) gave **16** as an off-white solid (62 % yield).

¹H NMR [400 MHz, CDCl₃]: δ_H = 8.77 (d, *J* = 1.6, 2H, Ph), 8.44 (dd, *J* = 7.7, 0.9, 2H, Ph), 8.07 (dd, *J* = 7.7, 1.1, 2H, Ph), 7.93 (t, *J* = 7.8, 1H, Py), 7.82 (d, *J* = 7.7, 2H, Py), 7.66 (dt, *J* = 7.8, 1.5 Hz, 2H, Ph), 4.56 (s, 4H, -CH₂-Br).

6.2.8 Synthesis of L⁸



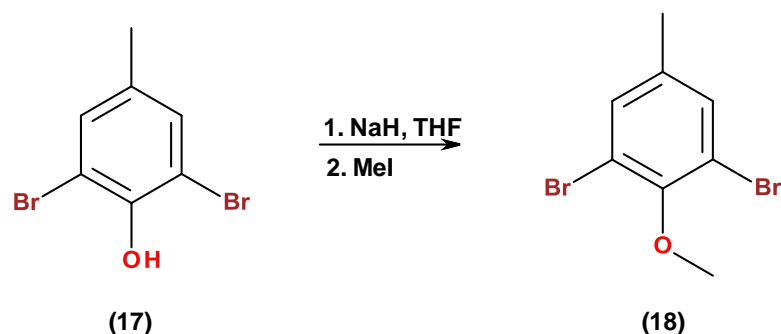
To a solution of 2,2'-bipyridine-6-thioamide (**9**) (0.06 g, 0.28 mmol) in ethanol (25 ml) was added the α -bromoacetyl (**16**) (0.057 g, 0.12 mmol) and the reaction refluxed for 8 h, during which time a precipitate was produced. This was isolated by filtration, whilst hot, followed by washing with EtOH and Et₂O (2 x 2 ml). The compound was isolated as the H.Br salt; to obtain the free ligand the product was suspended in concentrated ammonia (0.88 S.G., 10 ml) for 24 h. Filtration and washing with d.H₂O, EtOH and Et₂O (2 x 2 ml) gave the desired ligand, L⁸, as a white powder (0.052 g, 61 % yield).

^1H NMR [400 MHz, DMSO- d_6]: δ_{H} = 9.09 (s, 2H, Ph), 8.69 (dq, J = 4.8, 0.8, 2H, Py^{term}), 8.53 (s, 2H, Tz), 8.42 (dd, J = 7.8, 0.8, 2H, Py), 8.39 (d, J = 7.9, 2H, Py^{term}), 8.31 (d, J = 8.1, 2H, Ph), 8.25 (dd, J = 7.7, 0.8, 2H, Py), 8.21 (d, J = 8.0, 2H, Ph), 8.16 (d, J = 6.6, 1H, Py^{cent}), 8.11 (t, J = 6.2, 2H, Py^{cent}), 8.00 (t, J = 7.8, 2H, Py), 7.97 (dt, J = 7.7, 0.7, 2H, Py^{term}), 7.71 (t, J = 7.7, 2H, Ph), 7.47 (ddd, J = 7.6, 4.8, 1.1 Hz, 2H, Py^{term}).

The poor solubility of the ligand precluded ^{13}C NMR analysis

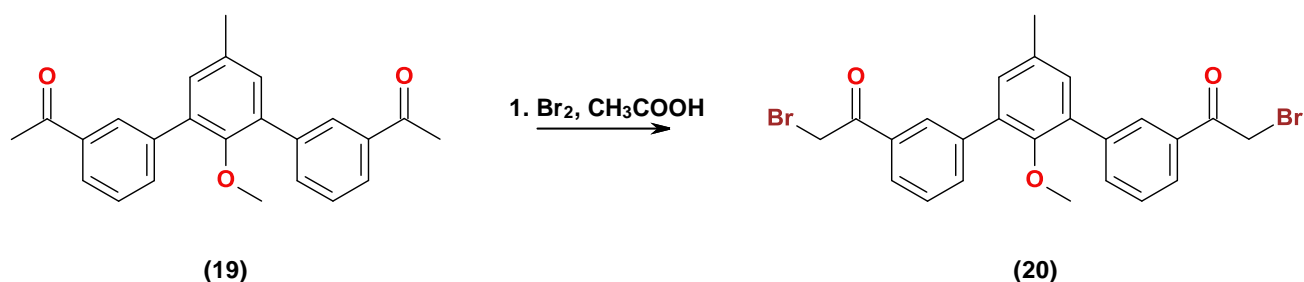
ESI-MS m/z 706 ($[\text{M}+\text{H}]^+$), HR ESI-MS found 706.1844 $\text{C}_{43}\text{H}_{27}\text{N}_7\text{S}_2$ requires 706.1842 (error 0.30 ppm).

6.2.9 Synthesis of 1,3-dibromo-2-methoxy-5-methylbenzene (**18**)¹⁷¹



A two necked round bottom flask charged with 2,6-dibromomethyl phenol (1.0 g, 3.8 mmol) and sodium hydride (60%, 0.3 g, 7.5 mmol), was placed under an atmosphere of dinitrogen, and anhydrous THF (20 ml) was added. To this methyl iodide (1ml) was added with care and the reaction was monitored *via* TLC (SiO_2 , 3:7 ethyl acetate: petroleum ether 40-60). Once all the starting material was consumed (48 h) methanol was added to the reaction (to react with any unreacted sodium hydride). The reaction was concentrated and $\text{d.H}_2\text{O}$ (40 ml) added, extracted into DCM (3 x 30 ml), the combined organic layers dried (MgSO_4) and solvent removed by rotary evaporation. Separation and purification *via* column chromatography (SiO_2 , 1:9 ethyl acetate: petroleum ether 40-60) gave **18** as a fine pink solid (0.76 g, 71 % yield).

6.2.11 Synthesis of **20**

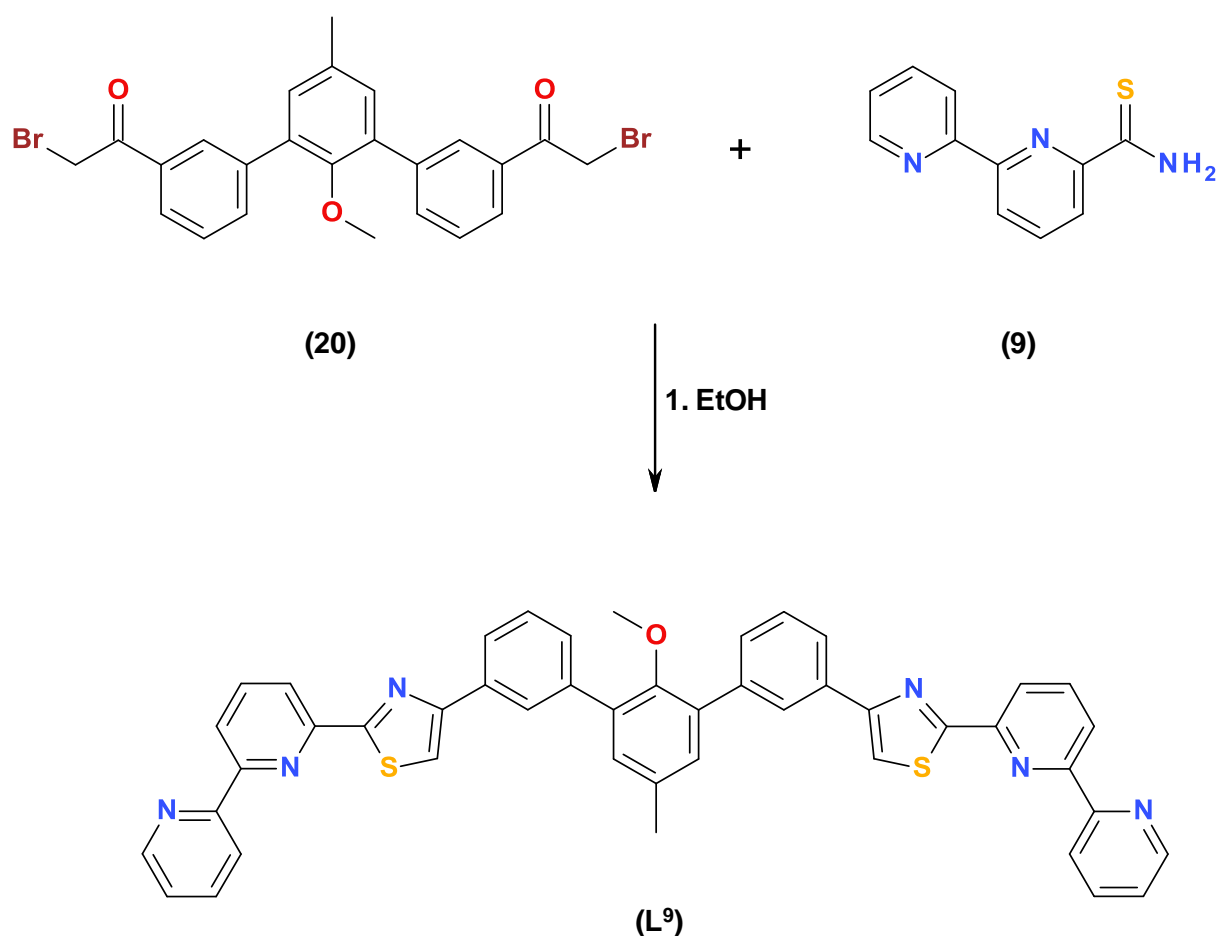


This compound was produced in an identical manner to compound **8**, except **19** was used in place of 3,3'-diacetylbiphenyl (**7**). The reaction was monitored *via* TLC (SiO₂, 0.5 % MeOH in DCM). Purification *via* column chromatography (SiO₂, 0.5 % MeOH in DCM) gave compound **20** as a white powder (44 % yield).

¹H NMR [500 MHz, CDCl₃]: δ_H = 8.23 (t, *J* = 1.6, 2H, Ph), 8.00 (dt, *J* = 7.8, 1.3, 2H, Ph), 7.89 (dt, *J* = 7.8, 1.3, 2H, Ph), 7.58 (t, *J* = 7.8 Hz, 2H, Ph), 7.22 (s, 2H, Ph^{cent}), 4.53 (s, 4H, -CH₂-Br), 3.13 (s, 3H, -O-CH₃), 2.44 (s, 3H, -ArCH₃).

ESI-MS *m/z* 536 ([M+Na]⁺), HR ESI-MS found 536.9671 C₂₄H₂₀Br₂ NaO₃ requires 536.9671 (error 0.10 ppm).

6.2.12 Synthesis of **L**⁹



To a solution of 2,2'-bipyridine-6-thioamide (**9**) (0.069 g, 0.32 mmol) in ethanol (25 ml) was added the α -bromoacetyl (**20**) (0.075 g, 0.15 mmol) and the reaction refluxed for 8 h, during which time a precipitate was produced. This was isolated by filtration, whilst hot, followed by washing with EtOH and Et₂O (2 x 2 ml). NaHCO_{3(aq)} (30 ml) was added to the resulting yellow powder, and the product was extracted into DCM (3 x 30 ml). The combined organic layers were dried (MgSO₄) and concentrated followed by purification *via* column chromatography (Al₂O₃, DCM). This gave the desired ligand, **L**⁹, as a light yellow powder (0.069 g, 65 % yield).

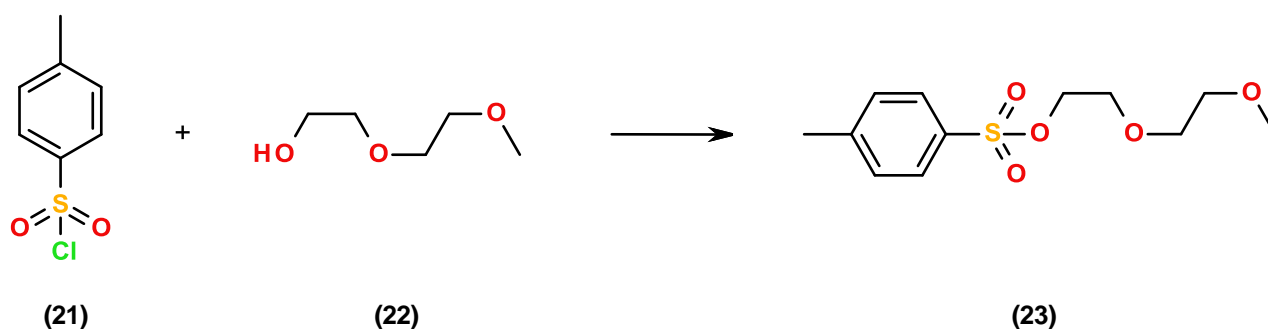
¹H NMR [500 MHz, DMSO-d₆]: δ_{H} = 8.75 (dq, J = 4.7, 0.9, 2H, Py^{term}), 8.50 (dt, J = 7.9, 1.0, 2H, Py^{term}), 8.49 (dd, J = 7.8, 0.9, 2H, Py), 8.43 (s, 2H, Tz), 8.33 (dd, J = 7.8, 0.9, 2H, Py), 8.28 (br s, 2H, Ph), 8.15 (t, J = 7.8, 2H, Py), 8.12 (dt, J =

6.7, 2, 2H, Ph), 8.06 (dt, $J = 7.7, 1.8$, 2H, Py^{term}), 7.61-7.60 (m, overlap, 4H, Ph), 7.53 (dq, $J = 7.5, 4.8, 1.2$ Hz, 2H, Py^{term}), 7.32 (s, 2H, Ph^{cent}), 3.21 (s, 3H, -OCH₃), 2.44 (s, 3H, -ArCH₃).

¹³C NMR [125 MHz, CDCl₃/CD₃OD]: $\delta_C = 169.1$ (quaternary, Q), 156.8 (Q), 155.2 (2 x Q), 152.9 (Q), 150.9 (Q), 148.7 (CH), 139.4 (Q), 138.1 (CH), 137.5 (CH), 135.3 (Q), 134.5 (Q), 133.7 (Q), 131.1 (CH), 129.3 (CH), 128.6 (CH), 127.3 (CH), 125.2 (CH), 124.1 (CH), 121.9 (CH), 121.6 (CH), 119.9 (CH), 115.5 (CH), 60.8 (OCH₃), 20.8 (CH₃).

ESI-MS m/z 749 ([M+H]⁺), HR ESI-MS found 749.2145 C₄₆H₃₃N₆OS₂ requires 749.2152 (error 0.89 ppm).

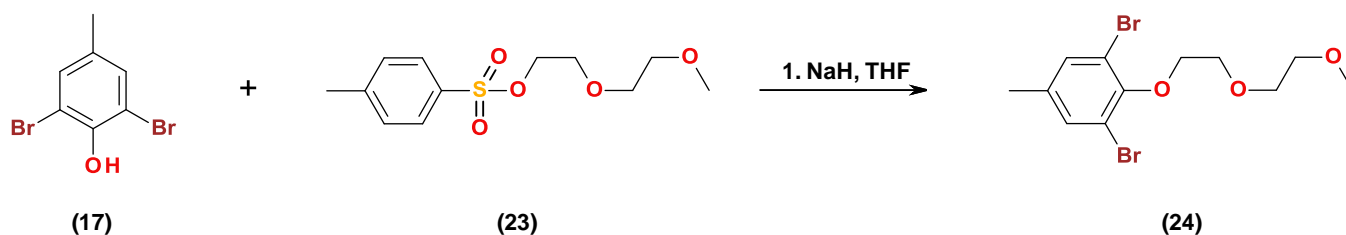
6.2.13 Synthesis of **23**¹⁷²



In a 250 ml round bottom flask charged with 2-(2-methoxyethoxy)ethanol (5 g, 0.04 mol) (**22**) pyridine was added (15 ml) and the mixture set to stir in an ice bath and left to cool (approx. 20 minutes). Once cool *p*-toluenesulfonyl chloride (**21**) (8 g, 0.04 mol) was added slowly over 2 h. After the complete addition of the *p*-toluenesulfonyl chloride the reaction was left to stir at RT for 24 h. Deionised water (100 ml) was added to the reaction flask producing an oil, this was left to stand at RT for 24 h. The water was decanted off; ether (100 ml) was added to the remaining oil. This was then washed with d.H₂O, HCl (2 M) and NaCl_(aq) (100 ml). The solvent was dried (MgSO₄) and the solvent removed, giving the desired product, **23**, as a viscous colourless oil.

^1H NMR [400 MHz, CDCl_3]: $\delta_{\text{H}} = 7.80$ (d, $J = 8.3$, 2H), 7.34 (d, $J = 8.1$, 2H), 4.17 (t, $J = 4.9$, 2H, $-\text{CH}_2$), 3.69 (t, $J = 4.9$ Hz, 2H, $-\text{CH}_2$), 3.58 (m, 2H, $-\text{CH}_2$), 3.48 (m, 2H, $-\text{CH}_2$), 3.35 (s, 3H, $-\text{CH}_3$), 2.45 (s, 3H, $-\text{ArCH}_3$).

6.2.14 Synthesis of **24**

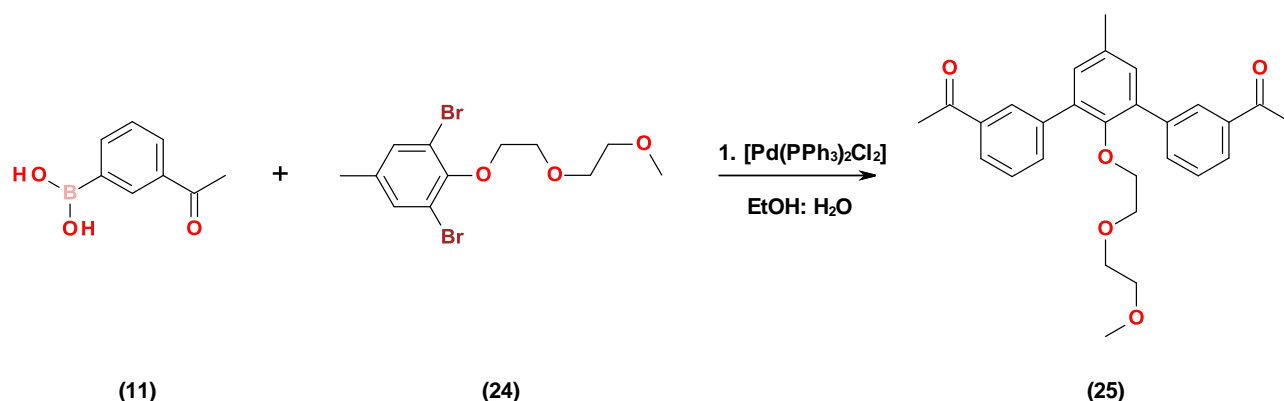


A two necked round bottom flask charged with 2,6-dibromo-4-methylphenol (**17**) (1.36 g, 5.1 mmol) and sodium hydride (0.12 g, 5.1 mmol) was placed under an atmosphere of dinitrogen, to this was added anhydrous THF (35 ml). This was left to stir at room temperature for 1h. After this time 2-(2-methoxyethoxy)ethyl 4-methylbenzenesulfonate (**23**) (0.71 g, 2.6 mmol) was added to the reaction and set to stir at 80°C. The reaction was monitored *via* TLC (SiO_2 , 2 % MeOH in DCM); once all the benzenesulfonate (**23**) was consumed methanol was added to the reaction whilst under $\text{N}_{2(\text{g})}$ (to react with any unreacted sodium hydride). The reaction was concentrated and $\text{NaHCO}_{3(\text{aq})}$ (50 ml) added to the reaction and the product extracted into ether (3 x 30 ml). The combined organic layers were dried (MgSO_4) and the solvent removed by rotary evaporation. Separation and purification *via* column chromatography (SiO_2 , 2 % MeOH in DCM) gave **24** as a green oil (0.52 g, 56 % yield).

^1H NMR [400 MHz, CDCl_3]: $\delta_{\text{H}} = 7.31$ (s, 2H, Ph), 4.18 (t, $J = 5.0$, 2H, $-\text{CH}_2$), 3.94 (t, $J = 5.2$, 2H, $-\text{CH}_2$), 3.78 (t, $J = 4.5$, 2H, $-\text{CH}_2$), 3.60 (t, $J = 4.5$ Hz, 2H, $-\text{CH}_2$), 3.41 (s, 3H, $-\text{CH}_3$), 2.28 (s, 3H, $-\text{ArCH}_3$).

ESI-MS m/z 388 ($[\text{M}+\text{Na}]^+$), HR ESI-MS found 388.9358 $\text{C}_{12}\text{H}_{16}\text{Br}_2\text{NaO}_3$ requires 388.9358 (error 1.09 ppm).

6.2.15 Synthesis of **25**

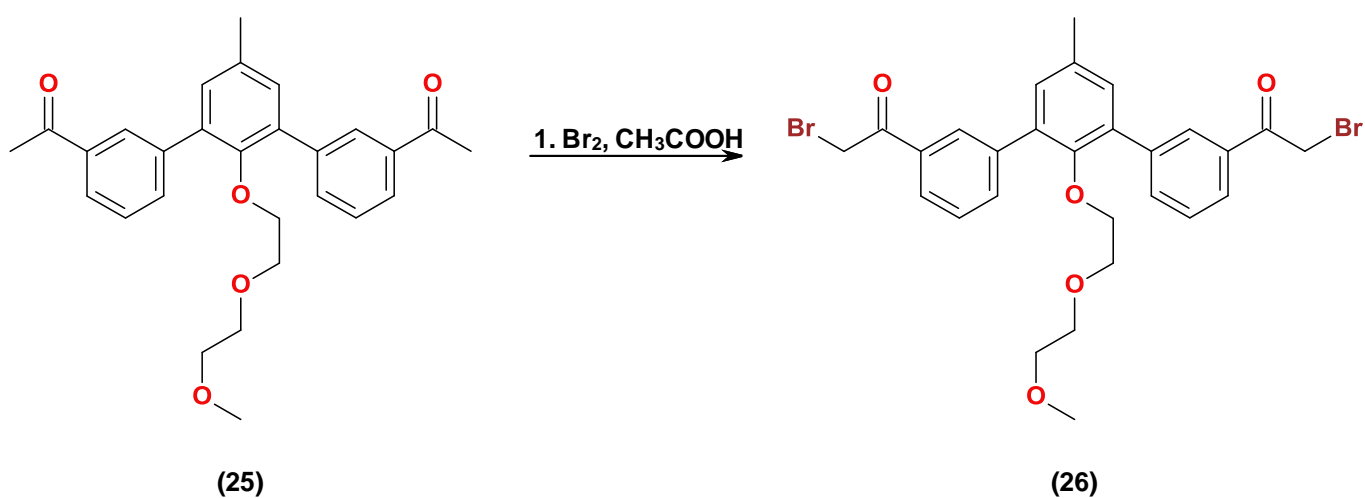


This compound was produced in an identical manner to compound **12**, except compound **24** was used in place of 1,3-dibromobenzene (**10**). The reaction was monitored *via* TLC (SiO₂, 1:1 ethyl acetate: petroleum ether 40-60). Purification *via* column chromatography (SiO₂, 1:1 ethyl acetate: petroleum ether 40-60) gave compound **25** as a yellow oil (89 % yield).

¹H NMR [400 MHz, CDCl₃]: δ_H = 8.21 (s, 2H, Ph), 7.95 (d, *J* = 7.7, 2H, Ph), 7.89 (d, *J* = 7.6, 2H, Ph), 7.53 (t, *J* = 7.7, 2H, Ph), 7.22 (s, 2H, Ph^{cent}), 3.35 (t, *J* = 5.0 Hz, 2H, -CH₂), 3.28-3.26 (m, overlap, 5H, -CH₂, -CH₃), 3.18-3.14 (m, overlap, 4H, 2 x -CH₂), 2.68 (s, 6H, -CH₃), 2.43 (s, 3H, -ArCH₃).

ESI-MS *m/z* 469 ([M+Na]⁺), HR ESI-MS found 469.2001 C₂₈H₃₀NaO₅ requires 469.1985 (error 3.32 ppm).

6.2.16 Synthesis of **26**

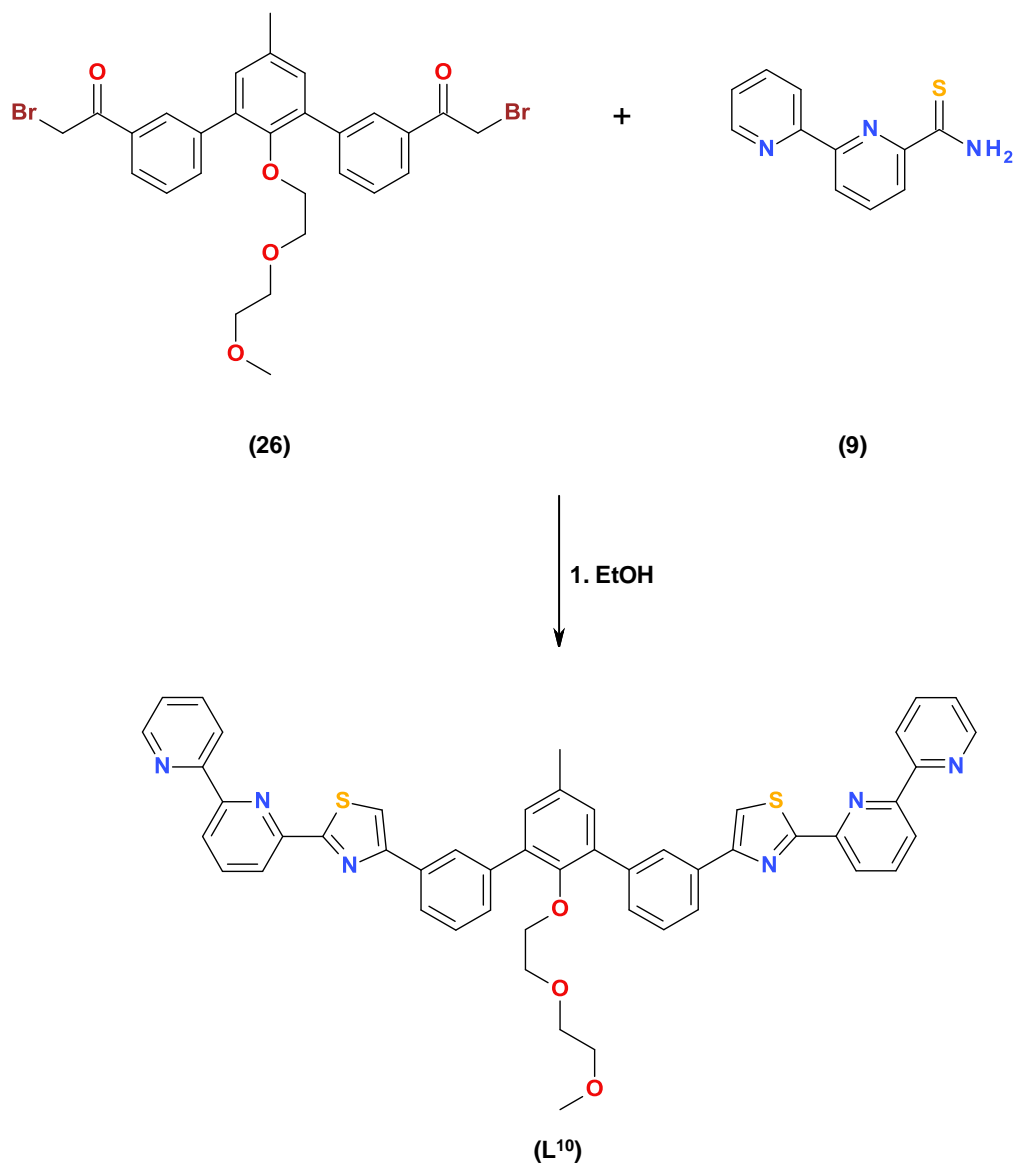


This compound was produced in an identical manner to compound **8**, except that compound **25** was used in place of 3,3'-diacetylbiphenyl (**7**). The reaction was monitored *via* TLC (SiO₂, 1:1 ethyl acetate: petroleum ether 40-60). Purification *via* column chromatography (SiO₂, 1:1 ethyl acetate: petroleum ether 40-60) gave compound **26** as a yellow oil (89 % yield).

¹H NMR [400 MHz, CDCl₃]: δ_H = 8.25 (s, 2H, Ph), 7.99 (d, *J* = 7.8, 2H, Ph), 7.92 (d, *J* = 7.7, 2H, Ph), 7.57 (t, *J* = 7.7, 2H, Ph), 7.22 (s, 2H, Ph^{cent}), 4.55 (s, 4H, -CH₂Br), 3.36 (t, *J* = 4.8 Hz, 2H, -CH₂), 3.29-3.26 (m, overlap, 5H, -CH₂, -CH₃), 3.19-3.15 (m, overlap, 4H, 2 x -CH₂), 2.43 (s, 3H, -ArCH₃).

ESI-MS *m/z* 625 ([M+Na]⁺), HR ESI-MS found 625.0206 C₂₈H₂₈Br₂NaO₅ requires 625.0196 (error 1.60 ppm).

6.2.17 Synthesis of ligand **L¹⁰**



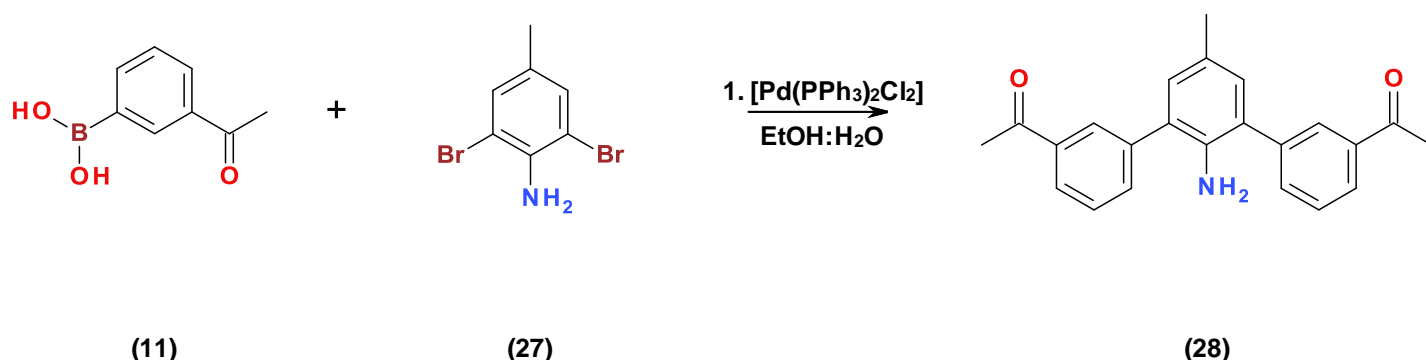
To a solution of 2,2'-bipyridine-6-thioamide (**9**) (0.098 g, 0.46 mmol) in ethanol (25 ml) was added the α -bromoacetyl (**26**) (0.125 g, 0.21 mmol) and the reaction refluxed for 8 h; the reaction was monitored *via* TLC (Al_2O_3 , 1 % MeOH in DCM). Upon completion the solvent was removed by rotary evaporation followed by purification *via* column chromatography (Al_2O_3 , 1 % MeOH in DCM) giving the final ligand, **L¹⁰**, as a fine white solid once completely dry (0.09 g, 51 % yield).

^1H NMR [400 MHz, CDCl_3]: δ_{H} = 8.72 (dt, J = 4.8, 0.8, 2H, Py^{term}), 8.61 (d, J = 8.0, 2H, Py^{term}), 8.50 (dd, J = 7.8, 0.9, 2H, Py), 8.37 (dd, J = 7.8, 0.9, 2H, Py), 8.28 (t, J = 1.5, 2H, Ph), 8.05 (dt, J = 7.7, 1.4, 2H, Ph), 7.97 (t, J = 7.8, 2H, Py), 7.90 (dt, J = 7.7, 1.7, 2H, Py^{term}), 7.73 (s, 2H, Tz), 7.69 (dt, J = 7.8, 1.3, 2H, Ph), 7.54 (t, J = 7.7, 2H, Ph), 7.36 (ddd, J = 7.8, 4.8, 1.1, 2H, Py^{term}), 7.31 (s, 2H, Ph^{cent}), 3.53 (t, J = 4.8, 2H, $-\text{CH}_2$), 3.28 (t, J = 4.8 Hz, 2H, $-\text{CH}_2$), 3.21-3.16 (m, overlap, 7H, 2 x $-\text{CH}_2$, $-\text{CH}_3$), 2.48 (s, 3H, $-\text{ArCH}_3$).

^{13}C NMR [125 MHz, $\text{CDCl}_3/\text{CD}_3\text{OD}$]: δ_{C} = 169.1 (quaternary, Q), 156.7 (Q), 155.5 (Q), 155.3 (Q), 151.9 (Q), 150.7 (Q), 149.1 (CH), 139.3 (Q), 138.1 (CH), 137.2 (CH), 135.5 (Q), 134.5 (Q), 133.8 (Q), 131.1 (CH), 129.6 (CH), 128.6 (CH), 127.4 (CH), 125.2 (CH), 124.1 (CH), 121.8 (CH), 121.4 (CH), 119.8 (CH), 115.6 (CH), 72.1 (OCH_2), 71.7 (OCH_2), 69.9 (OCH_2), 69.8 (OCH_2), 58.9 (OCH_3), 20.9 (ArCH_3).

ESI-MS m/z 837 ($[\text{M}+\text{H}]^+$), HR ESI-MS found 837.2661 $\text{C}_{50}\text{H}_{41}\text{N}_6\text{O}_3\text{S}_2$ requires 837.2676 (error 1.75 ppm).

6.2.18 Synthesis of **28**

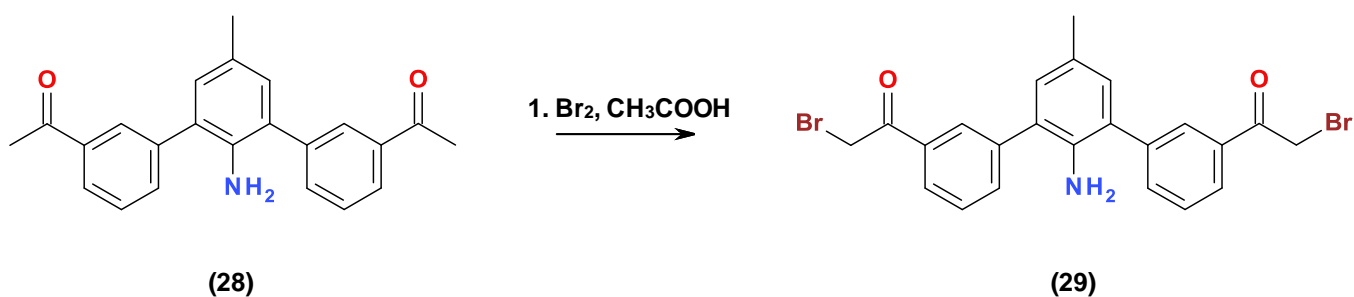


This compound was produced in an identical manner to compound **12**, except 2,6-dibromo-*p*-toluidine (**27**) was used in place of 1,3-dibromobenzene (**10**). The reaction was monitored *via* TLC (SiO_2 , 3:7 ethyl acetate : petroleum ether 40-60). Purification *via* column chromatography (SiO_2 , 1:2 ethyl acetate : petroleum ether 40-60) gave **28** as a yellow oil (49 % yield).

^1H NMR [400 MHz, CDCl_3]: δ_{H} = 8.10 (s, 2H, Ph), 7.97 (d, J = 7.8, 2H, Ph), 7.74 (d, J = 7.7, 2H, Ph), 7.57 (t, J = 7.7 Hz, 2H, Ph), 7.00 (s, 2H, Ph^{cent}), 3.64 (br s, 2H, $-\text{NH}_2$), 2.66 (s, 6H, $-\text{CH}_3$), 2.34 (s, 3H, $-\text{ArCH}_3$).

ESI-MS m/z 366 ($[\text{M}+\text{Na}]^+$), HR ESI-MS found 366.1465 $\text{C}_{23}\text{H}_{21}\text{NNaO}_2$ requires 366.1464 (error 0.24 ppm).

6.2.19 Synthesis of **29**

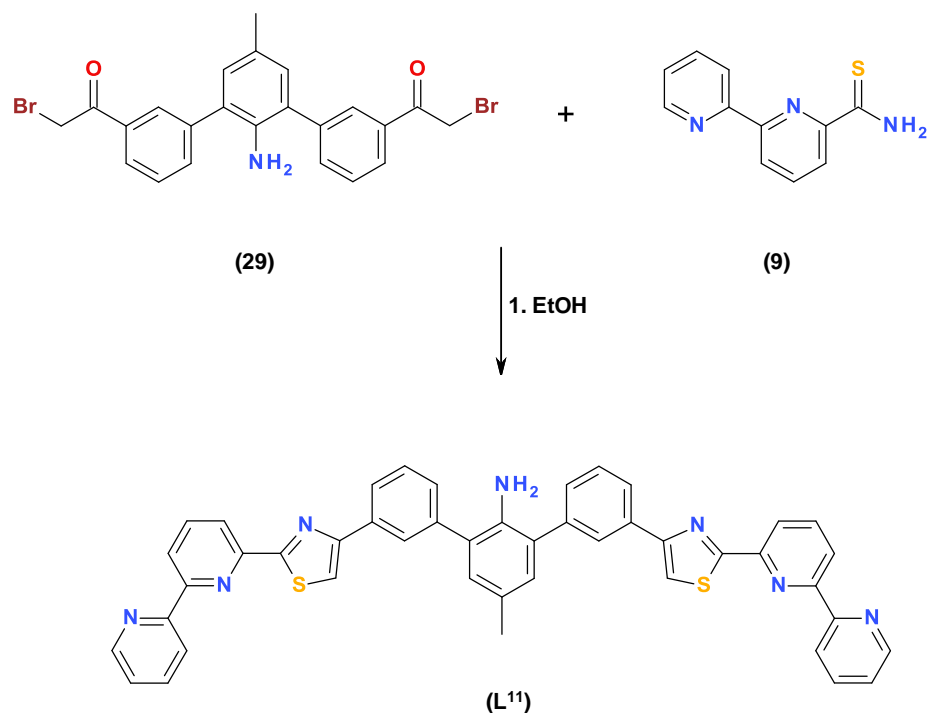


This compound was produced in an identical manner to compound **8**, except **28** was used in place of 3,3'-diacetylbiphenyl (**7**). The reaction was monitored *via* TLC (SiO_2 , 3:7 ethyl acetate: petroleum ether 40-60). Purification *via* column chromatography (SiO_2 , 3:7 ethyl acetate: petroleum ether 40-60) gave compound **29** as a dark yellow oil (38 % yield).

^1H NMR [400 MHz, CDCl_3]: δ_{H} = 8.22 (s, 2H, Ph), 8.00 (d, J =7.3, 2H, Ph), 7.79 (d, J =7.0, 2H, Ph), 7.61 (t, J =7.7 Hz, 2H, Ph), 7.01 (s, 2H, Ph^{cent}), 4.50 (s, 4H, $-\text{CH}_2\text{Br}$), 3.69 (br s, 2H, $-\text{NH}_2$), 2.34 (s, 3H, $-\text{ArCH}_3$).

ESI-MS m/z 499 ($[\text{M}+\text{H}]^+$), HR ESI-MS found 499.9854 $\text{C}_{23}\text{H}_{20}\text{Br}_2\text{NO}_2$ requires 499.9855 (error 0.33 ppm).

6.2.20 Synthesis of L¹¹

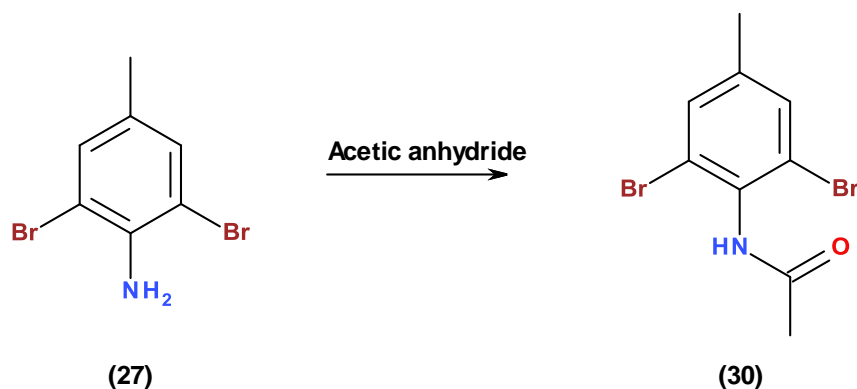


To a solution of 2,2'-bipyridine-6-thioamide (**9**) (0.052 g, 0.24 mmol) in ethanol (25 ml) was added the α -bromoacetyl (**29**) (0.06 g, 0.12 mmol) and the reaction refluxed for 8 h, during which time a precipitate was produced. This was isolated by filtration, whilst hot, followed by washing with EtOH and Et₂O (2 x 2 ml). The compound was isolated as the H.Br salt; to obtain the free ligand the product was suspended in concentrated ammonia (0.88 S.G., 10 ml) for 24 h. Filtration and washing with d.H₂O, EtOH and Et₂O (2 x 2 ml) gave the ligand, L¹¹, as an off-white powder (0.026 g, 30 % yield).

¹H NMR [400 MHz, CDCl₃]: δ_{H} = 8.72 (dd, J = 4.8, 0.8, 2H, Py^{term}), 8.61 (d, J = 8.6, 2H, Py^{term}), 8.50 (dd, J = 7.8, 0.9, 2H, Py), 8.35 (dd, J = 7.8, 0.9, 2H, Py), 8.19 (s, 2H, Ph), 8.04 (dt, J = 7.0, 1.8, 2H, Ph), 7.97 (t, J = 7.8, 2H, Py), 7.90 (dt, J = 7.8, 1.8, 2H, Py^{term}), 7.70 (s, 2H, Tz), 7.60-7.53 (m, overlap, 4H, Ph), 7.37 (ddd, J = 7.4, 4.8, 1.2 Hz, 2H, Py^{term}), 7.10 (s, 2H, Ph^{cent}), 3.84 (br s, 2H, -NH₂), 2.39 (s, 3H, -ArCH₃).

ESI-MS m/z 734 ($[M+H]^+$), HR ESI-MS found 734.2150 $C_{45}H_{31}N_7S_2$ requires 734.2155 (error 0.66 ppm).

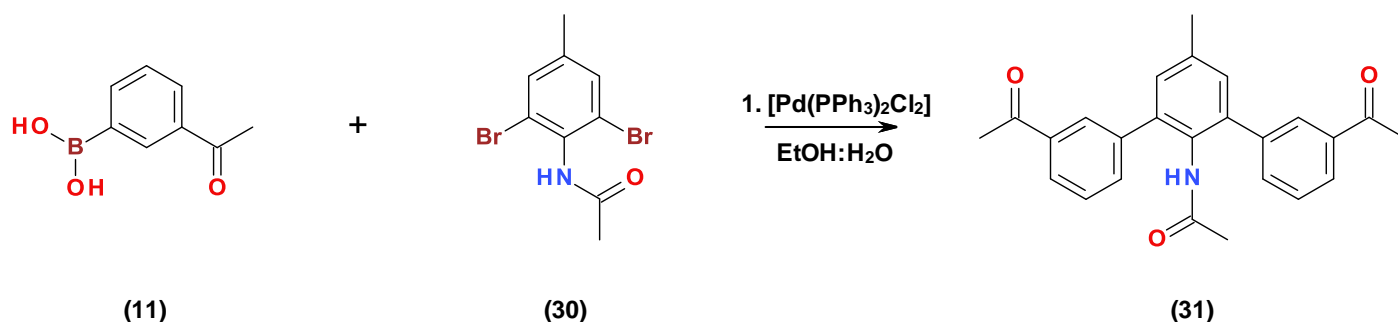
7.2.21 Synthesis of **30**¹⁷³



In a 50 ml round bottom flask 2,6-dibromo-*p*-toluidine (**27**) (1.0 g, 3.77 mmol) was dissolved in acetic anhydride (10 ml) and the reaction was set to stir at 60 °C for 1 h. After this time the reaction was left to stand at RT for 48 h. Over this time a crystalline solid was produced. The excess acetic anhydride was decanted off; the remaining solid was suspended in ether. This ether was decanted off, leaving the desired product **30** as a colourless crystalline solid (0.6 g, 70% yield).

^1H NMR [400 MHz, DMSO- d_6]: δ_{H} = 7.41 (s, 2H, Ph), 6.92 (br s, 1H, -NH), 2.32 (s, 3H, -ArCH₃) 2.23 (s, 3H, -CH₃).

6.2.22 Synthesis of **31**

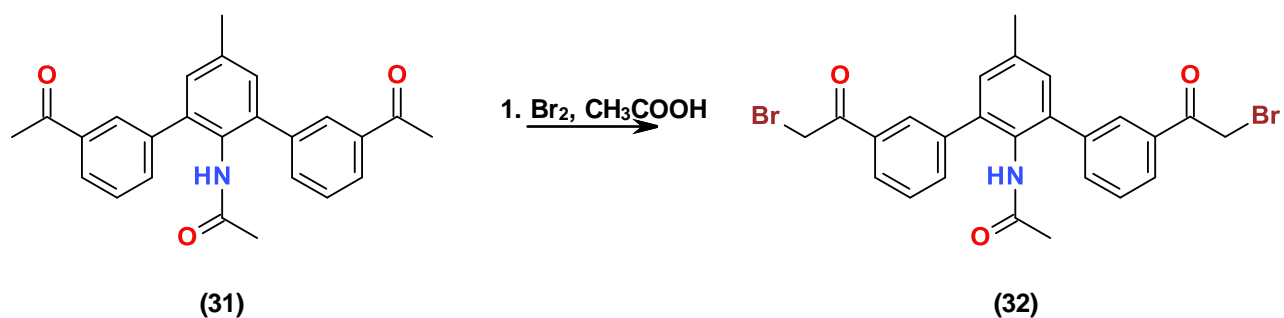


This compound was produced in an identical manner to compound **12**, except N-(2,6-dibromo-4-methylphenyl)acetamide (**30**) was used in place of 1,3-dibromobenzene (**10**). The reaction was monitored *via* TLC (SiO_2 , 2:3 ethyl acetate: petroleum ether 40-60). Purification *via* column chromatography (SiO_2 , 2:3 ethyl acetate: petroleum ether 40-60) gave compound **31** as a white solid (79 % yield).

^1H NMR [400 MHz, CDCl_3]: δ_{H} = 8.00 (s, 2H, Ph), 7.96 (d, J = 7.8, 2H, Ph), 7.62 (d, J = 7.6, 2H, Ph), 7.52 (t, J = 7.6 Hz, 2H, Ph), 7.24 (s, 2H, Ph^{cent}), 6.58 (s, 1H, -NH), 2.63 (s, 6H, - CH_3), 2.45 (s, 3H, -Ar CH_3), 1.68 (s, 3H, - CH_3).

ESI-MS m/z 408 ($[\text{M}+\text{Na}]^+$), HR ESI-MS found 408.1571 $\text{C}_{25}\text{H}_{23}\text{NNaO}_3$ requires 408.1570 (error 0.20 ppm).

6.2.23 Synthesis of **32**

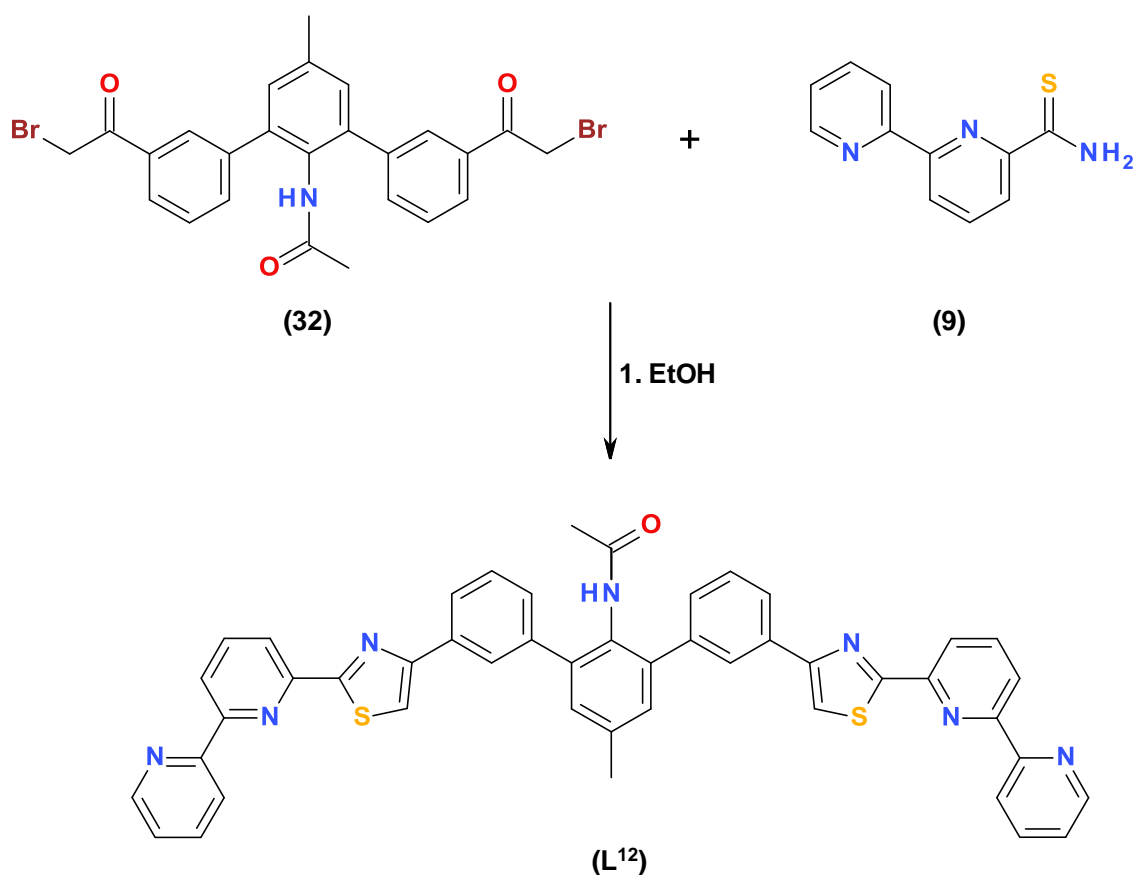


This compound was produced in an identical manner to compound **8**, except **31** was used in place of 3,3'-diacetylphenyl (**7**). The reaction was monitored *via* TLC (SiO₂, 2:3 ethyl acetate: petroleum ether 40-60). Purification *via* column chromatography (SiO₂, 2:3 ethyl acetate: petroleum ether 40-60) gave **32** as a white solid (58 % yield).

¹H NMR [400 MHz, CDCl₃]: δ_H = 8.02 (t, *J* = 1.6, 2H, Ph), 7.99 (dt, *J* = 7.7, 1.6, 2H, Ph), 7.67 (dt, *J* = 7.6, 1.6, 2H, Ph), 7.56 (t, *J* = 7.7 Hz, 2H, Ph), 7.24 (s, 2H, Ph^{cent}), 6.56 (s, 1H, -NH), 4.47 (s, 4H, -CH₂Br), 2.49 (s, 3H, -ArCH₃), 1.70 (s, 3H, -CH₃).

ESI-MS *m/z* 563 ([M+Na]⁺), HR ESI-MS found 563.9788 C₂₅H₂₁Br₂NNaO₃ requires 563.9780 (error 1.40 ppm).

6.2.24 Synthesis of L¹²



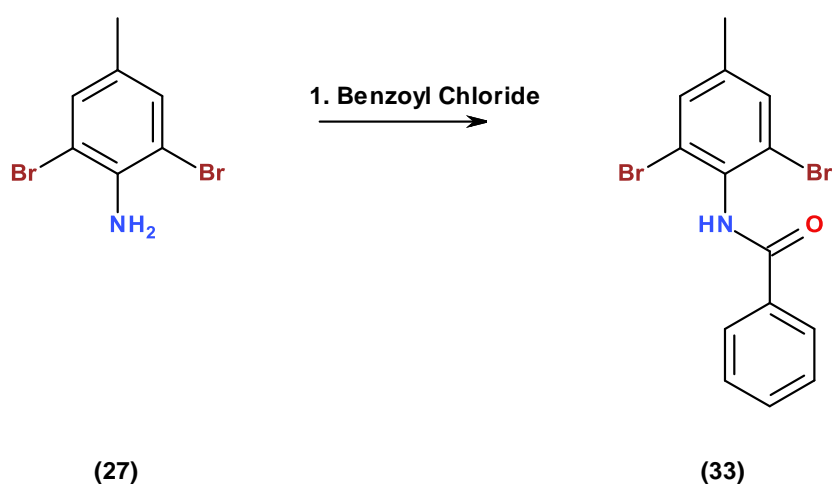
To a solution of 2,2'-bipyridine-6-thioamide (**9**) (0.079 g, 0.37 mmol) in ethanol (25 ml) was added the α -bromoacetyl (**32**) (0.100 g, 0.18 mmol) and the reaction refluxed for 8 h, during which time a precipitate was produced. This was isolated by filtration followed by washing with EtOH and Et₂O (2 x 2 ml). The compound was isolated as the H.Br salt; to obtain the free ligand the product was suspended in concentrated ammonia (0.88 S.G., 10 ml) for 24 h. Filtration and washing with d.H₂O, EtOH and Et₂O (2 x 2 ml) gave the desired ligand as an off-white powder. (0.125 g, 84 % yield).

¹H NMR [400 MHz, CDCl₃]: δ_{H} = 8.71 (d, J = 4.8, 2H, Py^{term}), 8.60 (d, J = 7.9, 2H, Py^{term}), 8.48 (d, J = 7.7, 2H, Py), 8.34 (d, J = 7.4, 2H, Py), 8.15 (s, 2H, Ph), 8.03 (d, J = 7.8, 2H, Ph), 7.96 (t, J = 7.8, 2H, Py), 7.90 (dt, J = 7.8, 1.7, 2H, Py^{term}), 7.69 (s, 2H, Tz), 7.55 (t, J = 7.5, 2H, Ph) 7.45 (d, J = 7.6 Hz, 2H, Ph),

7.39-7.33 (m, overlap, 4H, Py^{term}, Ph^{cent}), 6.59 (s, 1H, -NH), 2.49 (s, 3H, -ArCH₃), 1.75 (s, 3H, -CH₃).

ESI-MS *m/z* 776 (M + H⁺), HR ESI-MS found 776.2263 C₄₇H₃₄N₇OS₂ requires 776.2261 (error 0.25 ppm).

6.2.25 Synthesis of N-(2,6-dibromo-4-methyl-phenyl)benzamide (**33**)

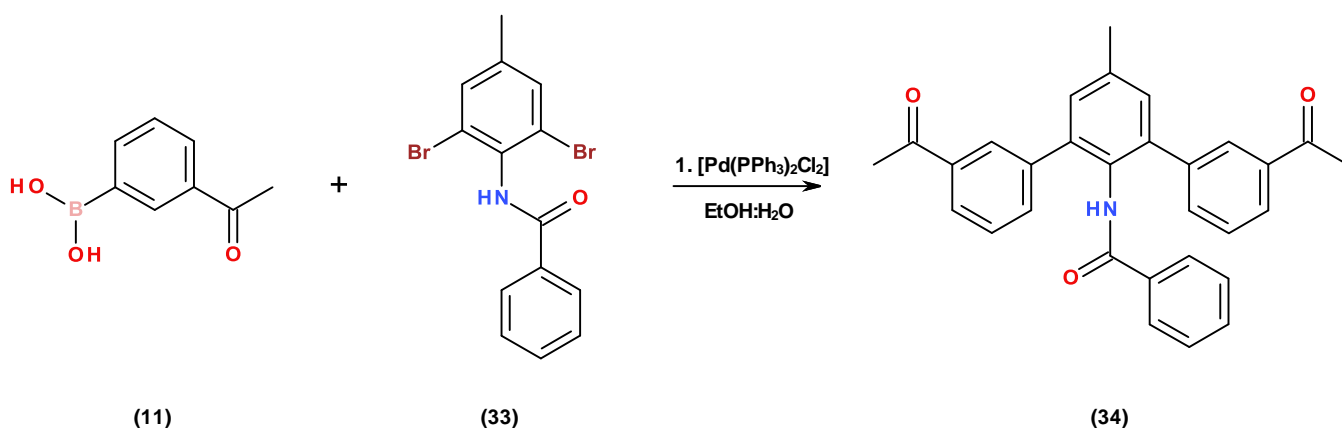


To a solution of **27** (0.67 g, 2.53 mmol) in DCM (25 ml) pyridine (0.20 g, 2.53 mmol) was added. This was set to stir at room temperature then a solution of benzoyl chloride (0.36 g, 2.53 mmol) in DCM (1 ml) was added drop-wise over a period of 1 h. The reaction was monitored by TLC (SiO₂, 1:1 ethyl acetate: petroleum ether 40-60). Upon completion DCM (25 ml) was added to the reaction, this was then washed with deionised water followed by NaHCO_{3(aq)} and finally washed with HCl (2 M) (2 x 30 ml). The resulting solution was dried (MgSO₄) and the solvent evaporated. Purification *via* column chromatography (SiO₂, 3:7 ethyl acetate: petroleum ether 40-60) gave **33** as a white powder (0.82 g, 88 % yield).

¹H NMR [400 MHz, CDCl₃]: δ_H= 7.98 (d, *J*= 7.4, 2H, Bz), 7.60 (t, *J*= 7.3 Hz, 1H, Bz), 7.53 (m overlap, 3H, -NH, Bz), 7.47 (s, 2H, Ph), 2.36 (s, 3H, -ArCH₃).

ESI-MS m/z 389 ($[M+Na]^+$), HR ESI-MS found 389.9094 $C_{14}H_{11}Br_2NNaO$ requires 389.9099 (error 1.41 ppm).

6.2.26 Synthesis of **34**

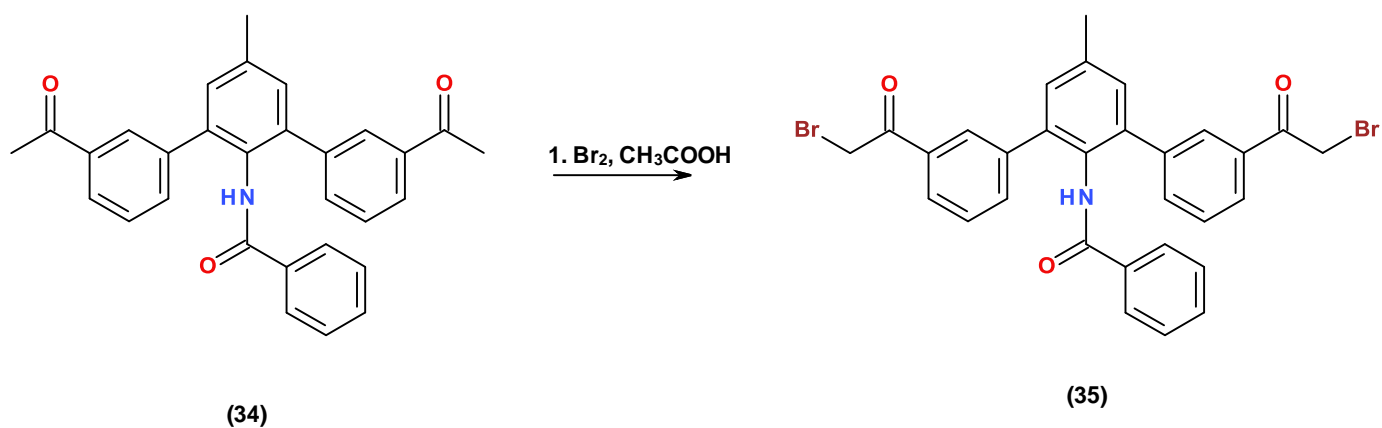


This compound was produced in an identical manner to compound **12**, except N-(2,6-dibromo-4-methyl-phenyl) benzamide (**33**) was used in place of 1,3-dibromobenzene (**10**). The reaction was monitored *via* TLC (SiO_2 , 1:1 ethyl acetate: petroleum ether 40-60). Upon completion the solvent was removed and $NaHCO_3$ (aq) (20 ml) added. This was extracted first with 1% MeOH in DCM (3 x 30 ml) followed by 3 % MeOH in DCM (3 x 30 ml) and finally 5 % MeOH in DCM (3 x 30 ml). The combined organic layers were dried over $MgSO_4$, filtered and evaporated. Once all the solvent had been removed DCM (\approx 2 ml) was added to the reaction and upon standing a precipitate was produced. This was isolated *via* filtration to give the desired compound, **34**, as a light grey powder (48 % yield).

1H NMR [400 MHz, $DMSO-d_6$]: δ_H = 9.82 (s, 1H, -NH), 8.06 (t, J = 1.6, 2H, Ph), 7.86 (dt, J = 7.8, 1.4, 2H, Ph), 7.71 (dt, J = 7.7, 1.4, 2H, Ph), 7.53-7.47 (m, overlap, 4H, Ph, Bz), 7.42 (tt, J = 7.4, 1.5, 1H, Bz), 7.34 (s, 2H, Ph^{cent}), 7.42 (t, J = 7.3 Hz, 2H, Bz), 2.51 (s, 6H, $-CH_3$), 2.46 (s, 3H, $-ArCH_3$).

ESI-MS m/z 470 ($[M+Na]^+$), HR ESI-MS found 470.1712 $C_{30}H_{25}NNaO_3$ requires 470.1727 (error 3.05 ppm).

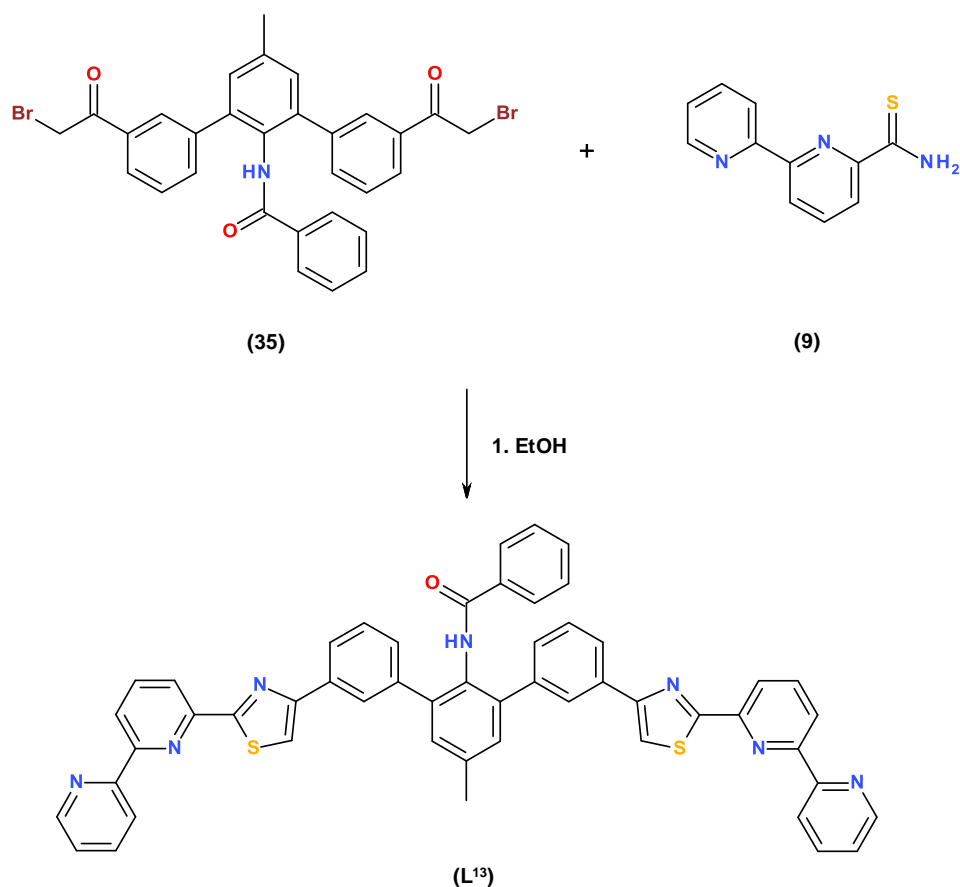
6.2.27 Synthesis of **35**



This compound was produced in a similar manner to compound **8**, except **34** was used in place of 3,3'-diacetylbiphenyl (**7**). The reaction was monitored *via* TLC (SiO_2 , 2:3 ethyl acetate: petroleum ether 40-60) until the starting material was consumed (approximately 3 h). After this time the reaction was allowed to cool, then poured over $NaHCO_{3(aq)}$ (30 ml), extracted using 1% MeOH in DCM (2 x 30 ml), 3% MeOH in DCM (2 x 30 ml) and 5% MeOH in DCM (2 x 30 ml). The combined organic layers were dried ($MgSO_4$), filtered and the solvent removed by rotary evaporation. After this DCM (5 ml) was added to the flask, upon reduction of solvent a precipitate was produced. Collection *via* filtration gave a crude orange-brown solid.

Note: Due to solubility problems this compound was not purified, thus characterisation of this compound cannot be reported.

6.2.28 Synthesis of **L**¹³



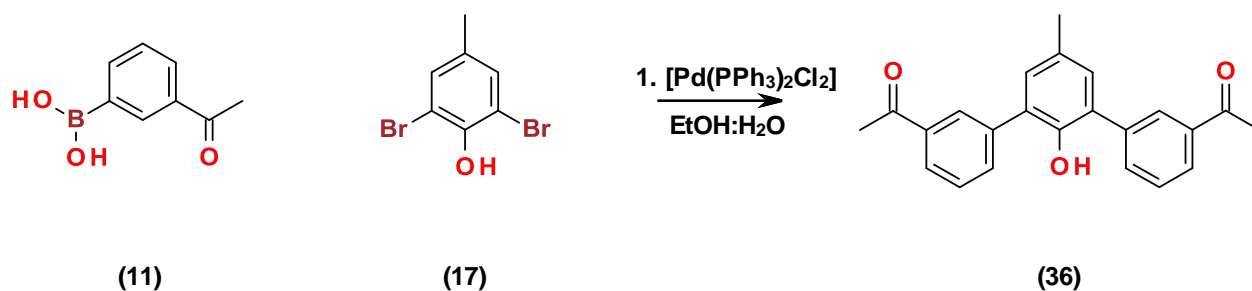
To a solution of 2,2'-bipyridine-6-thioamide (**9**) (0.071 g, 0.33 mmol) in ethanol (25 ml) was added the α -bromoacetyl (**35**) (0.10 g, 0.17 mmol) and the reaction heated under reflux for 8 h. The reaction was allowed to cool, which resulted in the production of a precipitate. This was isolated by filtration, followed by washing with EtOH and Et₂O (2 x 2 ml) giving the ligand, **L**¹³, as a cream powder (0.039 g, 45 % yield).

¹H NMR [500 MHz, DMSO-d₆]: δ_{H} = 9.90 (s, 1H, -NH), 8.76 (dq, J = 4.8, 0.9 2H, Py^{term}), 8.52-8.49 (m, overlap, 4H, Py, Py^{term}), 8.35 (dd, J = 7.8, 1.0, 2H, Py), 8.33 (s, 2H, Ph), 8.30 (s, 2H, Tz), 8.16 (t, J = 7.8, 2H, Py), 8.08 (dt, J = 7.7, 1.8, 2H, Py^{term}), 8.01 (dt, J = 7.3, 1.7, 2H, Ph), 7.64 (dd, J = 7.1, 1.3, 2H, Bz), 7.57-

7.49 (m, overlap, 6H, Py^{term}, Ph), 7.42 (s, 2H, Ph^{cent}), 7.28 (t, $J = 7.4$, 1H, Bz), 7.13 (t, $J = 7.9$ Hz, 2H, Bz), 2.63 (s, 3H, -ArCH₃).

ESI-MS m/z 838 ([M+H]⁺), HR ESI-MS found 838.2439 C₅₂H₃₆N₇OS₂ requires 838.2417 (error 2.63 ppm)

6.2.29 Synthesis of **36**

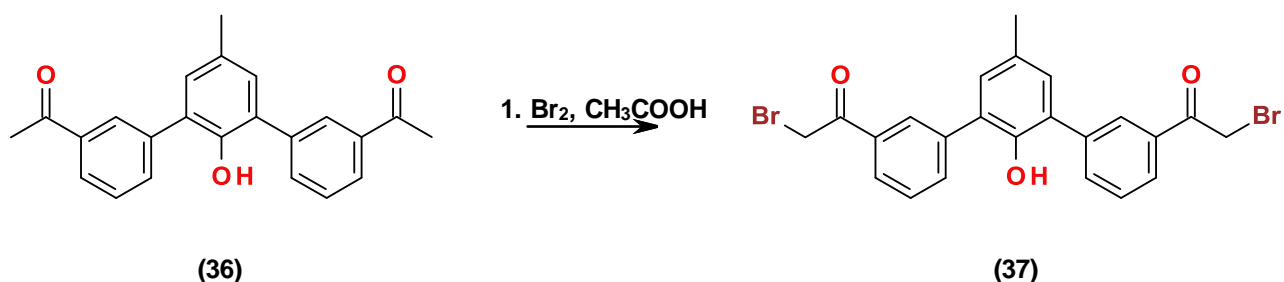


This compound was produced in an identical manner to compound **12**, except 2,6-dibromo-4-methylphenol (**17**) was used in place of 1,3-dibromobenzene (**10**). The reaction was monitored *via* TLC (SiO₂, 1:3 ethyl acetate: petroleum ether 40-60). Purification *via* column chromatography (SiO₂, 1:3 ethyl acetate: petroleum ether 40-60) gave compound **36** as a yellow oil (65 % yield).

¹H NMR [400 MHz, CDCl₃]: $\delta_{\text{H}} = 8.13$ (t, $J = 7.7$, 2H, Ph), 7.98 (dt, $J = 7.7$, 1.5, 2H, Ph), 7.78 (dt, $J = 7.7$, 1.5, 2H, Ph), 7.58 (t, $J = 7.8$ Hz, 2H, Ph), 7.14 (s, 2H, Ph^{cent}), 5.15 (s, 1H, -OH), 2.65 (s, 6H, -CH₃), 2.05 (s, 3H, -ArCH₃).

ESI-MS m/z 367 ([M+Na]⁺), HR ESI-MS found 367.1302 C₂₃H₂₀NaO₃ requires 367.1304 (error 0.60 ppm).

6.2.30 Synthesis of **37**

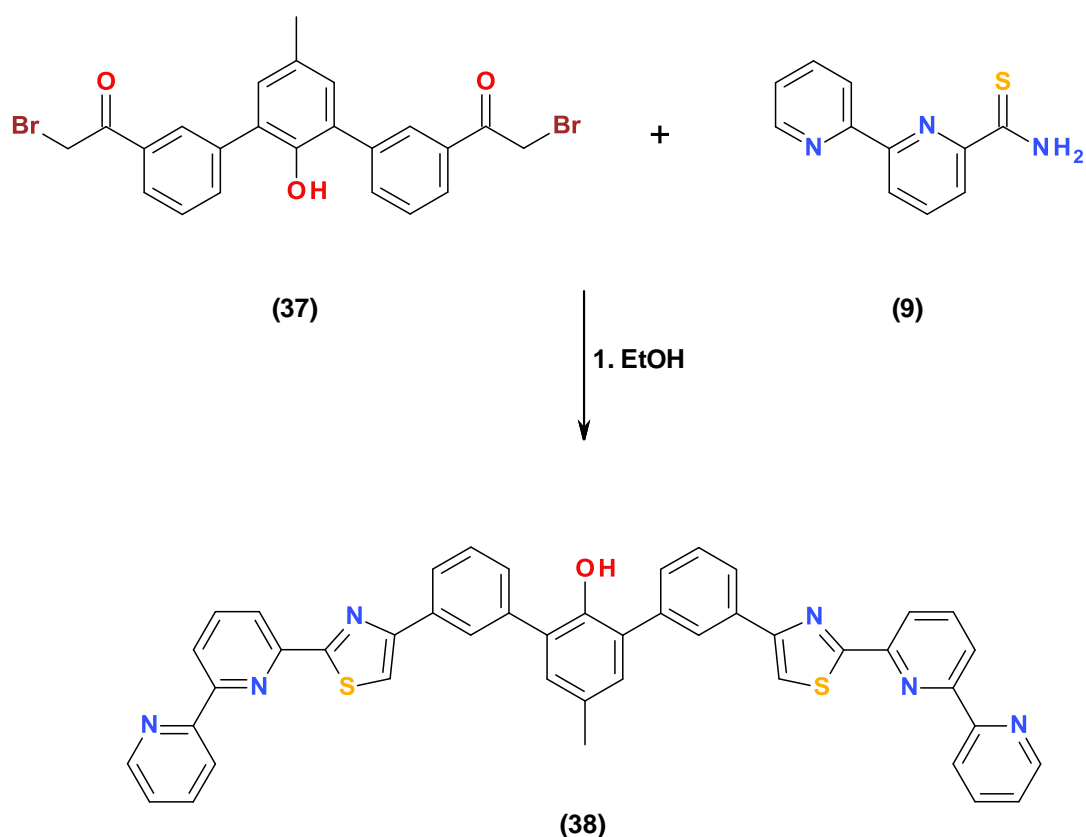


This compound was produced in an identical manner to compound **8**, except **36** was used in place of 3,3'-diacetylbiphenyl (**7**). The reaction was monitored *via* TLC (SiO_2 , 1 % MeOH in DCM). Purification *via* column chromatography (SiO_2 , 1 % MeOH in DCM) gave compound **37** as an off-white powder (89 % yield).

^1H NMR [400 MHz, CDCl_3]: δ_{H} = 8.17 (t, J = 1.6, 2H, Ph), 8.02 (dd, J = 7.8, 1.2, 2H, Ph), 7.82 (dd, J = 7.7, 1.1, 2H, Ph), 7.62 (t, J = 7.8 Hz, 2H, Ph), 7.15 (s, 2H, Ph^{cent}), 5.08 (s, 1H, -OH), 4.50 (s, 4H, $-\text{CH}_2\text{Br}$), 2.40 (s, 3H, $-\text{ArCH}_3$).

ESI-MS m/z 523 ($[\text{M}+\text{Na}]^+$), HR ESI-MS found 522.9520 $\text{C}_{23}\text{H}_{18}\text{Br}_2\text{NaO}_3$ requires 522.9515 (error 0.90 ppm).

6.2.31 Synthesis of **38**

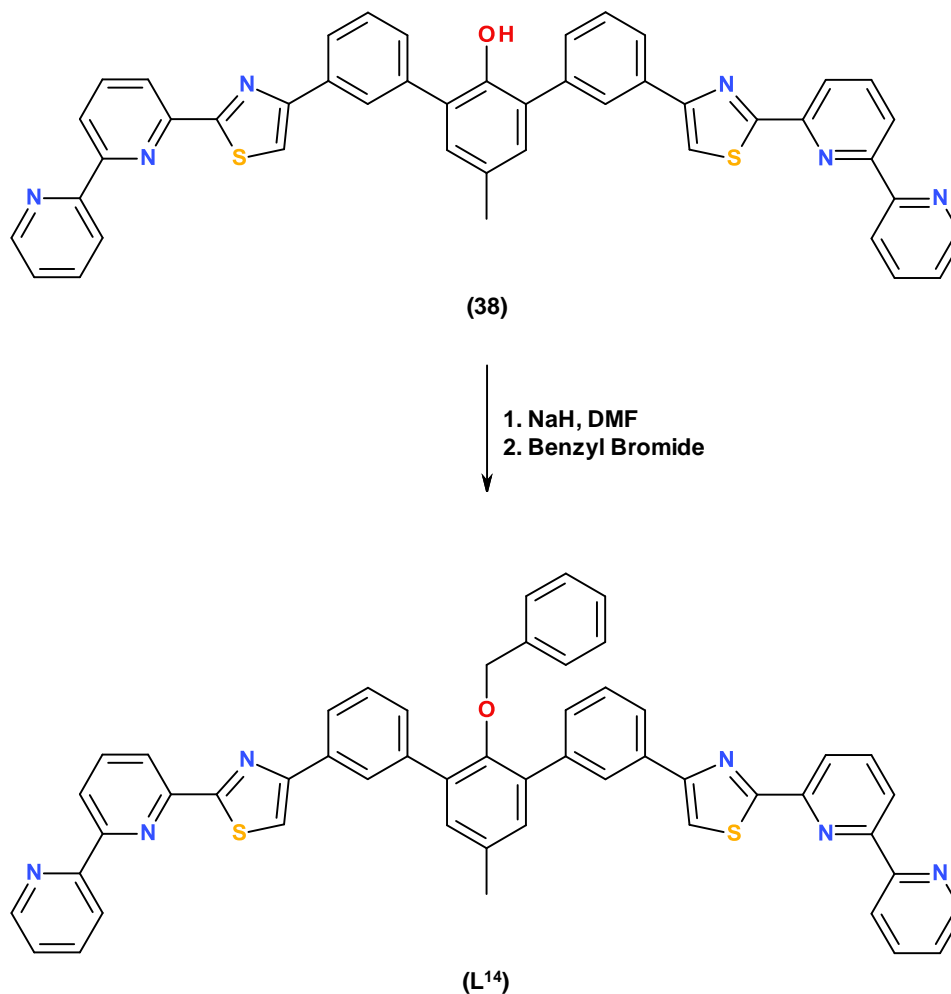


To a solution of 2,2'-bipyridine-6-thioamide (**9**) (0.113 g, 0.53 mmol) in ethanol (25 ml) was added the α -bromoacetyl (**37**) (0.120 g, 0.24 mmol) and the reaction refluxed for 8 h during which time a precipitate was produced. This was isolated by filtration, followed by washing with EtOH and Et₂O (2 x 2 ml). The compound was isolated as the H.Br salt; to obtain the free ligand the product was suspended in concentrated ammonia (0.88 S.G., 10 ml) for 24 h. Filtration and washing with d.H₂O, EtOH and Et₂O (2 x 2 ml) gave the desired product as a light brown powder (79 % yield).

¹H NMR [500 MHz, CDCl₃]: δ_{H} = 8.71 (dq, J = 4.8, 0.9, 2H, Py^{term}), 8.60 (dt, J = 7.9, 0.9, 2H, Py^{term}), 8.48 (dd, J = 7.9, 1.0, 2H, Py), 8.35 (dd, J = 7.8, 1.0, 2H, Py), 8.24 (br s, 2H, Ph), 8.06-8.04 (m, 2H, Ph), 7.96 (t, J = 7.8, 2H, Py), 7.89 (dt, J = 7.7, 1.7, 2H, Py^{term}), 7.69 (s, 2H, Tz), 7.60-7.59 (m, overlap, 4H, 2 x Ph), 7.36 (ddd, J = 7.5, 4.8, 1.2 Hz, 2H, Py^{term}), 7.24 (s, 2H, Ph^{cent}), 5.45 (s, 1H, -OH), 2.42 (s, 3H, -ArCH₃).

ESI-MS m/z 735 ($[M+H]^+$), HR ESI-MS found 735.1994 $C_{45}H_{31}N_6OS_2$ requires 735.1995 (error 0.19 ppm).

6.2.32 Synthesis of **L¹⁴**



A two necked round bottom flask charged with **38** (0.14 g, 0.19 mmol) and sodium hydride (0.04 g, 0.95 mmol), was placed under an atmosphere of $N_{2(g)}$, to this anhydrous DMF (5 ml) was added. This was left to stir at $80^\circ C$ for 1h. After this time benzyl bromide (0.07 g, 0.38 mmol) was added to the reaction and set to stir at $80^\circ C$. The reaction was monitored *via* TLC (Al_2O_3 , 1% hexane in DCM); once all the starting material had been consumed methanol was added to the reaction whilst under $N_{2(g)}$ (to react with any unreacted sodium hydride). The reaction was concentrated and $NaHCO_{3(aq)}$ (30 ml) added and the

reaction extracted into DCM (3 x 30 ml). The combined organic layers were dried (MgSO₄) and the solvent removed by rotary evaporation. Separation and purification *via* column chromatography (Al₂O₃, 1% hexane in DCM) gave **L¹⁴** as a fine cream powder once dry (0.052 g, 56 % yield)

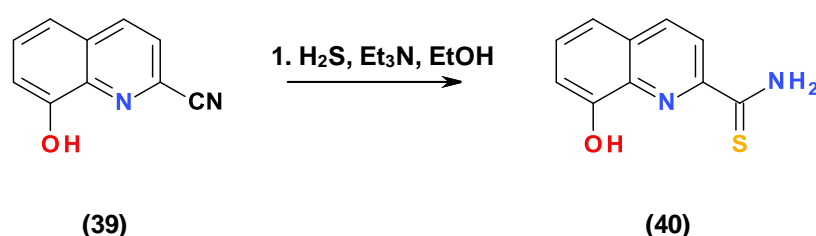
¹H NMR [400 MHz, CDCl₃]: δ_H = 8.72 (dq, *J* = 4.8, 0.8 2H, Py^{term}), 8.62 (d, *J* = 7.9, 2H, Py^{term}), 8.50 (dd, *J* = 7.9, 0.8, 2H, Py), 8.36 (dd, *J* = 7.7, 0.9, 2H, Py), 8.31 (t, *J* = 1.6, 2H, Ph), 8.09 (d, *J* = 7.8, 2H, Ph), 7.98 (t, *J* = 7.8, 2H, Py), 7.91 (dt, *J* = 7.7, 1.8, 2H, Py^{term}), 7.71 (d, *J* = 7.8, 2H, Ph), 7.62 (s, 2H, Tz), 7.56 (t, *J* = 7.7, 2H, Ph), 7.37 (ddd, *J* = 7.5, 4.8, 1.1, 2H, Py^{term}), 7.36 (s, 2H, Ph^{cent}), 7.08 (t, *J* = 7.2, 1H, Bn), 7.03 (t, *J* = 7.2, 2H, Bn), 6.79 (d, *J* = 6.9 Hz, 2H, Bn), 4.29 (s, 2H, O-CH₂-), 2.50 (s, 3H, -ArCH₃).

¹³C NMR [125 MHz, CDCl₃]: δ_C = 169.2 (quaternary, Q), 156.7 (Q), 155.7 (Q), 155.4 (Q), 151.4 (Q), 150.8 (Q), 149.2 (CH), 139.2 (Q), 138.0 (CH), 137.0 (CH), 136.7 (Q), 135.8 (Q), 134.5 (Q), 134.1 (Q), 131.0 (CH), 129.7 (CH), 128.7 (CH), 128.6 (CH), 128.0 (CH), 127.7 (CH), 127.5 (CH), 125.3 (CH), 124.1 (CH), 121.7 (CH), 121.3 (CH), 119.8 (CH), 115.6 (CH), 75.0 (CH₂, Bn), 21.0 (CH₃).

ESI-MS *m/z* 825 ([M+H]⁺), HR ESI-MS found 825.2455 C₅₂H₃₇N₆OS₂ requires 825.2465 (error 1.24 ppm).

6.3 Preparation of (**L¹⁵**- **L¹⁷**)

6.3.1 Synthesis of 8-hydroxyquinoline-2-carbothioamide **40**



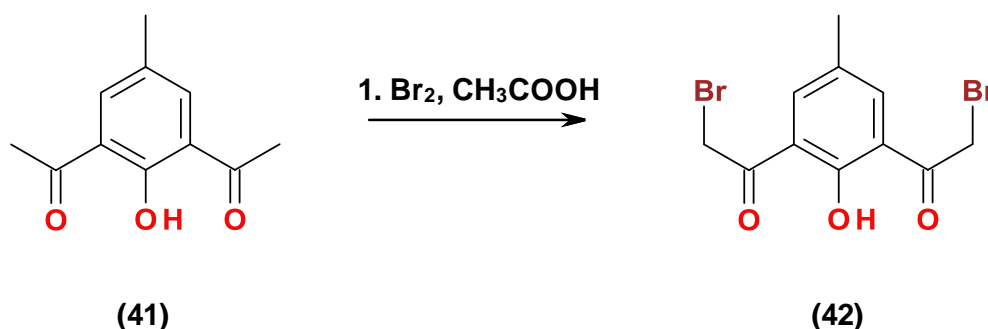
To a solution of 8-hydroxyquinoline-2-carbonitrile (**39**) (1.0 g, 5.9 mmol) in ethanol (20 ml), triethylamine (1.0 g, 9.9 mmol) was added and H₂S_(g) slowly

bubbled through the solution which turned yellow after a few minutes. The solution was then left to stand at room temperature for 48 h during which time a precipitate was produced. Filtration gave the thioamide, **40**, as a dark yellow powder (1.1 g, 91 % yield).

$^1\text{H NMR}$ [400 MHz, CDCl_3]: $\delta_{\text{H}} = 9.21$ (br s, 1H, $-\text{NH}_2$), 8.85 (d, $J = 8.7$, 1H, Py), 8.32 (d, $J = 8.7$, 1H, Py), 7.76 (br s, 1H, $-\text{NH}_2$), 7.63 (s, 1H, $-\text{OH}$), 7.59 (t, $J = 8.0$, 1H, Ph), 7.44 (dd, $J = 8.3$, 1.0 Hz, 1H, Ph), 7.27 (m, overlap with solvent peak, 1H, Ph).

ESI-MS m/z 227 ($[\text{M}+\text{Na}]^+$), HR ESI-MS found 227.0253 $\text{C}_{10}\text{H}_8\text{N}_2\text{NaOS}$ requires 227.0250 (error 1.55 ppm).

6.3.2 Synthesis of **42**

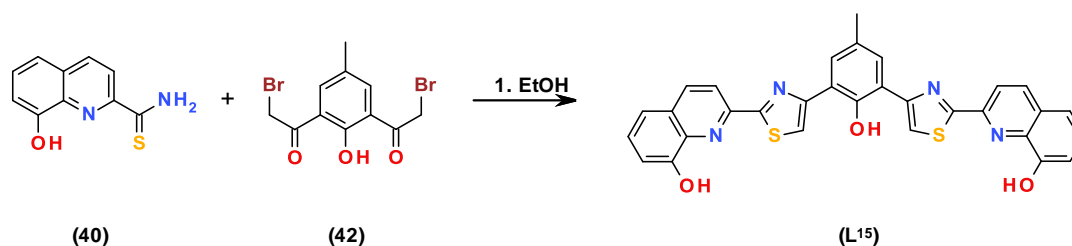


Diacetyl cresol (**41**) (0.2 g, 1.0 mmol) was dissolved in acetic acid (25 ml) and set to stir at 80 °C under an atmosphere of $\text{N}_2(\text{g})$. Bromine (0.33 g, 2.0 mmol) was diluted to 1 ml with acetic acid (approx. 0.9 ml) to allow slow addition to the reaction. The reaction was monitored *via* TLC (SiO_2 , 1% hexane in DCM) once the starting material was consumed the reaction was allowed to cool to room temperature, then poured over deionised water (30 ml) and NaHCO_3 (0.1 g) was added to neutralise the reaction. The product was extracted into DCM (3 x 30 ml) and the combined organic layers dried over MgSO_4 . Removal of the solvent left the crude product as an orange oil. Purification *via* column chromatography (SiO_2 , 1 % hexane in DCM) gave the desired product as an off-white solid (**42**). (0.15 g, 41 % yield)

^1H NMR [400 MHz, CDCl_3]: δ_{H} = 12.78 (s, 1H, -OH), 7.89 (s, 2H, Ph), 4.60 (s, 4H, $-\text{CH}_2\text{Br}$), 2.39 (s, 3H, Ar- CH_3).

ESI-MS m/z 370 ($[\text{M}+\text{Na}]^+$), HR ESI-MS found 370.8889 $\text{C}_{11}\text{H}_{10}\text{Br}_2\text{NaO}_3$ requires 370.8889 (error 0.07 ppm).

6.3.3 Synthesis of L^{15}



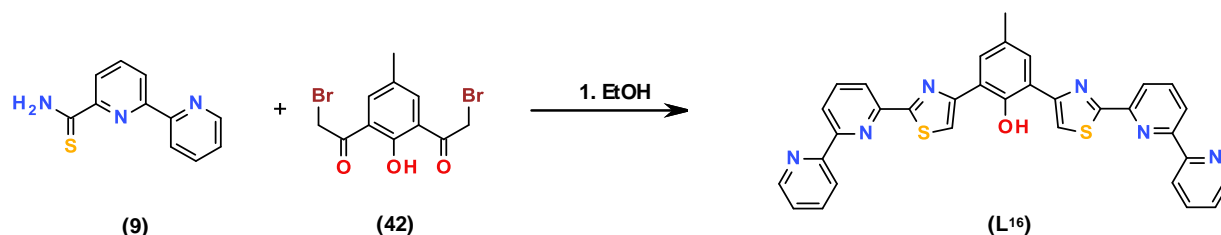
To a solution of 8-hydroxyquinoline-2-carbothioamide (**40**) (0.058 g, 0.28 mmol) in ethanol (25 ml) the α -bromoacetyl, **42**, (0.045 g, 0.13 mmol) was added and the solution refluxed for 5 h. After this time the resulting yellow precipitate was filtered, washed with ethanol (2 ml) and ether (2 ml) giving the bromide salt of the ligand. This was suspended in ammonia (0.88 S.G., 10 ml) and left for 12 h. Filtration and washing with d. H_2O , EtOH and Et_2O (2 x 2 ml) gave L^{15} as a light yellow powder (0.056 g, 78 % yield)

^1H NMR [400 MHz, $\text{DMSO}-d_6$]: δ_{H} = 12.59 (s, 1H, -OH), 9.98 (s, 2H, -OH), 8.59 (s, 2H, Tz), 8.54 (d, J = 8.6, 2H, Py), 8.40 (d, J = 8.6, 2H, Py), 8.04 (s, 2H, Ph^{cent}), 7.52-7.49 (m, overlap, 4H, 2 x Ph), 7.21 (dd, J = 6.6, 2.3 Hz, 2H, Ph), 2.45 (s, 3H, Ar- CH_3).

^{13}C NMR [100 MHz, CDCl_3]: δ_{C} = 167.8 (quaternary, Q), 153.8 (Q), 153.2 (Q), 151.5 (Q), 148.5 (Q), 138.6 (Q), 138.2 (CH), 129.9 (Q), 129.2 (CH), 129.0 (CH), 128.6 (Q), 120.4 (Q), 120.3 (Q), 118.5 (CH), 118.1 (CH), 113.2 (CH), 20.9 (- CH_3).

ESI-MS m/z 583 ($[\text{M}+\text{Na}]^+$), HR ESI-MS found 583.0869 $\text{C}_{31}\text{H}_{20}\text{N}_4\text{NaO}_3\text{S}_2$ requires 583.0869 (error 0.07 ppm)

6.3.4 Synthesis of L¹⁶



To a 50 ml round bottom flask charged with 2,2'-bipyridine-6-thioamide (**9**) (0.203 g, 0.94 mmol) and the α -bromoacetyl, **42**, (0.15 g, 0.43 mmol) was added DMF (10 ml) and the resulting solution was heated at 80 °C for 24 h. After this time the resulting yellow precipitate was filtered, washed with ethanol and ether (2 x 2 ml) giving the bromide salt of the ligand. This compound was suspended in ammonia (0.88 S.G., 10 ml) and left for 24 h. Filtration and washing with d.H₂O, EtOH and Et₂O (2 x 2 ml) gave L¹⁶ as a fine yellow solid (0.21 g, 84 % yield).

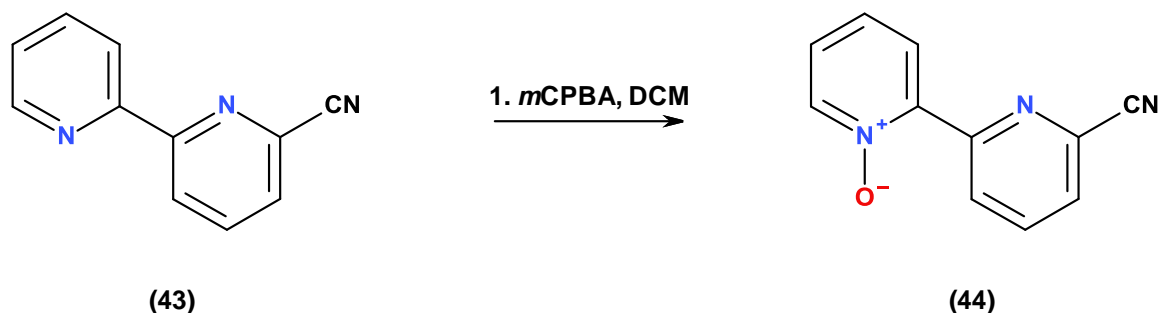
¹H NMR [500 MHz, DMSO-d₆]: δ_{H} = 12.33 (s, 1H, -OH), 8.77 (dq, J = 4.7, 1.8, 0.9, 2H, Py^{term}), 8.54-8.52 (m, overlap, 4H, Py, Py^{term}), 8.51 (s, 2H, Tz), 8.34 (dd, J = 7.7, 1.0, 2H, Py), 8.21 (t, J = 7.7, 2H, Py), 8.07 (dt, J = 7.7, 1.8, 2H, Py^{term}), 8.02 (s, 2H, Ph), 7.54 (ddd, J = 7.5, 4.8, 1.2 Hz, 2H, Py^{term}), 2.47 (s, 3H, Ar-CH₃).

The poor solubility of the ligand precluded ¹³C NMR analysis.

IR (solid, ν/cm^{-1}) 3138, 3117, 2982, 1580, 1571, 1560, 1526, 1514, 1480, 1452, 1429, 1297, 1275, 1252, 1144, 1091, 1076, 1027, 1016, 852, 823, 776, 740, 730, 688, 652.

ESI-MS m/z 605 ([M+Na]⁺), HR ESI-MS found 605.1183 C₃₃H₂₂N₆NaOS₂ requires 605.1189 (error 0.96 ppm)

6.3.5 Synthesis of 6'-cyano-2,2'-bipyridine-N-oxide (**44**)¹⁶⁹

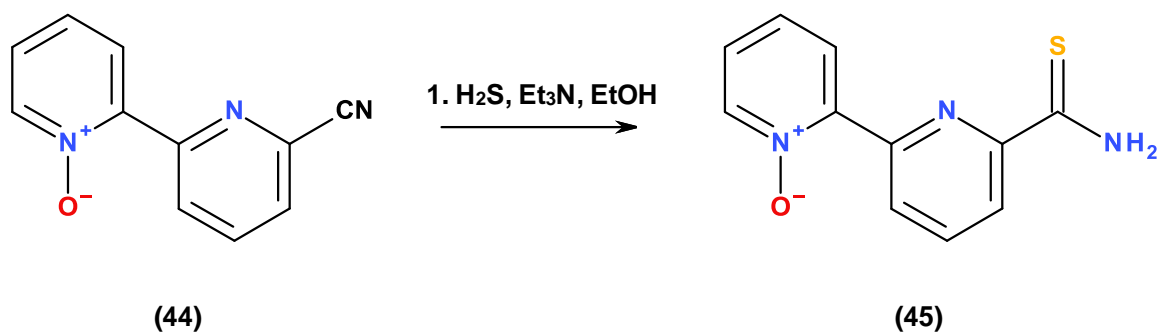


To a solution of 6-cyano-2,2'-bipyridine (**43**) (0.2 g, 1.1 mmol) in DCM (25 ml), *m*CPBA (0.27 g, 1.2 mmol, (77%)) was added slowly, over a period of 2 h after which the reaction was allowed to stir for 8 h. The solvent was removed by rotary evaporation and the resulting solid purified *via* column chromatography (Al₂O₃, 1% MeOH in DCM). This gave the desired compound, **44**, as a cream solid (0.17 g, 78 % yield)

¹H NMR [400 MHz, CDCl₃]: δ_H = 9.27 (dd, *J* = 8.3, 1.0, 1H, Py^{N-oxide}), 8.33 (dd, *J* = 6.4, 0.9, 1H, Py), 8.27 (dd, *J* = 8.0, 2.1, 1H, Py^{N-oxide}), 7.99 (t, *J* = 8.0, 1H, Py), 7.75 (dd, *J* = 6.4, 0.9, 1H, Py), 7.43 (dt, *J* = 7.8, 1.3, 1H, Py^{N-oxide}), 7.36 (ddd, *J* = 8.0, 5.9, 2.2 Hz, 1H, Py^{N-oxide}).

ESI-MS *m/z* 220 ([M+Na]⁺), HR ESI-MS found 220.0480 C₁₁H₇N₃NaO requires 220.0481 (error 0.46 ppm).

6.3.6 Synthesis of Synthesis of *N*-oxide-2,2'-bipyridine-6'-thioamide (**45**)¹⁶⁹

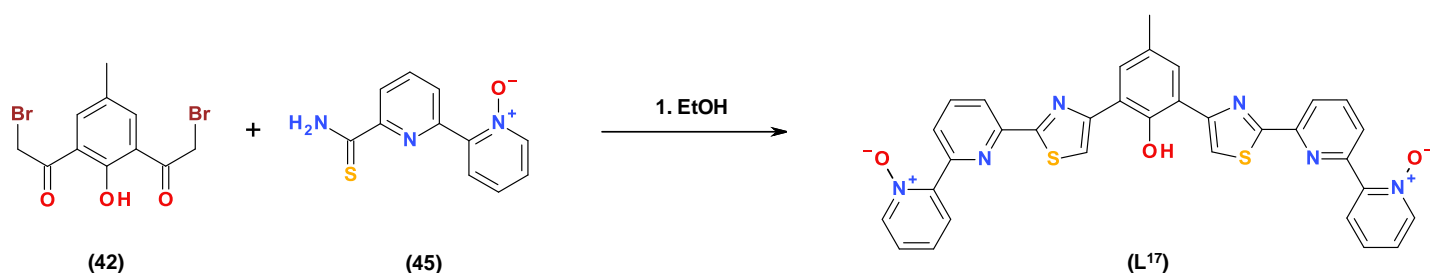


This compound was produced in a similar manner to 8-hydroxyquinoline-2-carbothioamide (**40**), except 6'-cyano-2,2'-bipyridine-*N*-oxide (**44**) was used in place of 8-hydroxyquinoline-2-carbonitrile (**39**). Filtration of the resulting precipitate gave **45** as a yellow powder (88 % yield).

¹H NMR [400 MHz, CDCl₃]: δ_H = 9.50 (br s, 1H, -NH₂), 8.97 (dd, *J* = 8.0, 0.7, 1H, Py^{N-oxide}), 8.78 (dd, *J* = 7.9, 0.7, 1H, Py^{N-oxide}), 8.36 (dd, *J* = 6.4, 0.7, 1H, Py), 8.04 (dd, *J* = 8.0, 2.1, 1H, Py), 8.01 (t, *J* = 7.5, 1H, Py), 7.76 (br s, 1H, -NH₂), 7.41 (dt, *J* = 7.7, 1.2 Hz, 1H, Py^{N-oxide}), 7.35 (m, 1H, Py^{N-oxide}).

ESI-MS *m/z* 254 ([M+Na]⁺), HR ESI-MS found 254.0371 C₁₁H₉N₃NaOS requires 254.0359 (error 4.79 ppm).

6.3.7 Synthesis of L^{17169}



To a solution of *N*-oxide-2,2'-bipyridine-6'-thioamide (**45**) (0.073 g, 0.31 mmol) in DMF (5 ml) the α -bromoacetyl, **42**, (0.050 g, 0.14 mmol) was added and the solution heated at 80 °C for 8 h. After this time the resulting yellow precipitate was filtered, washed with ethanol and ether (2 x 2 ml) giving the bromide salt of the ligand. This compound was suspended in ammonia (0.88 S.G., 10 ml) and left for 24 h. Filtration and washing with d.H₂O, EtOH and Et₂O (2 x 2 ml) gave L^{17} as a fine yellow powder (0.053 g, 62 % yield).

IR (solid, ν/cm^{-1}) 3112, 2955, 2359, 2343, 1738, 1675, 1581, 1567, 1515, 1490, 1450, 1494, 1393, 1292, 1285, 1231, 1211, 1155, 1023, 1011, 773, 760, 736.

Note: Due to poor solubility of this compound in organic solvents no NMR could be recorded.

6.4 Synthesis of complexes

For each ligand a selection of different metal ions, generally as the perchlorate, tetrafluoroborate or triflate salt, were employed in each case to investigate their coordination chemistry. The complexes reported here are those which produced crystals of sufficient quality for X-ray diffraction.

6.4.1 Synthesis of $[\text{Zn}_5(\text{L}^1)_5](\text{CF}_3\text{SO}_3)_{10}$

To a suspension of L^1 (5 mg, 0.008 mmol) in acetonitrile (1 ml) was added $\text{Zn}(\text{CF}_3\text{SO}_3)_2$ (3 mg, 0.08 mmol) and the suspension sonicated until all the ligand had dissolved. Ethyl acetate was then slowly allowed to diffuse into the solution giving colourless crystals, which were filtered and dried under vacuum (0.04 g, 50%). NMR and mass spectroscopy data are discussed in the text. Found: C, 42.9; H, 3.7; N, 12.2%. Calculated for $\text{C}_{170}\text{H}_{160}\text{N}_{30}\text{F}_{30}\text{O}_{40}\text{S}_{20}\text{Zn}_5$: C, 42.5; H, 3.4; N, 11.9%.

All the other ligand complexes (L^2 – L^4) were synthesised in an identical manner. $[\text{Zn}_5(\text{L}^2)_5](\text{CF}_3\text{SO}_3)_{10}$ (yield = 45%) Found: C, 39.3; H, 2.7; N, 11.9%. Calculated for $\text{C}_{160}\text{H}_{120}\text{N}_{30}\text{O}_{60}\text{S}_{20}\text{F}_{30}\text{Zn}_5$: C, 38.7; H, 2.4; N, 11.5%. $[\text{Zn}_5(\text{L}^3)_5](\text{CF}_3\text{SO}_3)_{10}$ (yield = 50%) Found: C, 42.6; H, 3.8; N, 7.4%. Calculated for $\text{C}_{190}\text{H}_{180}\text{N}_{30}\text{O}_{60}\text{S}_{20}\text{F}_{30}\text{Zn}_5$: C, 42.4; H, 3.4; N, 7.8%. $[\text{Zn}_5(\text{L}^4)_5](\text{CF}_3\text{SO}_3)_{10}$ (yield = 55%) Found: C, 47.5; H, 3.2; N, 10.1%. Calculated for $\text{C}_{230}\text{H}_{180}\text{N}_{30}\text{O}_{60}\text{S}_{20}\text{F}_{30}\text{Zn}_5$: C, 47.1; H, 3.1; N, 9.7%.

6.4.2 Synthesis of the complex $[\text{Cu}_2(\text{L}^6)_2](\text{ClO}_4)_4$

To a suspension of L^6 (5.0 mg, 0.008 mmol) in acetonitrile (2 ml) was added $\text{Cu}(\text{ClO}_4)_2 \cdot 6\text{H}_2\text{O}$ (2.9 mg, 0.008 mmol) and the suspension sonicated until all the ligand had dissolved giving a light green solution. Filtration followed by the slow diffusion of diethyl ether vapour into the acetonitrile solution resulted in the formation of green crystals of $[\text{Cu}_2(\text{L}^6)_2](\text{ClO}_4)_4$. ESI-MS m/z 1683 corresponding to $\{[\text{Cu}_2(\text{L}^6)_2](\text{ClO}_4)_3\}^+$. $[\text{Cu}_2(\text{L}^6)_2](\text{ClO}_4)_4$ (yield = 72 %).

6.4.3 Synthesis of the complex $[\text{Fe}_2(\text{L}^7)_2](\text{ClO}_4)_4$

To a suspension of L^7 (5.0 mg, 0.007 mmol) in nitromethane (2 ml) was added $\text{Fe}(\text{ClO}_4)_2 \cdot 6\text{H}_2\text{O}$ (2.6 mg, 0.007 mmol) and the suspension sonicated until all the ligand had dissolved giving a deep purple solution. Filtration followed by the slow diffusion of diethyl ether vapour into the nitromethane solution resulted in the formation of purple crystals of $[\text{Fe}_2(\text{L}^7)_2](\text{ClO}_4)_4$. ESI-MS m/z 1819 corresponding to $\{[\text{Fe}_2(\text{L}^7)_2](\text{ClO}_4)_3\}^+$. $[\text{Fe}_2(\text{L}^7)_2](\text{ClO}_4)_4$ (yield = 75 %). Found: C, 54.3; H, 2.6; N, 9.6%. Calculated for $\text{C}_{89}\text{H}_{59}\text{Cl}_4\text{Fe}_2\text{N}_{13}\text{O}_{18}\text{S}_4$: C, 54.0; H, 3.0; N, 9.2%.

6.4.4 Synthesis of the complex $[\text{Hg}_2(\text{L}^8)_2](\text{ClO}_4)_4$

To a suspension of L^8 (5.0 mg, 0.007 mmol) in nitromethane (2 ml) was added $\text{Hg}(\text{ClO}_4)_2 \cdot 6\text{H}_2\text{O}$ (3.6 mg, 0.007 mmol) and the suspension sonicated until all the ligand had dissolved giving a pale yellow solution. Filtration followed by the slow diffusion of diisopropyl ether vapour into the nitromethane solution resulted in the formation of colourless crystals of $[\text{Hg}_2(\text{L}^8)_2](\text{ClO}_4)_4$. ESI-MS m/z 2111 corresponding to $\{[\text{Hg}_2(\text{L}^8)_2](\text{ClO}_4)_3\}^+$. $[\text{Hg}_2(\text{L}^8)_2](\text{ClO}_4)_4$ (yield = 44 %).

6.4.5 Synthesis of L^9 complexes

6.4.5.1 Synthesis of the complex $[\text{Co}_2(\text{L}^9)_2](\text{BF}_4)_4$

To a suspension of L^9 (5.0 mg, 0.007 mmol) in nitromethane (2 ml) was added $\text{Co}(\text{BF}_4)_2 \cdot 6\text{H}_2\text{O}$ (2.3 mg, 0.007 mmol) and the suspension sonicated until all the ligand had dissolved giving an orange solution. Filtration followed by the slow diffusion of chloroform vapour into the nitromethane solution resulted in the formation of orange crystals of $[\text{Co}_2(\text{L}^9)_2](\text{BF}_4)_4$. ESI-MS m/z 1876 corresponding to $\{[\text{Co}_2(\text{L}^9)_2](\text{BF}_4)_3\}^+$. $[\text{Co}_2(\text{L}^9)_2](\text{BF}_4)_4$ (yield = 45 %). Found: C, 56.4; H, 2.9; N, 9.0 %. Calculated for $\text{C}_{92}\text{H}_{64}\text{B}_4\text{Co}_2\text{F}_{16}\text{N}_{12}\text{O}_2\text{S}_4$: C, 56.3; H, 3.3; N, 8.6 %

6.4.5.2 Synthesis of the complex $[\text{Cd}_2(\text{L}^9)_2](\text{ClO}_4)_4$

To a suspension of L^9 (5.0 mg, 0.007 mmol) in acetonitrile (2 ml) was added $\text{Cd}(\text{ClO}_4)_2 \cdot 6\text{H}_2\text{O}$ (2.8 mg, 0.007 mmol) and the suspension sonicated until all

the ligand had dissolved giving a pale yellow solution. Filtration followed by layering with diethyl resulted in the formation X-ray quality crystals of $[\text{Cd}_2(\text{L}^9)_2](\text{ClO}_4)_4$. ESI-MS m/z 2022 corresponding to $\{[\text{Cd}_2(\text{L}^9)_2](\text{ClO}_4)\}^+$. $[\text{Cd}_2(\text{L}^9)_2](\text{ClO}_4)_4$ (yield = 63 %). Found: C, 51.8; H, 3.0; N, 8.1%. Calculated for $\text{C}_{94}\text{H}_{67}\text{Cd}_2\text{Cl}_4\text{N}_{13}\text{O}_{18}\text{S}_4$: C, 52.2; H, 3.1; N, 8.4%.

6.4.6 Synthesis of the complex $[\text{Fe}_2(\text{L}^{10})_2](\text{ClO}_4)_4$

To a suspension of L^{10} (5.0 mg, 0.006 mmol) in acetonitrile (2 ml) was added $\text{Fe}(\text{ClO}_4)_2 \cdot 6\text{H}_2\text{O}$ (2.2 mg, 0.007 mmol) and the suspension sonicated until all the ligand had dissolved giving a deep purple solution. Filtration followed by the slow diffusion of chloroform vapour into the acetonitrile solution resulted in the formation of purple crystals of $[\text{Fe}_2(\text{L}^{10})_2](\text{ClO}_4)_4$. ESI-MS m/z 2084 corresponding to $\{[\text{Fe}_2(\text{L}^{10})_2](\text{ClO}_4)_3\}^+$. $[\text{Fe}_2(\text{L}^{10})_2](\text{ClO}_4)_4$ (yield = 75%). Found: C, 52.5; H, 3.2; N, 6.8%. Calculated for $\text{C}_{101}\text{H}_{81}\text{Cl}_7\text{Fe}_2\text{N}_{12}\text{O}_{22}\text{S}_4$: C, 52.7; H, 3.6; N, 7.3%.

6.4.7 Synthesis of the complex $[\text{Cd}_2(\text{L}^{11})_2](\text{ClO}_4)_4$

To a suspension of L^{11} (5.0 mg, 0.007 mmol) in nitromethane (2 ml) was added $\text{Cd}(\text{ClO}_4)_2 \cdot 6\text{H}_2\text{O}$ (2.9 mg, 0.007 mmol) and the suspension sonicated until all the ligand had dissolved. To this was added camphorsulfonic acid* (1.6 mg, 0.007 mmol) giving a pale yellow solution. Filtration followed by the slow diffusion of dichloromethane vapour into the nitromethane solution resulted in the formation of yellow crystals of $[\text{Cd}_2(\text{L}^{11})_2](\text{ClO}_4)_4$. ESI-MS m/z 1990 corresponding to $\{[\text{Cd}_2(\text{L}^{11})_2](\text{ClO}_4)_3\}^+$. $[\text{Cd}_2(\text{L}^{11})(\text{L}^{11}+\text{H})](\text{ClO}_4)_5$ (yield = 48%). Found: C, 49.0; H, 2.7; N, 8.7 %. Calculated for $\text{C}_{90}\text{H}_{63}\text{Cd}_2\text{Cl}_5\text{N}_{14}\text{O}_{20}\text{S}_4$: C, 49.3; H, 2.9; N, 9.0%.

6.4.8 Synthesis of the complex $[\text{Zn}_2(\text{L}^{12})_2](\text{ClO}_4)_4$

To a suspension of L^{12} (5.0 mg, 0.006 mmol) in nitromethane (2 ml) was added $\text{Zn}(\text{ClO}_4)_2 \cdot 6\text{H}_2\text{O}$ (2.4 mg, 0.006 mmol) and the suspension sonicated until all the ligand had dissolved giving a colourless solution. Filtration followed by the slow diffusion of dichloromethane vapour into the nitromethane solution

resulted in the formation of colourless crystals of $[\text{Zn}_2(\text{L}^{12})_2](\text{ClO}_4)_4$. ESI-MS m/z 1981 corresponding to $\{[\text{Zn}_2(\text{L}^{12})_2](\text{ClO}_4)_3\}^+ \cdot [\text{Zn}_2(\text{L}^{12})_2](\text{ClO}_4)_4$ (yield = 46%).

6.4.9 Synthesis of the complex $[\text{Zn}_2(\text{L}^{13})_2](\text{ClO}_4)_4$

To a suspension of L^{13} (5.0 mg, 0.006 mmol) in nitromethane (2 ml) was added $\text{Zn}(\text{ClO}_4)_2 \cdot 6\text{H}_2\text{O}$ (2.2 mg, 0.006 mmol) and the suspension sonicated until all the ligand had dissolved giving a colourless solution. Filtration followed by the slow diffusion of dichloromethane vapour into the nitromethane solution resulted in the formation of colourless crystals of $[\text{Zn}_2(\text{L}^{13})_2](\text{ClO}_4)_4$. ESI-MS m/z 2105 corresponding to $\{[\text{Zn}_2(\text{L}^{13})_2](\text{ClO}_4)_3\}^+ \cdot [\text{Zn}_2(\text{L}^{13})_2](\text{ClO}_4)_4$ (yield = 57 %).

6.4.10 Synthesis of the complex $[\text{Cd}_2(\text{L}^{14})_2](\text{ClO}_4)_4$

To a suspension of L^{14} (5.0 mg, 0.006 mmol) in acetonitrile (2 ml) was added $\text{Cd}(\text{ClO}_4)_2 \cdot 6\text{H}_2\text{O}$ (2.5 mg, 0.006 mmol) and the suspension sonicated until all the ligand had dissolved giving a colourless solution. Filtration followed by the slow diffusion of dichloromethane vapour into the acetonitrile solution resulted in the formation of colourless crystals of $[\text{Cd}_2(\text{L}^{14})_2](\text{ClO}_4)_4$. ESI-MS m/z 2173 corresponding to $\{[\text{Cd}_2(\text{L}^{14})_2](\text{ClO}_4)_3\}^+ \cdot [\text{Cd}_2(\text{L}^{14})_2](\text{ClO}_4)_4$ (yield = 55 %). Found: C, 55.2; H, 3.4; N, 7.1%. Calculated for $\text{C}_{104}\text{H}_{72}\text{Cd}_2\text{Cl}_4\text{N}_{12}\text{O}_{18}\text{S}_4$: C, 54.9; H, 3.2; N, 7.4%.

6.4.11 Synthesis of the complex $[\text{Cd}_2(\text{L}^{10})_2][\text{Cd}_2(\text{L}^{12}-\text{H})_2](\text{ClO}_4)_{10}$

To a suspension of L^{10} (5.0 mg, 0.006 mmol) and L^{11} (4.4 mg, 0.006 mmol) in nitromethane (2 ml) was added $\text{Cd}(\text{ClO}_4)_2 \cdot 6\text{H}_2\text{O}$ (5.0 mg, 0.012 mmol) and the suspension sonicated until all the ligand had dissolved. To this was added camphorsulfonic acid* (1.4 mg, 0.006 mmol) giving a colourless solution. Filtration followed by the slow diffusion of dichloromethane vapour into the nitromethane solution resulted in the formation of large colourless crystals of $[\text{Cd}_2(\text{L}^{10})_2][\text{Cd}_2(\text{L}^{12}-\text{H})_2](\text{ClO}_4)_{10}$. $[[\text{Cd}_2(\text{L}^{10})_2][\text{Cd}_2(\text{L}^{11}-\text{H})_2]](\text{ClO}_4)_{10}$ (yield = 62 %). Found: C, 48.8; H, 2.9; N, 7.5%. Calculated for $\text{C}_{190}\text{H}_{148}\text{Cd}_4\text{Cl}_{10}\text{N}_{26}\text{O}_{48}\text{S}_8$: C, 49.3; H, 3.2; N, 7.9%.

* Camphorsulfonic acid is used as it's a non-hygroscopic solid which is easy to weigh accurately and is soluble in a wide variety of solvents.

6.4.12 Synthesis of the complex $[(L^{15})_2Eu_2(H_2O)_2](CF_3SO_3)_4$

To a suspension of L^{15} (5.0 mg, 0.010 mmol) in nitromethane (2 ml) was added $Eu(CF_3SO_3)_3$ (5.9 mg, 0.010 mmol) and the suspension sonicated until all the ligand had dissolved giving a yellow solution. Filtration followed by the slow diffusion of chloroform vapour into the nitromethane solution resulted in the formation of yellow crystals of $[(L^{15})_2Eu_2(H_2O)_2](CF_3SO_3)_4$. ESI-MS m/z 1869 corresponding to $\{[(L^{15})_2Eu_2](CF_3SO_3)_3\}^+$. $[(L^{15})_2Eu_2](CF_3SO_3)_4$ (yield = 64%). Found C, 37.2; H, 2.0; N, 4.9%. Calculated for $C_{67}H_{41}Cl_3Eu_2F_{12}N_8O_{18}S_8$: C, 37.6; H, 1.8; N, 5.2%.

6.4.13 Synthesis of the complex $[(L^{16})_2La_2(H_2O)_2(CF_3SO_3)_2](CF_3SO_3)_4$

To a suspension of L^{16} (5.0 mg, 0.009 mmol) in nitromethane (2 ml) was added $La(CF_3SO_3)_3$ (5.0 mg, 0.009 mmol) and the suspension sonicated until all the ligand had dissolved giving a yellow solution. Filtration followed by the slow diffusion of diisopropyl ether vapour into the nitromethane solution resulted in the formation of X-ray quality crystals of $[(L^{16})_2La_2(H_2O)_2(CF_3SO_3)_2](CF_3SO_3)_4$. ESI-MS m/z 1887 corresponding to $\{[(L^{16})_2La_2](CF_3SO_3)_3\}^+$. $[(L^{16})_2La_2](CF_3SO_3)_4$ (yield = 50%). Found: C, 40.1; H, 2.0; N, 7.8%. Calculated for $C_{70}H_{46}F_{12}La_2N_{12}O_{16}S_8$: C, 40.5; H, 2.2; N, 8.1%

6.4.14 Synthesis of the complex $[(L^{17})_2Tb_2](CF_3SO_3)_4$

To a suspension of L^{17} (5.0 mg, 0.008 mmol) in nitromethane (2 ml) was added $Tb(CF_3SO_3)_3$ (4.9 mg, 0.008 mmol) and the suspension sonicated until all the ligand had dissolved giving a yellow solution. Filtration followed by the slow diffusion of diethyl ether vapour into the nitromethane solution resulted in the formation of X-ray quality crystals of $[(L^{17})_2Tb_2](CF_3SO_3)_4$. ESI-MS m/z 1991 corresponding to $\{[(L^{17})_2Tb_2](CF_3SO_3)_3\}^+$. $[(L^{17})_2Tb_2](CF_3SO_3)_4$ (yield = 59%). Found C, 38.4; H, 1.8; N, 7.9%. Calculated for $C_{71}H_{45}F_{12}N_{13}O_{20}S_8Tb_2$: C, 38.7; H, 2.1; N, 8.3%.

References

1. J. M. Lehn, *Supramolecular Chemistry: Concepts and Perspectives : a Personal Account Built Upon the George Fisher Baker Lectures in Chemistry at Cornell University [and The] Lezione Lincee, Accademia Nazionale Dei Lincei, Roma*, VCH, 1995.
2. P. D. Beer, P. A. Gale and D. K. Smith, *Supramolecular Chemistry*, Oxford University Press, 1999.
3. L. Jean-Marie, *Reports on Progress in Physics*, 2004, **67**, 249.
4. J. W. Steed, D. R. Turner and K. J. Wallace, *Core concepts in supramolecular chemistry and nanochemistry*, John Wiley, 2007.
5. J. W. Steed and J. L. Atwood, *Supramolecular Chemistry*, Wiley, 2000.
6. D. A. House and N. F. Curtis, *Journal of the American Chemical Society*, 1962, **84**, 3248-3250.
7. E. G. Jäger and E. Uhlig, *Zeitschrift für Chemie*, 1964, **4**, 437-437.
8. J. D. Curry and D. H. Busch, *Journal of the American Chemical Society*, 1964, **86**, 592-594.
9. C. J. Pedersen, *Journal of the American Chemical Society*, 1967, **89**, 2495-2496.
10. B. Dietrich, J. M. Lehn and J. P. Sauvage, *Journal of the Chemical Society D: Chemical Communications*, 1970, 1055-1056.
11. K. N. Trueblood, C. B. Knobler, E. Maverick, R. C. Helgeson, S. B. Brown and D. J. Cram, *Journal of the American Chemical Society*, 1981, **103**, 5594-5596.
12. D. B. Smithrud, E. M. Sanford, I. Chao, S. B. Ferguson, D. R. Carcanague, J. D. Evanseck, K. N. Houk and F. Diederich, *Pure Appl. Chem*, 1990, **62**, 2227-2236.
13. [http://www.docbrown.info/page04/4_72bond2.htm\(09-12-13\)](http://www.docbrown.info/page04/4_72bond2.htm(09-12-13)).
14. C. A. Hunter, K. R. Lawson, J. Perkins and C. J. Urch, *Journal of the Chemical Society, Perkin Transactions 2*, 2001, 651-669.
15. D. J. Cram, *Angewandte Chemie International Edition in English*, 1986, **25**, 1039-1057.
16. E. Fischer, *Berichte der deutschen chemischen Gesellschaft*, 1894, **27**, 2985-2993.

17. C. J. Pedersen, *Journal of the American Chemical Society*, 1967, **89**, 7017-7036.
18. C. J. Pedersen, *Angewandte Chemie International Edition in English*, 1988, **27**, 1021-1027.
19. C. J. Pedersen, *Journal of the American Chemical Society*, 1970, **92**, 391-394.
20. H. K. Frensdorff, *Journal of the American Chemical Society*, 1971, **93**, 600-606.
21. C. J. Pedersen, *Journal of the American Chemical Society*, 1970, **92**, 386-391.
22. R. D. Hancock and A. E. Martell, *Comments on Inorganic Chemistry*, 1988, **6**, 237-284.
23. B. Dietrich, J. M. Lehn and J. P. Sauvage, *Tetrahedron Letters*, 1969, **10**, 2889-2892.
24. B. Dietrich, J. M. Lehn and J. P. Sauvage, *Tetrahedron*, 1973, **29**, 1647-1658.
25. D. J. Cram, T. Kaneda, R. C. Helgeson and G. M. Lein, *Journal of the American Chemical Society*, 1979, **101**, 6752-6754.
26. D. J. Cram and G. M. Lein, *Journal of the American Chemical Society*, 1985, **107**, 3657-3668.
27. J. S. Bradshaw and P. E. Stott, *Tetrahedron*, 1980, **36**, 461-510.
28. J. C. Lockhart, A. C. Robson, M. E. Thompson, S. D. Furtado, C. K. Kaura and A. R. Allan, *Journal of the Chemical Society, Perkin Transactions 1*, 1973, 577-581.
29. J. Ennen and T. Kauffmann, *Angewandte Chemie International Edition in English*, 1981, **20**, 118-119.
30. G. W. Gokel, D. M. Dishong and C. J. Diamond, *Journal of the Chemical Society, Chemical Communications*, 1980, 1053-1054.
31. D. Philp and J. F. Stoddart, *Angewandte Chemie International Edition in English*, 1996, **35**, 1154-1196.
32. D. B. Amabilino and J. F. Stoddart, *Chemical Reviews*, 1995, **95**, 2725-2828.
33. J.-M. Lehn, *Proceedings of the National Academy of Sciences*, 2002, **99**, 4763-4768.

34. P. Linnartz and C. A. Schacly, 2004, **1**.
35. F. M. Raymo and J. F. Stoddart, *Chemical Reviews*, 1999, **99**, 1643-1664.
36. I. T. Harrison and S. Harrison, *Journal of the American Chemical Society*, 1967, **89**, 5723-5724.
37. R. B. Merrifield, *Journal of the American Chemical Society*, 1963, **85**, 2149-2154.
38. I. T. Harrison, *Journal of the Chemical Society, Perkin Transactions 1*, 1974, 301-304.
39. A. G. Kolchinski, D. H. Busch and N. W. Alcock, *Journal of the Chemical Society, Chemical Communications*, 1995, 1289-1291.
40. B. Chatterjee, *Organic Molecular Shuttles based on Rotaxanes*.
41. I. T. Harrison, *Journal of the Chemical Society, Chemical Communications*, 1972, 231-232.
42. P. R. Ashton, M. C. T. Fyfe, C. Schiavo, J. F. Stoddart, A. J. P. White and D. J. Williams, *Tetrahedron Letters*, 1998, **39**, 5455-5458.
43. D. B. Amabilino, P. R. Ashton, M. Belohradsky, F. M. Raymo and J. F. Stoddart, *Journal of the Chemical Society, Chemical Communications*, 1995, 747-750.
44. C. M. Keaveney and D. A. Leigh, *Angewandte Chemie International Edition*, 2004, **43**, 1222-1224.
45. L. Hogg, D. A. Leigh, P. J. Lusby, A. Morelli, S. Parsons and J. K. Y. Wong, *Angewandte Chemie International Edition*, 2004, **43**, 1218-1221.
46. E. C. Constable and A. M. W. C. Thompson, *Journal of the Chemical Society, Dalton Transactions*, 1994, 1409-1418.
47. M. Fujita, J. Yazaki and K. Ogura, *Journal of the American Chemical Society*, 1990, **112**, 5645-5647.
48. S. Roche, C. Haslam, S. L. Heath and J. A. Thomas, *Chemical Communications*, 1998, 1681-1682.
49. J. R. Nitschke and J.-M. Lehn, *Proceedings of the National Academy of Sciences*, 2003, **100**, 11970-11974.
50. G. S. Hanan, U. S. Schubert, D. Volkmer, E. Rivière, J.-M. Lehn, N. Kyritsakas and J. Fischer, *Canadian Journal of Chemistry*, 1997, **75**, 169-182.
51. J.-M. Lehn, *Chemical Society Reviews*, 2007, **36**, 151-160.

52. E. Breuning, M. Ruben, J.-M. Lehn, F. Renz, Y. Garcia, V. Ksenofontov, P. Gütllich, E. Wegelius and K. Rissanen, *Angewandte Chemie International Edition*, 2000, **39**, 2504-2507.
53. G. S. Hanan, D. Volkmer, U. S. Schubert, J.-M. Lehn, G. Baum and D. Fenske, *Angewandte Chemie International Edition in English*, 1997, **36**, 1842-1844.
54. G. F. Swiegers and T. J. Malefetse, *Chemical Reviews*, 2000, **100**, 3483-3538.
55. K. Nicole Power, T. L. Hennigar and M. J. Zaworotko, *New Journal of Chemistry*, 1998, **22**, 177-181.
56. P. N. W. Baxter, G. S. Hanan and J.-M. Lehn, *Chemical Communications*, 1996, 2019-2020.
57. H. Sleiman, P. Baxter, J.-M. Lehn and K. Rissanen, *Journal of the Chemical Society, Chemical Communications*, 1995, 715-716.
58. S. R. Seidel and P. J. Stang, *Accounts of Chemical Research*, 2002, **35**, 972-983.
59. M. Fujita, K. Umemoto, M. Yoshizawa, N. Fujita, T. Kusukawa and K. Biradha, *Chemical Communications*, 2001, 509-518.
60. M. Fujita, D. Oguro, M. Miyazawa, H. Oka, K. Yamaguchi and K. Ogura, *Nature*, 1995, **378**, 469-471.
61. P. J. Stang and D. H. Cao, *Journal of the American Chemical Society*, 1994, **116**, 4981-4982.
62. M. Fujita, O. Sasaki, T. Mitsuhashi, T. Fujita, J. Yazaki, K. Yamaguchi and K. Ogura, *Chemical Communications*, 1996, 1535-1536.
63. F. Ibukuro, T. Kusukawa and M. Fujita, *Journal of the American Chemical Society*, 1998, **120**, 8561-8562.
64. N. K. Al-Rasbi, I. S. Tidmarsh, S. P. Argent, H. Adams, L. P. Harding and M. D. Ward, *Journal of the American Chemical Society*, 2008, **130**, 11641-11649.
65. M. D. Ward, *Chemical Communications*, 2009, 4487-4499.
66. S. P. Argent, H. Adams, T. Riis-Johannessen, J. C. Jeffery, L. P. Harding and M. D. Ward, *Journal of the American Chemical Society*, 2005, **128**, 72-73.

67. S. P. Argent, H. Adams, T. Riis-Johannessen, J. C. Jeffery, L. P. Harding, O. Mamula and M. D. Ward, *Inorganic Chemistry*, 2006, **45**, 3905-3919.
68. M. D. Ward, J. A. McCleverty and J. C. Jeffery, *Coordination Chemistry Reviews*, 2001, **222**, 251-272.
69. P. L. Jones, A. J. Amoroso, J. C. Jeffery, J. A. McCleverty, E. Psillakis, L. H. Rees and M. D. Ward, *Inorganic Chemistry*, 1997, **36**, 10-18.
70. R. L. Paul, A. J. Amoroso, P. L. Jones, S. M. Couchman, Z. R. Reeves, L. H. Rees, J. C. Jeffery, J. A. McCleverty and M. D. Ward, *Journal of the Chemical Society, Dalton Transactions*, 1999, 1563-1568.
71. I. S. Tidmarsh, T. B. Faust, H. Adams, L. P. Harding, L. Russo, W. Clegg and M. D. Ward, *Journal of the American Chemical Society*, 2008, **130**, 15167-15175.
72. J. M. Lehn, A. Rigault, J. Siegel, J. Harrowfield, B. Chevrier and D. Moras, *Proceedings of the National Academy of Sciences*, 1987, **84**, 2565-2569.
73. C. Piguet, G. Bernardinelli and G. Hopfgartner, *Chemical Reviews*, 1997, **97**, 2005-2062.
74. E. C. Constable, F. R. Heitzler, M. Neuburger and M. Zehnder, *Supramolecular Chemistry*, 1995, **5**, 197-200.
75. E. C. Constable, F. R. Heitzler, M. Neuburger and M. Zehnder, *Chemical Communications*, 1996, 933-934.
76. E. C. Constable, F. Heitzler, M. Neuburger and M. Zehnder, *Journal of the American Chemical Society*, 1997, **119**, 5606-5617.
77. E. C. Constable, S. M. Elder, J. Healy, M. D. Ward and D. A. Tocher, *Journal of the American Chemical Society*, 1990, **112**, 4590-4592.
78. E. C. Constable and J. V. Walker, *Journal of the Chemical Society, Chemical Communications*, 1992, 884-886.
79. M. Barley, E. C. Constable, S. A. Corr, R. C. S. McQueen, J. C. Nutkins, M. D. Ward and M. G. B. Drew, *Journal of the Chemical Society, Dalton Transactions*, 1988, 2655-2662.
80. E. C. Constable, M. G. B. Drew and M. D. Ward, *Journal of the Chemical Society, Chemical Communications*, 1987, 1600-1601.

81. B. Hasenknopf, J. M. Lehn, G. Baum and D. Fenske, *Proceedings of the National Academy of Sciences of the United States of America*, 1996, **93**, 1397-1400.
82. V. C. M. Smith and J.-M. Lehn, *Chemical Communications*, 1996, 2733-2734.
83. Within reference 77 it is noted that Ligand J has been shown to form homoduplex helicates with Fe(II) or Ni(II). This work is however unpublished (B.Hasenknopf and J-M. Lehn)
84. V. Chaurin, E. C. Constable and C. E. Housecroft, *New Journal of Chemistry*, 2006, **30**, 1740-1744.
85. E. C. Constable, A. J. Edwards, P. R. Raithby, D. R. Smith, J. V. Walker and L. Whall, *Chemical Communications*, 1996, 2551-2552.
86. E. C. Constable, in *Progress in Inorganic Chemistry*, John Wiley & Sons, Inc., Editon edn., 2007, pp. 67-138.
87. E. C. Constable, A. J. Edwards, P. R. Raithby and J. V. Walker, *Angewandte Chemie International Edition in English*, 1993, **32**, 1465-1467.
88. T. Moeller, in *Werner Centennial*, AMERICAN CHEMICAL SOCIETY, Editon edn., 1967, vol. 62, pp. 306-317.
89. C. Piguet, C. Edder, S. Rigault, G. Bernardinelli, J.-C. G. Bunzli and G. Hopfgartner, *Journal of the Chemical Society, Dalton Transactions*, 2000, 3999-4006.
90. K. Meurer and F. Vögtle, Springer Berlin / Heidelberg, Editon edn., 1985, vol. 127, pp. 1-76.
91. E. C. Constable, T. Kulke, M. Neuburger and M. Zehnder, *Chemical Communications*, 1997, 489-490.
92. E. C. Constable, T. Kulke, G. Baum and D. Fenske, *Chemical Communications*, 1997, 2043-2044.
93. E. C. Constable, T. Kulke, G. Baum and D. Fenske, *Inorganic Chemistry Communications*, 1998, **1**, 80-82.
94. N. C. Fletcher, F. R. Keene, H. Viebrock and A. von Zelewsky, *Inorganic Chemistry*, 1997, **36**, 1113-1121.
95. O. Mamula, A. von Zelewsky, P. Brodard, C.-W. Schläpfer, G. Bernardinelli and H. Stoeckli-Evans, *Chemistry – A European Journal*, 2005, **11**, 3049-3057.

96. H. Mürner, A. von Zelewsky and G. Hopfgartner, *Inorganica Chimica Acta*, 1998, **271**, 36-39.
97. H.-L. Kwong, H.-L. Yeung, W.-S. Lee and W.-T. Wong, *Chemical Communications*, 2006, 4841-4843.
98. C. Piguet, G. Hopfgartner, B. Bocquet, O. Schaad and A. F. Williams, *Journal of the American Chemical Society*, 1994, **116**, 9092-9102.
99. M. Albrecht, *Chemistry – A European Journal*, 2000, **6**, 3485-3489.
100. M. Albrecht, *Chemical Society Reviews*, 1998, **27**, 281-288.
101. T. K. Ronson, H. Adams, T. Riis-Johannessen, J. C. Jeffery and M. D. Ward, *New Journal of Chemistry*, 2006, **30**, 26-28.
102. T. K. Ronson, H. Adams and M. D. Ward, *Inorganica Chimica Acta*, 2005, **358**, 1943-1954.
103. B. Hasenknopf, J.-M. Lehn, B. O. Kneisel, G. Baum and D. Fenske, *Angewandte Chemie International Edition in English*, 1996, **35**, 1838-1840.
104. B. Hasenknopf, J.-M. Lehn, N. Boumediene, A. Dupont-Gervais, A. Van Dorsselaer, B. Kneisel and D. Fenske, *Journal of the American Chemical Society*, 1997, **119**, 10956-10962.
105. C. Bonnefous, N. Bellec and R. P. Thummel, *Chemical Communications*, 1999, 1243-1244.
106. J. Hamblin, F. Tuna, S. Bunce, L. J. Childs, A. Jackson, W. Errington, N. W. Alcock, H. Nierengarten, A. Van Dorsselaer, E. Leize-Wagner and M. J. Hannon, *Chemistry – A European Journal*, 2007, **13**, 9286-9296.
107. L. Bain, S. Bullock, L. Harding, T. Riis-Johannessen, G. Midgley, C. R. Rice and M. Whitehead, *Chemical Communications*, 2010, **46**, 3496-3498.
108. K. E. Allen, R. A. Faulkner, L. P. Harding, C. R. Rice, T. Riis-Johannessen, M. L. Voss and M. Whitehead, *Angewandte Chemie International Edition*, 2010, **49**, 6655-6658.
109. O. Mamula, A. von Zelewsky and G. Bernardinelli, *Angewandte Chemie International Edition*, 1998, **37**, 289-293.
110. H. B. Tanh Jeazet, K. Gloe, T. Doert, O. N. Kataeva, A. Jager, G. Geipel, G. Bernhard, B. Buchner and K. Gloe, *Chemical Communications*, 2010, **46**, 2373-2375.
111. H. Cheng, D. Chun-ying, F. Chen-jie and M. Qing-jin, *Journal of the Chemical Society, Dalton Transactions*, 2000, 2419-2424.

112. N. Yoshida and K. Ichikawa, *Chemical Communications*, 1997, 1091-1092.
113. J. Rebek, *Accounts of Chemical Research*, 1984, **17**, 258-264.
114. J. Rebek and R. V. Wattlely, *Journal of the American Chemical Society*, 1980, **102**, 4853-4854.
115. C. J. Baylies, T. Riis-Johannessen, L. P. Harding, J. C. Jeffery, R. Moon, C. R. Rice and M. Whitehead, *Angewandte Chemie International Edition*, 2005, **44**, 6909-6912.
116. N. C. Gianneschi, P. A. Bertin, S. T. Nguyen, C. A. Mirkin, L. N. Zakharov and A. L. Rheingold, *Journal of the American Chemical Society*, 2003, **125**, 10508-10509.
117. D. A. Jose, I. Mon, H. Fernández-Pérez, E. C. Escudero-Adán, J. Benet-Buchholz and A. Vidal-Ferran, *Organic Letters*, 2011, **13**, 3632-3635.
118. T. Gunnlaugsson and F. Stomeo, *Organic & Biomolecular Chemistry*, 2007, **5**, 1999-2009.
119. C. Lincheneau, J. P. Leonard, T. McCabe and T. Gunnlaugsson, *Chemical Communications*, 2011, **47**, 7119-7121.
120. D. P. Funeriu, J.-M. Lehn, K. M. Fromm and D. Fenske, *Chemistry – A European Journal*, 2000, **6**, 2103-2111.
121. D. P. Funeriu, J.-M. Lehn, G. Baum and D. Fenske, *Chemistry – A European Journal*, 1997, **3**, 99-104.
122. R. Chotalia, E. C. Constable, M. Neuburger, D. R. Smith and M. Zehnder, *Journal of the Chemical Society, Dalton Transactions*, 1996, 4207-4216.
123. C. R. Rice, S. Worl, J. C. Jeffery, R. L. Paul and M. D. Ward, *Chemical Communications*, 2000, 1529-1530.
124. C. R. Rice, C. J. Baylies, J. C. Jeffery, R. L. Paul and M. D. Ward, *Inorganica Chimica Acta*, 2001, **324**, 331-335.
125. C. R. Rice, C. J. Baylies, H. J. Clayton, J. C. Jeffery, R. L. Paul and M. D. Ward, *Inorganica Chimica Acta*, 2003, **351**, 207-216.
126. A. Pfeil and J.-M. Lehn, *Journal of the Chemical Society, Chemical Communications*, 1992, 838-840.
127. R. Kramer, J. M. Lehn and A. Marquis-Rigault, *Proceedings of the National Academy of Sciences*, 1993, **90**, 5394-5398.

128. R. Krämer, J.-M. Lehn, A. De Cian and J. Fischer, *Angewandte Chemie International Edition in English*, 1993, **32**, 703-706.
129. It has been found that the chemical shift of the central phenylene unit is very susceptible to a change in the nuclearity of the circular helicate and lower nuclearity species (e.g. [M4L4]8+ compared with [M5L5]10+) tend to have a higher chemical shift compared to the pentanuclear species; the difference in chemical shift is also quite pronounced (>0.3 ppm), C.R. Rice, unpublished results.
130. S. G. Telfer, T. M. McLean and M. R. Waterland, *Dalton Transactions*, 2011, **40**, 3097-3108.
131. M. Ziegler and A. von Zelewsky, *Coordination Chemistry Reviews*, 1998, **177**, 257-300.
132. S. G. Telfer, N. Tajima and R. Kuroda, *Journal of the American Chemical Society*, 2004, **126**, 1408-1418.
133. M. Albrecht and S. Kotila, *Angewandte Chemie International Edition in English*, 1995, **34**, 2134-2137.
134. M. Albrecht and S. Kotila, *Chemical Communications*, 1996, **0**, 2309-2310.
135. M. Albrecht and C. Riether, *Chemische Berichte*, 1996, **129**, 829-832.
136. M. Meyer, B. Kersting, R. E. Powers and K. N. Raymond, *Inorganic Chemistry*, 1997, **36**, 5179-5191.
137. J. Xu, T. N. Parac and K. N. Raymond, *Angewandte Chemie International Edition*, 1999, **38**, 2878-2882.
138. F. Cui, S. Li, C. Jia, J. S. Mathieson, L. Cronin, X.-J. Yang and B. Wu, *Inorganic Chemistry*, 2011, **51**, 179-187.
139. M. C. Young, A. M. Johnson, A. S. Gamboa and R. J. Hooley, *Chemical Communications*, 2013, **49**, 1627-1629.
140. E. Burda, W. Bauer, W. Hummel and H. Gröger, *ChemCatChem*, 2010, **2**, 67-72.
141. W. Meng, J. K. Clegg, J. D. Thoburn and J. R. Nitschke, *Journal of the American Chemical Society*, 2011, **133**, 13652-13660.
142. A. Stephenson and M. D. Ward, *Chemical Communications*, 2012, **48**, 3605-3607.

143. A. Lavalette, F. Tuna, G. Clarkson, N. W. Alcock and M. J. Hannon, *Chemical Communications*, 2003, 2666-2667.
144. C. Piguet, A. F. Williams and G. Bernardinelli, *Angewandte Chemie International Edition in English*, 1992, **31**, 1622-1624.
145. N. Kaltsoyannis and P. Scott, *The f elements*, Oxford University Press, 1999.
146. B. V. Harbuzaru, A. Corma, F. Rey, J. L. Jordá, D. Ananias, L. D. Carlos and J. Rocha, *Angewandte Chemie International Edition*, 2009, **48**, 6476-6479.
147. S. J. A. Pope and R. H. Laye, *Dalton Transactions*, 2006, **0**, 3108-3113.
148. G. Muller, *Dalton Transactions*, 2009, **0**, 9692-9707.
149. J.-M. Senegas, S. Koeller, G. Bernardinelli and C. Piguet, *Chemical Communications*, 2005, **0**, 2235-2237.
150. B. Bocquet, G. Bernardinelli, N. Ouali, S. Floquet, F. Renaud, G. Hopfgartner and C. Piguet, *Chemical Communications*, 2002, **0**, 930-931.
151. M. Albrecht, O. Osetska, J.-C. G. Bünzli, F. Gummy and R. Fröhlich, *Chemistry – A European Journal*, 2009, **15**, 8791-8799.
152. M. Albrecht, Y. Liu, S. S. Zhu, C. A. Schalley and R. Frohlich, *Chemical Communications*, 2009, **0**, 1195-1197.
153. J. Leonard and T. Gunnlaugsson, *Journal of Fluorescence*, 2005, **15**, 585-595.
154. M. Albrecht and O. Osetska, *European Journal of Inorganic Chemistry*, 2010, **2010**, 4678-4682.
155. M. Elhabiri, R. Scopelliti, J.-C. G. Bünzli and C. Piguet, *Journal of the American Chemical Society*, 1999, **121**, 10747-10762.
156. N. Martin, J.-C. G. Bünzli, V. McKee, C. Piguet and G. Hopfgartner, *Inorganic Chemistry*, 1998, **37**, 577-589.
157. C. Piguet, J. C. G. Bünzli, G. Bernardinelli, G. Hopfgartner and A. F. Williams, *Journal of the American Chemical Society*, 1993, **115**, 8197-8206.
158. S. Torelli, D. Imbert, M. Cantuel, G. Bernardinelli, S. Delahaye, A. Hauser, J.-C. G. Bünzli and C. Piguet, *Chemistry – A European Journal*, 2005, **11**, 3228-3242.
159. C. Piguet, G. Hopfgartner, A. F. Williams and J.-C. G. Bünzli, *Journal of the Chemical Society, Chemical Communications*, 1995, **0**, 491-493.

160. C. Piguet, G. Bernardinelli, J.-C. G. Bünzli, S. Petoud and G. Hopfgartner, *Journal of the Chemical Society, Chemical Communications*, 1995, **0**, 2575-2577.
161. S. Floquet, M. Borkovec, G. Bernardinelli, A. Pinto, L.-A. Leuthold, G. Hopfgartner, D. Imbert, J.-C. G. Bünzli and C. Piguet, *Chemistry – A European Journal*, 2004, **10**, 1091-1105.
162. Y.-X. Chi, S.-Y. Niu, J. Jin, R. Wang and Y. Li, *Dalton Transactions*, 2009, **0**, 7653-7659.
163. S.-Y. Lin, L. Zhao, Y.-N. Guo, P. Zhang, Y. Guo and J. Tang, *Inorganic Chemistry*, 2012, **51**, 10522-10528.
164. B. El Aroussi, L. Guénée• e, P. Pal and J. Hamacek, *Inorganic Chemistry*, 2011, **50**, 8588-8597.
165. S. K. Mandal and K. Nag, *Journal of the Chemical Society, Dalton Transactions*, 1983, **0**, 2429-2434.
166. I. Antonini, F. Claudi, G. Cristalli, P. Franchetti, M. Grifantini and S. Martelli, *Journal of Medicinal Chemistry*, 1981, **24**, 1181-1184.
167. T. Riis-Johannessen, L. P. Harding, J. C. Jeffery, R. Moon and C. R. Rice, *Dalton Transactions*, 2007, **0**, 1577-1587.
168. N. M. Shavaleev, R. Scopelliti, F. Gumy and J.-C. G. Bünzli, *Inorganic Chemistry*, 2009, **48**, 7937-7946.
169. S. J. Bullock, L. P. Harding, M. P. Moore, A. Mills, S. A. F. Piela, C. R. Rice, L. Towns-Andrews and M. Whitehead, *Dalton Transactions*, 2013, **42**, 5805-5811.
170. A. P. Swain and S. K. Naegele, *Journal of the American Chemical Society*, 1957, **79**, 5250-5253.
171. A. Kayal, A. F. Ducruet and S. C. Lee, *Inorganic Chemistry*, 2000, **39**, 3696-3704.
172. R. Li, P. Ma, S. Dong, X. Zhang, Y. Chen, X. Li and J. Jiang, *Inorganic Chemistry*, 2007, **46**, 11397-11404.
173. S. T. Kadam and S. S. Kim, *Synthesis*, 2008, **2008**, 267-271.

Appendix 1: Crystal data tables

In general single crystal X-ray diffraction data was collected at 150(2) K on a Bruker Apex Duo diffractometer equipped with a graphite monochromated Mo(K α) radiation source and a cold stream of N₂ gas. Solutions were generated by conventional heavy atom Patterson or direct methods and refined by full-matrix least squares on all F^2 data, using SHELXS-97 and SHELXL software respectively.⁵ Absorption corrections were applied based on multiple and symmetry-equivalent measurements using SADABS.⁶ A number of crystal structures contained anion and/or solvent disorder this was modelled depending on the requirements of the data.

For example within $[\text{Zn}_5(\text{L}^1)_5](\text{CF}_3\text{SO}_3)_{10}$ a number of triflate anions and terminal diethylamide fragments were refined with geometric similarity restraints (SAME and SIMU). Additionally four triflate anions were modelled using two-component disorder models. Each component was treated as a rigid body (AFIX 9). The unit cell contained large amounts of diffuse electron density, presumably due to highly disordered interstitial solvent. However, attempts at modelling this were unsuccessful and the relevant scattering contributions were thus removed using the SQUEEZE routine in PLATON.

Generally anion and/or solvent disorder was modelled in two positions using the part instructions and constrained using DELU, SIMU, SADI and ISOR instructions in the least squares refinements. Specifically, for $[\text{Fe}_2(\text{L}^7)_2][\text{ClO}_4]_4$ the terminal phenyl spacer showed slight positional disorder resulting in large anisotropic displacement parameters. For simplicity five carbon atoms were constrained using DELU and SIMU constrains and one was further constrained using ISOR. Additionally $[\text{Cd}_2(\text{L}^9)_2][\text{ClO}_4]_4$ contained a substitution disorder comprising of a molecule of acetonitrile and a water molecule and these were modelled in two positions using the part instruction and were both constrained

⁵ SHELXTL Program System, Vers. 5.1, Bruker Analytical X-ray Instruments Inc., Madison, WI, 1998.

⁶ G. M. Sheldrick, SADABS: A Program for Absorption Correction with the Siemens SMART System, University of Göttingen (Germany), 1996

using DELU and SIMU and the bond lengths of the acetonitrile molecule constrained using DFIX.

The crystals of $[\text{Zn}_2(\mathbf{L}^9)]_2[\text{CF}_3\text{SO}_3]_2$ decomposed rapidly and despite exhaustive attempts to collect data and growing the crystals under different conditions (changing solvents, counter ions and temperature) only very poorly diffracting crystals were formed. However, despite this data was collected and a gross molecular structure was obtained but contained severe disorder of a triflate counter ion and solvent molecules and to obtain data of reasonable quality the diffuse electron density was removed using the solvent mask facility in Olex2,⁷ resulting in very large voids in the crystal structure. The solvent mask removed a total of 611.4 electrons in the unit cell which corresponds to triflate anion and one ethyl acetate and nitromethane solvent molecules per helicate complex (which corresponds to a total of 612 electrons in the unit cell). Given the obvious problems associated with extensive anion disorder in this crystal structure any structural discussion has been omitted manuscript apart from being confident that the gross solution is correct and that the complex is isostructural with $[\text{Co}_2(\mathbf{L}^9)]_2[\text{BF}_4]_4$ (i.e. a *meso*-helicate).

For the one-dimensional chain $[[\text{Cd}_2(\mathbf{L}^{10})_2][\text{Cd}_2(\mathbf{L}^{11}\text{-H})_2]](\text{ClO}_4)_{10}$ the crystals of this species diffracted poorly so data was limited to $2\theta = 50$. The glycol chain was refined isotropically as a satisfactory anisotropic disordered model could not be found. The majority of the solvent water positions, one CH_2Cl_2 and two ClO_4 anions were refined isotropically. The C-Cl distances of one CH_2Cl_2 and the Cl-O distances of one ClO_4 were restrained to be chemically reasonable.

⁷ O. V. Dolomanov, L. J. Bourhis, R. J. Gildea, J. A. K. Howard and H. Puschmann, OLEX2: a complete structure solution, refinement and analysis program. *J. Appl. Cryst.* (2009). **42**, 339-341.

Table A1. Crystallographic data of L^1 complex $[Zn_5(L^1)_5]^{10+}$

Compound	$[Zn_5(L^1)_5](CF_3SO_3)_{10}$
Formula	$C_{230}H_{270}F_{30}N_{40}O_{60}S_{20}Zn_5$
M	6092.91
Crystal system	Triclinic
Space group	P-1
Unit cell dimensions	
a (Å)	20.3776(13)
b (Å)	21.5461(15)
c (Å)	28.7397(19)
α (°)	79.876(2)
β (°)	85.013(2)
γ (°)	77.697(2)
V (Å ³)	12120.6(1)
Z	2
ρ_{calc} (Mg cm ⁻³)	1.669
$F(000)$	6300
Crystal dimensions (mm)	0.5, 0.2, 0.2
Reflections collected	131442
Range	$1.44 \leq \theta \leq 23.37^\circ$
hkl range indices	$-22 \leq h \leq 22, -24 \leq k \leq 23, -31 \leq l \leq 32$
Unique reflections	35025
R_{int}	0.0667
R_w	0.2819
R	0.1032
Reflections with $I > 2\sigma(I)$	22284
GOF	1.069
Refined parameters	2360
Restraints	369
Largest peak and hole (e Å ⁻³)	1.417, -1.425

Table A2. Crystallographic data of L^6 complex $[Cu_2(L^6)_2]^{4+}$

Compound	$[Cu_2(L^6)_2][ClO_4]_4$
Formula	$C_{84.37} H_{62.06} Cl_4 Cu_2 N_{16.18} O_{16} S_4$
M	1955.71
Crystal system	Triclinic
Space group	P-1
Unit cell dimensions	
a (Å)	15.2185(8)
b (Å)	17.9346(11)
c (Å)	18.4590(12)
α (°)	112.4660(10)
β (°)	94.9120(10)
γ (°)	98.333(2)
V (Å ³)	4551.5(5)
Z	2
ρ_{calc} (Mg cm ⁻¹)	1.427
$F(000)$	1999
Crystal dimensions (mm)	0.3, 0.25, 0.1
Reflections collected	104298
Range	$1.88 \leq \theta \leq 31.37^\circ$
hkl range indices	$-21 \leq h \leq 22, -25 \leq k \leq 25, -26 \leq l \leq 26$
Unique reflections	28137
R_{int}	0.0566
R_w	0.2031
R	0.0687
Reflections with $I > 2\sigma(I)$	16524
GOF	1.02
Refined parameters	1224
Restraints	85
Largest peak and hole (e Å ⁻³)	1.680, -0.707

Table A3. Crystallographic data of L^7 complex $[Fe_2(L^7)_2]^{4+}$

Compound	$[Fe_2(L^7)_2][ClO_4]_4$
Formula	$C_{45}H_{31}Cl_2FeN_7O_{10}S_2$
M	1020.64
Crystal system	Orthorhombic
Space group	Cmca
Unit cell dimensions	
a (Å)	45.5093(11)
b (Å)	22.2219(5)
c (Å)	17.1211(4)
α (°)	90
β (°)	90
γ (°)	90
V (Å ³)	17314.6(7)
Z	16
ρ_{calc} (Mg cm ⁻¹)	1.566
$F(000)$	8352
Crystal dimensions (mm)	0.5, 0.4, 0.2
Reflections collected	46105
Range	$1.79 \leq \theta \leq 28.42^\circ$
hkl range indices	$-60 \leq h \leq 60, -29 \leq k \leq 25, -22 \leq l \leq 15$
Unique reflections	10977
R_{int}	0.0544
R_w	0.1368
R	0.0552
Reflections with $I > 2\sigma(I)$	6702
GOF	1.019
Refined parameters	620
Restraints	48
Largest peak and hole (e Å ⁻³)	1.129, -0.828

Table A4. Crystallographic data of L^8 complex $[Hg_2(L^8)_2]^{4+}$

Compound	$[Hg_2(L^8)_2][ClO_4]_4$
Formula	$C_{89}H_{63}Cl_4Hg_2N_{17}O_{22}S_4$
M	2393.78
Crystal system	Monoclinic
Space group	P2(1)/c
Unit cell dimensions	
a (Å)	17.5144(7)
b (Å)	26.3233(10)
c (Å)	19.1644(7)
α (°)	90
β (°)	98.5960(10)
γ (°)	90
V (Å ³)	8736.2(6)
Z	4
ρ_{calc} (Mg cm ⁻¹)	1.82
F(000)	4736
Crystal dimensions (mm)	0.3, 0.3, 0.2
Reflections collected	83581
Range	$1.66 \leq \theta \leq 27.88^\circ$
hkl range indices	$-23 \leq h \leq 23, -34 \leq k \leq 34, -25 \leq l \leq 25$
Unique reflections	20762
R_{int}	0.0579
R_w	0.0569
R	0.0324
Reflections with $I > 2\sigma(I)$	15429
GOF	0.999
Refined parameters	1274
Restraints	18
Largest peak and hole (e Å ⁻³)	1.131, -0.793

Table A5. Crystallographic data of L^9 complex $[Zn_2(L^9)_2]^{4+}$

Compound	$[Zn_2(L^9)_2][CF_3SO_3]_4$
Formula	$C_{101} H_{75} F_{12} N_{13} O_{18} S_8 Zn_2$
M	1926.81
Crystal system	monoclinic
Space group	C 2/c
Unit cell dimensions	
a (Å)	40.525(4)
b (Å)	24.073(2)
c (Å)	12.188(1)
α (°)	90
β (°)	105.746(2)
γ (°)	90
V (Å ³)	11443.7(18)
Z	4
ρ_{calc} (Mg cm ⁻¹)	1.1183
$F(000)$	3951.1988
Crystal dimensions (mm)	0.30, 0.15, 0.15
Reflections collected	53010
Range	$1.74 \leq \theta \leq 28.46^\circ$
hkl range indices	$-54 \leq h \leq 52, 0 \leq k \leq 32, 0 \leq l \leq 16$
Unique reflections	14217
R_{int}	0.0675
R_w	0.2050
R	0.0635
Reflections with $I > 2\sigma(I)$	6799
GOF	0.9818
Refined parameters	578
Restraints	0
Largest peak and hole (e Å ⁻³)	0.7212, -0.9532

Table A6. Crystallographic data of L^9 complex $[Co_2(L^9)_2]^{4+}$

Compound	$[Co_2(L^9)_2][BF_4]_4$
Formula	$C_{96} H_{68} B_4 Cl_{12} Co_2 F_{16} N_{12} O_2 S_4$
M	2440.36
Crystal system	Triclinic
Space group	P-1
Unit cell dimensions	
a (Å)	11.2403(4)
b (Å)	14.2668(6)
c (Å)	15.9890(6)
α (°)	97.9160(10)
β (°)	102.7040(10)
γ (°)	91.6320(10)
V (Å ³)	2472.85(16)
Z	1
ρ_{calc} (Mg cm ⁻¹)	1.639
$F(000)$	1230
Crystal dimensions (mm)	0.30, 0.30, 0.15
Reflections collected	56159
Range	$1.32 \leq \theta \leq 30.51^\circ$
hkl range indices	$-16 \leq h \leq 16, -20 \leq k \leq 20, -22 \leq l \leq 22$
Unique reflections	14975
R_{int}	0.0518
R_w	0.1684
R	0.0611
Reflections with $I > 2\sigma(I)$	9866
GOF	1.041
Refined parameters	669
Restraints	0
Largest peak and hole (e Å ⁻³)	1.469, -1.185

Table A7. Crystallographic data of L^9 complex $[Cd_2(L^9)_2]^{4+}$

Compound	$[Cd_2(L^9)_2][ClO_4]_4$
Formula	$C_{201}H_{152}Cd_4C_{18}N_{33}O_{38}S_8$
M	4627.24
Crystal system	Triclinic
Space group	P-1
Unit cell dimensions	
a (Å)	12.6829(8)
b (Å)	16.4451(10)
c (Å)	25.0185(14)
α (°)	94.6030(10)
β (°)	101.5490(10)
γ (°)	97.467(2)
V (Å ³)	5038.7(5)
Z	1
ρ_{calc} (Mg cm ⁻³)	1.525
F(000)	2349
Crystal dimensions (mm)	0.2, 0.2, 0.1
Reflections collected	112792
Range	$1.43 \leq \theta \leq 30.03^\circ$
hkl range indices	$-17 \leq h \leq 17, -23 \leq k \leq 23, -35 \leq l \leq 33$
Unique reflections	29420
R_{int}	0.0807
R_w	0.1302
R	0.0591
Reflections with $I > 2\sigma(I)$	16062
GOF	1.018
Refined parameters	1360
Restraints	30
Largest peak and hole (e Å ⁻³)	1.095, -0.989

Table A8. Crystallographic data of L^{10} complex $[Fe_2(L^{10})_2][ClO_4]_4^{4+}$

Compound	$[Fe_2(L^{10})_2][ClO_4]_4$
Formula	$C_{108}H_{90}Cl_{16}Fe_2N_{14}O_{22}S_4$
M	2743.08
Crystal system	Triclinic
Space group	P-1
Unit cell dimensions	
a (Å)	11.7211(6)
b (Å)	13.4503(8)
c (Å)	21.2922(12)
α (°)	104.0930(10)
β (°)	96.2950(10)
γ (°)	110.1670(10)
V (Å ³)	2986.2(3)
Z	1
ρ_{calc} (Mg cm ⁻¹)	1.525
$F(000)$	1400
Crystal dimensions (mm)	0.50, 0.26, 0.03
Reflections collected	55213
Range	$1.69 \leq \theta \leq 28.72^\circ$
hkl range indices	$-15 \leq h \leq 14, -17 \leq k \leq 17, -28 \leq l \leq 28$
Unique reflections	14883
R_{int}	0.0774
R_w	0.1325
R	0.0596
Reflections with $I > 2\sigma(I)$	8603
GOF	1.016
Refined parameters	751
Restraints	0
Largest peak and hole (e Å ⁻³)	1.518, -1.128

Table A9. Crystallographic data of L^{11} complex $[Cd_2(L^{11})(L^{11}-H)]^{5+}$

Compound	$[Cd_2(L^{11})(L^{11}-H)_2](ClO_4)_5$
Formula	$C_{94.86}H_{75.57}Cd_2Cl_{13}N_{14.86}O_{22.71}S_4$
M	2600.83
Crystal system	Triclinic
Space group	P-1
Unit cell dimensions	
a (Å)	13.8209(7)
b (Å)	18.3351(9)
c (Å)	21.5994(10)
α (°)	95.0080(10)
β (°)	92.1730(10)
γ (°)	107.4850(10)
V (Å ³)	5188.8(4)
Z	2
ρ_{calc} (Mg cm ⁻³)	1.665
F(000)	2622.8
Crystal dimensions (mm)	0.40, 0.3, 0.01
Reflections collected	118786
Range	$1.43 \leq \theta \leq 30.51$
hkl range indices	$-19 \leq h \leq 19, -26 \leq k \leq 26, -30 \leq l \leq 30$
Unique reflections	31560
R_{int}	0.0580
R_w	0.1514
R	0.0588
Reflections with $I > 2\sigma(I)$	20025
GOF	1.045
Refined parameters	1401
Restraints	52
Largest peak and hole (e Å ⁻³)	1.888, -1.980

Table A10. Crystallographic data of L^{12} complex $[Zn_2(L^{12})_2]^{4+}$

Compound	$[Zn_2(L^{12})_2][ClO_4]$
Formula	C24 H18 Cl N4 O5.5 S Zn0.5
M	550.65
Crystal system	Triclinic
Space group	P-1
Unit cell dimensions	
a (Å)	12.5839(5)
b (Å)	12.9897(6)
c (Å)	19.7481(8)
α (°)	85.377(1)
β (°)	82.463(1)
γ (°)	68.636(1)
V (Å ³)	2978.4(2)
Z	4
ρ_{calc} (Mg cm ⁻¹)	1.2279
$F(000)$	1130.2089
Reflections collected	55104
Range	$1.68 \leq \theta \leq 27.88^\circ$
hkl range indices	$-16 \leq h \leq 16, -17 \leq k \leq 17, -25 \leq l \leq 25$
Unique reflections	14123
R_{int}	0.0538
R	0.048156
Reflections with $I > 2\sigma(I)$	9827
GOF	1.013791
Refined parameters	661
Restraints	0
Largest peak and hole (e Å ⁻³)	1.086330, -0.891055

Table A11. Crystallographic data of L^{13} complex $[Zn_2(L^{13})_2]^{4+}$

Compound	$[Zn_2(L^{13})_2][ClO_4]_4$
Formula	$C_{114.956} H_{94} Cl_{22.333} N_{15.789} O_{22.579} S_4 Zn_2$
M	3108.71
Crystal system	Triclinic
Space group	P -1
Unit cell dimensions	
a (Å)	14.4009(7)
b (Å)	20.9146(11)
c (Å)	22.4441(12)
α (°)	80.955(1)
β (°)	84.776(1)
γ (°)	83.257(1)
V (Å ³)	6611.5(6)
Z	2
ρ_{calc} (Mg cm ⁻¹)	1.5614
$F(000)$	3167.1135
Crystal dimensions (mm)	0.5, 0.3, 0.2
Reflections collected	120152
Range	$1.43 \leq \theta \leq 28.28^\circ$
hkl range indices	$-19 \leq h \leq 19, -27 \leq k \leq 27, -29 \leq l \leq 29$
Unique reflections	32500
R_{int}	0.0712
R	0.0665
Reflections with $I > 2\sigma(I)$	18703
GOF	1.0786
Refined parameters	1699
Restraints	174
Largest peak and hole (e Å ⁻³)	2.0134, -1.4919

Table A12. Crystallographic data of L^{14} complex $[Cd_2(L^{14})_2]^{4+}$

Compound	$[Cd_2(L^{14})_2][ClO_4]_4$
Formula	$C_{110.95} H_{82.43} Cd_2 Cl_4 N_{15.47} O_{18} S_4$
M	2415.24
Crystal system	Monoclinic
Space group	P 1 21/c
Unit cell dimensions	
a (Å)	21.7000(11)
b (Å)	12.4488(6)
c (Å)	22.2200(11)
α (°)	90
β (°)	117.0500(10)
γ (°)	90
V (Å ³)	5345.9(5)
Z	2
ρ_{calc} (Mg cm ⁻¹)	1.500
$F(000)$	2457
Crystal dimensions (mm)	0.4, 0.15, 0.12
Reflections collected	53131
Range	$1.84 \leq \theta \leq 28.33^\circ$
hkl range indices	$-28 \leq h \leq 28, -8 \leq k \leq 16, -29 \leq l \leq 29$
Unique reflections	13301
R_{int}	0.0618
R_w	0.1503
R	0.0546
Reflections with $I > 2\sigma(I)$	8746
GOF	1.023
Refined parameters	734
Restraints	60
Largest peak and hole (e Å ⁻³)	2.560, -0.920

Table A13. Crystallographic data of L^{10} and L^{11} complex $[\text{Cd}_2(L^{10})_2][\text{Cd}_2(L^{11}-\text{H})_2]^{10+}$

Compound	$[\text{Cd}_2(L^{10})_2][\text{Cd}_2(L^{11}-\text{H})_2]^{10+}$
Formula	$\text{C}_{98}\text{H}_{93}\text{Cd}_2\text{Cl}_{10}\text{N}_{13}\text{O}_{30.50}\text{S}_4$
M	2648.39
Crystal system	Monoclinic
Space group	P2(1)/c
Unit cell dimensions	
a (Å)	13.3018(3)
b (Å)	20.7598(4)
c (Å)	44.2313(9)
α (°)	90
β (°)	91.2640(10)
γ (°)	90
V (Å ³)	12211.2(4)
Z	4
ρ_{calc} (Mg cm ⁻¹)	1.441
$F(000)$	5384
Crystal dimensions (mm)	0.50, 0.18, 0.07
Reflections collected	104867
Range	$1.35 \leq \theta \leq 25.00^\circ$
hkl range indices	$-15 \leq h \leq 15, -246 \leq k \leq 24, -52 \leq l \leq 52$
Unique reflections	21329
R_{int}	0.0686
R_w	0.3254
R	0.1202
Reflections with $I > 2\sigma(I)$	13700
GOF	2.239
Refined parameters	1304
Restraints	6
Largest peak and hole (e Å ⁻³)	2.296, -1.509

Table A14. Crystallographic data of L^{15} complex $[(L^{15})_2Eu_2]^{4+}$

Compound	$[(L^{15})_2Eu_2](CF_3SO_3)_4$
Formula	$C_{70.907}H_{44}Cl_{7.561}Eu_2F_{12}N_{10.386}O_{24.773}S_8$
M	2494.35
Crystal system	Monoclinic
Space group	$C2/c$
Unit cell dimensions	
a (Å)	22.4400(4)
b (Å)	17.4669(3)
c (Å)	23.2350(5)
α (°)	90
β (°)	91.603
γ (°)	90
V (Å ³)	9103.6(3)
Z	4
ρ_{calc} (Mg cm ⁻³)	1.671
$F(000)$	4934.5601
Crystal dimensions (mm)	0.25, 0.25, 0.15
Reflections collected	53586
Range	$1.71 \leq \theta \leq 30.03^\circ$
hkl range indices	$-31 \leq h \leq 31, -24 \leq k \leq 24, -32 \leq l \leq 32$
Unique reflections	13292
R_{int}	0.0396
R_w	0.0831
R	0.0345
Reflections with $I > 2\sigma(I)$	10278
GOF	1.059
Refined parameters	567
Restraints	31
Largest peak and hole (e Å ⁻³)	1.342, -1.296

Table A15. Crystallographic data of L^{16} complex $[(L^{16})_2La_2]^{4+}$

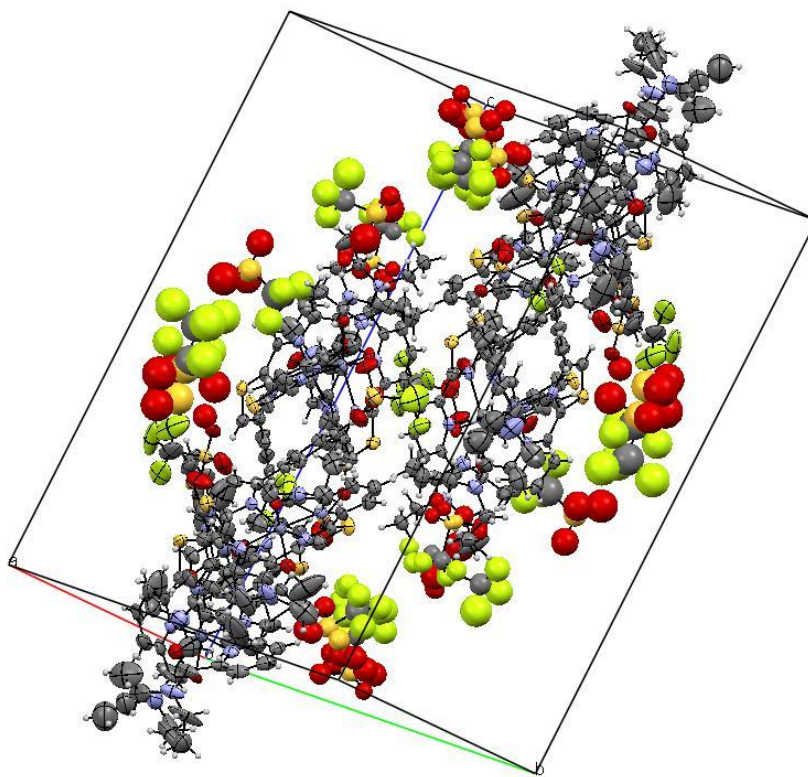
Compound	$[(L^{16})_2La_2](CF_3SO_3)_4$
Formula	$C_{36.50} H_{27.50} F_6 La N_{7.50} O_{11} S_4$
M	1128.31
Crystal system	Triclinic
Space group	P-1
Unit cell dimensions	
a (Å)	14.3142(13)
b (Å)	17.3019(16)
c (Å)	17.810(2)
α (°)	88.810(3)
β (°)	89.053(3)
γ (°)	70.987(5)
V (Å ³)	4169.1(7)
Z	x
ρ_{calc} (Mg cm ⁻¹)	1.798
$F(000)$	2248
Crystal dimensions (mm)	0.20, 0.20, 0.10
Reflections collected	28806
Range	$1.50 \leq \theta \leq 24.81^\circ$
hkl range indices	$-16 \leq h \leq 16, -20 \leq k \leq 20, -20 \leq l \leq 20$
Unique reflections	14150
R_{int}	0.0736
R_w	0.0886
R	0.0494
Reflections with $I > 2\sigma(I)$	8826
GOF	0.954
Refined parameters	1210
Restraints	78
Largest peak and hole (e Å ⁻³)	0.954, -0.977

Table A16. Crystallographic data of L^{17} complex $[(L^{17})_2Tb_2]^{4+}$

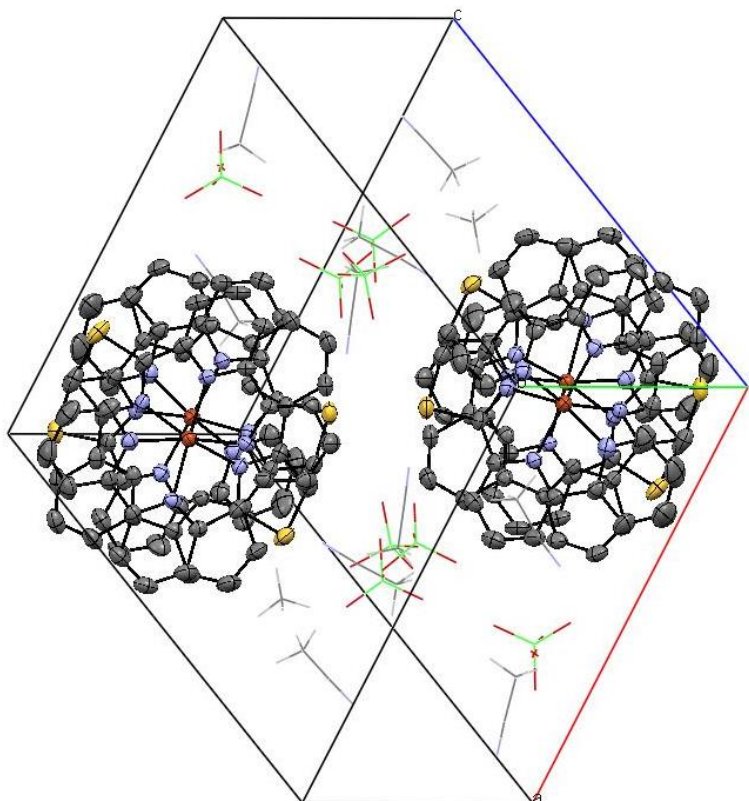
Compound	$[(L^{17})_2Tb_2](CF_3SO_3)_4$
Formula	$C_{75.10} H_{57.29} F_{12} N_{17.10} O_{27.75} S_8 Tb_2$
M	2445.45
Crystal system	Monoclinic
Space group	P2(1)/n
Unit cell dimensions	
a (Å)	19.1137(8)
b (Å)	20.0995(8)
c (Å)	24.0305(10)
α (°)	90
β (°)	99.2700(10)
γ (°)	90
V (Å ³)	9111.4(6)
Z	4
ρ_{calc} (Mg cm ⁻¹)	1.783
$F(000)$	4862
Crystal dimensions (mm)	0.30, 0.20, 0.20
Reflections collected	88947
Range	$1.48 \leq \theta \leq 27.88^\circ$
hkl range indices	$-25 \leq h \leq 25, -26 \leq k \leq 26, -31 \leq l \leq 31$
Unique reflections	21738
R_{int}	0.0602
R_w	0.1299
R	0.0508
Reflections with $I > 2\sigma(I)$	15968
GOF	1.053
Refined parameters	1493
Restraints	633
Largest peak and hole (e Å ⁻³)	2.554, -1.750

Appendix 2: Crystal packing

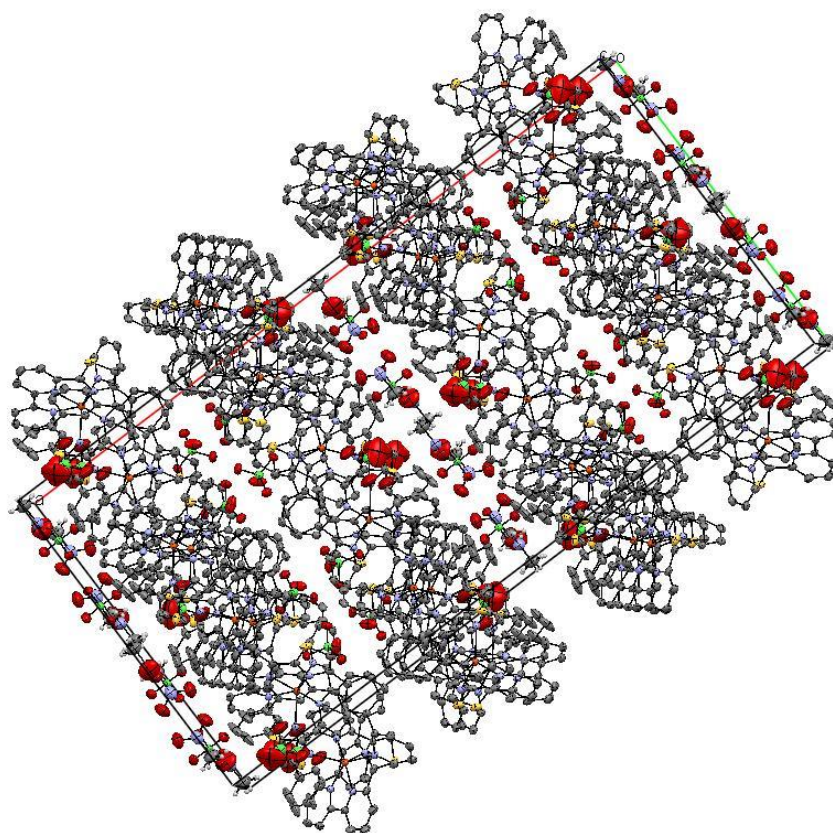
A2.1. Packing of L^1 complex $[Zn_5(L^1)_5]^{10+}$



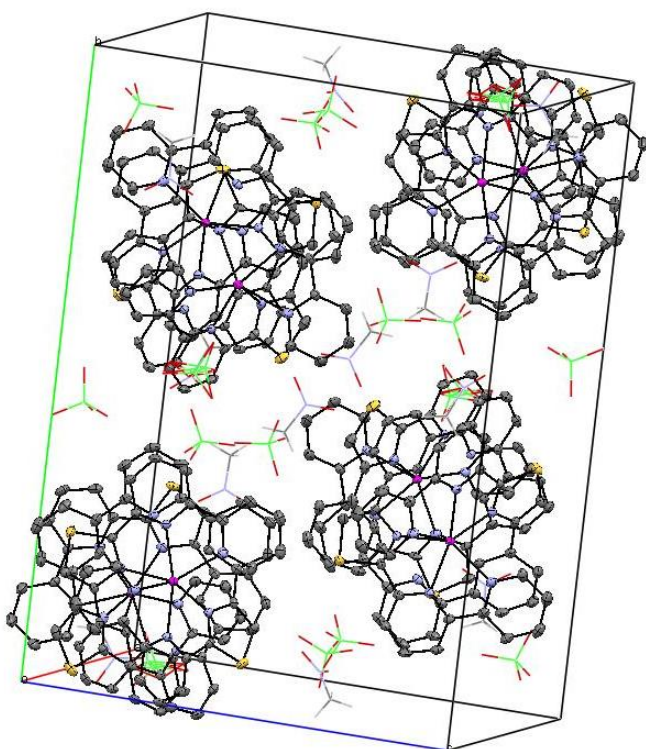
A2.2 Packing of L^6 complex $[Cu_2(L^6)_2]^{4+}$



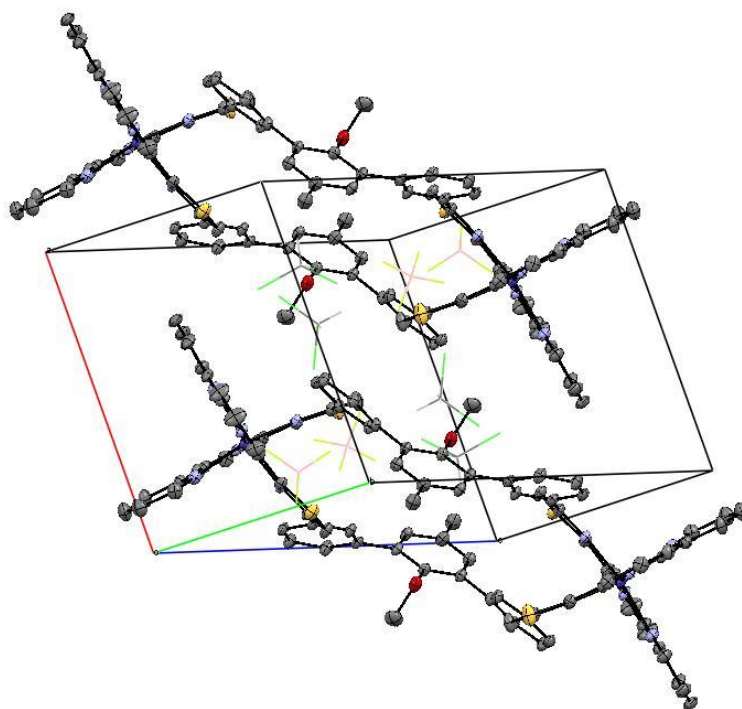
A2.3. Packing of L^7 complex $[Fe_2(L^7)_2]^{4+}$



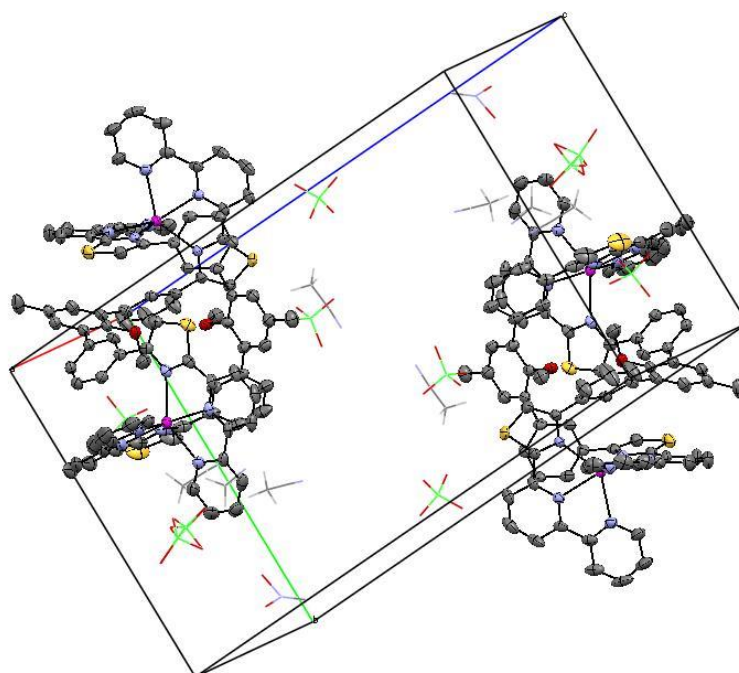
A2.4. Packing of L^8 complex $[Hg_2(L^8)_2]^{4+}$



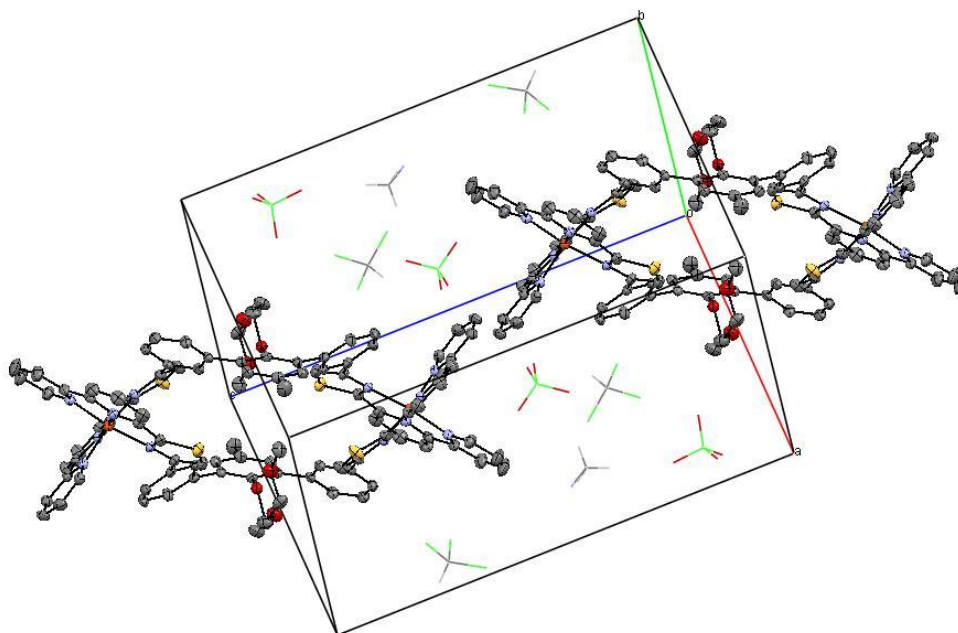
A2.5. Packing of L^9 complex $[Co_2(L^9)_2]^{4+}$



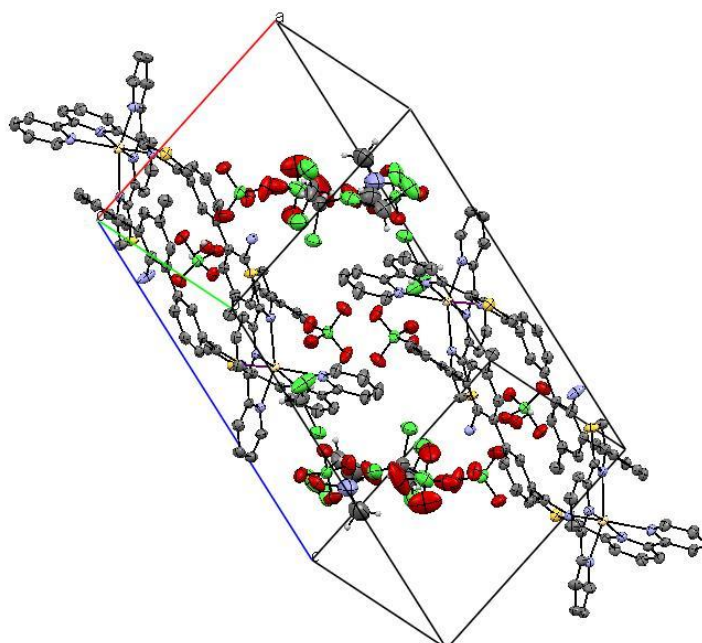
A2.6. Packing of L^9 complex $[Cd_2(L^9)_2]^{4+}$



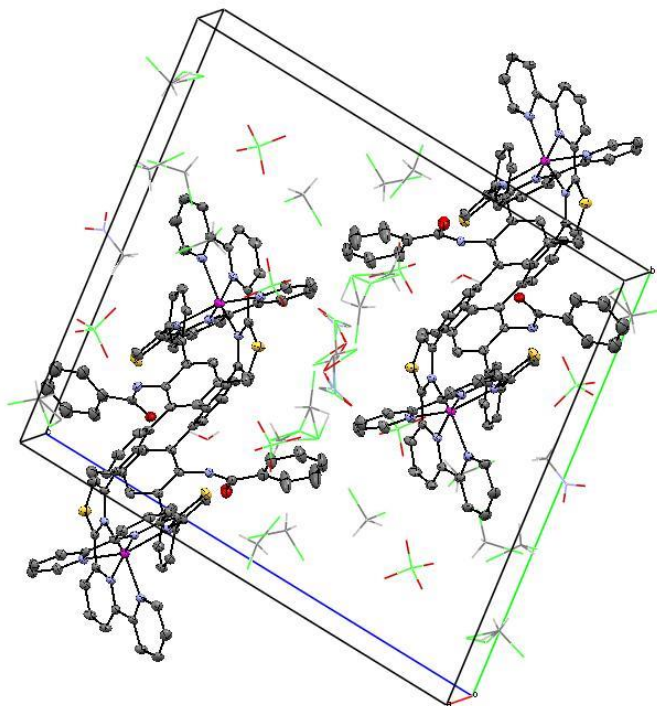
A2.7. Packing of L^{10} complex $[Fe_2(L^{10})_2]^{4+}$



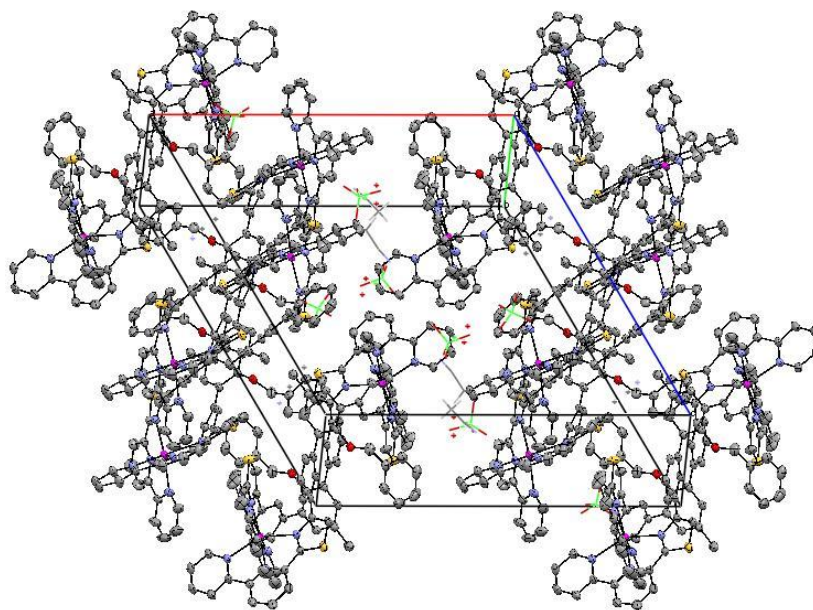
A2.8. Packing of L^{11} complex $[Cd_2(L^{11})(L^{11}-H)]^{5+}$



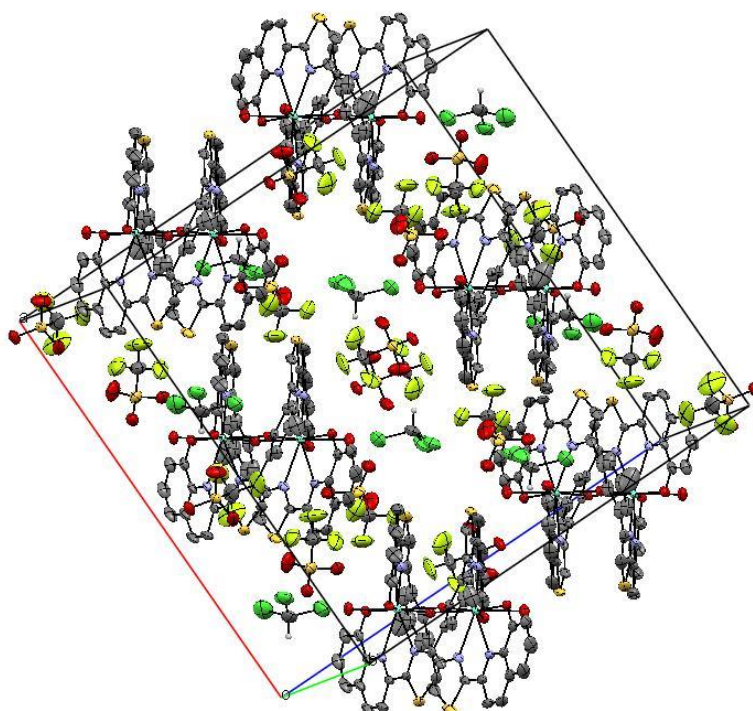
A2.9. Packing of L^{13} complex $[Zn_2(L^{13})_2]^{4+}$



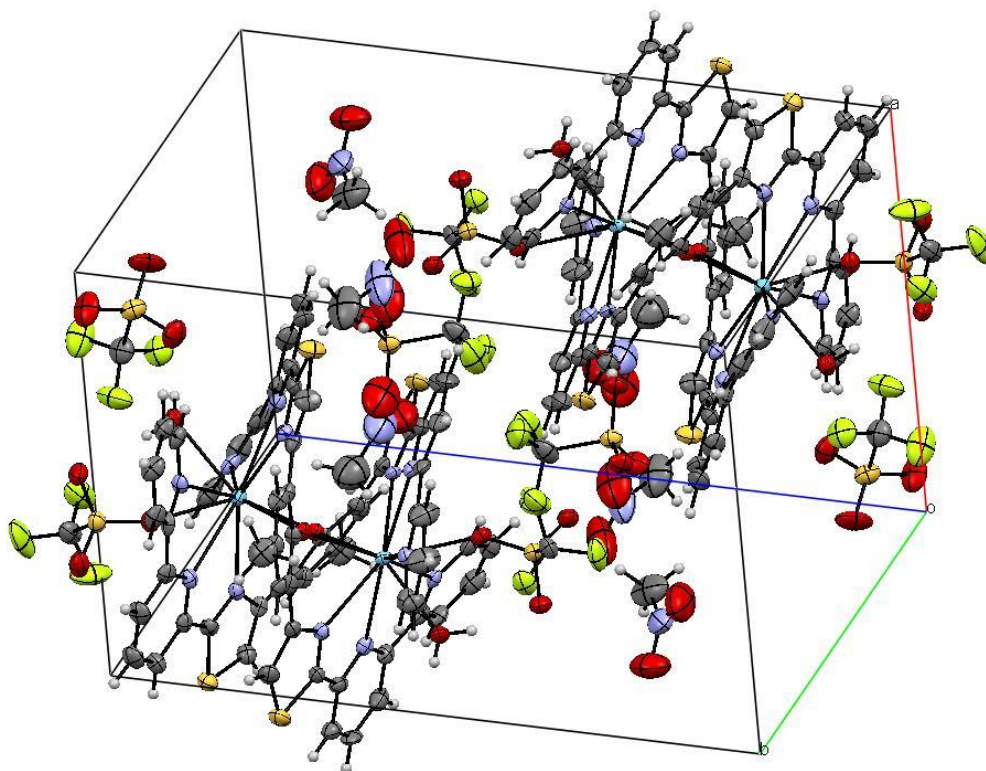
A2.10. Packing of L^{14} complex $[Cd_2(L^{14})_2]^{4+}$



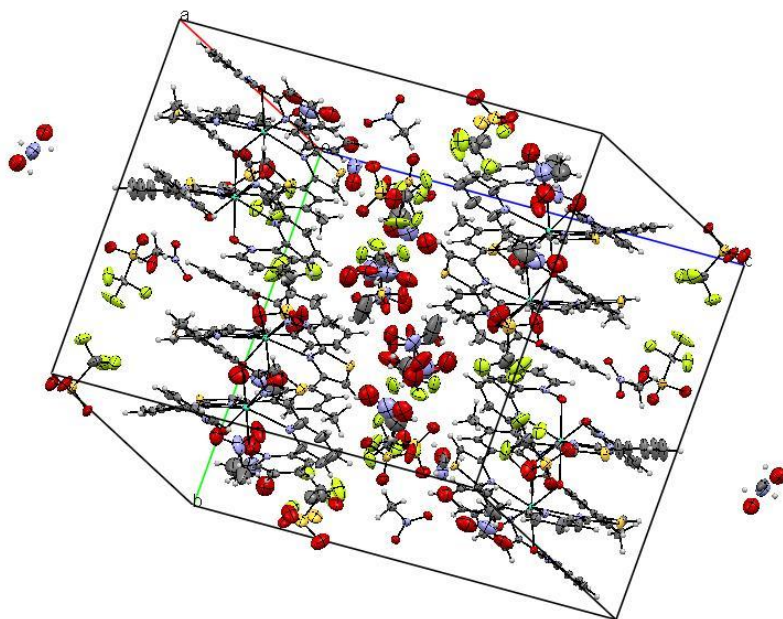
A2.11. Packing of L^{15} complex $[(L^{15})_2Eu_2]^{4+}$



A2.12. Packing of L^{16} complex $[(L^{16})_2La_2]^{4+}$



A2.13. Packing of L^{17} complex $[(L^{17})_2Tb_2]^{4+}$



Appendix 3: Publications